

**STUDY OF AXIALLY LOADED POST GROUTED DRILLED
SHAFTS USING CPT BASED LOAD TRANSFER CURVES**

by

Miguel E. Ruiz

A thesis submitted in partial fulfillment of the requirements for the degree of

MASTER OF SCIENCE
in
CIVIL ENGINEERING

UNIVERSITY OF PUERTO RICO
MAYAGÜEZ CAMPUS
2005

Approved by:

Juan Carlos Virella, Ph.D.
Member, Graduate Committee

Date

Américo L. Fernández, Ph.D.
Member, Graduate Committee

Date

Miguel A. Pando, Ph.D.
President, Graduate Committee

Date

Genock Portela, Ph.D.
Representative of Graduate Studies

Date

Ismael Pagán Trinidad, MSCE
Chairperson of the Department

Date

ABSTRACT

Post-grouted drilled shafts (PGDS) have been reported to have increased axial capacity and to experience smaller settlements, for a certain load level, compared to conventional piles installed under similar conditions. The main objectives of this study are to develop a load transfer methodology for estimating load-settlement behavior of axially loaded piles, and investigate by using the developed methodology the factors responsible for the observed improved performance of PGDS foundations with respect to conventional drilled shafts. The first objective was met through the development of a new load transfer methodology which resulted in the program TZASP, which was validated against five well documented field case studies involving load tests on instrumented drilled shafts. The proposed methodology was used to analyze several case histories involving field load tests of instrumented PGDS foundations. The analytical work revealed the following factors responsible for the improved performance of PGDS foundations: soil compaction and stiffening under the pile tip, shear stress reversal along the pile shaft, and enlarged pile tip area due to the formation of a grout bulb. The results of the PGDS numerical models were used to develop a new PGDS design procedure.

RESUMEN

Se ha reportado en la literatura que la inyección de lechada cementicia en la punta de pilotes excavados aumenta la capacidad de carga axial del pilote. Además, se ha encontrado que los pilotes con inyección de lechada cementicia experimentan menores asentamientos, para un determinado nivel de sollicitación, que pilotes convencionales instalados bajo las mismas condiciones. Este trabajo consta de dos objetivos principales. El primer objetivo es desarrollar una metodología, basada en el método de transferencia de carga, para estudiar el comportamiento de carga-desplazamiento de pilotes individuales solicitados axialmente. El segundo objetivo es investigar los factores que controlan el aumento de capacidad de carga de pilotes inyectados con lechada cementicia a través de la aplicación de la metodología desarrollada. Para satisfacer el primer objetivo se desarrolló una nueva metodología para estimar asentamientos de pilotes. Esta nueva metodología se implementó en un programa de computadora denominado TZASP que fue desarrollado para este trabajo. El programa se validó con resultados de cinco pruebas de cargas llevadas a cabo en pilotes excavados que se encontraban adecuadamente instrumentados. Esta misma metodología se utilizó para analizar los resultados de nueve pruebas de carga llevadas a cabo con pilotes inyectados con lechada cementicia, también

adecuadamente instrumentados. Los resultados de estos análisis muestran que existen al menos tres factores que controlan el aumento de capacidad de carga de pilotes inyectados: densificación del suelo debajo de la punta del pilote, desarrollo de fricción negativa a lo largo del fuste, y el aumento del área de la punta del pilote debido a la formación de un bulbo de lechada cementicia. Con los resultados de los modelos numéricos realizados se desarrolló una metodología para diseñar pilotes inyectados con lechada cementicia.

© Miguel E. Ruiz, 2005

ACKNOWLEDGEMENTS

The author would like to thank the following people without whom this research would not have been possible:

- Professor Miguel Pando for offering me the opportunity of studying at the University of Puerto Rico. Professor Pando acted as my main advisor and contributed in all aspects of this research. He also helped with partial economic support for this research. His support and friendship are greatly appreciated.
- Dr. Américo L. Fernández for being the co-advisor of this work. Dr. Fernández was a valuable reviewer of this research. He provided an important amount of information, without which, this project could not have been carried out. His support and friendship are greatly appreciated.
- Drs. Juan Carlos Virella and Genock Portela for their patience in reviewing and editing the final draft of this work.
- Civil Engineering Department for providing partial economic support during the two years journey at the UPRM.

TABLE OF CONTENTS

ABSTRACT	II
RESUMEN	III
ACKNOWLEDGEMENTS	VI
TABLE OF CONTENTS	VII
LIST OF FIGURES	X
LIST OF TABLES	XVIII
1 INTRODUCTION	2
1.1 OBJECTIVES	4
1.2 BACKGROUND ON POST GROUTED PILES	5
1.3 ORGANIZATION OF THIS THESIS	7
2 BACKGROUND AND REVIEW	8
2.1 INTRODUCTION	8
2.2 PILE SETTLEMENTS	9
2.2.1 <i>Introduction</i>	9
2.2.2 <i>The Load Transfer method</i>	10
2.2.2.1 Background of the load transfer method for pile settlement prediction	10
2.2.2.2 Empirical Load-Transfer functions	13
2.2.2.3 Theoretically based Load-Transfer functions	15
2.3 POST GROUTED PILES	19
2.3.1 <i>Background of post grouted piles</i>	20
2.3.2 <i>Construction procedure for post grouted piles</i>	22
2.3.3 <i>Current design procedure for post grouted piles</i>	25
3 PROPOSED METHODOLOGY FOR ESTIMATING SINGLE PILE SETTLEMENTS	29
3.1 INTRODUCTION	29
3.2 METHODOLOGY FOR DERIVING THEORETICAL LOAD TRANSFER CURVES	30
3.2.1 <i>Theoretical load transfer curves for the pile shaft (T-Z_s curves)</i>	30
3.2.1.1 Radial variation of shear stresses	32
3.2.1.2 Radial variation of shear modulus	35
3.2.1.3 Radius of influence of the pile	38
3.2.1.4 Variation of shear modulus with shear stress level	41
3.2.1.5 Recommended Procedure to derive theoretic load transfer curves	45
3.2.2 <i>Theoretical load transfer curves for the pile tip (Q_b-Z_b curves)</i>	49
3.3 PROPOSED METHODOLOGY FOR SETTLEMENT ANALYSIS OF AXIALLY LOADED PILES	51
3.3.1 <i>Methods for estimating axial pile capacity using CPT or SCPT data</i>	53
3.3.2 <i>Initial shear modulus at very low strains from CPT data</i>	58
3.3.3 <i>Methodology for Estimating Pile Settlements</i>	61
3.4 SUMMARY AND CONCLUSIONS	62
4 APPLICATION OF THE PROPOSED METHODOLOGY FOR ESTIMATING PILE SETTLEMENTS TO FIVE CASE STUDIES	64
4.1 INTRODUCTION	64
4.2 CASE STUDIES IN THE SOUTHERN PIEDMONT PROVINCE	65
4.2.1 <i>Drilled shaft at Opelika Site, Auburn University, Alabama</i>	66
4.2.2 <i>Drilled Shaft in coweta county, Georgia</i>	70

4.2.3	<i>Drilled shaft at Georgia Tech Campus</i>	75
4.2.4	<i>Drilled Shaft at NGES near Texas A&M University, Texas</i>	80
4.2.5	<i>Drilled shaft in a project in the Old San Juan area, Puerto Rico</i>	86
4.3	PILE CAPACITY PREDICTION USING THE PROPOSED METHODOLOGY	89
4.4	SUMMARY AND CONCLUSIONS.....	92
5	LOAD SETTLEMENT BEHAVIOR OF POST GROUTED PILES	94
5.1	INTRODUCTION.....	94
5.2	BEHAVIOR OF POST GROUTED DRILLED SHAFTS	95
5.3	FACTOR 1: SOIL COMPRESSION UNDER THE PILE TIP	97
5.4	FACTOR 2: STRESS REVERSAL ALONG THE SHAFT	100
5.5	FACTOR 3: INCREASED TIP AREA DUE TO FORMATION OF A GROUT BULB UNDER THE PILE TIP..	104
5.6	SUMMARY AND CONCLUSIONS.....	112
6	POST GROUTED PILES: CASE STUDIES	114
6.1	INTRODUCTION.....	114
6.2	ORGANIZATION OF CASE STUDIES	115
6.3	SITE I: CLEARWATER, FLORIDA	119
6.3.1	<i>Control pile</i>	122
6.3.2	<i>PGDS Installed using Flat Jack grouting Apparatus</i>	124
6.3.2.1	Flat jack I (FJ I).....	124
6.3.2.2	Flat jack II (FJ II).....	129
6.3.3	<i>PGDS Installed using Sleeve Port grouting apparatus</i>	134
6.3.3.1	Sleeve port I (SP I).....	134
6.3.3.2	Sleeve Port II (SP II).....	140
6.4	LOAD TESTS AT THE UNIVERSITY OF HOUSTON	144
6.4.1	<i>Control pile</i>	147
6.4.2	<i>PGDS: S2</i>	149
6.5	LOAD TESTS AT THE NGES AT AUBURN UNIVERSITY	155
6.5.1	<i>Control pile</i>	158
6.5.2	<i>PGDS: TS1</i>	160
6.5.3	<i>PGDS: TS2</i>	166
6.5.4	<i>PGDS: TS3</i>	172
6.6	DRILLED SHAFT IN A SOUTH CAROLINA STATE PROJECT.....	177
6.6.1	<i>PGDS at Carolina Bays project</i>	178
6.7	SUMMARY AND CONCLUSIONS.....	184
7	THEORETICALLY BASED DESIGN CHARTS FOR POST GROUTED DRILLED SHAFTS	186
7.1	INTRODUCTION	186
7.2	THEORETICALLY DERIVED TIP CAPACITY MULTIPLIERS.....	187
7.3	MODIFIED DESIGN PARAMETERS	194
7.3.1	<i>Shaft Grout Pressure Index (SGPI)</i>	194
7.3.2	<i>Axial Capacity Multiplier (ACM)</i>	197
7.3.3	<i>Ultimate Capacity Multiplier (DCM)</i>	199
7.4	TOTAL CAPACITY DESIGN CHARTS	200
7.5	SUMMARY AND CONCLUSIONS.....	206
8	DESIGN METHODOLOGY FOR POST GROUTED DRILLED SHAFTS	208
8.1	INTRODUCTION.....	208
8.2	PROPOSED METHODOLOGY	208
8.3	DESIGN EXAMPLE.....	217
8.4	SUMMARY AND CONCLUSIONS.....	224

9	SUMMARY AND CONCLUSIONS.....	226
9.1	INTRODUCTION	226
9.2	SUMMARY AND CONCLUSIONS	228
9.2.1	<i>Literature review</i>	228
9.2.2	<i>Load settlement technique</i>	228
9.2.3	<i>Analytical study of PGDS axial behavior</i>	229
9.2.4	<i>Proposed procedure for PGDS design</i>	230
9.3	RECOMMENDATIONS FOR FUTURE RESEARCH	231
	• <i>Methodology for estimating pile settlements</i>	232
	• <i>Design methodology for PGDS</i>	232
	REFERENCES.....	235
	APPENDIX A	243
	APPENDIX B.....	262

LIST OF FIGURES

FIGURE 2-1 DISCRETIZATION ASSUMED BY THE LOAD-TRANSFER APPROACH	12
FIGURE 2-2 TYPICAL SIDE LOAD TRANSFER CURVE	16
FIGURE 2-3 PILE LOAD TEST RESULTS FOR GROUTED AND UNGROUTED DRILLED SHAFTS IN MARACAIBO, VENEZUELA (SILWINSKI AND FLEMING, 1984)	22
FIGURE 2-4 PILE LOAD TEST RESULTS FOR GROUTED AND UNGROUTED DRILLED SHAFTS IN WEST PALM BEACH, FLORIDA (MULLINS AND WINTERS, 2004)	22
FIGURE 2-5 TYPICAL APPARATUS FOR GROUTING (ADAPTED FROM LIZZI, 1981)	23
FIGURE 2-6 TYPICAL CONSTRUCTION PROCEDURE FOR POST GROUTED DRILLED SHAFTS	24
FIGURE 2-7 DESIGN CHART FOR TIP ULTIMATE SETTLEMENT OF 5% OF THE PILE DIAMETER (ADAPTED FROM MULLINS AND WINTERS, 2004)	28
FIGURE 3-1 CONCENTRIC CYLINDER APPROACH	32
FIGURE 3-2 STRESSES IN A DIFFERENTIAL SOIL ELEMENT	33
FIGURE 3-3 RADIAL DISTRIBUTION OF THE SHEAR MODULUS DUE TO SOIL DISTURBANCES DURING PILE INSTALLATION	36
FIGURE 3-4 ASSUMED RADIAL VARIATION OF SHEAR MODULUS	36
FIGURE 3-5 VARIATION OF SHEAR MODULUS WITH SHEAR STRAIN IN SOILS (ADAPTED FROM MAYNE AND SCHENIDER, 2001)	43
FIGURE 3-6 DEGRADATION OF SHEAR MODULUS FOR DIFFERENT NON-LINEAR SOIL MODELS	44
FIGURE 3-7 LINEAR, HYPERBOLIC AND MODIFIED HYPERBOLIC LOAD TRANSFER CURVES	49
FIGURE 3-8 TYPICAL LOAD TRANSFER CURVES FOR THE PILE BASE	51
FIGURE 4-1 SOUTHERN PIEDMONT PROVINCE AND RELATIVE LOCATION OF CASE HISTORIES 1 THROUGH 3 ...	66
FIGURE 4-2 SHEAR WAVE VELOCITY PROFILE AND CPT SOUNDINGS ADVANCED AT OPELIKA SITE, ALABAMA	67
FIGURE 4-3 STATIC AXIAL PILE CAPACITY AND SHEAR MODULUS PROFILE FOR A 0.915 DIAMETER DRILLED SHAFT AT OPELIKA SITE	68
FIGURE 4-4 TYPE A PREDICTIONS FOR AXIAL PILE AT OPELIKA SITE	69
FIGURE 4-5 LOAD TRANSFERRED THROUGH THE SHAFT AND THE PILE TIP FOR THE PILE TESTED AT OPELIKA SITE FOR MODEL 2	70
FIGURE 4-6 SHEAR WAVE VELOCITY AND CPT SOUNDING ADVANCED IN COWETA COUNTY, GEORGIA	71
FIGURE 4-7 STATIC AXIAL PILE CAPACITY AND SHEAR MODULUS PROFILE FOR A 0.915 DIAMETER DRILLED SHAFT IN COWETA COUNTY, GEORGIA	72
FIGURE 4-8 TYPE A PREDICTIONS FOR AXIAL PILE UNDER A BRIDGE IN COWETA COUNTY	73

FIGURE 4-9 MODIFIED TYPE A PREDICTION FOR AXIAL PILE UNDER A BRIDGE IN COWETA COUNTY	74
FIGURE 4-10 SHEAR WAVE VELOCITY AND CPT SOUNDING ADVANCED AT GEORGIA TECH CAMPUS, GEORGIA	76
FIGURE 4-11 STATIC AXIAL PILE CAPACITY AND SHEAR MODULUS PROFILE FOR A 0.76 DIAMETER DRILLED SHAFT AT GEORGIA TECH CAMPUS, GEORGIA.....	77
FIGURE 4-12 TYPE A PREDICTIONS FOR AXIAL PILE TESTED AT GT CAMPUS.....	78
FIGURE 4-13 TYPE B PREDICTION FOR THE PILE TESTED AT GT CAMPUS	79
FIGURE 4-14 PREDICTED VS. MEASURED LOAD TRANSFER WITH DEPTH FOR MODEL 2.....	80
FIGURE 4-15 SHEAR WAVE VELOCITY AND CPT SOUNDING ADVANCED AT TEXAS A&M CAMPUS, TEXAS...	81
FIGURE 4-16 STATIC AXIAL PILE CAPACITY AND SHEAR MODULUS PROFILE FOR A 0.91 DIAMETER DRILLED SHAFT AT TEXAS A&M CAMPUS, TEXAS	82
FIGURE 4-17 TYPE A PREDICTIONS FOR AXIAL PILE TESTED AT NGES IN TEXAS	83
FIGURE 4-18 PREDICTED VS. MEASURED LOAD TRANSFER WITH DEPTH FOR MODEL 1	84
FIGURE 4-19 PREDICTED VS. MEASURED LOAD TRANSFER WITH DEPTH FOR MODEL 2.....	85
FIGURE 4-20 PREDICTED VS. MEASURED LOAD TRANSFER WITH DEPTH FOR MODEL 3.....	86
FIGURE 4-21 SHEAR WAVE VELOCITY AND CPT SOUNDINGS ADVANCED IN THE OLD SAN JUAN AREA, PUERTO RICO	87
FIGURE 4-22 STATIC AXIAL PILE CAPACITY AND SHEAR MODULUS PROFILE FOR A 0.41 DIAMETER DRILLED SHAFT IN THE OLD SAN JUAN AREA, PUERTO RICO	88
FIGURE 4-23 TYPE A PREDICTIONS FOR AXIAL PILE TESTED AT A PROJECT IN THE OLD SAN JUAN AREA, PUERTO RICO	89
FIGURE 4-24 ULTIMATE PILE CAPACITY PREDICTED VS DAVISSON FAILURE LOAD FROM LOAD TEST FOR CASE STUDIES ONE THROUGH FIVE.....	91
FIGURE 4-25 DAVISSON FAILURE LOAD ESTIMATED USING THE PROPOSED CPT BASED LOAD TRANSFER APPROACH METHODOLOGY	92
FIGURE 5-1 PILE CAPACITY IMPROVEMENT FOR A DRILLED SHAFT IN (A) VENEZUELA AND (B) FLORIDA	96
FIGURE 5-2 EFFECT OF SOIL COMPRESSION UNDER THE BOTTOM OF THE PILE ON THE LOAD-TRANSFER CURVE AT THE TIP	98
FIGURE 5-3 EFFECT OF AN INCREASED SOIL SHEAR MODULUS ON THE Q_b -Z CURVE.....	99
FIGURE 5-4 EFFECT OF STRESS REVERSAL ON THE LOAD-TRANSFER CURVE OF SOIL ALONG THE SHAFT	101
FIGURE 5-5 MASING RULE APPLIED TO A TZ CURVE	103
FIGURE 5-6 EFFECT OF THE AUGMENTED TIP AREA ON THE LOAD-TRANSFER AT THE TIP	106
FIGURE 5-7 EFFECT OF AN INCREASED PILE TIP AREA ON THE LOAD TRANSFER CURVE Q_b -Z	107
FIGURE 5-8 POST GROUTED LABORATORY SPECIMEN WITH FRACTURED GROUT BULB (FROM MULLINS AND WINTERS, 2004)	110

FIGURE 5-9 POST GROUTED LABORATORY SPECIMENS WITH GROUT BULB (FROM MULLINS AND WINTERS, 2004).....	111
FIGURE 6-1 SITE I LAYOUT.....	120
FIGURE 6-2 GEOTECHNICAL INFORMATION GATHERED AT TESTING SITE I, CLEARWATER, FLORIDA.....	121
FIGURE 6-3 EQUIVALENT STATIC LOAD TEST DATA FOR FOUR PGDS AND ONE CONTROL PILE AT CLEARWATER, FLORIDA.....	122
FIGURE 6-4 TYPE A PREDICTION FOR CONTROL SHAFT IN SITE I.....	123
FIGURE 6-5 PREDICTED LOAD SETTLEMENT CURVE FOR AN UNGROUTED DRILLED SHAFT AT FJ I LOCATION.....	125
FIGURE 6-6 FJ I – FACTOR 1: PREDICTION OF THE LOAD-SETTLEMENT CURVE OF PGDS WITH DENSIFIED SOIL UNDER THE PILE TIP.....	126
FIGURE 6-7 FJ I – FACTOR 2: PREDICTION OF THE LOAD-SETTLEMENT CURVE OF PGDS CONSIDERING STRESS REVERSAL ALONG THE SHAFT.....	127
FIGURE 6-8 FJ I – FACTOR 3: PREDICTION OF THE LOAD-SETTLEMENT CURVE OF PGDS CONSIDERING AUGMENTED TIP AREA.....	128
FIGURE 6-9 FJ I – FACTORS 2 AND 3: CALIBRATED LOAD-SETTLEMENT CURVE.....	129
FIGURE 6-10 PREDICTED LOAD SETTLEMENT CURVE FOR AN UNGROUTED DRILLED SHAFT AT FJ II LOCATION.....	130
FIGURE 6-11 FJ II – FACTOR 1: PREDICTION OF THE LOAD-SETTLEMENT CURVE OF PGDS WITH DENSIFIED SOIL UNDER THE PILE TIP.....	131
FIGURE 6-12 FJ II – FACTOR 2: PREDICTION OF THE LOAD-SETTLEMENT CURVE OF PGDS CONSIDERING STRESS REVERSAL ALONG THE SHAFT.....	132
FIGURE 6-13 FJ II – FACTOR 3: PREDICTION OF THE LOAD-SETTLEMENT CURVE OF PGDS CONSIDERING AUGMENTED TIP AREA.....	133
FIGURE 6-14 FJ II – FACTORS 2 AND 3: CALIBRATED LOAD-SETTLEMENT CURVE.....	134
FIGURE 6-15 PREDICTED LOAD SETTLEMENT CURVE FOR AN UNGROUTED DRILLED SHAFT AT SP I LOCATION.....	135
FIGURE 6-16 SP I – FACTOR 1: PREDICTION OF THE LOAD-SETTLEMENT CURVE OF PGDS WITH DENSIFIED SOIL UNDER THE PILE TIP.....	136
FIGURE 6-17 SP I – FACTOR 2: PREDICTION OF THE LOAD-SETTLEMENT CURVE OF PGDS CONSIDERING STRESS REVERSAL ALONG THE SHAFT.....	137
FIGURE 6-18 SP I – FACTOR 3: PREDICTION OF THE LOAD-SETTLEMENT CURVE OF PGDS CONSIDERING AUGMENTED TIP AREA.....	138
FIGURE 6-19 SP I – FACTORS 1, 2 AND 3: CALIBRATED LOAD-SETTLEMENT CURVE.....	139
FIGURE 6-20 PREDICTED LOAD SETTLEMENT CURVE FOR AN UNGROUTED DRILLED SHAFT AT SP II LOCATION.....	140

FIGURE 6-21 SP II – FACTOR 1: PREDICTION OF THE LOAD-SETTLEMENT CURVE OF PGDS WITH DENSIFIED SOIL UNDER THE PILE TIP	141
FIGURE 6-22 SP II – FACTOR 2: PREDICTION OF THE LOAD-SETTLEMENT CURVE OF PGDS CONSIDERING STRESS REVERSAL ALONG THE SHAFT	142
FIGURE 6-23 SP II – FACTOR 3: PREDICTION OF THE LOAD-SETTLEMENT CURVE OF PGDS CONSIDERING AUGMENTED TIP AREA	143
FIGURE 6-24 SP II – FACTORS 2 AND 3: CALIBRATED LOAD-SETTLEMENT CURVE	144
FIGURE 6-25 GEOTECHNICAL INFORMATION GATHERED AT TESTING SITE NEAR UNIVERSITY OF HOUSTON, TEXAS	146
FIGURE 6-26 LAYOUT OF SITE NEAR THE UNIVERSITY OF HOUSTON	147
FIGURE 6-27 EQUIVALENT STATIC LOAD TEST DATA FOR PGDS S2 AND CONTROL PILE S1 AT THE TESTING NEAR UNIVERSITY OF HOUSTON.....	148
FIGURE 6-28 PREDICTED AND MEASURED CONTROL PILE LOAD SETTLEMENT CURVES FOR THE TEXAS DOT DEMO (TYPE A PREDICTION).....	149
FIGURE 6-29 CALIBRATED CONTROL PILE MODEL FOR THE TEXAS DOT DEMO.....	150
FIGURE 6-30 S2 – FACTOR 1: PREDICTION OF THE LOAD-SETTLEMENT CURVE OF PGDS WITH DENSIFIED SOIL UNDER THE PILE TIP	150
FIGURE 6-31 S2 – FACTOR 2: PREDICTION OF THE LOAD-SETTLEMENT CURVE OF PGDS CONSIDERING STRESS REVERSAL ALONG THE SHAFT	151
FIGURE 6-32 S2 – FACTOR 3: PREDICTION OF THE LOAD-SETTLEMENT CURVE OF PGDS CONSIDERING AUGMENTED TIP AREA	153
FIGURE 6-33 S 2 – FACTORS 1 AND 2: CALIBRATED LOAD-SETTLEMENT CURVE.....	155
FIGURE 6-34 GEOTECHNICAL INFORMATION GATHERED AT NGES AT AUBURN UNIVERSITY	156
FIGURE 6-35 LAYOUT OF FIVE DRILLED SHAFTS TESTED AT NGES AUBURN UNIVERSITY.....	157
FIGURE 6-36 EQUIVALENT STATIC LOAD TEST DATA FOR PGDS S2 AND CONTROL PILE S1 AT THE TESTING NEAR UNIVERSITY OF HOUSTON.....	158
FIGURE 6-37 TYPE A PREDICTION FOR CONTROL SHAFT AT NGES AT AUBURN UNIVERSITY	159
FIGURE 6-38 TYPE A PREDICTION FOR UNGROUTED PILES USING DATA FROM 5 CPT SOUNDINGS ADVANCED AT THE SITE	160
FIGURE 6-39 TS 1 – FACTOR 1: PREDICTION OF THE LOAD-SETTLEMENT CURVE OF PGDS WITH DENSIFIED SOIL UNDER THE PILE TIP	162
FIGURE 6-40 TS 1 – FACTOR 2: PREDICTION OF THE LOAD-SETTLEMENT CURVE OF PGDS CONSIDERING STRESS REVERSAL ALONG THE SHAFT	163
FIGURE 6-41 TS 1 – FACTOR 3: PREDICTION OF THE LOAD-SETTLEMENT CURVE OF PGDS CONSIDERING AUGMENTED TIP AREA	164
FIGURE 6-42 TS 1 – FACTORS 2 AND 3: CALIBRATED LOAD-SETTLEMENT CURVE.....	165

FIGURE 6-43 TS 2 – FACTOR 1: PREDICTION OF THE LOAD-SETTLEMENT CURVE OF PGDS WITH DENSIFIED SOIL UNDER THE PILE TIP	167
FIGURE 6-44 TS 2 – FACTOR 2: PREDICTION OF THE LOAD-SETTLEMENT CURVE OF PGDS CONSIDERING STRESS REVERSAL ALONG THE SHAFT	168
FIGURE 6-45 TS 2 – FACTOR 3: PREDICTION OF THE LOAD-SETTLEMENT CURVE OF PGDS CONSIDERING AUGMENTED TIP AREA	169
FIGURE 6-46 TS 2 – FACTORS 2 AND 3: CALIBRATED LOAD-SETTLEMENT CURVE.....	171
FIGURE 6-47 TS 3 – FACTOR 1: PREDICTION OF THE LOAD-SETTLEMENT CURVE OF PGDS WITH DENSIFIED SOIL UNDER THE PILE TIP	173
FIGURE 6-48 TS 3 – FACTOR 2: PREDICTION OF THE LOAD-SETTLEMENT CURVE OF PGDS CONSIDERING STRESS REVERSAL ALONG THE SHAFT	174
FIGURE 6-49 TS 3 – FACTOR 3: PREDICTION OF THE LOAD-SETTLEMENT CURVE OF PGDS CONSIDERING AUGMENTED TIP AREA	175
FIGURE 6-50 TS 3 – FACTORS 1, 2 AND 3: CALIBRATED LOAD-SETTLEMENT CURVE.....	176
FIGURE 6-51 GEOTECHNICAL INFORMATION GATHERED AT CAROLINA BAYS PROJECT	178
FIGURE 6-52 PREDICTED LOAD SETTLEMENT CURVE FOR AN UNGROUTED DRILLED SHAFT AT CAROLINA BAYS PROJECT	179
FIGURE 6-53 CAROLINA BAYS – FACTOR 1: PREDICTION OF THE LOAD-SETTLEMENT CURVE OF PGDS WITH DENSIFIED SOIL UNDER THE PILE TIP	180
FIGURE 6-54 CAROLINA BAYS – FACTOR 2: PREDICTION OF THE LOAD-SETTLEMENT CURVE OF PGDS CONSIDERING STRESS REVERSAL ALONG THE SHAFT.....	181
FIGURE 6-55 CAROLINA BAYS – FACTOR 3: PREDICTION OF THE LOAD-SETTLEMENT CURVE OF PGDS CONSIDERING AUGMENTED TIP AREA.....	182
FIGURE 6-56 CAROLINA BAYS – FACTORS 1, 2 AND 3: CALIBRATED LOAD-SETTLEMENT CURVE	183
FIGURE 7-1 TCM VS. GPI APPLIED TO UNGROUTED TIP CAPACITIES AT 1% OF DIAMETER DISPLACEMENT ..	189
FIGURE 7-2 TCM VS. GPI APPLIED TO UNGROUTED TIP CAPACITIES AT 2% OF DIAMETER DISPLACEMENT ..	190
FIGURE 7-3 TCM VS. GPI APPLIED TO UNGROUTED TIP CAPACITIES AT 5% OF DIAMETER DISPLACEMENT ..	191
FIGURE 7-4 TOTAL CAPACITY DESIGN CHART APPLIED TO GROUTED TOTAL CAPACITIES CORRESPONDING TO GROUTED PILE HEAD DISPLACEMENTS OF 1%, 2%, AND 5% OF DIAMETER	201
FIGURE 7-5 UCM VS. SGPI DESIGN CHART.....	203
FIGURE 7-6 DESIGN CHART TO APPROXIMATELY ESTIMATE THE GROUT BULB RADIUS OF A PGDS IN TERMS OF THE SGPI.....	204
FIGURE 8-1 EXAMPLE OF CALCULATION OF THE PGDS TOTAL CAPACITY AT PILE HEAD DISPLACEMENT FOR A GIVEN MGPI.....	213
FIGURE 8-2 EXAMPLE OF THE APPLICATION OF THE RESULTING MODIFIED HYPERBOLIC T-Z CURVE AFTER APPLYING THE MASING RULE TO CONSIDER STRESS REVERSAL	214

FIGURE 8-3 EXAMPLE FOR THE ESTIMATION OF THE BULB RADIUS USING THE MGPI PARAMETER	215
FIGURE 8-4 EXAMPLE FOR CHECKING THE PGDS DAVISSON FAILURE LOAD	216
FIGURE 8-5 SHEAR WAVE VELOCITY AND CPT SOUNDINGS ADVANCED AT THE LOCATION OF AN ADDITIONAL CPT SOUNDING (CPT 67) ADVANCED AT SITE I, CLEARWATER, FLORIDA	217
FIGURE 8-6 STATIC AXIAL PILE CAPACITY AND SHEAR MODULUS PROFILE FOR A 0.61 M DIAMETER DRILLED SHAFT AT THE LOCATION OF CPT 67 AT SITE I, CLEARWATER, FLORIDA	218
FIGURE 8-7 LOAD SETTLEMENT CURVE FOR THE UNGROUTED PILE	219
FIGURE 8-8 TOTAL CAPACITY MULTIPLIERS FOR PILE HEAD DISPLACEMENTS OF 1 %, 2 %, AND 5 % OF THE PILE DIAMETER	220
FIGURE 8-9 ESTIMATED GROUT BULB RADIUS FROM DESIGN CHART	221
FIGURE 8-10 LOAD SETTLEMENT CURVE FOR THE PGDS ASSUMING A GROUT BULB RADIUS 1.7 TIMES THE SHAFT RADIUS AND STRESS REVERSAL OF 30 KPA ALONG THE SHAFT.....	222
FIGURE 8-11 DAVISSON FAILURE LOAD FOR THE DESIGNED PGDS	223
FIGURE A - 1 SHEAR WAVE VELOCITY AND CPT SOUNDINGS ADVANCED AT THE LOCATION OF CONTROL PILE AT SITE I, CLEARWATER, FLORIDA.....	243
FIGURE A - 2 STATIC AXIAL PILE CAPACITY AND SHEAR MODULUS PROFILE FOR A 0.61 M DIAMETER CONTROL PILE AT SITE I, CLEARWATER, FLORIDA	244
FIGURE A - 3 SHEAR WAVE VELOCITY AND CPT SOUNDINGS ADVANCED AT THE LOCATION OF DRILLED SHAFT FJ 1 AT SITE I, CLEARWATER, FLORIDA.....	244
FIGURE A - 4 STATIC AXIAL PILE CAPACITY AND SHEAR MODULUS PROFILE FOR A 0.61 M DIAMETER DRILLED SHAFT FJ 1 LOCATION AT SITE I, CLEARWATER, FLORIDA.....	245
FIGURE A - 5 SHEAR WAVE VELOCITY AND CPT SOUNDINGS ADVANCED AT THE LOCATION OF DRILLED SHAFT FJ 2 AT SITE I, CLEARWATER, FLORIDA.....	245
FIGURE A - 6 STATIC AXIAL PILE CAPACITY AND SHEAR MODULUS PROFILE FOR A 0.61 M DIAMETER DRILLED SHAFT FJ 2 LOCATION AT SITE I, CLEARWATER, FLORIDA.....	246
FIGURE A - 7 SHEAR WAVE VELOCITY AND CPT SOUNDINGS ADVANCED AT THE LOCATION OF DRILLED SHAFT SP 1 AT SITE I, CLEARWATER, FLORIDA	246
FIGURE A - 8 STATIC AXIAL PILE CAPACITY AND SHEAR MODULUS PROFILE FOR A 0.61 M DIAMETER DRILLED SHAFT SP 1 LOCATION AT SITE I, CLEARWATER, FLORIDA	247
FIGURE A - 9 SHEAR WAVE VELOCITY AND CPT SOUNDINGS ADVANCED AT THE LOCATION OF DRILLED SHAFT SP 2 AT SITE I, CLEARWATER, FLORIDA	247
FIGURE A - 10 STATIC AXIAL PILE CAPACITY AND SHEAR MODULUS PROFILE FOR A 0.61 M DIAMETER DRILLED SHAFT SP 2 LOCATION AT SITE I, CLEARWATER, FLORIDA.....	248
FIGURE A - 11 SHEAR WAVE VELOCITY AND CPT SOUNDINGS ADVANCED AT THE LOCATION OF AN ADDITIONAL CPT SOUNDING (CPT 67) ADVANCED AT SITE I, CLEARWATER, FLORIDA.....	248

FIGURE A - 12 STATIC AXIAL PILE CAPACITY AND SHEAR MODULUS PROFILE FOR A 0.61 M DIAMETER DRILLED SHAFT AT THE LOCATION OF CPT 67 AT SITE I, CLEARWATER, FLORIDA	249
FIGURE A - 13 SHEAR WAVE VELOCITY AND SOUNDING CPT 2 ADVANCED AT UNIVERSITY OF HOUSTON, TEXAS	250
FIGURE A - 14 SHEAR WAVE VELOCITY AND SOUNDING CPT 4 ADVANCED AT UNIVERSITY OF HOUSTON, TEXAS	251
FIGURE A - 15 SHEAR WAVE VELOCITY AND SOUNDING CPT 5 ADVANCED AT UNIVERSITY OF HOUSTON, TEXAS	251
FIGURE A - 16 SHEAR WAVE VELOCITY AND SOUNDING CPT 6 ADVANCED AT THE LOCATION OF DRILLED SHAFT S2 AT UNIVERSITY OF HOUSTON, TEXAS	252
FIGURE A - 17 SHEAR WAVE VELOCITY AND AVERAGE CPT SOUNDING OBTAINED FROM SOUNDINGS DEPICTED IN FIGURE A - 13 THROUGH FIGURE A - 16.....	252
FIGURE A - 18 STATIC AXIAL PILE CAPACITY AND SHEAR MODULUS PROFILE FOR A 1.22 M DIAMETER DRILLED SHAFT USING THE AVERAGE SOIL PROFILE DEPICTED IN FIGURE A - 17	253
FIGURE A - 19 SHEAR WAVE VELOCITY AND CPT SOUNDINGS ADVANCED AT THE LOCATION OF CONTROL PILE TS-4 AT NGES AT AUBURN UNIVERSITY, ALABAMA	254
FIGURE A - 20 STATIC AXIAL PILE CAPACITY AND SHEAR MODULUS PROFILE FOR A 1.06 M DIAMETER CONTROL PILE TS-4 AT AUBURN UNIVERSITY, ALABAMA	255
FIGURE A - 21 SHEAR WAVE VELOCITY AND CPT SOUNDINGS ADVANCED AT THE LOCATION OF DRILLED SHAFT TS-1 AT NGES AT AUBURN UNIVERSITY, ALABAMA.....	255
FIGURE A - 22 STATIC AXIAL PILE CAPACITY AND SHEAR MODULUS PROFILE FOR A 1.06 M DIAMETER DRILLED SHAFT TS-1 AT AUBURN UNIVERSITY, ALABAMA	256
FIGURE A - 23 SHEAR WAVE VELOCITY AND CPT SOUNDINGS ADVANCED AT THE LOCATION OF DRILLED SHAFT TS-2 AT NGES AT AUBURN UNIVERSITY, ALABAMA.....	256
FIGURE A - 24 STATIC AXIAL PILE CAPACITY AND SHEAR MODULUS PROFILE FOR A 1.06 M DIAMETER DRILLED SHAFT TS-2 AT AUBURN UNIVERSITY, ALABAMA	257
FIGURE A - 25 SHEAR WAVE VELOCITY AND CPT SOUNDINGS ADVANCED AT THE LOCATION OF DRILLED SHAFT TS-3 AT NGES AT AUBURN UNIVERSITY, ALABAMA.....	257
FIGURE A - 26 STATIC AXIAL PILE CAPACITY AND SHEAR MODULUS PROFILE FOR A 1.06 M DIAMETER DRILLED SHAFT TS-3 AT AUBURN UNIVERSITY, ALABAMA	258
FIGURE A - 27 SHEAR WAVE VELOCITY AND CPT SOUNDINGS ADVANCED AT THE LOCATION OF DRILLED SHAFT TS-5 AT NGES AT AUBURN UNIVERSITY, ALABAMA.....	258
FIGURE A - 28 STATIC AXIAL PILE CAPACITY AND SHEAR MODULUS PROFILE FOR A 1.06 M DIAMETER DRILLED SHAFT TS-5 AT AUBURN UNIVERSITY, ALABAMA	259
FIGURE A - 29 SHEAR WAVE VELOCITY AND CPT SOUNDINGS ADVANCED AT THE LOCATION OF THE PGDS AT THE CAROLINA BAYS PROJECT, SOUTH CAROLINA.....	260

FIGURE A - 30 STATIC AXIAL PILE CAPACITY AND SHEAR MODULUS PROFILE FOR A 1.372 M DIAMETER DRILLED SHAFT AT THE CAROLINA BAYS PROJECT, SOUTH CAROLINA	261
FIGURE B-1 "INSTRUCTIONS" WORKSHEET OF THE LOAD TRANSFER PROGRAM: PILE DISCRETIZATION.....	263
FIGURE B-2 "INSTRUCTIONS" WORKSHEET OF THE LOAD TRANSFER PROGRAM: GENERAL INSTRUCTIONS TO RUN ANALYSIS AND VARIABLE DEFINITION.....	264
FIGURE B-3 "GENERAL DATA" WORKSHEET OF THE LOAD TRANSFER PROGRAM: GENERAL MODEL DATA AND PILE PROPERTIES	265
FIGURE B-4 "INSTRUCTIONS" WORKSHEETS OF THE LOAD TRANSFER PROGRAM: GENERAL INSTRUCTIONS TO RUN ANALYSIS AND VARIABLE DEFINITION.....	266
FIGURE B-5 RESULTS FILE: ECHO OF INPUT DATA.....	267

LIST OF TABLES

TABLE 2-1 EMPIRICAL LOAD-TRANSFER CURVES	14
TABLE 2-2 SOME THEORETICAL LOAD-TRANSFER CURVES.....	17
TABLE 3-1 SUGGESTED VALUES TO CONSIDER MODULUS DEGRADATION DUE TO INSTALLATION EFFECTS (AFTER KRAFT ET AL. 1981)	37
TABLE 3-2 MODELS OF SHEAR MODULUS DEGRADATION.....	42
TABLE 3-3 STEPS REQUIRED TO DEFINED THEORETICAL TZ CURVES.....	46
TABLE 3-4 VARIABLES REQUIRED TO DEFINE LOAD TRANSFER CURVES.....	52
TABLE 3-5 VALUES FOR AGE SCALING FACTOR ASF (AFTER ANDRUS ET AL., 2004)	59
TABLE 3-6 STEPS OF THE PROPOSED COUPLED CPT – LOAD TRANSFER METHODOLOGY.....	61
TABLE 4-1 PREDICTED AXIAL PILE CAPACITY FOR A DRILLED SHAFT AT OPELIKA SITE.....	68
TABLE 4-2 PREDICTED AXIAL PILE CAPACITY FOR A DRILLED SHAFT IN COWETA COUNTY	72
TABLE 4-3 CORRECTED AXIAL PILE CAPACITY FOR A DRILLED SHAFT IN COWETA COUNTY	74
TABLE 4-4 PREDICTED AXIAL PILE CAPACITY FOR A DRILLED SHAFT AT GT CAMPUS	77
TABLE 4-5 PREDICTED AXIAL PILE CAPACITY FOR A DRILLED SHAFT IN TEXAS	82
TABLE 4-6 PREDICTED AXIAL PILE CAPACITY FOR A DRILLED SHAFT IN PUERTO RICO	88
TABLE 6-1 PGDS CASE HISTORIES	118
TABLE 7-1 EMPIRICAL AND THEORETICAL SLOPES AND INTERCEPTS FOR THE DESIGN CHARTS PROPOSED BY MULLINS AND WINTERS (2004) FOR UNGROUTED TIP DISPLACEMENT $J = 1\%$	189
TABLE 7-2 EMPIRICAL AND THEORETICAL SLOPES AND INTERCEPTS FOR THE DESIGN CHARTS PROPOSED BY MULLINS AND WINTERS (2004) FOR UNGROUTED TIP DISPLACEMENT $J = 2\%$	190
TABLE 7-3 EMPIRICAL AND THEORETICAL SLOPES AND INTERCEPTS FOR THE DESIGN CHARTS PROPOSED BY MULLINS AND WINTERS (2004) FOR UNGROUTED TIP DISPLACEMENT $J = 5\%$	191
TABLE 9-1 DETAILED PROJECT OBJECTIVES	227

1 INTRODUCTION

This thesis describes the main aspects of a research on the applications of post grouting techniques to improve the performance of piled foundations. The term post-grouted deep foundations refers to drilled shafts (PGDS) or driven piles (PGDP) in which cementitious slurry is injected through the pile tip after pile installation in order to improve axial pile capacity and stiffness. The injection takes place through grout pipes left inside the pile during construction. The grout injected at the tip elevation is expected to (a) create a grout bulb below the tip that will improve pile capacity to resist axial loads through increased tip resistance and (b) decrease pile settlements through increased stiffness of the soil near the tip. Post grouted piles have been reported as been used in Argentina (Bolognesi and Moretto, 1973), Germany (Stoker, 1983), and Taipei (Mullins, 1999).

So far, post grouted piles have not been widely used in the US, probably due to the lack of familiarity with this foundation technique and lack of well documented case histories that could help promote the use of post grouted piles. Mullins et al. (2001) presented a comprehensive study of this type of foundation and proposed an

empirical design method for post grouted piles based on the few load tests available on this type of piles. The design method proposed by these authors is a good initial design approach. The method is constantly being updated and verified as more load test data becomes available. A drawback of this methodology is that it is based solely on available empirical observations that to this date are limited and that it is not complemented by a theoretical framework.

The main focus of this research is to propose a theoretical framework to study the behavior of post grouted piles. Through the review of the available experimental data using such theoretical approach, this research hopes to contribute to the design method currently available. Among a number of theoretical methods available to study post grouted pile behavior, the load transfer approach (or T-Z method) was considered as a simple and flexible method to study the behavior of these piles and to predict their settlements with reasonable accuracy.

The T-Z method has been intensively improved since it was originally proposed in 1950. It has evolved to become a very versatile tool, which allows the modeling of a great variety of soil profiles and pile types. The method provides enough accuracy to be applied in common engineering problems. Due to its simplicity, relative high accuracy and the availability of numerous commercial programs, the T-Z method is one of the most used techniques in the mainstream engineering practice in US to estimate pile settlements.

1.1 OBJECTIVES

This thesis has the following two main objectives:

1. Develop a methodology for estimating settlements of single piles.
2. Study the behavior of post grouted drilled shafts by means of the load transfer method.

More specific objectives of this research are:

Concerning the first main objective:

- (1.a) Obtain approximate theoretical expressions to estimate the radius of influence of the pile.
- (1.b) Include in the methodology the effects that soil disturbances due to pile installation have on the load-transfer curves and on the load-settlement curve of the pile.
- (1.c) Develop a computer program to incorporate the proposed methodology.

Concerning the second main objective:

- (2.a) Identify factors that contribute to the improvement of pile performance using the load-settlement methodology developed in (1).
- (2.b) Derive theoretically based design curves for post-grouted piles using the load-transfer method.
- (2.c) Propose a design methodology for post grouted drilled shafts

1.2 BACKGROUND ON POST GROUTED PILES

In the last 30 years, the trend in the design of piled foundations has been moving towards large diameters piles (Stoker, 1983). However, constructions problems and high costs in small to medium projects, construction difficulties, lower skin-friction-to pile-self-weight ratio and higher associated costs still contribute to favor conventional designs using smaller pile diameters (Stocker, 1983). This is one of the reasons why continuous attempts are being made to improve deep foundation performance (i.e., higher capacity and lower settlements) without increasing pile diameter.

While post-grouting of pile tips has been used as a method to increase pile capacity in numerous projects at several locations (Bruce, 1986), little use of this technique in US mainstream engineering practice has been observed. Although grouted piles have shown good performance (Bolognesi and Moretto, 1973; Brusey, 2000; Stocker, 1983) there is still some reticence in the US engineering community to implement the use of post-grouted piles. Probably, the main reason for which post-grouting is not being used by practitioners, is the lack of knowledge about the effectiveness of post-grouting and its effects on the overall behavior of the pile (Mullins et al., 2001).

Until the present, post-grouted piles have been designed with the aid of either empirical methods or experience. Currently, an empirically developed design method of post-grouted drilled shafts is available to US engineers. The absence of a more robust theoretical-design procedure may attempt against the use of post-grouted piles in US. Therefore, a deeper understanding of grouting process through theoretical analyses is required to strengthen the design method available.

For this study the load transfer approach (or T-Z method) was selected to assess the behavior of PGDS because of its relative simplicity, their fairly accurate results and its straightforward implementation in a computer program.

In order to make reliable predictions on the behavior of PGDS a general methodology data is proposed for estimating pile settlements that combines the load-transfer methodology and the CPT continuous soil information data. Commercial programs such as FB-Pier (Hoit et al., 2000), Shaft (Ensoft, 1998), and CAXPILE (Dawkins, 1982) have made the load transfer method more accessible to the community of engineers. Currently, load-transfer methodology is commonly used by FHWA and US transportation agencies. However, commercial programs are quite expensive and its code is completely unknown by the user. On the contrary to that, an in-house load-transfer program specially developed to study both grouted and ungrouted piles, would allow a better handling of model parameters in that the code would be fully open.

There is a need to improve the understanding of post grouted pile behavior in order to achieve a rationale and safe design. Constructions costs may be significantly reduced if piles with conventional diameters but high capacity could be designed. The aid of a simple but reliable methodology to study the grouted and ungrouted pile behavior is required to study their load transfer behavior and to evaluate the current empirically-based design method for grouted piles.

1.3 ORGANIZATION OF THIS THESIS

This thesis comprises 10 chapters and two appendixes. In Chapter 2, a literature review on pile settlements and post grouted piles is presented. Particular attention is paid to the estimation of settlements using the load transfer method and post grouting of piles by means of compaction high pressure grouting, since both aspects constitute the central topics of this work. A methodology for studying settlements of axially loaded single piles using the load transfer approach and theoretically derived load transfer curves is presented in Chapter 3. The methodology is validated with several case studies presented in Chapter 4. An investigation of the different factors that may contribute to the observed improved resistance of post grouted piles are covered in Chapter 5. Load transfer analyses of available case histories of load tested post grouted piles are presented and discussed in Chapter 6 to test the suitability of the analysis performed in Chapter 5. The design charts initially proposed by Mullins et al. (2001) are reproduced in Chapter 7 using the results of the numerical analyses from Chapter 6. In Chapter 7 new design charts based on the results of the load transfer analyses carried out in this work are presented and discussed. In Chapter 8 a methodology for designing PGDS and approximately estimating its settlements is proposed. Conclusions and main findings that arise from this study are presented in Chapter 9. Two appendixes are presented at the end of this work. Appendix A presents geotechnical information for case studies included in chapter 6. Appendix B presents the main aspects of the Load Transfer program developed to perform numerical analyses for this work.

2 BACKGROUND AND LITERATURE REVIEW

2.1 INTRODUCTION

Pile settlements have always been of great concern within the geotechnical community since the behavior of a superstructure would depend on the settlements experienced by its foundation. Numerous investigators have developed methods for estimating pile settlements, and several investigations have been conducted to study the possibility of reducing foundation settlements. One of the available methods to reduce pile settlements is by means of the post grouting technique.

Since this research is concerned with the estimation of post grouted pile settlements and the study of the behavior of post grouted piles, the literature review presented in this chapter is divided into two parts. The first, Section 2.2, deals with pile settlements estimation by means of the load transfer method. The second, Section 2.3, presents a review on post grouted piles, paying special attention to the construction procedure, current post grouting techniques, and the current design method available.

2.2 PILE SETTLEMENTS

For many years, the design of pile foundations was primarily based on empirical methods and experience (Poulos, 1989). However, in the last few decades new theoretical methods have been formulated implying a progress in the area. Several methods have been proposed to predict load-settlement behavior of single axially loaded piles. They are somehow based on rigorous theoretical fundamentals. In this chapter, an approximate method known as the load transfer method is covered in detail since it has been the method chosen for this work.

2.2.1 INTRODUCTION

Several procedures have been proposed to predict load-settlement behavior of single axially loaded piles. Among these, closed form solutions and approximate numerical solutions have become quite popular.

Closed form solutions are available for a number of pile-soil systems. For instance, a solution for a single pile embedded in a homogeneous linear elastic half-space has been proposed by Satou (1965) and Murff (1975). Extensions to this solution, such as layered systems of Gibson soil profile, have been made by Guo, 2000. However, none of the closed form models could accurately model the behavior of a pile embedded in an arbitrarily non-homogeneous soil profile, which has been found to have great influence in pile settlements (Guo, 1996).

The load settlement behavior of single axially loaded piles can be solved via numerical solutions such as Finite Element Method (FEM), Boundary Element Method (BEM), Variational Elements, and Load-transfer method. The load-transfer method will be

described in the next subsection, since it was the methodology selected for this research. Details of the FE method can be found in Zienkiewicz (1971) and its application to geotechnical problems is covered in Desai and Christian (1977). The BEM is covered in Butterfield and Banerjee (1971). Finally, additional information on the Variational Elements method applied to piles can be found in Rajapakse (1990).

2.2.2 THE LOAD TRANSFER METHOD

Approximate solutions using numerical methods are useful alternatives when closed form solutions cannot be obtained. Probably the main advantage of numerical solutions is that they are capable of modeling almost any pile geometry and soil profile. Among these approaches, the load transfer method stands as a simple but accurate method to study pile behavior and to predict pile settlements.

In the following section a background on the load-transfer method is provided. In sections 2.2.2.2 and 2.2.2.3 the most common load-transfer curves (empirical and theoretical, respectively) are reviewed.

2.2.2.1 BACKGROUND OF THE LOAD TRANSFER METHOD FOR PILE SETTLEMENT PREDICTION

Seed and Reese (1957) were one of the first researchers who proposed the load transfer approach as a mean to calculate the local load-displacement relation of piles. Since then, numerous researchers have worked in the load transfer method (e.g., Seed and Reese, 1957; Coyle and Reese, 1966; Coyle and Sulaiman, 1967; Randolph and Wroth, 1978; Kraft et al., 1981; Guo and Randolph, 1997 Guo, 2000; Zhu and Chang; 2002; and Pando 2003, among others).

In essence, the load-transfer method consists in subdividing the pile in a discrete number of segments, which are connected by springs that represent the axial stiffness of the pile. Each pile segment is linked, on the side, to a vertical spring, which represents the shear resistance of the surrounding soil. The ultimate resistance of this spring is a function of the soil–pile interface friction, usually termed skin friction in deep foundation design. The last segment, at the bottom, is also supported by a vertical spring that represents the tip resistance of the pile. The discretization assumed by the load transfer approach is shown schematically in Figure 2-1.

The load transfer approach is a mean of obtaining the load-displacement curve of the pile using an iterative procedure. The procedure consists in back-calculating the load that must be applied to the pile head at each step to produce an assumed pile tip settlement. Each load step must satisfy vertical equilibrium and include the forces along the pile that result from the lateral springs and pile tip spring. The pile head displacement is calculated for each load step by summing the displacements of each segment, the assumed tip displacement (of the step), and the elastic shortening of each pile segment. A detailed description of the iterative process can be found in Coyle and Reese (1966), and Poulos and Davis (1980).

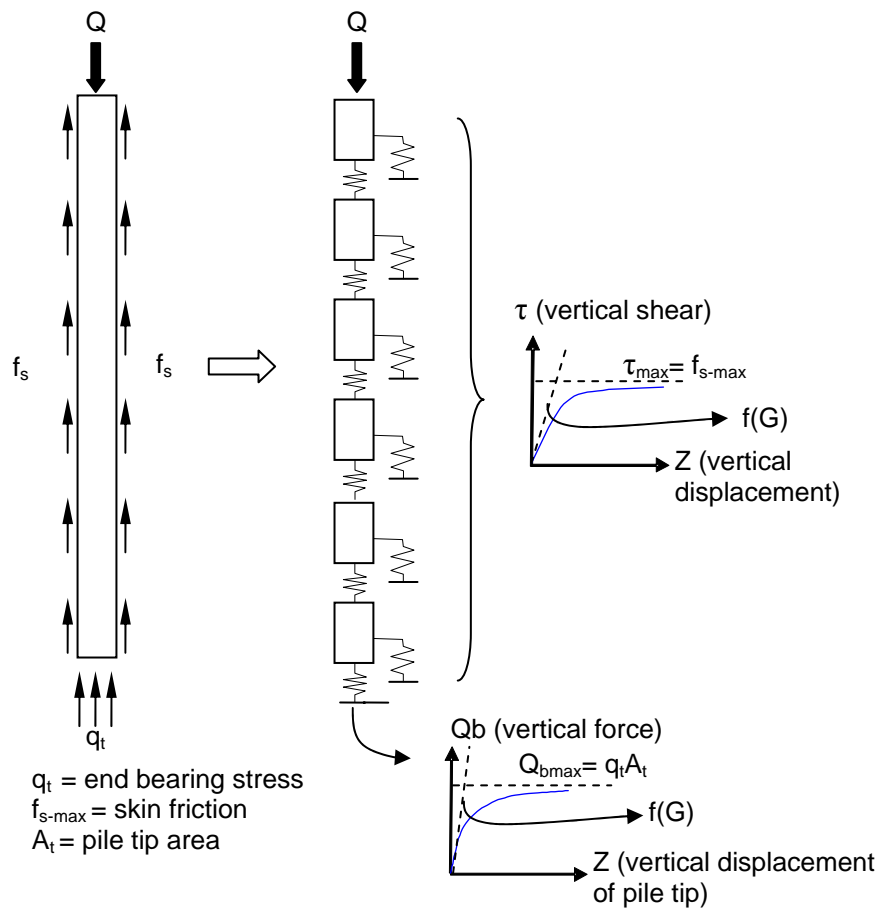


Figure 2-1 Discretization assumed by the load-transfer approach

The load-transfer approach offers great flexibility to handle soil non-homogeneity and can be used, in conjunction with an appropriate numerically fitted function, to model viscoelastic soil behavior (Guo, 1996). Such fitted transfer function can be defined as a mathematical expression that associates the increments in load transferred from a structural element to the soil, with the variation in relative displacement of the element with respect to the surrounding soil (Everett, 1991).

As it can be seen in Figure 2-1, the load-transfer method is actually based on two sets of load transfer functions: one set characterizes the load-transfer that takes place along the shaft of the pile. They are commonly referred to as T-Z curves; the other set

characterizes the load transfer that takes place at the tip of the pile and are commonly referred to as Q_b -Z curves. The second load transfer function relates the pile tip force to the tip settlement. T-Z constitutive curves are assigned to the lateral springs of the model, as shown in Figure 2-1. The Q_b -Z curve is assigned to the spring located at the pile tip.

A broad number of load-transfer functions have been proposed in the literature, having either an empirical or a theoretical basis. The next two sections summarize the most common load transfer functions of each category.

2.2.2.2 EMPIRICAL LOAD-TRANSFER FUNCTIONS

The first implementations of the load-transfer method were based on measurements of load and local displacements obtained from load tests of instrumented piles (e.g., Seed and Reese, 1957; Coyle and Reese, 1966; and Coyle and Sulaiman, 1967). A number of researchers have proposed empirically based load-transfer functions to fit experimental data. For example, empirical functions have been proposed by Reese et al., 1969; Vijayvergiya, 1977; and API, 1993; exponential functions have been proposed by Kezdi, 1975; Liu and Meyerhof, 1987; Vaziri and Xie, 1990, Georgiadis and Saflekou, 1990; and Everett, 1991; polygonal functions have been proposed by Frank and Zhao, 1982; Frank, et al., 1991; Zhao, 1991; Tan and Johnston, 1991; and Kodikara and Johnston, 1994; Romberg-Osgood functions have been proposed by Abendroth and Greimann, 1988; and O'Neill and Raines, 1991, and hyperbolic functions have been also proposed by Hirayama, 1990. In Table 2-1 some empirical load transfer functions are listed.

Table 2-1 Empirical load-transfer curves

Author	T-Z curve for side springs	Q _b -Z curve for tip spring												
API	$\tau_s = \tau_{\max} \frac{z_s}{z_c} \text{ for } (z_s \leq z_c)$ $\tau_s = \tau_{\max} \text{ for } (z_s > z_c)$	Tabulated curve: <table border="1" style="margin-left: auto; margin-right: auto;"> <thead> <tr> <th>Z_b/D</th> <th>P_b/P_{max}</th> </tr> </thead> <tbody> <tr> <td>0.002</td> <td>0.25</td> </tr> <tr> <td>0.13</td> <td>0.50</td> </tr> <tr> <td>0.042</td> <td>0.75</td> </tr> <tr> <td>0.073</td> <td>0.90</td> </tr> <tr> <td>0.100</td> <td>1.00</td> </tr> </tbody> </table>	Z _b /D	P _b /P _{max}	0.002	0.25	0.13	0.50	0.042	0.75	0.073	0.90	0.100	1.00
Z _b /D	P _b /P _{max}													
0.002	0.25													
0.13	0.50													
0.042	0.75													
0.073	0.90													
0.100	1.00													
Vijayvergiya (1977)	$\tau_0 = \tau_{\max} \left(2 \sqrt{\frac{z_s}{z_c} - \frac{z_s}{z_c}} \right) \text{ (for } z_s \leq z_c)$ $\tau_0 = \tau_{\max} \text{ (for } z_s > z_c)$	$Q_b = \left(\frac{z_b}{z_c} \right)^{\frac{1}{3}} Q_{b-\max} \text{ (for } z_b \leq z_c)$ $Q_b = Q_{b-\max} \text{ (for } z_b > z_c)$												
Hirayama (1990)	$\tau_0 = \frac{\tau_f z_s}{(0.0025 + z_s)}$	$Q_b = \frac{z_b}{a_b + b_b z_b}$												

Notation in Table 2-1:

Q_b = load at the pile tip

Q_{b-max} = Ultimate base resistance

τ₀ = shear stress at the soil-pile interface

a_b and b_b = curve-fitting constants

z_c = Displacement at failure

z_s = Shaft segment displacement

z_b = Tip displacement

τ_{max} = Maximum soil shear stress

The aforementioned functions were adjusted to fit experimental data. However, as pointed out by Guo (1996), a typical load-transfer function should depend on several physical factors, such as:

- Poisson ratio of the soil
- Ratio of the depth of an stiff underlying soil layer to length of pile
- Shear modulus variation with depth
- Pile slenderness ratio (defined as length to diameter ratio)

Most empirical load-transfer functions do not take into consideration these factors and therefore their applicability is usually restricted to the soil type and pile characteristics for which they were derived.

2.2.2.3 THEORETICALLY BASED LOAD-TRANSFER FUNCTIONS

This section presents the background and the general methodology used for pile settlement prediction using theoretically based load transfer curves. Most of the work in this area is based on the pioneering work by Randolph and Wroth (1978) and by Kraft et al. (1981).

Theoretical shaft load transfer functions (T-Z curve) are commonly derived by assuming that soil deformations around a pile shaft can be idealized by concentric cylinders in shear (Randolph and Wroth, 1978). This idealization assumes that soil displacement due to the pile axial loads is predominantly vertical and that radial displacements are negligible. Studies by Frank (1974) and Baguelin et al. (1975) have shown that the concentric cylinder approach is a good approximation of the deformation pattern obtained using more rigorous analyses such as the finite element method.

Load-transfer functions for the pile tip can be obtained using one of the available elastic solutions for the punch of a rigid body acting on a half space or in the interior of a semi-infinite elastic medium.

Solutions such as those proposed by Mindlin (1936) and Boussinesq (1885) have been used to derive load transfer functions for the pile tip. Ramberg-Osgood functions have been proposed also to represent load-transfer functions at the pile tip and along the shaft (e.g., Armaleh and Desai, 1987). Some of these theoretically derived load-transfer curves are listed in Table 2-2.

In both, side (T-Z) and tip (Q_b -Z) theoretical load transfer curves two important components can be distinguished: (1) the initial slope of the curve and (2) the asymptotic value the curve approaches as displacements tend to infinite (Figure 2-2). The initial slope of the curve is defined by the soil shear modulus, while the asymptotic value can be defined when the pile reaches ultimate side friction or at the ultimate tip capacity of the pile tip (τ_{max} , and Q_{b-max}). Some authors proposed a softening behavior after the peak resistance of the soil has been reached (available literature, e.g. Kraft et al., 1981).

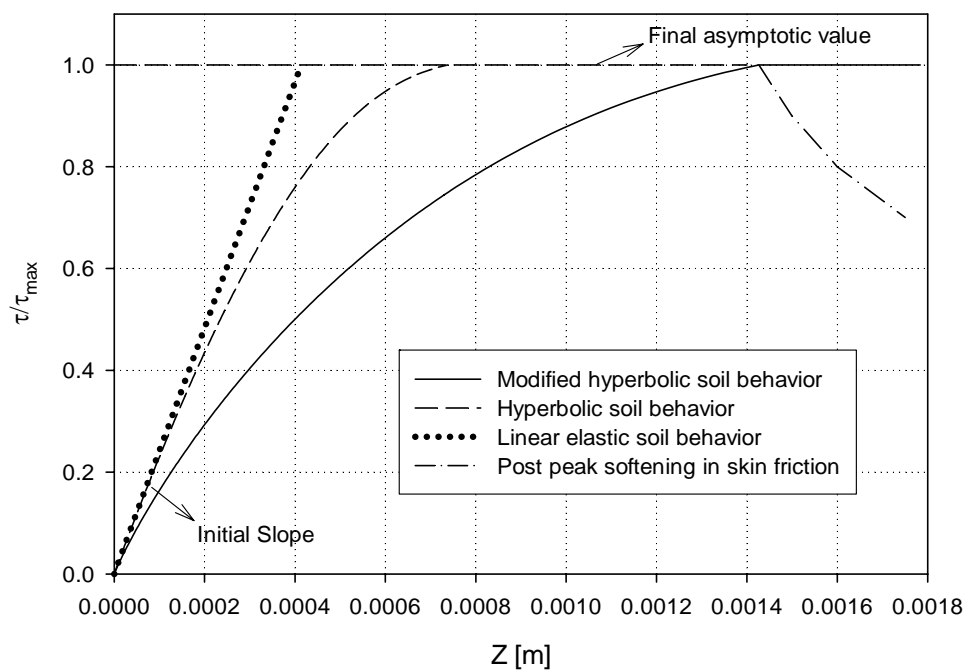


Figure 2-2 Typical side load transfer curve

Table 2-2 Some theoretical load-transfer curves

Author	Type	T-Z curve for side springs	Q _b -Z curve for tip spring
Randolph and Wroth (1978)	Linear	$z_s = \frac{\tau_0 r_0}{G} \ln \left(\frac{r_m}{r_0} \right)$	$z_b = \frac{Q_b (1-\nu)}{4r_0 G} \eta$
Kraft et al. (1981)	Hyperbolic	$z_s = \frac{\tau_0 r_0}{G} \ln \left(\frac{\frac{r_m - R_f}{r_0} \frac{\tau_0}{\tau_{\max}}}{1 - R_f \frac{\tau_0}{\tau_{\max}}} \right)$	$z_b = \frac{Q_b D (1-\nu^2)}{E} \eta$
Armaleh and Desai (1987)	Ramber-Osgood	$\tau_0 = \frac{(k_{os} - k_{fs}) z_s}{\left(1 + \left \frac{(k_{os} - k_{fs}) z_s}{\tau_{\max}} \right ^{m_s} \right)^{1/m_s}} + k_{fs} z_s$	$Q_b = \frac{(k_{ob} - k_{fb}) z_b}{\left(1 + \left \frac{(k_{ob} - k_{fb}) z_b}{Q_{b-\max}} \right ^{m_b} \right)^{1/m_b}} + k_{fb} z_b$
McVay et al. (1989)	Hyperbolic	$z_s = \frac{\tau_0 r_0}{G} \left[\ln \left(\frac{r_m - \beta}{r_0 - \beta} \right) + \frac{\beta (r_m - r_0)}{(r_m - \beta)(r_0 - \beta)} \right]$	$z_b = \frac{Q_b (1-\nu)}{4r_0 G \left(1 - Q_b \frac{R_f}{Q_{b-\max}} \right)^2}$
Zhu and Chang (2002), Pando (2003)	Modified Hyperbolic	$z_s = \frac{\tau_0 r_0}{G} \ln \left(\frac{\left(\frac{r_m}{r_0} \right)^g - f \left(\frac{\tau_0}{\tau_{\max}} \right)^g}{1 - f \left(\frac{\tau_0}{\tau_{\max}} \right)^g} \right)$	$z_b = \frac{Q_b (1-\nu)}{4Gr_0 \left[1 - f \cdot \left(\frac{P_b}{Q_{b-\max}} \right)^g \right]}$

Notation in Table 2-2:

Q_{b-max}=load at the pile tip

ν=poisson ratio of the soil under the pile tip

G=shear modulus of soil layer

η=factor to consider depth of pile tip

r₀ and r_m= radius of pile and radius of influence of pile, respectively

τ₀=shear stress at the soil-pile interface

R_f=Stress-strain curve fitting constant

E=Young modulus of soil

k_{0s} and k_{0t}=initial side and tip spring stiffness, respectively

k_{fs} and k_{ft} = final side and tip spring stiffness, respectively

τ_{max} and Q_{b-max} = side friction and pile end bearing (asymptotic values for the curves)

m_s and m_t =order of the T-Z and Q_b-Z curve, respectively

f and g=curve-fitting constants

$\beta = r_0 \tau_0 R_f / \tau_{\max}$

The transition, from the initial slope to the asymptotic value, depends on the constitutive model for the soil. For example, a perfectly linear-elastic soil yields an elastic-perfectly plastic T-Z curve (Randolph and Wroth, 1978). This T-Z curve works well if a secant modulus is used in the model (Poulos, 2001). Successful application of a linear theory to solve a non-linear problem requires judicious selection of the elastic properties. However, field and laboratory tests have extensively shown that soil behaves in a marked non-linear fashion (e.g., Kondner 1963; Duncan and Chang, 1970; and Atkinson, 2000). Soil non-linearity is associated with degradation of the shear modulus with shear strain. In recent years, geophysical and dynamic methods have been used in geotechnical engineering practice to measure the soil shear modulus at very low strains ($\gamma < 0.001\%$). This shear modulus is referred to as the initial shear modulus (G_0 or G_{\max}) and is the maximum shear modulus of the soil since it is measured in the linear range of the material.

Load transfer functions should incorporate an adequate rate of soil modulus degradation depending on the initial slope of the curve, in order to capture the actual soil non-linear behavior. Thus, hyperbolic functions (Kraft et al., 1981; and McVay et al., 1989), modified hyperbolic functions (Zhu and Chang, 2002; and Pando, 2003) and Ramberg-Osgood functions (e.g., Armaleh and Desai, 1987) have been proposed to model the non-linear transition from the initial slope to the asymptotic value of the curve considering shear modulus degradation (Figure 2-2).

To perform a non-linear pile settlement analysis, the initial shear modulus profile along the length of the pile must be estimated. Some researchers derived closed form

solutions using the load transfer approach assuming linear or exponential variation of soil rigidity with depth (e.g., Randolph and Wroth, 1978; and Guo, 1997 and 2000). In this regard, functions listed in Table 2-2 are defined under a discrete approach, therefore they allow soil modeling with an arbitrary variation of soil initial shear modulus with depth.

Some authors (Xiao, 2003; Liu and Zhang, 2003; and Liu, et al., 2004) proposed a separate approach to study pile settlements within the load-transfer method. This approach includes a set of transfer matrices, which relate load and displacement at the pile head to load and displacement at the pile tip. They used polygonal constitutive models for soil along the shaft and a multi linear polygonal constitutive load for the soil under the pile tip. These methods will not be used in this work.

2.3 POST GROUTED PILES

This thesis evaluates the application of non-linear load-transfer pile settlement analyses to the study and evaluation of post grouted piles behavior. In essence, post grouted piles consist of conventional piles that incorporate grouting pipes along the shaft during the construction process. In this research project only post grouted bored piles (also known as drilled shafts, cast-in-situ piles, rotary bored piles or simply shafts) were studied. Although the term “pile” is commonly used to designate driven piles, for the sake of simplicity, the term “pile” will be also used to refer to bored piles throughout the thesis. After pile installation and predetermined concrete strength gain, grout is injected through these grouting tubes exiting through the pile tip in order to improve the soil behavior around the tip area. A not so common variation of this post grouting technique is to inject grout laterally along the shaft (usually termed shaft grouting). The injection of

the grout is used to improve the overall pile capacity and to reduce settlements required to mobilize the design bearing capacity. This work aims only at studying post grouting of pile tips and therefore not piles with post grouted shafts.

In the following subsection a general background on post-grouted piles is provided. Section 2.3.2 summarizes the most widely used post-grouting technique in US and their construction procedure. Finally the current design method proposed by Mullins et al. (2001) is presented in the last subsection.

2.3.1 BACKGROUND OF POST GROUTED PILES

The post-grouting technique has been used as a method to reduce pile settlements and improve pile tip capacity since the early 1960's and has been reported many times in the literature (Simons, et al., 1963; Houdin, et al., 1968; Schmitt, 1971; and Bolognesi and Moretto, 1973; Gouvenot and Gabiax, 1975; Stocker, 1983; Bruce, 1986; Mullins et al., 2001; and Mullins and Winters, 2004).

Currently, post grouting of pile tips has become a routine process in many parts around the world (Bruce, 1986). The increasing requirement of small settlements for high pile capacity in large projects without the enlargement of pile diameters has encouraged the use of pile tip post grouting techniques (Stocker, 1983; and Mullins et al., 2001).

The post grouting technique consists of the injection of cementitious slurry under the pile tip or along the pile shaft after the concrete has been poured and set. The injection of the slurry takes place through pipes installed within the pile shaft and attached to the steel reinforcement cage. The main effects of post grouting are: the pre-compression of the soil

beneath the pile tip (Bolognesi and Moretto, 1973); and the densification of the soil around and under the pile tip (Mullins et al., 2001). The post grouting process at the pile tip is believed to develop a grout bulb under the pile tip (Mullins et al., 2001). The extent of such beneficial effects will depend to a large extent on the post-grouting technique mechanism used (Mullins et al., 2001).

Silwinski and Fleming (1984) reported load-settlement curves for grouted and ungrouted drilled shafts tested at a project in Maracaibo, Venezuela. The typical load-displacement curves obtained by the authors are shown in Figure 2-3. The results show that, for any given applied load, grouted pile settlements are significant smaller compared to those measured for the to the ungrouted pile. Mullins et al. (2001) and Mullins and Winters (2004) also reported several load tests on grouted and ungrouted piles. They found a general improved performance in the grouted piles, as shown in Figure 2-4.

The applicability of the post grouting procedure depends primarily on the soil type at the tip elevation. Post grouting techniques have been found to improve to different extents in cohesive soils, soft rocks, and cohesionless soils. Test results show that they are most effective in cohesionless soils (Baker and Broadrick, 1997).

This is confirmed by the several reported case histories where post grouted piles have been successfully used in sites with cohesionless soil (e.g., Piccione, 1984; Sliwinski and Fleming, 1984; Logie, 1984; Stoker 1983; and Solera and Mitchell, 1991). In all cases, results showed large improvement of end bearing capacities of post grouted piles in sands and silts. In sites with clays, post grouting seems to produce minimal improvements in pile capacity only (Mullins et al., 2001).

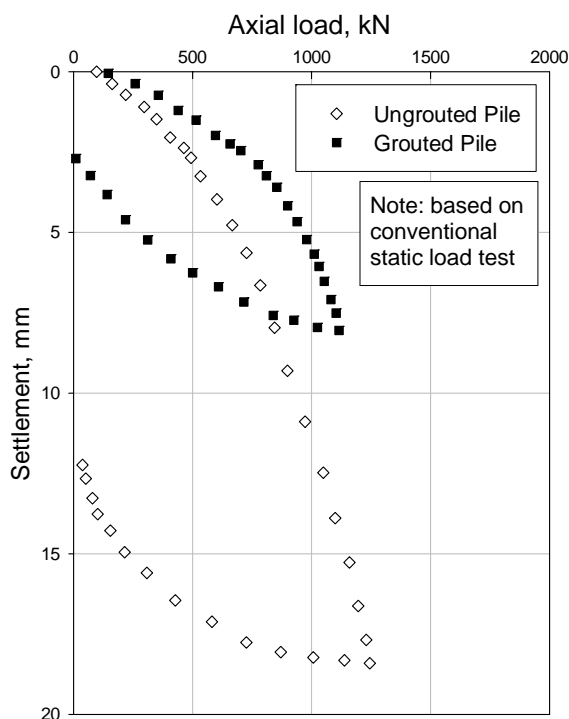


Figure 2-3 Pile load test results for grouted and ungrouted drilled shafts in Maracaibo, Venezuela (Silwinski and Fleming, 1984)

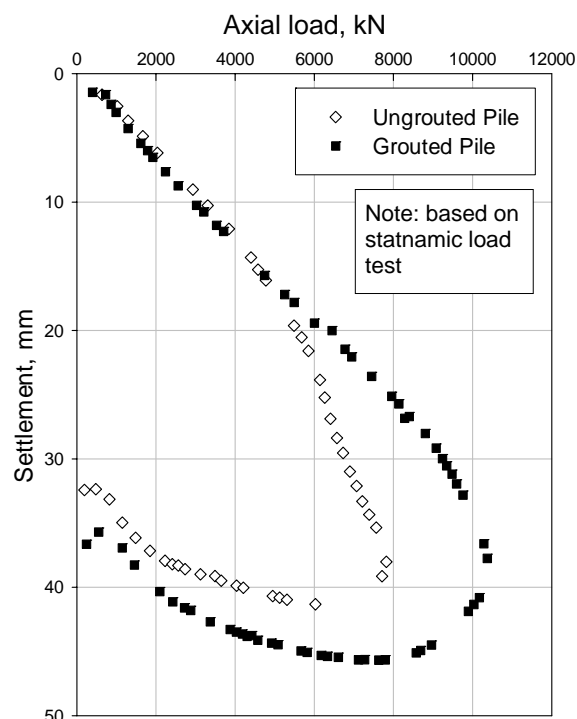


Figure 2-4 Pile load test results for grouted and ungrouted drilled shafts in West Palm Beach, Florida (Mullins et al., 2001)

2.3.2 CONSTRUCTION PROCEDURE FOR POST GROUTED PILES

This section describes the construction procedure commonly used in the United States, which involves pile tip grouting by means of compaction grouting. Some other pile post grouting techniques, used in other parts of the world such as permeation grouting and staged grouting (Bolognesi and Moretto, 1973), will not be discussed in this work. A typical high pressure grouting apparatus is shown in Figure 2-5. Post grouted piles are relatively new in the United States. The patent holder for this type of piles is A. H. Beck Foundation Co. Inc.

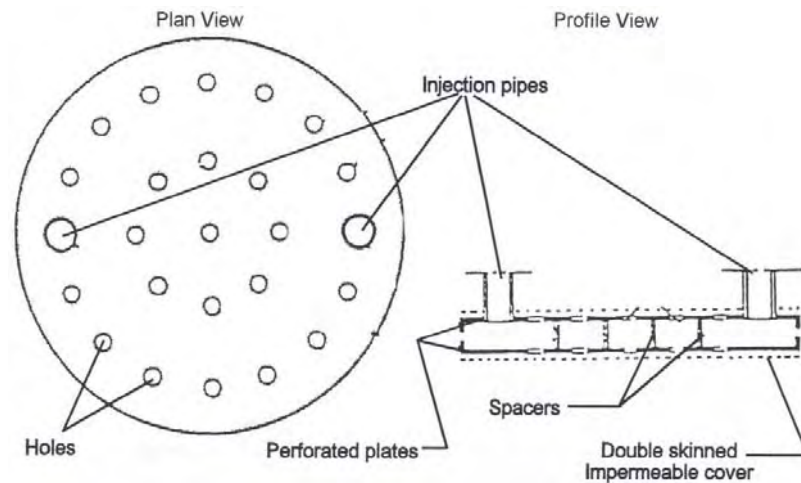


Figure 2-5 Typical apparatus for grouting (adapted from Lizzi, 1981)

A typical construction procedure for post grouted drilled shafts can be summarized in four steps, as shown in Figure 2-6. The shaft is installed by drilling a cylindrical hole in the ground and lowering the reinforcement cage into the excavation (steps 1 and 2). PVC grouting pipes should be previously attached to the reinforcement cage in order to be used for the injection of the cementitious slurry during the post grouting stage. Concrete is then poured into the excavation and cured until concrete compressive strength reaches its design value (step 3). Steps (1) through (3) do not differ much from the construction procedure for a conventional drilled shaft. Post-grouting takes place after the specified setting of the concrete is attained, then grout is injected at high pressure via the grouting pipes and through a steel grouting plate placed at the bottom, which holds an expansion control membrane (step 4).

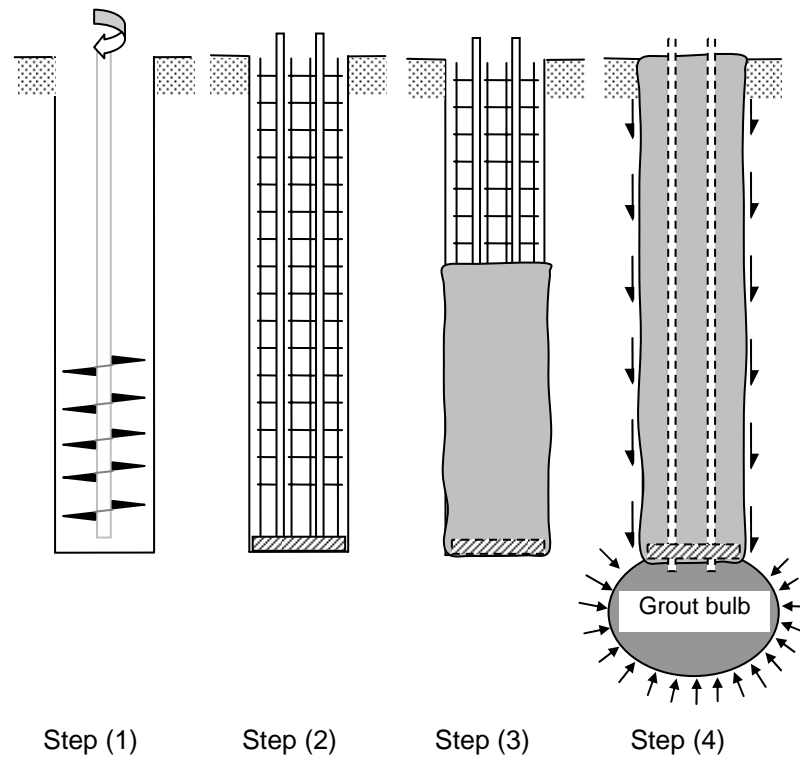


Figure 2-6 Typical construction procedure for post grouted drilled shafts

Although the construction procedure described above only concerns to drilled shafts, the grouting procedure can be equally applied to some types of driven piles, provided that grouting pipes have been left inside the pile during its casting.

In compaction grouting the injected slurry is initially prevented to enter into the soil by means of the control membrane mentioned above. The control membrane typically consists of a very flexible elastic membrane that accommodates the initial volume of grout through expansion and thus ensures grouting pipe communication by providing separation between the grout and the soil under the pile tip. It is very common that the membrane breaks or separates from the steel base plate after a certain grout volume has been injected.

In summary, during the post grouting stage, the slurry is injected into a flexible membrane, which is deformed and pushed against the soil by the grout pressure, thus compressing and densifying the soil through a process analogous to cavity expansion. At the end of the grouting process a grout bulb is expected to form at the bottom of the pile.

2.3.3 CURRENT DESIGN PROCEDURE FOR POST GROUTED PILES

To date, in US the available design procedure for predicting post grouted drilled shaft capacity is the one proposed by Mullins et al. (2001). The procedure has been developed with a strong empirical component, based on observations from an extensive laboratory and field testing programs which involved 13 laboratory load tests and 16 load test are full scale post grouted drilled shafts. The method is currently being updated as more field data of load test on post grouted piles becomes available.

Mullins et al. (2001) estimate the level of pile capacity improvement by comparing the load test results of control piles (ungROUTED) and post grouted piles tested with similar soil conditions, pile dimensions, and construction technique (except the pile tip modification due to grouting).

In essence, the method attributes the overall pile performance improvement to an increased pile tip capacity. Mullins et al. (2001) proposed using a factor called tip capacity multiplier (TCM) to estimate the improved pile tip resistance due to grouting. Measured TCM values were empirically obtained from pile load tests as the ratio between the measured post grouted tip capacity and the ungrouted tip capacity of the

control pile. Both capacities were obtained at a predefined service and ultimate tip displacements:

$$TCM_{i,j} = \frac{(q_t^{grouted})_i}{(q_t^{ungrounded})_j} \quad (2.1)$$

Where: $(q_t^{grouted})_i$ = Unit tip resistance of grouted pile at displacement i

$(q_t^{ungrounded})_j$ = Unit tip resistance of ungrouted pile at displacement j

i = Displacement of grouted tip, as a percentage of pile diameter.

j = Displacement of ungrouted tip, as a percentage of pile diameter.

$TCM_{i,j}$ = Tip Capacity Multiplier at displacement i given an ungrouted tip capacity at displacement j .

The authors developed design charts to estimate TCM as a function of a parameter predefined as the grout pressure index (GPI) and the level of displacement of the tip desired. The GPI was defined as the ratio of the maximum sustained grouting pressure to the maximum ungrouted tip capacity.

$$GPI = \frac{P_{\max}}{(q_t^{ungrounded})_j} \quad (2.2)$$

Design charts were developed by plotting the values of GPI, obtained from field tests, in the horizontal axis and values of TCM in the vertical axis. Values of TCM were obtained from field test for ultimate and service tip displacements of 1%, 2%, and 5% of the pile diameter. Linear regressions between GPI and TCM factors were made for tip displacements of 1%, 2%, and 5% of the pile diameter.

In summary, the method consists of estimating the TCM for a given GPI and calculating the grouted capacity of the pile tip by means of Equation (2.1). A typical design chart proposed by Mullins et al. (2001) is shown in Figure 2-7. The chart corresponds to an ungrouted pile tip displacement (j) of 1 % diameter and has best linear fits for 3 levels of grouted pile tip displacement ($j = 1 \%$, 2% , and 5%). The TCM values are obtained for a given GPI, and i displacement level. For example, for $GPI = 5$ and $i = 2 \%$ diameter, the TCM is about 7. This represents a 700 % increase of pile tip capacity due to post grouting. The design method proposed by Mullins and Winters consists of seven steps, which are summarized below:

1. Calculate or estimate the ungrouted tip capacity of the pile corresponding to a certain level of tip displacement, $q_t^{ungrouted}$.
2. Estimate the ultimate side resistance of the pile, S_{ult} .
3. Establish the maximum allowable service displacement and express it as a percentage of the pile diameter.
4. Determine the maximum available pressure that the grout can exert upon the pile tip, as:

$$P_{\max} = \frac{S_{ult}}{A_{tip}} \quad (2.3)$$

5. Calculate de Grout Pressure Index as the ratio of pressures from step 3 and step 1, using formula (2.2).

6. Obtain the Tip Capacity Multiplier (TCM) from the design charts using the GPI from step 4 for a designed level of tip displacement.

7. Estimate the tip capacity of the grouted pile multiplying the ungrouted tip capacity by the TCM:

$$(q_t^{grouted})_i = TCM_{i,j} \times (q_t^{ungrouted})_j \tag{2.4}$$

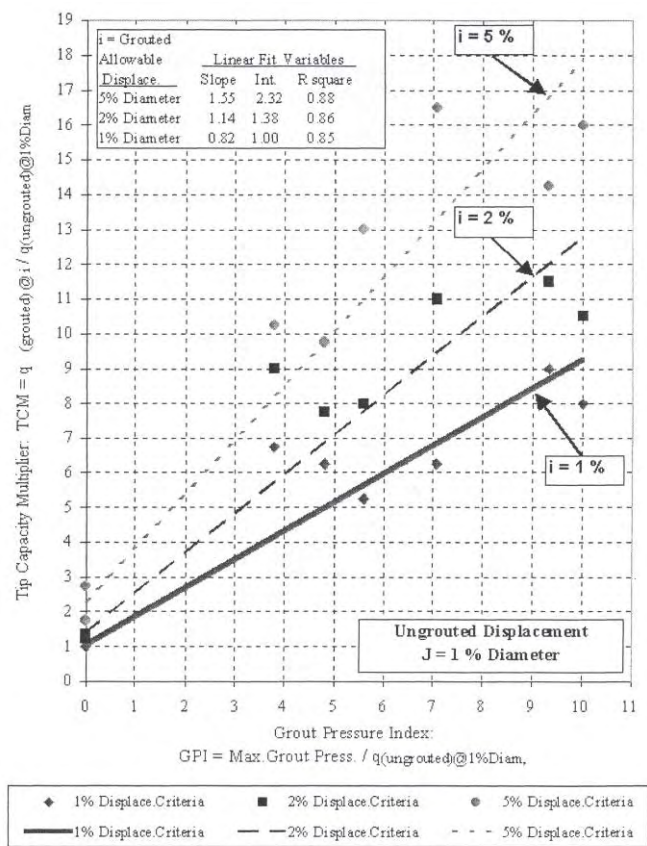


Figure 2-7 Design chart for tip ultimate settlement of 5% of the pile diameter (adapted from Mullins and Winters, 2004)

3 PROPOSED METHODOLOGY FOR ESTIMATING SINGLE PILE SETTLEMENTS

3.1 INTRODUCTION

This chapter describes the proposed general methodology for estimating settlements of single piles. The chapter is divided into four subsections. The first describes the methodology used for deriving the theoretical load transfer curves for the shaft side friction and the pile tip or base. The following subsection presents the proposed methodology for estimating pile settlements using the derived theoretical load transfer curves presented before. The last subsection of this chapter presents a summary and conclusions.

One of the principal objectives of this chapter is to develop a robust methodology for studying axially loaded single piles. This methodology would provide the basis for the study of the behavior of post grouted drilled shafts, which will be discussed in the following chapters.

The new methodology proposed herein, is based on combining CPT data and the load transfer method for estimating pile settlements. The use of CPT data allows incorporating soil non-homogeneity and thin layering for estimating the profile of shear stiffness in the soil deposit. The load transfer method is incorporated using theoretical load transfer curves, following the work by Kraft et al. (1981) and Randolph and Wroth (1978). The procedure for deriving theoretic load transfer curves allows considering shear modulus degradation due to installation effects, a modified radius of influence of the pile, and arbitrary radial distribution of shear stresses.

3.2 METHODOLOGY FOR DERIVING THEORETICAL LOAD TRANSFER CURVES

3.2.1 THEORETICAL LOAD TRANSFER CURVES FOR THE PILE SHAFT (T-Z_s CURVES)

A load transfer function can be defined as a mathematical expression, which associates the load transferred from a structural element to the soil with the relative displacement between the element and the surrounding soil (Everett, 1991). In general, this relation can be expressed as

$$z_s = f(\tau) \quad (3.1)$$

Where z_s = vertical relative displacement of the shaft

τ = shear stress transferred to the soil along the shaft

Assuming a radial stress distribution, an expression of the form of Equation (3.1) can be derived by first expressing the angular distortions in a soil element near a loaded pile, as follows:

$$\gamma(y, r) = \frac{\partial u}{\partial y} + \frac{\partial z_s}{\partial r} \quad (3.2)$$

Where z_s = vertical relative displacement of the soil element

u = radial displacement of the soil element

y = vertical coordinate, measured from the pile head

r = radial coordinate, measured from the center of the pile

In addition, it is assumed a constitutive law for the soil of the form

$$\tau(r) = G(r, \tau) \cdot \gamma(y, r) \quad (3.3)$$

Where $G(r, \tau)$ is the secant shear modulus of the soil, which is considered, in general, to be a function of the shear stress level in the soil; and the radial distance to the center of the pile. $\gamma(y, r)$ is the angular distortion in the soil defined in Equation (3.2).

An alternative expression to the form of Equation (3.1) can be found replacing Equation (3.2) in Equation (3.3) and solving for ∂z_s , as follows:

$$\partial z_s = \left(\frac{\tau(r)}{G(r, \tau)} - \frac{\partial u}{\partial y} \right) \partial r \quad (3.4)$$

The total vertical displacement of the pile shaft can be found by integrating Equation (3.4) within the range affected by the loaded pile. The integration is usually done between a radial distance r_0 and a certain distance r_m beyond which the deformations in the soil are considered negligible. The resulting expression is:

$$z_s = \int_{r_0}^{r_m} \left[\frac{\tau(r)}{G(r, \tau)} - \frac{\partial u}{\partial y} \right] dr \quad (3.5)$$

From Equation (3.5) it can be seen that in order to obtain a theoretical load transfer curve, the radial variation of shear stresses and the variation of the shear modulus with respect to both, shear stress and radial distance to the pile, have to be defined. Another important consideration is the value of the upper integration limit r_m . This value has to be defined in order to evaluate the integral in Equation (3.5). These four aspects of the load transfer formulation are covered in the following subsections.

3.2.1.1 RADIAL VARIATION OF SHEAR STRESSES

Randolph and Wroth (1978) suggested that the deformation of the soil around an axially loaded single pile can be idealized as a series of concentric cylinders subject to pure shear loading, as shown in Figure 3-1.

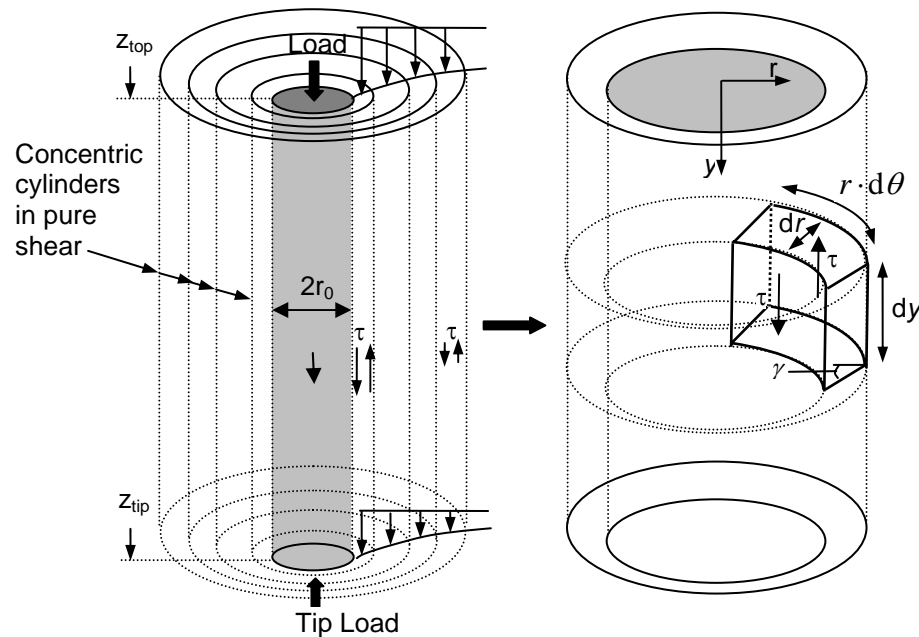


Figure 3-1 Concentric cylinder approach

Assume a single pile of radius r_0 , embedded in a uniform soil characterized by its shear modulus, G , and shear resistance, τ_{\max} . For a differential element of soil (Figure 3-2), located at a distance r of the center of a pile, the equation of vertical equilibrium can be written as follows:

$$\begin{aligned} & \left(\tau(r) + \frac{\partial \tau(r)}{\partial r} dr \right) \cdot (r + dr) \cdot d\theta \cdot dy - \tau(r) \cdot r \cdot d\theta \cdot dy + \\ & + \left(\sigma_y + \frac{\partial \sigma_y}{\partial y} \cdot dy \right) \cdot \left(r + \frac{dr}{2} \right) \cdot d\theta \cdot dr - \sigma_y \cdot \left(r + \frac{dr}{2} \right) \cdot d\theta \cdot dr = 0 \end{aligned} \quad (3.6)$$

The term definitions of Equation (3.6) are specified in Figure 3-2.

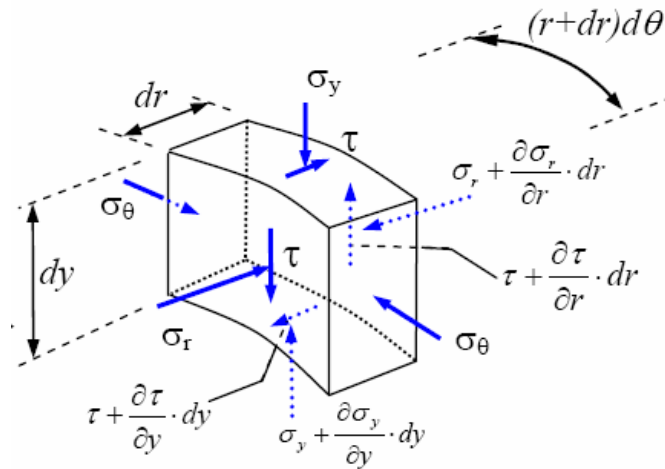


Figure 3-2 Stresses in a differential soil element

Simplifying and neglecting second order terms in (3.6), the vertical equilibrium equation reduces to

$$\frac{\partial(\tau(r) \cdot r)}{\partial r} + \frac{\partial(\sigma_y)}{\partial y} r = 0 \quad (3.7)$$

Randolph and Wroth (1978) suggest that for axially loaded piles the rate of change of the vertical stress with respect to depth is much less than the rate of change of shear stress

with respect to radial distance. Thus, neglecting the second term of Equation (3.7) results in:

$$\frac{\partial(\tau(r) \cdot r)}{\partial r} \approx 0 \quad (3.8)$$

Which can be integrated between the radius of the pile (r_0) and a radius r to obtain the following expression of radial variation of shear stress:

$$\tau(r) = \frac{\tau_0 r_0}{r} \quad (3.9)$$

Where τ_0 = shear stress at the pile-soil interface

r = radial distance from center of the pile

$\tau(r)$ = shear stress in the soil at a radial distance r

Substituting Equation (3.9) into Equation (3.5):

$$z_s = \int_{r_0}^{r_m} \left[\frac{\tau_0 r_0}{r \cdot G(r, \tau)} - \frac{\partial u}{\partial y} \right] dr \quad (3.10)$$

Equation (3.10) was obtained neglecting the variation of vertical stress with depth, which is equivalent to assuming that the annular soil elements are subjected to a stress state of pure shear. According to a pure shear stress state, the primary displacement will be vertical. With regard to this, Baguelin and Frank (1979) have shown by means of the Finite Element Method, that the vertical loading upon the pile produces almost no radial movements. Thus, the term $\partial u / \partial y$ can be ignored and the general expression for TZ curves becomes:

$$z_s = \tau_0 r_0 \int_{r_0}^{r_m} \frac{dr}{r \cdot G(r, \tau)} \quad (3.11)$$

To obtain the final load transfer expression, it is needed to address $G(r, \tau)$ and r_m .

The following subsections discuss these terms.

3.2.1.2 RADIAL VARIATION OF SHEAR MODULUS

If a pile could be installed without disturbing the surrounding material and the soil deposit is assumed uniform and homogeneous with no variation of properties laterally or with depth, a radial distribution of the shear modulus of the soil as the one shown in Figure 3-3-a may be assumed. However, the soil near the pile tends to be disturbed because of the installation process. The magnitude and extent of this disturbance is difficult to quantify and is still subject to investigation. Some authors (Kraft et al., 1981, Baguelin and Frank, 1979) have proposed to account for construction effects by assuming a linear variation of shear modulus with radial distance as shown in Figure 3-3-b. This still assumes laterally uniform soil conditions. Kraft et al. (1981) also considered the possibility of a stiffer soil resulting after pile installation, as shown in Figure 3-3-c.

Typically, pile installation procedures result in disturbances of soil shear resistance and soil shear modulus. In this subsection only the disturbance of the shear modulus of the soil adjacent to the pile is addressed. The effects that construction procedures have on soil shear resistance are not considered here since it is accounted for by the methods used to estimate the ultimate axial capacity of piles (see subsection 3.3.1).

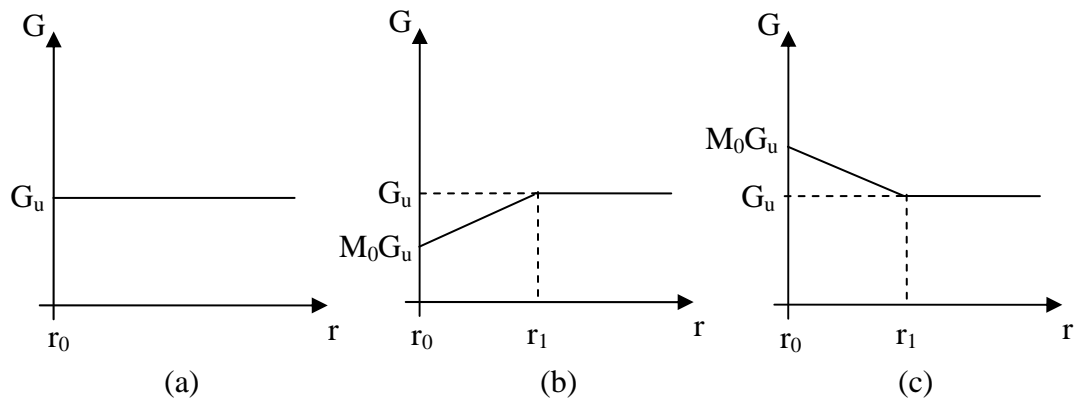


Figure 3-3 Radial distribution of the shear modulus due to soil disturbances during pile installation

To account for construction effects, a linear variation of shear modulus with radial distance was proposed by Kraft et al. (1981), as shown in Figure 3-4.

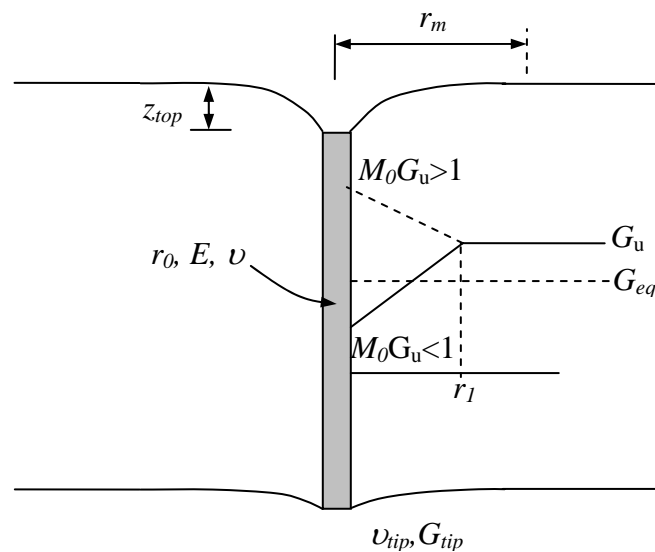


Figure 3-4 Assumed radial variation of shear modulus

As shown in this figure, the shear modulus varies from a value equal to $M_0 G_u$, at the soil-pile interface, to an undisturbed value of G_u at a distance r_1 measured from the center of the pile. This shear modulus variation can be expressed as:

$$G(r) = G_u(\tau) \cdot \left(M_0 + \frac{(1-M_0) \left(\frac{r}{r_0} \right)}{\frac{r_1}{r_0} - 1} \right) \quad (3.12)$$

Where M_0 = empirical coefficient such that $M_0 G_u$ is the disturbed value of the shear modulus of the soil at the pile interface after pile installation

r_1 = extent of the disturbed zone

$G_u(\tau)$ = Undisturbed shear modulus

Values of the ratio r_1/r_0 and M_0 proposed by Kraft et al. (1981) are listed in Table 3-1.

Table 3-1 Suggested values to consider modulus degradation due to installation effects (after Kraft et al. 1981)

Condition	Load	r_1/r_0	M_0
Immediately after installation	Small	16	0.65
	Large ($f > 0.6S_u$)	15.2	0.2
After consolidation	Small	4	1.3
	Large ($f > 0.4S_u$)	12	0.8
	Large ($f = S_u$)	14.1	0.4

Notes:

S_u = Ultimate soil shear resistance

f = stress along the shaft

The integral in (3.11) can be modified to account for construction effects as follows

(assuming $r > r_1$):

$$z_s = \int_{r_0}^{r_1} \frac{\tau(r)}{G(r_1, M_0, \tau)} dr + \int_{r_1}^{r_m} \frac{\tau(r)}{G_u(\tau)} dr \quad (3.13)$$

In order to facilitate the implementation of the proposed radial distribution in the load transfer curve, Kraft et al. (1981) proposed to define an equivalent constant shear modulus such that vertical displacements of the pile shaft calculated with the equivalent

modulus are equal to those obtained with the actual radial distribution of G . In other words, Equation (3.5) using G_{eq} must be equal to Equation (3.13), as follows:

$$\int_{r_0}^{r_1} \frac{\tau(r)}{G(r_1, M_0, \tau)} dr + \int_{r_1}^{r_m} \frac{\tau(r)}{G_u(\tau)} dr = \frac{1}{G_{eq}(\tau)} \int_{r_0}^{r_m} \tau(r) dr \quad (3.14)$$

The above equation results in the following expression for the equivalent shear modulus:

$$G_{eq}(\tau) = \frac{\int_{r_0}^{r_m} \tau(r) dr}{\int_{r_0}^{r_1} \frac{\tau(r)}{G(r_1, M_0, \tau)} dr + \int_{r_1}^{r_m} \frac{\tau(r)}{G_u(\tau)} dr} \quad (3.15)$$

The hyperbolic shear stress distribution found in section 1.2.1.1 can be replaced in (3.15) to obtain:

$$G_{eq}(\tau) = \frac{\int_{r_0}^{r_m} \frac{1}{r} dr}{\int_{r_0}^{r_1} \frac{1}{r \cdot G(r_1, M_0, \tau)} dr + \int_{r_1}^{r_m} \frac{1}{r \cdot G_u(\tau)} dr} \quad (3.16)$$

The same procedure can be used to obtain similar expressions for the equivalent shear modulus for shear stress distributions different from (3.9), if available. Using the equivalent shear modulus, the integral for calculating the theoretical TZ curve becomes:

$$z_s = \tau_0 r_0 \int_{r_0}^{r_m} \frac{1}{r \cdot G_{eq}(\tau)} dr \quad (3.17)$$

3.2.1.3 RADIUS OF INFLUENCE OF THE PILE

The radius of influence of a pile can be defined as the radial distance at which shear stresses or displacements induced in the soil by the axially loaded pile become negligible.

The shape of the affected zone is assumed to be cylindrical with radius r_m . However, the extent of the affected zone is still under investigation. Randolph and Wroth (1978) proposed the following formula to estimate the radius of influence of a pile:

$$r_m = C \cdot l_p \cdot \rho \cdot (1 - \nu) \quad (3.18)$$

Where: C = coefficient equal to 2.5 when the pile is embedded in an infinite half space and equal to 2 when a rigid layer is located at a depth of $2.5l_p$

l_p = length of pile

ρ = heterogeneity factor equal to the ratio of the soil shear modulus at a depth of $l_p/2$ to the soil shear modulus of the soil under the pile tip.

ν = Poisson's ratio of the soil

Note that if the pile is embedded in a homogeneous soil profile the heterogeneity factor becomes 1 whereas if it is embedded in a non-homogeneous Gibson-type soil (i.e. the soil shear modulus of the soil deposit increases linearly with depth) ρ becomes equal to 0.5.

Although the above formula has few parameters that are easy to estimate, it can not account for an arbitrary variation of soil rigidity with depth. In addition, expression (3.18) does not consider the fact that the load level applied to the pile also affects the radius of influence.

Such limitations can be satisfactorily overcome if radius of influence is defined as the maximum value of r at which pile-induced displacements or shear stresses in the soil

become negligible or below a certain predefined small value. This can be accomplished by differentiating Equation (3.11) with respect to r and equating the resulting expression to zero:

$$dz_s = \frac{\tau_0 r_0}{r_m \cdot G(r, \tau)} = 0 \quad (3.19)$$

Expression (3.19) shows that only for $r_m = \infty$ displacements would become zero. This is consistent with the definition of the soil mass as a continuum as discussed before by Equation (3.9). However, for practical purposes a finite radius of influence must be defined. Therefore, a parameter δ can be defined such that δ is sufficiently small to be considered equal to zero for practical purposes. Then the radius of influence of the pile can be derived from (3.19):

$$\begin{aligned} \frac{\tau_0 r_0}{r \cdot G(r, \tau)} &= \delta \\ \therefore r_m &= \frac{\tau_0 r_0}{\delta \cdot G(r, \tau)} \end{aligned} \quad (3.20)$$

The value for r_m can be calculated straightforward once $G(r, \tau)$ is defined. The derivation is also valid for shear stress distributions distinct from that described by (3.9), providing that Equation (3.5) is used in the derivations instead of Equation (3.11). As expected and confirmed from expression (3.20) the radius of influence of the pile depends upon the load level on the pile (given by τ_0) and the soil properties (given by G).

The value of the parameter δ was calibrated to match experimental data and was found to range between 1×10^{-5} m and 1×10^{-7} m in order to obtain similar results as those obtained with the approach proposed by Randolph and Wroth (1978).

The benefits of calculating the radius of influence using Equation (3.20) relies on the fact that an arbitrary soil profile can be considered and no additional parameters, such as the heterogeneity factor are needed. Since numerical models using r_m calculated from (3.18) and from (3.20) gave almost identical results, the latter equation may be more convenient for cases where ρ cannot be easily calculated.

3.2.1.4 VARIATION OF SHEAR MODULUS WITH SHEAR STRESS LEVEL

The problem here is to find a relation, which can accurately represent the degradation of soil stiffness (given by the soil shear modulus) as shear stresses in the soil mass increase. This can be expressed as:

$$\frac{G(\tau)}{G_i} = f(\tau) \quad (3.21)$$

Where: $G(\tau)$ = secant shear modulus of the soil for shear stress τ

G_i = initial reference value of shear modulus

Probably, the most widely used soil models to represent soil stiffness degradation are hyperbolic expressions (Kondner 1963; Kondner and Zelasko 1963; and Duncan and Chang 1970); modified hyperbolic function (Fahey and Carter 1993) and linear elastic-plastic relationships (Randolph and Wroth, 1978). These models are listed in Table 3-2.

Table 3-2 Models of shear modulus degradation

Model type	Expression	Explanation	Reference
Linear	$\frac{G(\tau)}{G_i} = 1$	No degradation of the initial shear modulus	Randolph and Wroth (19780)
Hyperbolic	$\frac{G(\tau)}{G_i} = 1 - R_f \frac{\tau}{\tau_{\max}}$	$R_f = \text{failure ratio} \leq 1$ $\tau_{\max} = R_f \tau_u = \text{failure stress}$ $\tau_u = \text{asymptotic shear stress value}$	Duncan and Chang (1970)
Modified Hyperbolic	$\frac{G(\tau)}{G_i} = 1 - f \left(\frac{\tau}{\tau_{\max}} \right)^g$	$f = \text{fitting constant that controls the amount of degradation}$ $g = \text{fitting constant that controls the rate of degradation}$	Fahey and Carter (1993)

From Table 1-2 it can be observed that both, linear and hyperbolic models can be seen as special cases of the modified hyperbolic model since this model reduces to the linear model for $f = 0$ and to the hyperbolic model for $f = R_f$ and $g = 1$.

The adequate use of the mentioned soil models depends on the value of initial shear modulus used as reference in Equation (3.21), which in turn, depends to a large extent on the shear strain imposed to the soil when measuring G_i . For example, seismic or geophysical methods allows the determination of shear modulus in the elastic range of the material (since very small strains are imposed to the soil with these methods i.e., shear strains of $1 \times 10^{-3} \%$ or below), resulting in the maximum shear modulus of the soil (referred to as G_0 or G_{max}). In the other hand, laboratory test on soil samples would lead to somewhat lower values of G_i since shear strains of the order of 0.001 % or above are imposed to the soil with most lab methods. Figure 3-5 shows a typical degradation curve of shear modulus with shear strain. In the same figure typical strain ranges of the shear strains induced with different test methods are indicated.

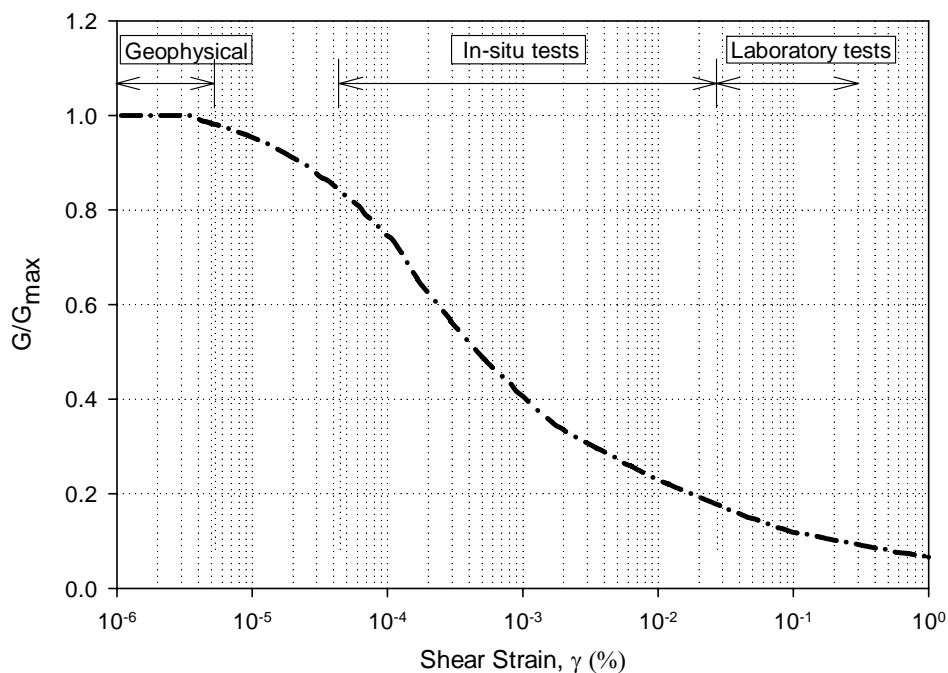


Figure 3-5 Variation of shear modulus with shear strain in soils (adapted from Mayne and Schneider, 2001)

Fitting constants f and g are used to define the degradation of the shear modulus with shear strain or stress. Parameter f controls the amount of degradation of shear modulus, and ranges between 0 and 1. However, results of case studies, presented later in this chapter, show that a value of $f = 0.98$ usually yields reasonably good results for most cases. The fitting constant g controls the rate of degradation of the shear modulus and typically ranges between 0.2 and 0.4 for most soil types (Mayne and Schneider, 2001). As shown later in this chapter, good results were obtained by setting $g = 0.3$. The rate of degradation of the different models listed in Table 1-2 is shown in Figure 3-6. This figure shows values of G/G_i plotted as a function of the shear level given by the ratio τ/τ_{max} . A faster level of degradation is necessary to capture the correct soil behavior when the

initial shear modulus G_{\max} is used as the initial reference value. From Figure 3-6, the faster shear modulus degradation is evidently the modified hyperbolic.

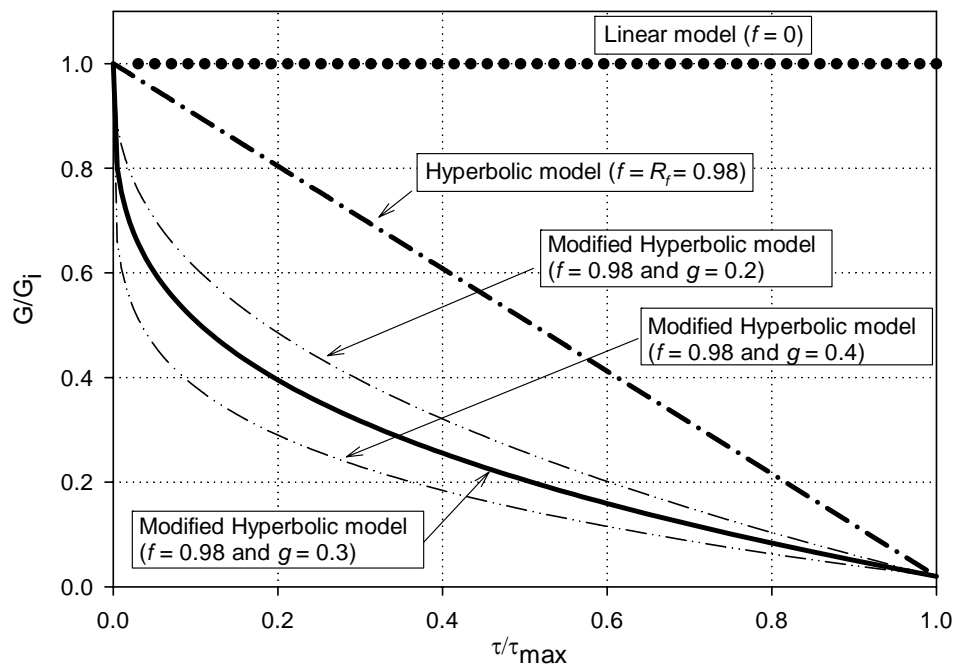


Figure 3-6 Degradation of shear modulus for different non-linear soil models

Expressions included in Table 1-2 can be used in conjunction with equations (3.11), (3.16), and (3.20) to obtain load transfer curves for linear, hyperbolic or modified hyperbolic models considering modulus degradation due to shear stresses, modulus disturbance due to construction effects and an approximate radius of influence.

Depending on the initial shear modulus available, either linear, hyperbolic or modified hyperbolic non-linear models should be used. The modified hyperbolic model was found accurate to capture the actual modulus degradation of the soil when the initial or reference value for the shear modulus is obtained from geophysical tests. These type of

tests usually measure shear wave velocity which can be used to calculate the shear modulus as follows:

$$G_0 = \rho \cdot V_s^2 \quad (3.22)$$

Where: V_s = shear wave velocity of the soil

ρ = soil density

G_0 = maximum shear modulus of the soil

The linear models may also yield satisfactory results if a secant shear modulus is used as initial reference (G_i). Estimating adequate secant shear modulus values requires experience and good engineering judgment.

3.2.1.5 RECOMMENDED PROCEDURE TO DERIVE THEORETIC LOAD TRANSFER CURVES

In the preceding sections, the different factors involved in the theoretical derivation of TZ curves were discussed. This section presents the procedure recommended to derive theoretical load transfer curves for the pile side friction. Table 1-3 summarizes the steps required for this derivation.

Table 3-3 Steps required to defined theoretical TZ curves

Step	Description
1	Assume a function to represent the radial variation of shear stresses. Good results have been found with the hyperbolic function as presented in Section 1.2.1.1 (Randolph and Wroth, 1978; Frank, 1974; and Baguelin et al. 1975).
2	Select a soil stiffness model to adequately capture the degradation of soil shear modulus. Table 1-2 lists some of the most commonly used models.
3	Incorporate soil disturbance due to pile installation. This can be done by using Equation (3.16) or (3.15). Note that $G_u(\tau)$ should be replaced by the expression selected in Step 2. If modulus degradation due to installation is not an issue, this step can be skipped.
5	Calculate the value of r_m either by means of Equation (3.18) or (3.20).
4	Integrate Equation (3.11) or (3.10) between r_0 and r_m to obtain the theoretical load transfer curve. Note that $G(r_l, M_0, \tau)$ is the expression obtained in Step 3. If Step 3 was skipped, $G(r_l, M_0, \tau)$ would be the expression for $G(\tau)$ selected in Step 2.

The derivation of theoretical load transfer curves used throughout this work is presented, following the procedure described in Table 3-3.

Step 1: A hyperbolic radial variation of shear stresses was selected. Thus, the load transfer curve would result from the integration of

$$z_s = \tau_0 r_0 \int_{r_0}^{r_m} \frac{dr}{r \cdot G(r, \tau)} \quad (3.11)$$

Step 2 and 3: For this work, the modified hyperbolic model was selected since the shear modulus for small strains will be used as initial reference.

The equivalent shear modulus considering installation effects can be derived using Equation (3.16):

$$G_{eq}(\tau) = \frac{\int_0^{r_m} \frac{1}{r} dr}{\int_{r_0}^{r_1} \frac{1}{r \cdot G \cdot \left(1 - f \cdot \left(\frac{\tau_0 \cdot r_0}{r \cdot \tau_{max}}\right)^g\right) \cdot \left(M_0 + \frac{(1-M_0) \left(\frac{r}{r_0}\right)}{\frac{r_1}{r_0} - 1}\right)} dr + \int_{r_1}^{r_m} \frac{1}{r \cdot G_0 \cdot \left(1 - f \cdot \left(\frac{\tau_0 \cdot r_0}{r \cdot \tau_{max}}\right)^g\right)} dr} \quad (3.23)$$

To obtain Equation (3.23) the following replacements were made in Equation (3.16):

$$G_u(\tau) = G_0 \cdot \left(1 - f \cdot \left(\frac{\tau_0 \cdot r_0}{r \cdot \tau_{max}}\right)^g\right)$$

$$G(r_1, M_0, \tau) = G_0 \cdot \left(1 - f \cdot \left(\frac{\tau_0 \cdot r_0}{r \cdot \tau_{max}}\right)^g\right) \cdot \left(M_0 + \frac{(1-M_0) \left(\frac{r}{r_0}\right)}{\frac{r_1}{r_0} - 1}\right)$$

$$\tau = \frac{\tau_0 r_0}{r}$$

Step 4: Replacing the modified hyperbolic model into Equation (3.11) and incorporating the radial shear distribution the integration yields

$$z_s = \tau_0 r_0 \int_{r_0}^{r_m} \frac{1}{r \cdot G_{eq} \cdot \left(1 - f \cdot \left(\frac{\tau_0 \cdot r_0}{r \cdot \tau_{max}}\right)^g\right)} dr \quad (3.24)$$

$$z_s = \frac{\tau_0 \cdot r_0}{g \cdot G_{eq}} \ln \left(\frac{\left(\frac{r_m}{r_0}\right)^g - f \left(\frac{\tau_0}{\tau_{max}}\right)^g}{1 - f \left(\frac{\tau_0}{\tau_{max}}\right)^g} \right) \quad (3.25)$$

Note that in Equation (3.25) an equivalent shear modulus was considered. The expression to calculate the equivalent shear modulus was presented in Step 3. If it is not desired to include installation effects, G_{eq} should be replaced by G_0 in (3.25).

Step 5: Finally, the approximate expression to estimate the radius of influence of the pile can be included in Equation (3.25) to yield the final expression for load transfer curve:

$$z_s = \frac{\tau_0 \cdot r_0}{g \cdot G_{eq}} \ln \left(\frac{\left(\frac{\tau_0}{\delta \cdot G_0 \cdot \left(1 - f \left(\frac{\tau_0}{\tau_{max}} \right)^g} \right)} \right)^g - f \left(\frac{\tau_0}{\tau_{max}} \right)^g}{1 - f \left(\frac{\tau_0}{\tau_{max}} \right)^g} \right) \quad (3.26)$$

If the expression for the radius of influence of the pile proposed by Randolph and Wroth (1978) is used Equation (3.26) turns to be

$$z_s = \frac{\tau_0 \cdot r_0}{g \cdot G_{eq}} \ln \left(\frac{\left(\frac{C \cdot l_p \cdot \rho \cdot (1 - \nu)}{r_0} \right)^g - f \left(\frac{\tau_0}{\tau_{max}} \right)^g}{1 - f \left(\frac{\tau_0}{\tau_{max}} \right)^g} \right) \quad (3.27)$$

Equation (3.27) has been used for drilled shafts embedded in residual soil (Zhu and Chang, 2002) and for driven composite piles Pando (2003). The application of these equations to the study of piles embedded in alluvial soils will be investigated in this work, in Chapter 4 and 6.

Note that equations (3.26) and (3.27) still hold for conventional hyperbolic models and linear elastic-plastic models providing that adequate values are given to the fitting constants f and g . Side shear load transfer curves resulting from linear, hyperbolic and modified hyperbolic soil models are shown in Figure 3-7.

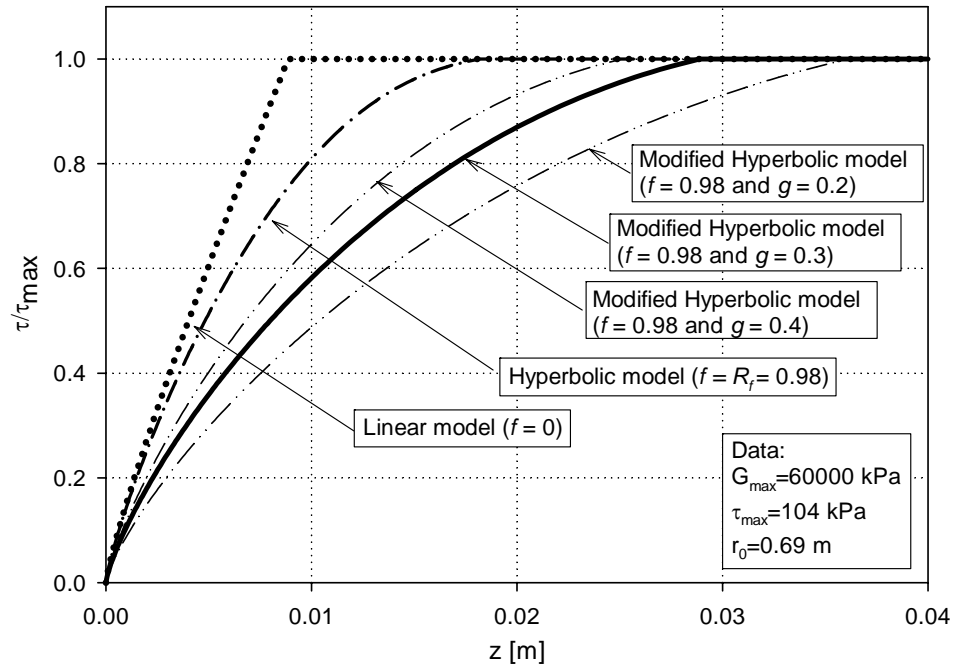


Figure 3-7 Linear, hyperbolic and modified hyperbolic load transfer curves

3.2.2 THEORETICAL LOAD TRANSFER CURVES FOR THE PILE TIP (Q_B - Z_B CURVES)

Derivation of load transfer curves for the pile tip is not as straightforward as for load transfer curves along the shaft. This is due to the complex distribution of shear stresses that develop under the pile tip that prevents from assuming a simple state of stress similar to the concentric cylinders. The problem of the load transfer at the pile base can be thought to be similar to that solved by Boussinesq (1885) for a rigid punch acting on an elastic half space. According to Boussinesq's solution the displacement of the rigid punch can be estimated by:

$$z_b = \frac{Q_b (1-\nu)}{4r_0 G} \omega \quad (3.28)$$

Where: z_b = displacement of the pile base

Q_b = load at the pile tip

ν = Poisson's ratio of the soil under the pile

r_0 = base radius

G = shear modulus of the soil under the pile

ω = shape and depth factor, which can be taken equal to 1.0 (Randolph and Wroth, 1978; and Armaleh and Desai, 1987)

Because the nature of the shear strain distribution below a pile tip is more complex it is not as straightforward to model soil non-linearity for Q-Z curves as it was for the T-Z curves. An initial approximation consists of assuming a hyperbolic variation of Equation (3.28), such as proposed by Chow (1986):

$$z_b = \frac{Q_b(1-\nu)}{4r_0G_0 \left(1 - f \left(\frac{Q_b}{Q_{b-\max}} \right)^g \right)} \quad (3.29)$$

Where: $Q_{b-\max}$ = ultimate pile base capacity

As for the case of TZ curves, the linear elastic-plastic and hyperbolic models are generated setting $f = 0$ and $f = R_f$ and $g = 1$ respectively, in Equation (3.29). Load transfer curves for the pile base for the modified hyperbolic, conventional hyperbolic and linear elastic models are depicted in Figure 3-8.

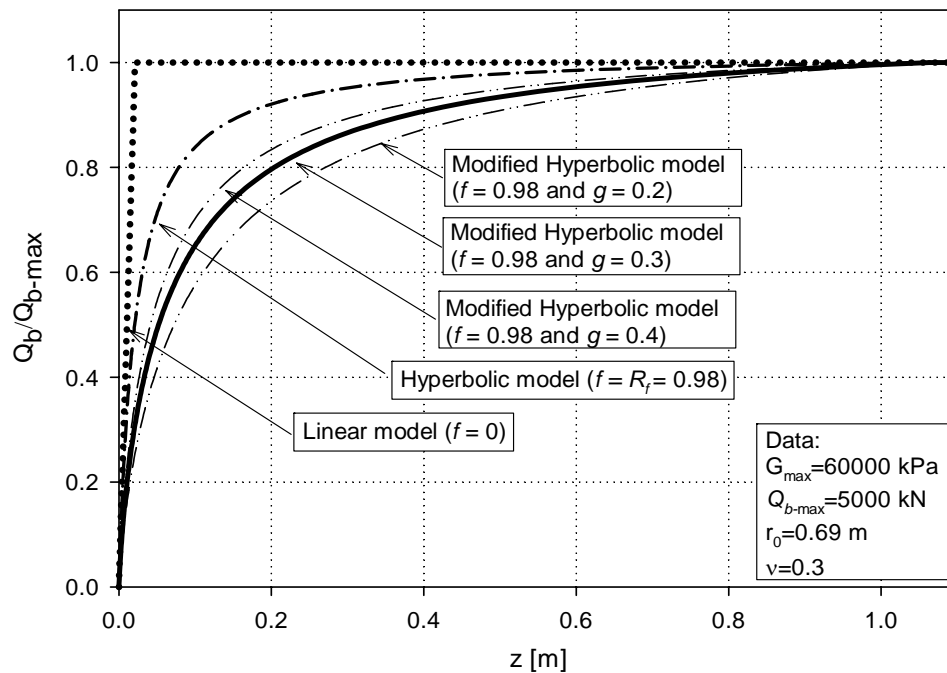


Figure 3-8 Typical load transfer curves for the pile base

As for case of shaft load transfer curves, the modified hyperbolic model simulates a faster degradation of the initial shear modulus of the soil compared to the other two soil models. The use of the modified hyperbolic model for the base load transfer curve was found necessary when the soil shear modulus for very low strains was used as initial reference in Equation (3.29).

3.3 PROPOSED METHODOLOGY FOR SETTLEMENT ANALYSIS OF AXIALLY LOADED PILES

A methodology combining the use of CPT data and the load transfer method is proposed to estimate the response of axially loaded piles. Theoretical load transfer curves included in the previous section are used to characterize soil layers. CPT data is used to compute the soil parameters that define the asymptotic values in the load transfer curves

and to incorporate non-homogeneity. Thereafter, the load transfer method, implemented into a computer program, is used to calculate the load settlement curve for the pile.

In order to effectively develop a systematic methodology that can be applied to any case at hand, the required input parameters to compute TZ and Q_bZ_b curves should be established first. These parameters are listed in Table 3-4.

Table 3-4 Variables required to define load transfer curves

Variable	How to calculate the variable
1 - Variables needed to calculate G_θ	
ρ	From empirical correlations (see subsection 1.3.2)
V_s	From SCPT soundings or empirical correlations (see subsection 1.3.2)
2 - Variables needed to calculate G_{eq}	
M_θ	Values suggested in Table 1-1
R_l	Values suggested in Table 1-1
G_θ	Use Equation (3.22)
r_m	Use Equation (3.18) or (3.20)
3 - Variables needed to define the modified hyperbolic TZ curve	
τ_{max}	From one of the available methods to estimate axial pile capacity (see subsection 1.3.1)
f and g	Suggested initial value of 0.3 and 0.98 respectively
G_{eq}	Use Equation (3.23) or (3.16)
4 - Variables to define the modified hyperbolic Q_bZ_b curve	
Q_{b-max}	From one of the methods to estimate axial pile capacity (see subsection 1.3.1)
f and g	Suggested initial value of 0.98 and 0.3 respectively
G_θ	Use Equation (3.22)

Most variables listed in Table 1-4, except Q_{b-max} and τ_{max} , were defined in the previous subsections. These two variables will be described in the following subsection where CPT – based static methods for estimating pile capacity are described.

3.3.1 METHODS FOR ESTIMATING AXIAL PILE CAPACITY USING CPT OR SCPT DATA

The Cone Penetration Test (CPT) and the Seismic Cone Penetration Test (SCPT) consist of an instrumented steel probe with standard geometry that is pushed into the soil at a constant rate. Originally, the cone was used to measure only tip resistance but currently, a number of geotechnical measurements are available from CPT soundings. Due to the addition of transducers into the cone tip, CPT soundings record a continuous profile of pore pressure, the friction along the lateral sleeve of the cone, and the arrival of seismic shear wave, which allows estimating shear wave velocity (Mitchell, 1988). The downside of CPT is that no soil samples are retrieved during the test. Therefore, sometimes CPT soundings are combined with other in-situ tests to extract soil samples to determine some soil properties (unit weight, moisture content, etc).

CPT data can be used to estimate axial pile capacity by means of indirect or direct methods. Indirect methods make use of the readings from CPT soundings to evaluate engineering soil parameters (e.g. modulus of elasticity, friction angle, undrained shear strength), which are used as input data for theoretical formulations employed to estimate pile capacity (Poulos, 1989). Direct methods, on the other hand, relate quantities measured in situ, during the test, to axial pile capacity by means of empirical correlations. The first indirect methods available used only the cone tip resistance (q_c) to estimate base and shaft capacity. Over the years, indirect methods have improved and the latest empirical correlations combine tip cone resistance, sleeve friction, and pore water pressure measurements to provide a more reliable estimation of pile capacity (Eslami and Fellenius, 1997). For this work direct methods for estimating axial pile capacity where

chosen because of its simplicity and ease of programming in conventional spreadsheets. The level of accuracy of currently available direct and indirect methods is considered comparable

Probably, the most widely used and accurate direct methods to estimate axial pile capacity from CPT soundings are the ones proposed by Bustamante and Gianeselli (1982), Eslami and Fellenius (1997), and Takesue et al., (1998). For the proposed methodology, the three methods were used to estimate asymptotic values of the load transfer curves and their results were compared. The three aforementioned methods are briefly reviewed below.

In general, the total axial pile capacity can be obtained by adding the contribution of the shaft resistance in skin friction and pile tip resistance as follows:

$$\begin{aligned}
 Q_u &= Q_t + Q_s \\
 Q_u &= f_t \cdot A_t + \int_0^{l_p} f_s(z) \cdot p(z) \cdot dz
 \end{aligned}
 \tag{3.30}$$

Where: Q_u = ultimate total axial pile capacity, units of [F]

Q_t = ultimate tip capacity, units of [F]

Q_s = ultimate shaft capacity, units of [F]

f_s = unit side shear, units of [F/L²]

f_t = unit end bearing, units of [F/L²]

A_t = pile tip area, units of [L²]

p = pile perimeter, units of [L]

z = depth, units of [L]

In general a continuous function to describe the skin friction is not known (because of soil heterogeneity), therefore soil profile is discretized into layers, which allows replacing the integral in Equation (3.30) by the following summation:

$$Q_u \approx f_t \cdot A_t + \sum_{i=1}^{\#layers} f_{si} \cdot p_i \cdot \Delta z_i \quad (3.31)$$

Where: f_{si} = unit side shear for layer i

p_i = pile perimeter at mid depth of layer i

Δz_i = thickness of layer i

From Equation (3.31) it is observed that both f_t and f_{si} have to be estimated in order to calculate total axial capacity of a given pile. The methods described in below use different empirical correlations to estimate these values.

- **Bustamante and Gianeselli (1982) – LCPC method**

The method is based on experimental work by the Laboratoire Central des Ponts et Chaussées (LCPC). This method is based on the results of 197 pile load (and extraction) tests with a wide range of soil types. The LCPC method has been continuously updated and many variations of the original method proposed by Bustamante and Gianeselli in 1982 are available.

The LCPC method uses only the cone tip resistance to estimate both shaft skin friction and end bearing. The general expressions proposed by the authors to estimate unit side shear and unit end bearing are:

$$f_{si} = \frac{q_c}{\alpha_{LCPC}} \quad (3.32)$$

$$f_t = k_c \cdot q_{ca}$$

Where q_c is the cone tip resistance at the elevation where f_{si} is evaluated and q_{ca} is a filtered average value of q_c over the range $1.5b$ above and $1.5b$ below the pile tip, with b equal to the pile diameter or pile width. The method also recommends the use of limiting values for both f_{si} and f_t depending on soil type, pile type and installation method. Additional information on this method can be found in Lunne et al. (1997).

This method will be referred to in this thesis as “Method 1” and numerical models based on axial pile capacity estimates using this method will be referred to as “Model 1”.

- **Eslami and Fellenius (1997) method**

This method is based on a large database of pile load tests composed of 102 case histories which includes both drilled shafts and driven piles. The distinctive aspect of this method is that the unit end bearing (f_t) is calculated using a geometric average of cone tip resistance over an influence zone extended from $8b$ above to $4b$ below the pile tip, with b equal to the pile diameter. For piles installed through a dense soil into a weak soil the zone of influence spans from $2b$ above and $4b$ below the pile tip. Cone tip resistance is corrected by subtracting the measured pore water pressure to the measured cone tip resistance:

$$q_E = q_t - u_2 \quad (3.33)$$

The expressions proposed by Eslami and Fellenius (1997) to estimate ultimate pile capacity are:

$$\begin{aligned} f_t &= C_t q_{E_g} \\ f_{si} &= C_s q_{E_g} \end{aligned} \quad (3.34)$$

Where: C_t = correlation coefficient equal to 0.98, but can be taken as unity

C_s = correlation coefficient which depends on soil type. Values for this coefficient can be found in Appendix A.

q_{E_g} = geometric average of q_E values within the influence zone

Values for coefficients C_s depend on the soil type. The method includes a soil classification chart based on measured sleeve friction and cone tip resistance which is used to classify soil layers in order to determine the value of C_s to be used in Equation (3.34).

This method will be referred to in this work as “Method 2” and numerical models based on axial pile capacity estimates using this method will be referred to as “Model 2”.

- **Takesue et al. (1998) method**

This method was proposed to estimate values of unit side shear f_{si} in both clays and sands for either driven piles or drilled shafts. The method incorporates measurements of excess pore water pressure and sleeve friction recorded during piezocone penetration.

The authors proposed the following expressions for estimating the unit side shear:

$$\begin{aligned} \text{For } \Delta u_b < 300 \text{ kPa} \quad f_{si} &= F_s \left(\frac{\Delta u_b}{1250} + 0.76 \right) \\ \text{For } \Delta u_b > 300 \text{ kPa} \quad f_{si} &= F_s \left(\frac{\Delta u_b}{200} - 0.50 \right) \end{aligned} \quad (3.35)$$

Where: F_s = cone sleeve friction

$\Delta u_b = u_2 - u_0$, where u_2 = pore pressure measured at the shoulder of the cone, in kPa and u_0 = the hydrostatic pore pressure, in kPa

Takesue et al. (1998) did not propose a formula to estimate pile base resistance. However, Mayne and Schneider (2001) obtained good agreements when combining values from Equation (3.35) with unit pile base resistance values from Eslami and Fellenius (1997) for pile tips resting on clays or with the following expression by Lee and Salgado (1999) for pile tips in sands:

$$\frac{f_t}{q_t} = \frac{1}{1.90 + \frac{0.62}{s/b}} \quad (3.36)$$

Where: q_t = cone tip resistance. For this work the geometric average q_{Eg} proposed by Eslami and Fellenius (1997) was used in formula (3.36).

s = tip settlement required to mobilize f_t

b = pile diameter or width

This method will be referred to in this work as “Method 3” and numerical models based on axial pile capacity estimates using this method will be referred to as “Model 3”.

3.3.2 INITIAL SHEAR MODULUS AT VERY LOW STRAINS FROM CPT DATA

The proposed methodology is based on the load transfer method using modified hyperbolic load transfer curves, such as those presented in the previous section, with asymptotic values based on static methods that use CPT data. The main reason leading to the use of the modified hyperbolic model is that a faster degradation of the shear modulus

is observed when G_0 at very low strains is used as initial reference in the TZ curves (Randolph 1994). As explained earlier, G_0 at very low strains can be reliably obtained from soil shear wave velocity by using Equation (3.22). If shear wave velocity data is not available, correlations between conventional CPT soundings and soil shear wave velocity could be used. Andrus, et al. (2004) suggested the following correlations to estimate shear wave velocity:

$$V_s = 26.3 \cdot q_c^{0.199} \cdot f_s^{0.003} \cdot \text{ASF} \quad \text{for sands} \quad (3.37)$$

$$V_s = 14.3 \cdot q_c^{0.280} \cdot f_s^{0.108} \cdot \text{ASF} \quad \text{for clays} \quad (3.38)$$

Where: V_s = shear wave velocity in m/s

q_c = uncorrected cone tip resistance in kPa

f_s = cone sleeve friction in kPa

ASF = age scaling factor. Values of ASF are in Table 3-5.

Table 3-5 Values for age scaling factor ASF (after Andrus et al., 2004)

Geologic Age	ASF for Sands	ASF for Clays
Holocene (<10000 years)	1	1
Pleistocene (10000 to 1.5 millions years)	1.44	1.18

After estimating V_s , the value for G_0 can be calculated using Equation (3.22). Soil density can be obtained by means of the following correlation proposed by Mayne et al. (1999).

$$\rho_{sat} = 1 + \frac{1}{0.614 + 58.7 \frac{(\log(z) + 1.095)}{V_s}} \quad (3.39)$$

In Equation (3.39) the depth of the soil layer, z , must be expressed in meters (m) and the shear wave velocity in meters per second (m/s). For layers above the ground water table the following relation can be used to estimate the dry density

$$\rho_{dry} = \frac{G_s (\rho_{sat} - 1)}{G_s - 1} \quad (3.40)$$

Where: G_s = specific gravity of the soil

Alternatively, G_0 can be estimated by direct correlations with CPT measurements.

Some of the most commonly used correlations are:

- Rix and Stokoe (1991):

$$\left(\frac{G_0}{q_c} \right)_{average} = 1634 \cdot \left(\frac{q_c}{\sqrt{\sigma'_{vo}}} \right)^{-0.75} \quad (3.41)$$

Where: σ'_{vo} = effective overburden pressure at depth of q_c . All values in expression (3.41) are in kPa.

- Chow (1996):

$$G_0 = \frac{q_c}{A + B\eta - C\eta^2}$$

and

$$\eta = \frac{q_c}{\sqrt{P_a \sigma'_v}} \quad (3.42)$$

Where: $A = 0.0203$, $B = 0.00125$, and $C = 1.216 \times 10^{-6}$

σ'_v = free-field effective overburden pressure

P_a = atmospheric pressure = 101 kPa

- Baldi et al. (1989):

$$\left(\frac{G_0}{q_c}\right)_{average} = 1615 \cdot \left(\frac{q_c}{\sqrt{\sigma'_{vo}}}\right)^{-0.764} \quad (3.43)$$

All terms in Equation (3.43) are those defined for the previous correlations.

3.3.3 METHODOLOGY FOR ESTIMATING PILE SETTLEMENTS

In the previous section the variables and constants required to define the load transfer curves using a modified hyperbolic model were discussed. In this subsection the methodology for estimating pile settlements is summarized in 5 steps which are listed in Table 3-6.

Table 3-6 Steps of the proposed methodology for estimating pile settlement using the load transfer method

Step	Description
1	Estimate the ultimate pile capacity. This can be done by using one of the methods presented in subsection 1.3.1. The methodology is not restricted to the use of these methods and the user can choose a different method if preferred.
2	Discretize soil profile into finite layers with uniform properties. Although this step is not strictly required, discretizing the soil profile into layers is recommended in order to simplify the analysis and improve accuracy.
3	Using shear wave velocity measurements from SCPT, geophysical tests, or correlations such as the ones presented in subsection 1.3.2 estimate the initial shear modulus for each of the layers present in the soil profile.
4	Define load transfer curves using equations (3.26) for the shaft and (3.29) for the tip. If it is not desired to include installation effects, use Equation (3.25) instead of (3.26) providing G_{eq} is replaced by the undisturbed modulus G_0 .
5	Define pile model data: E (Young modulus) and ν (pile Poisson's ratio)

The systematic application of these steps has yielded results that were found to be in good agreement with field load tests, as will be shown in Chapter 4.

3.4 SUMMARY AND CONCLUSIONS

The methodology presented to systematically generate load transfer curves for the pile shaft and pile tip was presented in Section 1.2. Although the procedure is based on the theoretical work by Kraft et al. (1981) and Randolph and Wroth (1978) three distinct aspects are submitted with the proposed methodology: (a) parameters for the load transfer curves derived from CPT or SCPT, (b) a methodology considering the linear and the conventional hyperbolic soil models as special cases of the modified hyperbolic model through fitting parameters f and g , yielding a more general approach, and (c) a more rational approach is proposed in order to estimate the radius of influence of the pile and shear modulus disturbance due to construction procedures can be considered in the load transfer curves.

Probably, one of the strengths of the proposed procedure is that fewer parameters are required to define load transfer curves and all of them can be reliably estimated from results of CPT or SCPT soundings.

The benefits of the proposed approach to calculate the radius of influence can be summarized in three aspects:

1. Allows for including the effect of shear modulus degradation on the radius of influence of the pile, through the fitting parameter g .

2. Allows for considering the stress level dependency of radius of influence of the pile.
3. It is not necessary to arbitrarily define the radius of influence since it is determined with the soil properties established for each layer.

The proposed methodology also allows for considering a disturbed shear modulus at the pile interface due to installation procedures. If the disturbed shear modulus can be reliably estimated, it can be easily incorporated into the load transfer models by means of equation (3.26).

The conventional hyperbolic and the linear soil models are special cases of the modified hyperbolic soil model. These soil models can be generated by setting appropriate values for the fitting constants f and g in Equation (3.26) or (3.27). This may be useful when a fast degradation of the shear modulus used as initial reference is not required to adequately simulate soil behavior (i.e., the maximum shear modulus measured at very low strains is not available and a secant shear modulus has to be used).

4 APPLICATION OF THE PROPOSED METHODOLOGY FOR ESTIMATING PILE SETTLEMENTS TO FIVE CASE STUDIES

4.1 INTRODUCTION

This chapter presents the results of the application of the proposed methodology for estimating pile settlements to the study of five case histories. For each case study three numerical models were developed using asymptotic values from the methods outlined in Chapter 3.

Type A predictions were carried out for all cases in order to assess the ability of the proposed procedure to predict the load settlement curve of a single pile and its Davisson failure load. Load transfer analyses were performed using typical values for the fitting constants f and g as those suggested in the previous chapter.

Cases one through three correspond to load tests on axial drilled shafts located in the southern piedmont geologic province of the United States. These cases are discussed in Section 4.2. The fourth case is from a test carried out at the national geotechnical experimentation site (NGES) near Texas A&M University, and the fifth example corresponds to a drilled shaft tested in a project in the Old San Juan area, in Puerto Rico. These last two cases are discussed in Section 4.4. For each case study, failure loads predicted by numerical models are compared to those obtained for the load settlement curve recorded in the field. The last subsection of this chapter summarizes the main findings obtained from the analyses of the case studies.

4.2 CASE STUDIES IN THE SOUTHERN PIEDMONT PROVINCE

Case studies 1 through 3 correspond to drilled shafts located at the southern end of the piedmont province, as shown in Figure 4-1. The southern piedmont province is bounded to the east by the Atlantic coastal plain, to the south by the Gulf of Mexico, and to the north by the Blue Ridge. The Piedmont is composed of residual silts and sands underlain by partially weathered rock.

A deep geotechnical site characterization of the southern piedmont geologic province of US was performed by Mayne et al. (2000).

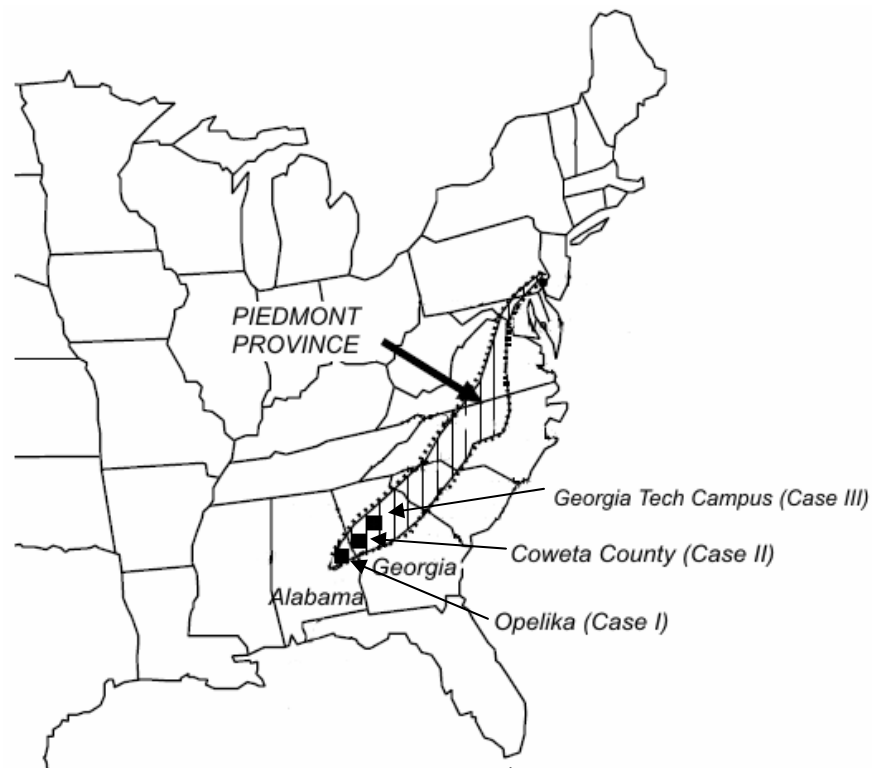


Figure 4-1 Southern piedmont province and relative location of case histories 1 through 3

4.2.1 DRILLED SHAFT AT OPELIKA SITE, AUBURN UNIVERSITY, ALABAMA

A load test program composed of ten drilled shafts was conducted at the NGES established by Auburn University and the Alabama Department of Transportation in Opelika, Alabama (Brown, 2002). Of the series of ten drilled shafts, a 11.6 m long pile with a radius of 0.915 m was modeled using the proposed methodology and the numerical results are compared with field test data in this section.

The NGES at Opelika has been extensively characterized by several researchers, such as Brown and Vinson (1998), Mayne et al. (2000), and Mayne and Brown, 2003. The site is underlain by residual soils derived the weathering of gneiss, schist and granite. The soil

profile is composed of a mixture of fine sandy silts to silty fine sands with trace mica (Mayne and Zavala, 2004). A detailed site characterization can be found in Mayne et al. (2000).

Two CPT soundings advanced at the site are shown in Figure 4-2. In the same figure the predicted and measured shear wave velocity profiles are also shown.

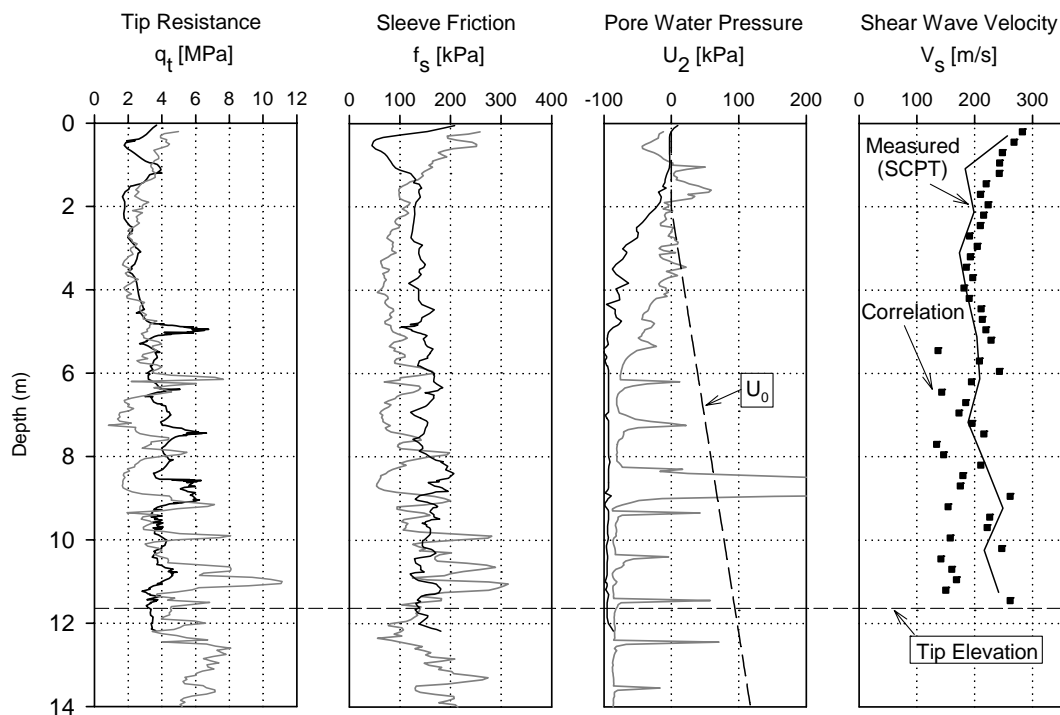


Figure 4-2 Shear wave velocity profile and CPT soundings advanced at Opelika Site, Alabama

In the following paragraphs, the results of the step by step proposed methodology are summarized.

Figure 4-3 shows the axial capacity for the drilled shaft at Opelika site estimated using each one of the three methods described in Chapter 3.

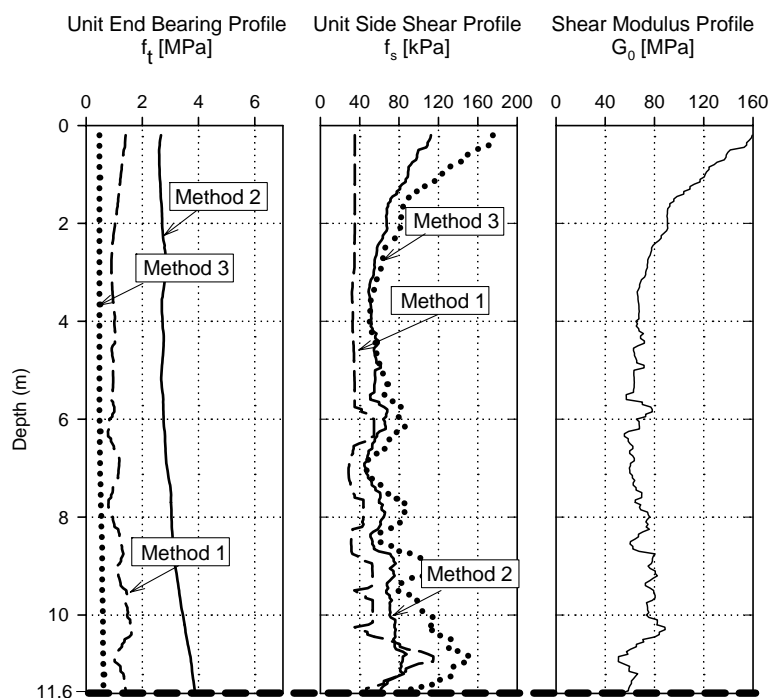


Figure 4-3 Static axial pile capacity and shear modulus profile for a 0.915 diameter drilled shaft at Opelika Site

Table 4-1 summarizes the results of the predicted axial pile capacity for each of the methods presented in the previous chapter.

Table 4-1 Predicted axial pile capacity for a drilled shaft at Opelika site

Method	Shaft Capacity [kN]	Tip Capacity [kN]	Ultimate Capacity [kN]	Davisson Load [kN]
1	1410	745	2155	2700
2	2200	2540	4740	2700
3	2894	320	3214	2700
Load Test	-	-	2900	2700

Results of class A predictions obtained with the numerical analyses are shown in Figure 4-4 for models 1 through 3.

Results from class A predictions show fairly good agreement with field measurements for the linear part of the curve up to an axial load of about 1200 kN. The best estimation

of the Davisson load was obtained with Model 2, Model 1 underpredicted the failure load by 30 % and model 3 overpredicted the Davisson failure load by 16 %.

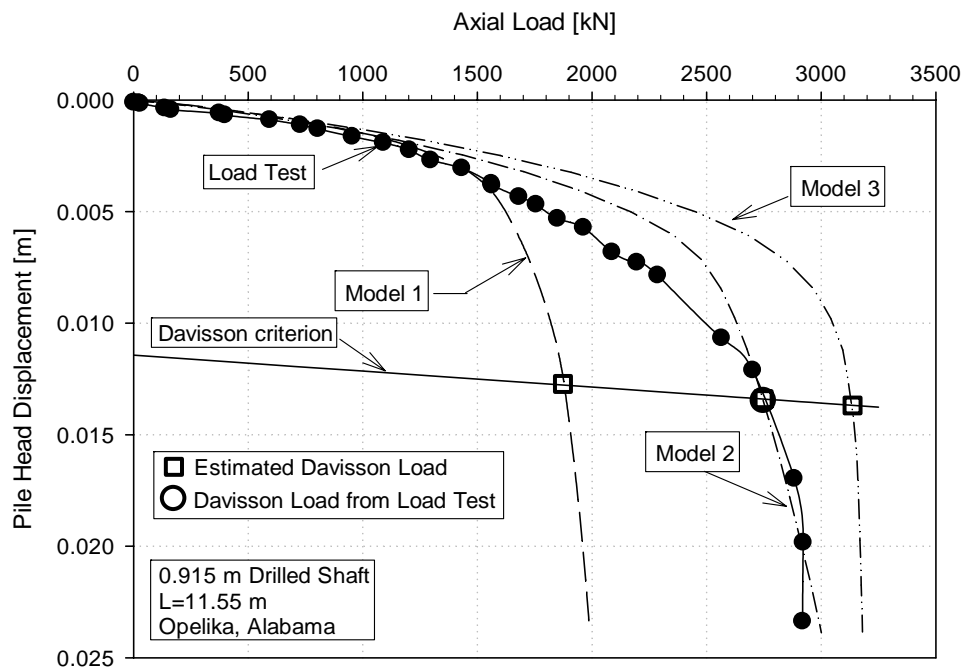


Figure 4-4 Type A predictions for axial pile at Opelika Site

The three models used the same shear modulus profile and profile soil layer discretization, differences in the predicted pile response are attributed mainly to the asymptotic values of the load transfer curves which correspond to the ultimate axial pile capacity. Due to incompatibility of deformations required to mobilize shaft friction and end bearing, only a small percentage of pile tip resistance is being mobilized while side friction has been fully mobilized. This can be observed in Figure 4-5, where load transferred through the shaft and through the pile tip were plotted in separate curves.

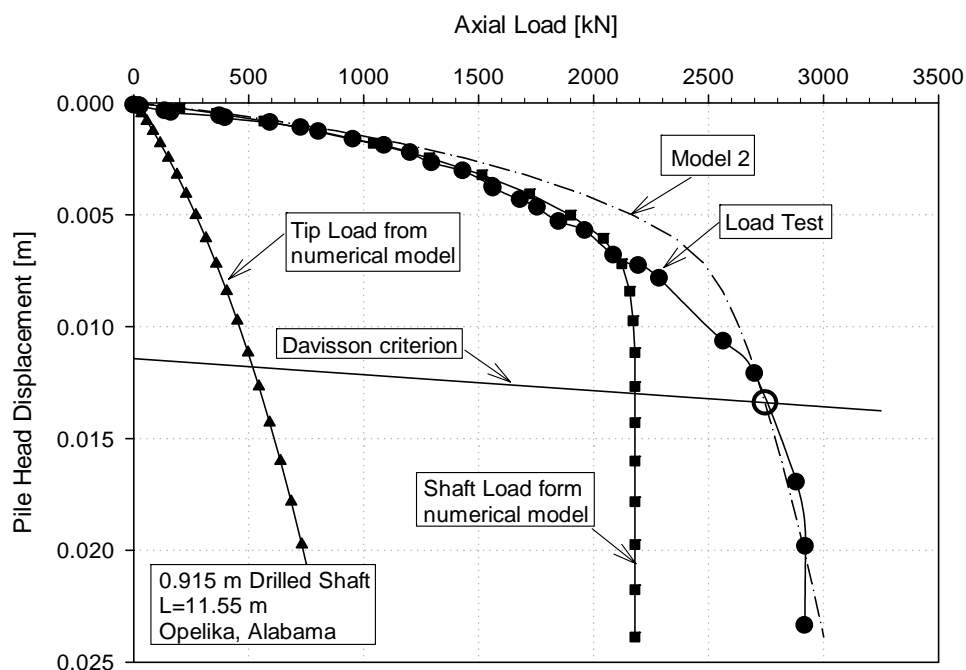


Figure 4-5 Load transferred through the shaft and the pile tip for the pile tested at Opelika site for model 2

Although a tip capacity of 2540 kN was predicted by Method 2, only 500 kN of tip load has been developed at Davisson failure. It can be seen that a tip load of 500 kN lies between ultimate base capacity predicted by Models 1 and 3. This shows that the load transfer method is capable of accounting for deformation incompatibility between side shear and end bearing.

4.2.2 DRILLED SHAFT IN COWETA COUNTY, GEORGIA

This case history corresponds to a drilled shaft constructed under a bridge for the widening of interstate I-85 in Coweta County, Georgia. The pile was 0.91 m in diameter and 19.2 m long. The pile was socketed in a partially weathered gneissic granite which underlies the residual soil characteristic of the southern piedmont geologic province.

CPT data revealed a rigid crust in the upper 2 m which was underlain by almost uniform clayey soil profile up to 14 meters deep. CPT tip resistance values of 32 MPa were recorded in the partially weathered rock that extended from 18 m deep and below.

The CPT sounding advanced at the site and used to develop the numerical model for the drilled shaft in Coweta County is shown in Figure 4-2. In the same figure the predicted and measured shear wave velocity profiles are also shown.

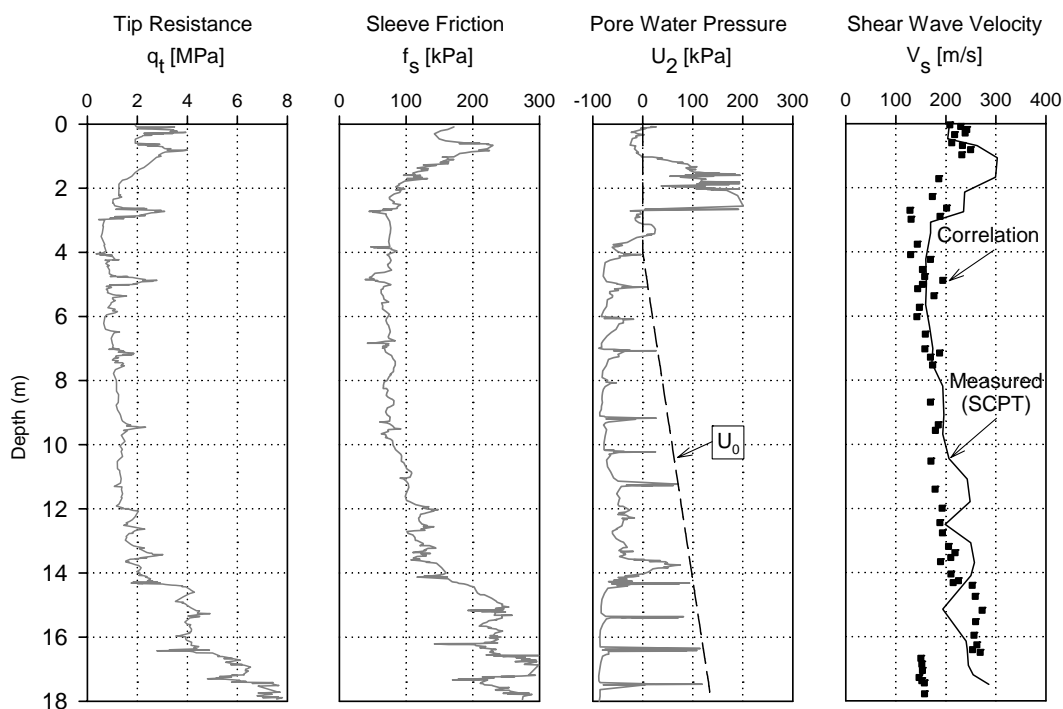


Figure 4-6 Shear wave velocity and CPT sounding advanced in Coweta County, Georgia

The results of the numerical model of the drilled shaft at Coweta County, obtained with the procedure outlined before are summarized in the following paragraphs.

Figure 4-7 shows the axial pile capacity for the drilled shaft in Coweta County estimated using each one of the three methods described in Chapter 3. Ultimate axial pile capacity is summarized in Table 4-2.

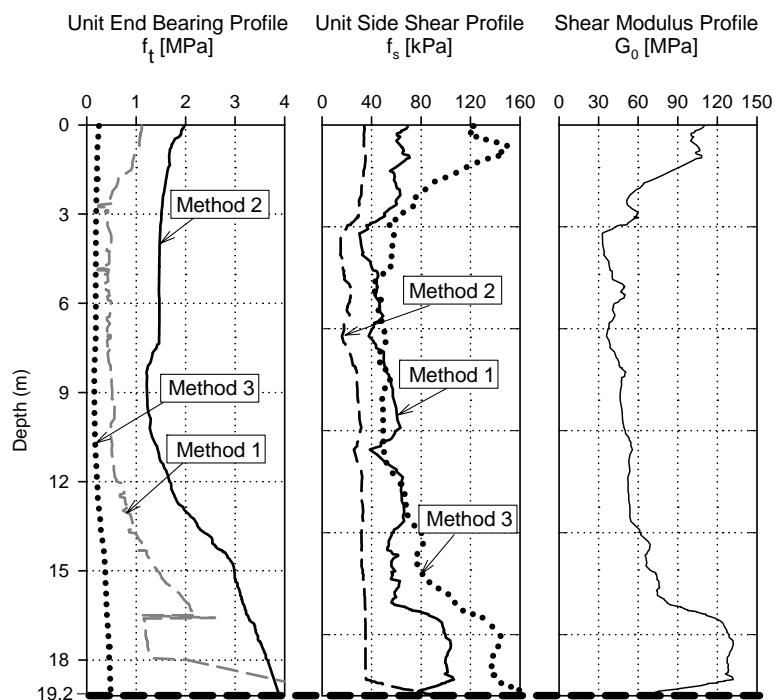


Figure 4-7 Static axial pile capacity and shear modulus profile for a 0.915 diameter drilled shaft in Coweta County, Georgia

Table 4-2 Predicted axial pile capacity for a drilled shaft in Coweta County

Method	Shaft Capacity [kN]	Tip Capacity [kN]	Ultimate Capacity [kN]	Davisson Load [kN]
1	2220	4360	6580	5260
2	3580	2530	6110	5260
3	4920	320	5240	5260
Load Test	-	-	> 7000	5260

Results of class A predictions obtained with the numerical analyses are shown in Figure 4-8 for Models 1 through 3.

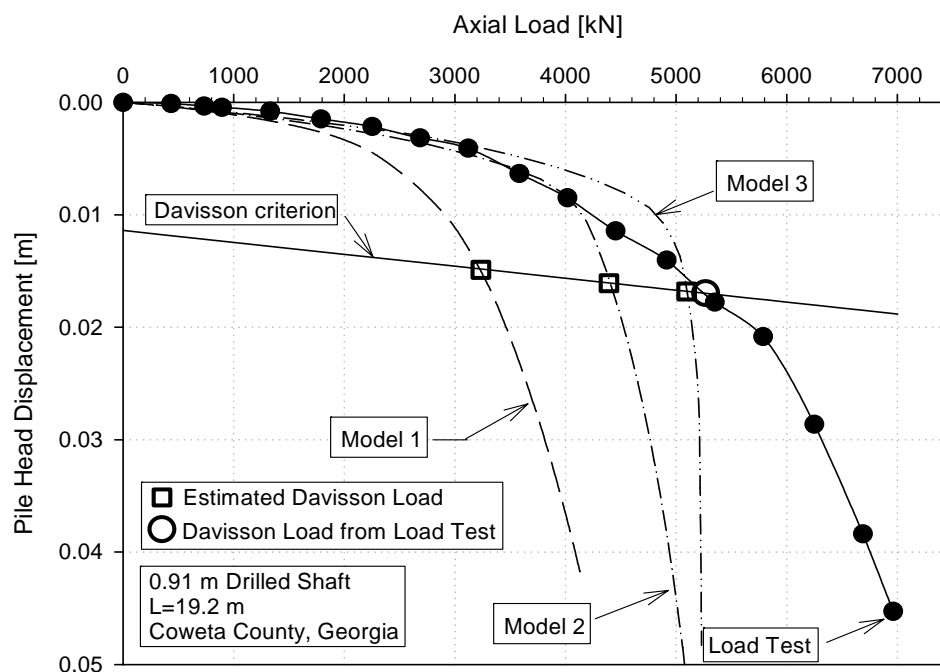


Figure 4-8 Type A predictions for axial pile under a bridge in Coweta County

Predicted load settlement curves did not show good agreement with the field measurements, particularly for the last portion of the curve beyond 4000 kN. The main reason believed to be responsible for this is the underestimated pile base capacity. This may be attributed to the averaging technique involved in the estimation of pile base capacity. The soil layers overlaying the weathered rock yielded cone tip resistance values ranging between 0.5 MPa and 8 MPa, which are many times lower than the 32 MPa measured in the weathered rock. This can be seen in the CPT sounding shown in Figure 4-6. This large cone tip resistance contrast resulted in a low average cone tip resistance for computation of the pile unit end bearing. A new set of calculations were made using a base pile capacity estimated without using the averaged cone tip resistance q_{ca} or q_{Eg} . The new set of calculations used q_{ca} or q_{Eg} equal to 32 MPa which is the average value

recorded in the weathered rock. The new set of pile capacities are summarized in Table 4-3.

Table 4-3 Corrected axial pile capacity for a drilled shaft in Coweta County

Method	Shaft Capacity [kN]	Tip Capacity [kN]	Total Capacity [kN]	Davisson Load [kN]
1	2220	6240	8460	5260
2	3580	20400	23980	5260
3	4920	2570	7490	5260
Load Test	-	-	> 7000	5260

Additional runs were carried out with the corrected tip capacity while keeping other model parameters constant (i. e. only values for Q_{b-max} were changed in the numerical models). The results obtained with the modified type A prediction are depicted in Figure 4-9.

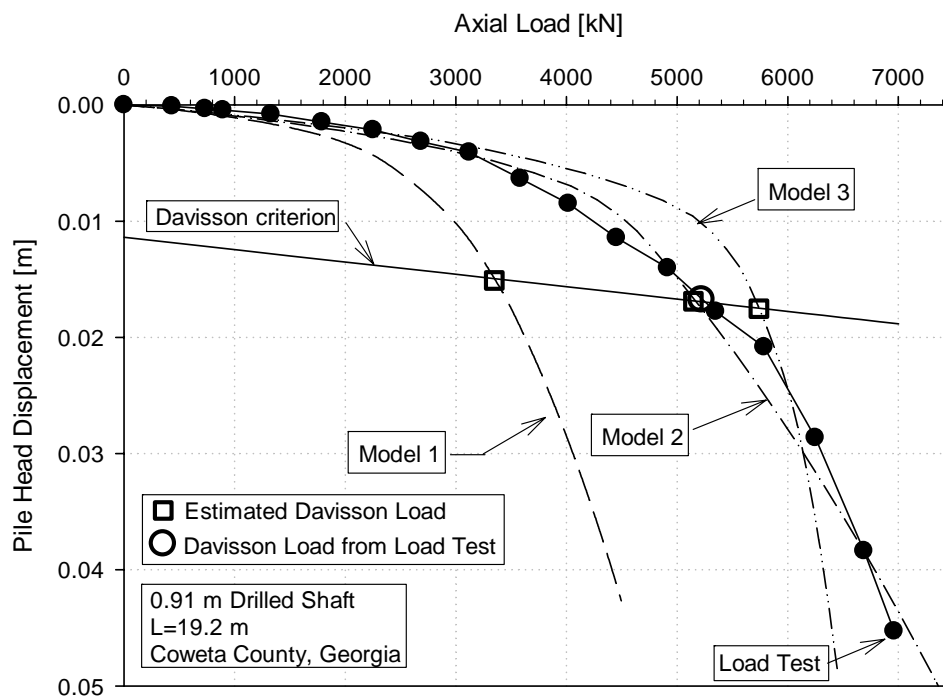


Figure 4-9 Modified Type A prediction for axial pile under a bridge in Coweta County

With the corrected pile base capacity good agreement was obtained for the entire load settlement curve for Model 2. Model 1 still underpredicted pile capacity by 40 % and Model 3 overpredicted Davisson failure load by 10 %.

Although Model 3 gave a reasonably good approximation for the initial portion of the curve, the predicted curve suggests that shaft capacity may have been overestimated. Model 1, in the other hand, underpredicted shaft capacity.

For the drilled shaft studied in this case, type A predictions using directly the three models presented earlier did not give accurate estimates of the Davisson failure load. However, as shown with the modified predictions with modified unit end bearings, this may be attributed to particular geotechnical conditions at the site which involved a large sudden contrast in CPT tip resistance at the soil weathered bedrock interface. This marked difference in resistance between adjacent layers was seen to greatly affect the estimation of the average cone tip resistance used to estimate the unit end bearing of the pile. Using higher unit end bearing values gave relatively good results. This modification was found justified since larger unit bearing capacity is expected in the weathered rock below the pile tip.

4.2.3 DRILLED SHAFT AT GEORGIA TECH CAMPUS

The third case history studied entailed a drilled shaft load testing program conducted at the Georgia Institute of Technology (GT) campus and described by Mayne and Dumas (1997). The analyzed drilled shaft had a length of 16.7 m and a diameter of 0.76 m. The site is located within the piedmont geologic province of the US, as were the two previous case studies. A complete geotechnical site characterization carried out for the load testing

program is presented in Mayne and Dumas (1997). Results from CPTs advanced at the site show a fairly uniform profile with a slight linear increase in soil resistance with depth. For this case history SASW (Spectral Analysis of Surface Waves) results were available to provide a shear wave velocity profile for the site.

The CPT sounding advanced at the site and used to develop the numerical model for the drilled shaft at Georgia Tech Campus is shown in Figure 4-10. In the same figure the predicted and measured shear wave velocity profiles are also shown.

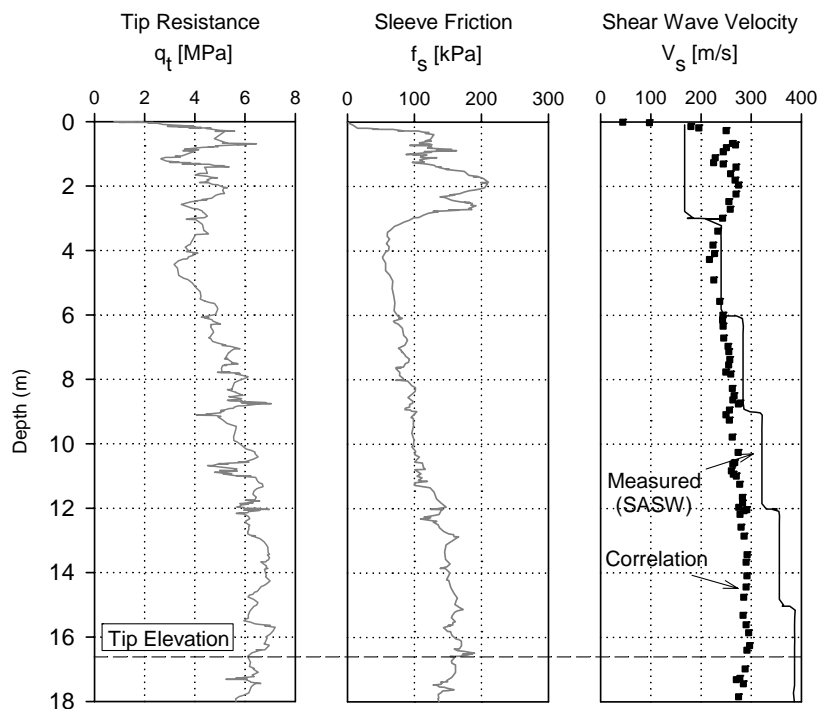


Figure 4-10 Shear wave velocity and CPT sounding advanced at Georgia Tech Campus, Georgia

The results of the numerical model of the drilled shaft at Georgia Tech Campus, obtained with the procedure outlined before are summarized in the following paragraphs.

Figure 4-11 shows the axial pile capacity with depth for the drilled shaft at Georgia Tech campus estimated using each one of the three methods described in Chapter 3. Ultimate axial pile capacity is summarized in Table 4-4.

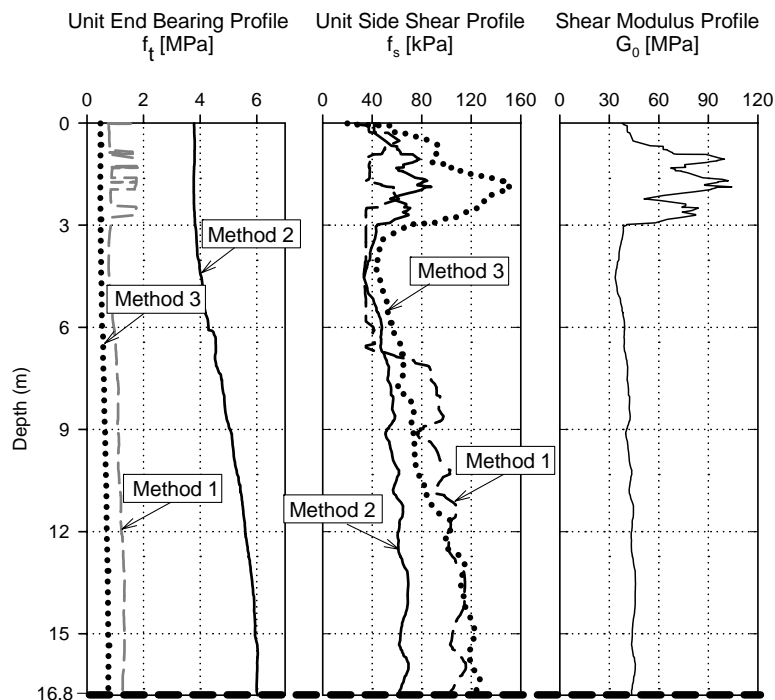


Figure 4-11 Static axial pile capacity and shear modulus profile for a 0.76 diameter drilled shaft at Georgia Tech Campus, Georgia

Table 4-4 Predicted axial pile capacity for a drilled shaft at GT campus

Method	Shaft Capacity [kN]	Tip Capacity [kN]	Total Capacity [kN]	Davisson Load [kN]
1	3030	570	3600	2870
2	2270	2730	5000	2870
3	3470	344	3814	2870
Load Test	-	-	> 4500	2870

Class A predictions obtained using the proposed numerical analysis are compared with pile load test results in Figure 4-12. In this figure, it can be seen that load settlement curves predicted by the numerical analyses showed good agreement with that measured

in the field for the initial portion of the load test curve. However the agreement is not as good for the last portion of the curve beyond 2800 kN of axial load. It can be seen, that models 1 and 3 overpredicted the Davisson failure load while model 2 gave a reasonably good estimate.

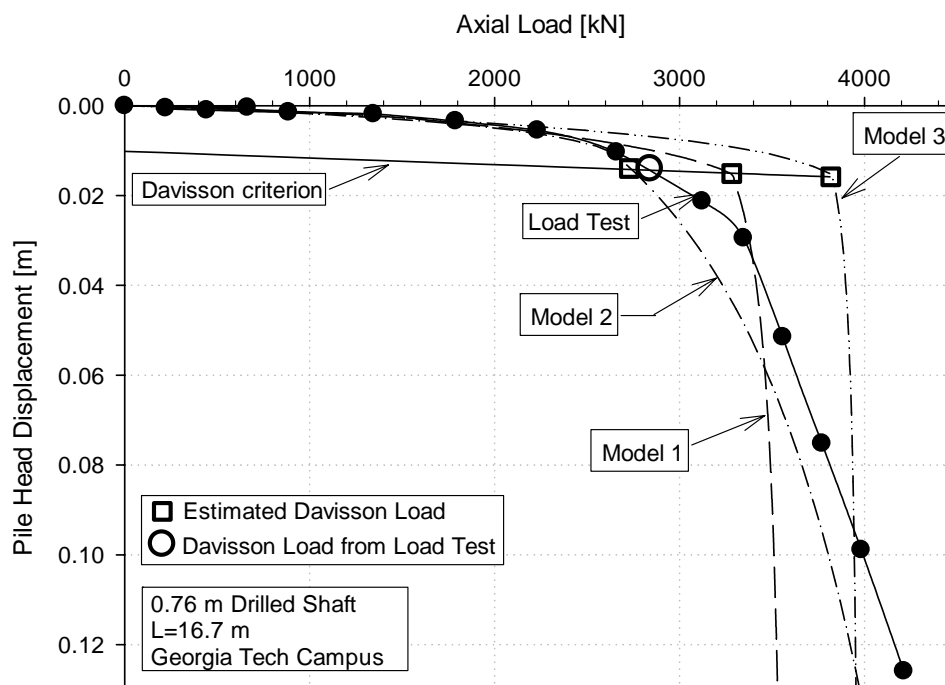


Figure 4-12 Type A predictions for axial pile tested at GT campus

In order to improve the agreement between predicted and measured load settlement curves for the entire measured load settlement curve a type B prediction for model 2 was performed adjusting parameter g and poisson ratio for the layer under the pile tip. No type B predictions were made for models based on methods 1 and 3 since it was found that in order to improve the agreement it was necessary to reduce the calculated shaft capacity of the pile. This was considered inappropriate since no logical reason was found to justify decreasing the side friction values for Models 1 and 3. The overpredicted

Davisson failure load for Models 1 and 3 seem to be related to the high unit side friction values.

The type B prediction obtained by setting the fitting parameter g equal to 0.4 and ν equal to 0.35 for the layer under the pile tip is shown in Figure 4-13. Original values for these parameters used in the type A prediction were 0.3. Very good agreement is observed for the adjusted model for the entire load settlement curve.

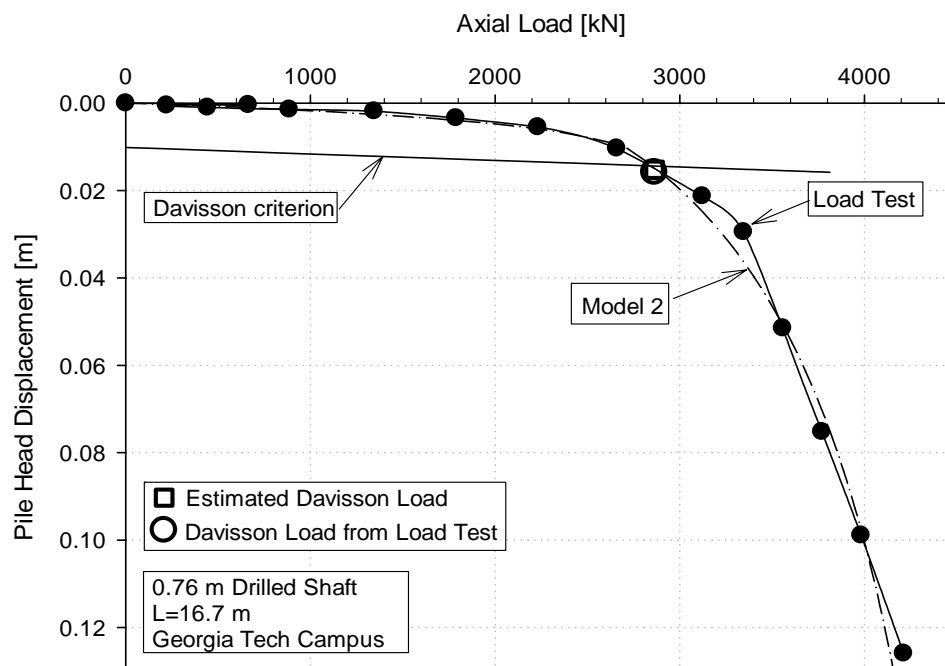


Figure 4-13 Type B prediction for the pile tested at GT campus

This case history had the advantage that load transfer data was available from readings in strain gages located at 9 m deep and a tell tale system cast in the pile tip during construction. Comparison of the load transfer along the shaft from the Type B prediction with the measured load transfer is shown in Figure 4-14. Good agreement is observed between predicted and measured values for almost the complete loading range.

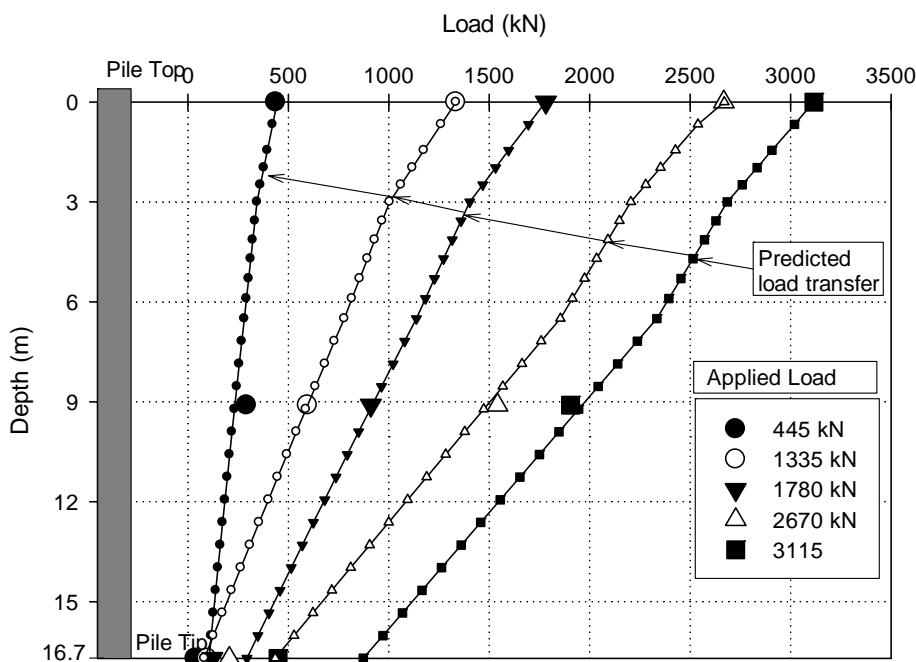


Figure 4-14 Predicted Vs. measured load transfer with depth for model 2

4.2.4 DRILLED SHAFT AT NGES NEAR TEXAS A&M UNIVERSITY, TEXAS

This case study involves a load test performed on an instrumented drilled shaft ($L = 10.4$ m and $D = 0.91$ m) tested at the National Geotechnical and Experimental Site near Texas A&M University. The site has been extensively characterized and detailed geotechnical information can be found elsewhere (Briaud and Gibbens, 1994). The generalized soil profile consists of silty to clayey sands up to 12.5 m underlain by hard clay shale. A representative SCPT sounding conducted at this site by Tumay and Bynoe (1998) is shown in Figure 4-15, together with predicted and measured shear wave velocities up to 15 m deep. The SCPT sounding showed a fairly uniform shear wave velocity profile with an average value of about 300 m/s from the ground surface to a 15 m depth.

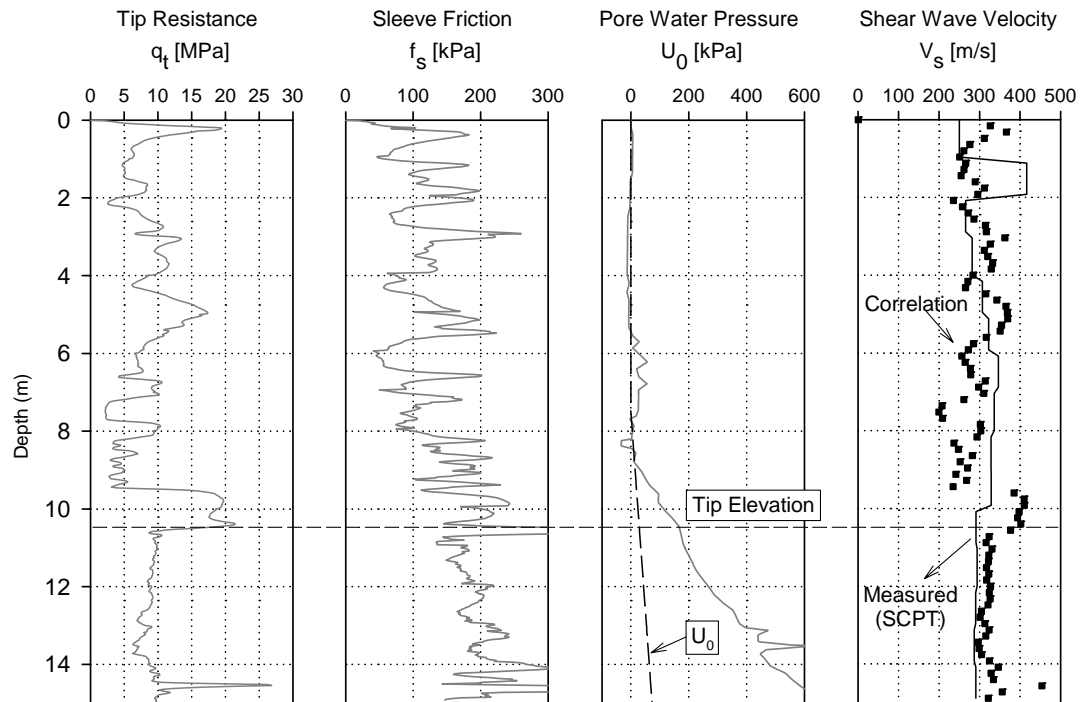


Figure 4-15 Shear wave velocity and CPT sounding advanced at Texas A&M Campus, Texas

The results of the numerical model of the drilled shaft at NGES near Texas A&M University, obtained with the procedure outlined before are summarized in the following paragraphs.

Figure 4-16 shows the axial pile capacity for the drilled shaft in the NGES near Texas A&M University estimated using each one of the three methods described in Chapter 3. Ultimate axial pile capacity is summarized in Table 4-5.

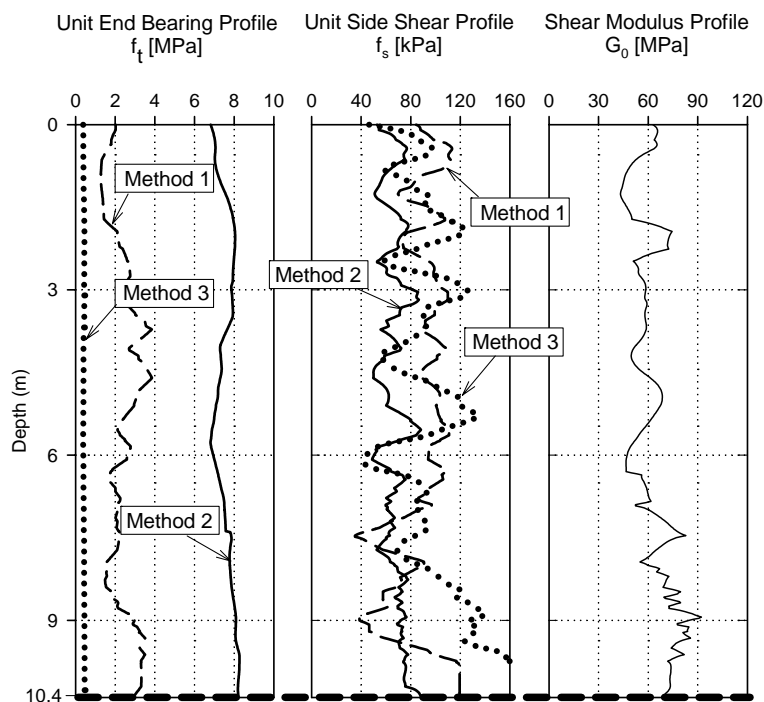


Figure 4-16 Static axial pile capacity and shear modulus profile for a 0.91 diameter drilled shaft at Texas A&M Campus, Texas

Table 4-5 Predicted axial pile capacity for a drilled shaft in Texas

Method	Shaft Capacity [kN]	Tip Capacity [kN]	Total Capacity [kN]	Davisson Load [kN]
1	2700	2190	4890	2945
2	2010	5450	7460	2945
3	2975	686	3661	2945
Load Test	-	-	3500	2945

As shown in Figure 4-17 all models predicted reasonably well the initial portion of the load test curve up to an axial load of about 2000 kN. From Figure 4-17 it may be inferred that Model 1 predicted reasonable well pile base capacity and overpredicted the shaft capacity. Since the slope in the non-linear part of the predicted and measured curves agree reasonably well. Model 3 seemed to have overpredicted pile shaft capacity for a similar amount as model 2, pile base capacity estimated by method 3 seems to be lower than the actual pile tip resistance. Model 2, on the other hand, seems to slightly

underpredict shaft capacity and to overpredict pile base capacity. However Model 2 gave the closest approximation to the Davisson failure load of the three models.

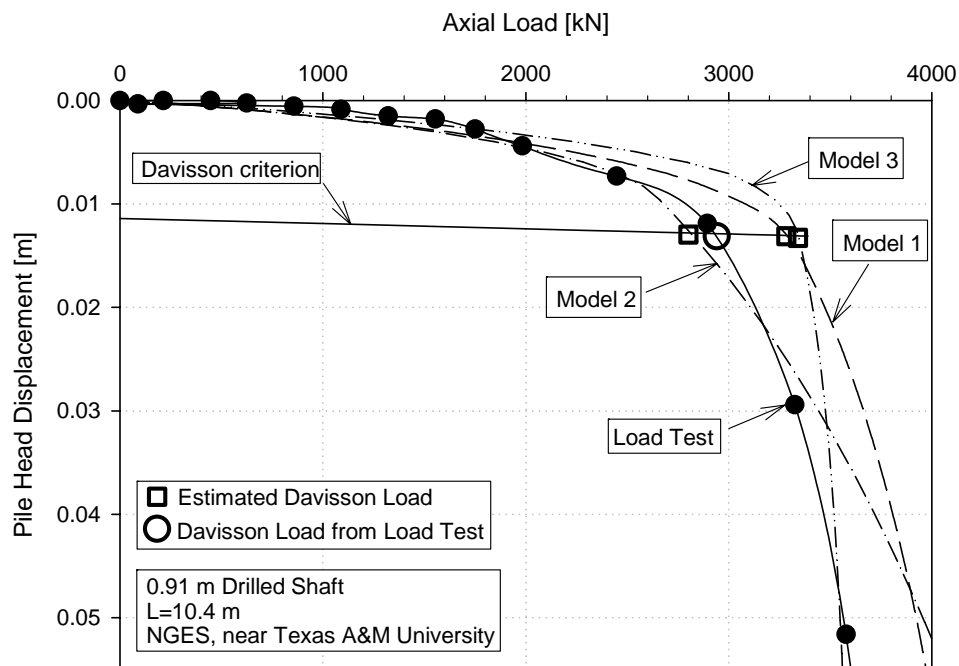


Figure 4-17 Type A predictions for axial pile tested at NGES in Texas

For this pile, the load transfer along the shaft was available through readings on three strain gages located at different elevations along the shaft. Load transfer for the model based in method 1 is depicted in Figure 4-18, where it can be seen that the model can accurately predict the load transfer for loads smaller than 2000 kN. However, for higher loads, the model tends to overpredict both shaft and base capacity giving as a result the stiffer load settlement curve shown in Figure 4-18.

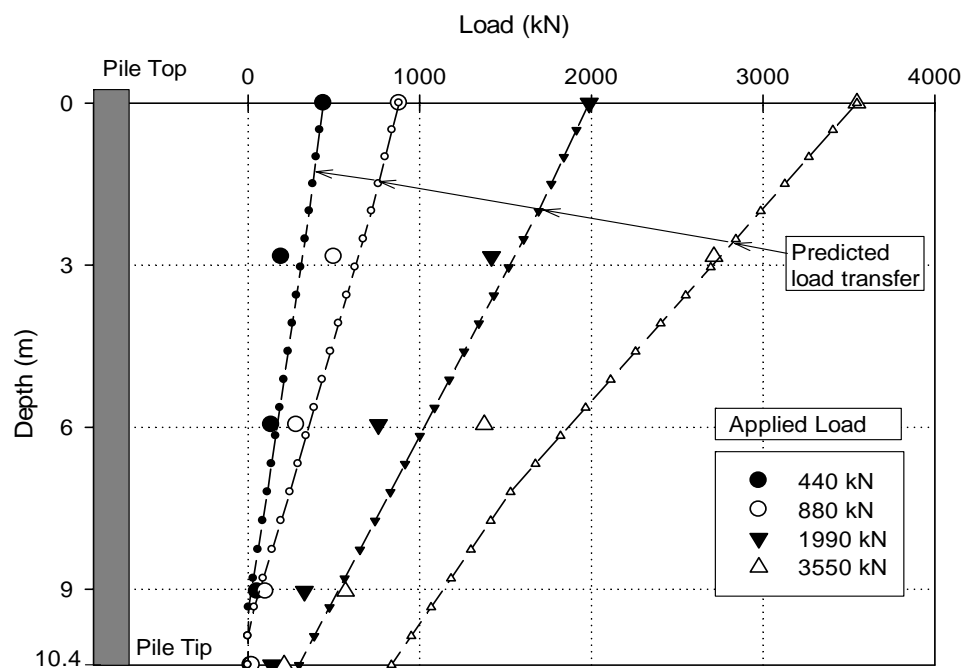


Figure 4-18 Predicted Vs. measured load transfer with depth for Model 1

The load transfer with depth for the second model is shown in Figure 4-19. Similar to model 1, the numerical solution gives higher tip loads than those actually developed during the field test. In the numerical model, however, this is counterbalanced by a slightly underpredicted shaft capacity to yield a fairly accurate Davisson failure load. For applied loads larger than 2000 kN side resistance had been fully mobilized in the numerical model, and any additional load must be carried through the pile tip, as evident from Figure 4-19.

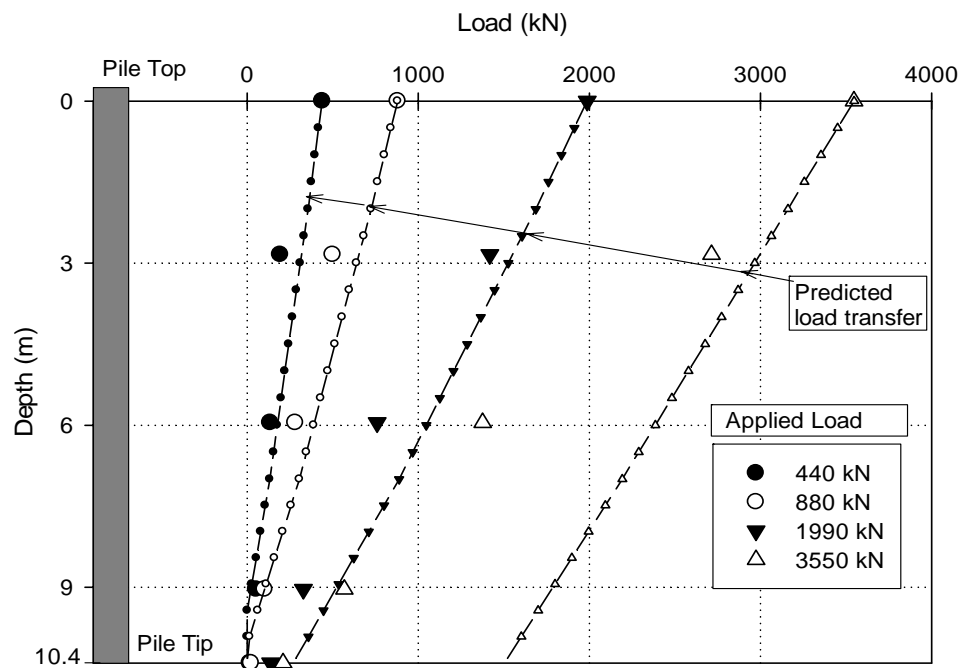


Figure 4-19 Predicted Vs. measured load transfer with depth for model 2

The load transfer with depth for the third model is shown in Figure 4-20. This case is similar to model 1 in that a small base capacity was predicted by static method 3 and pile shaft capacity was slightly over predicted. This can be seen in Figure 4-20 where for loads higher than 2000 kN load transfer curves depart from the measured values at approximately mid length of the pile. However, despite model three did not give the best estimation of the failure load it did give the best representation of the actual load transfer behavior with depth.

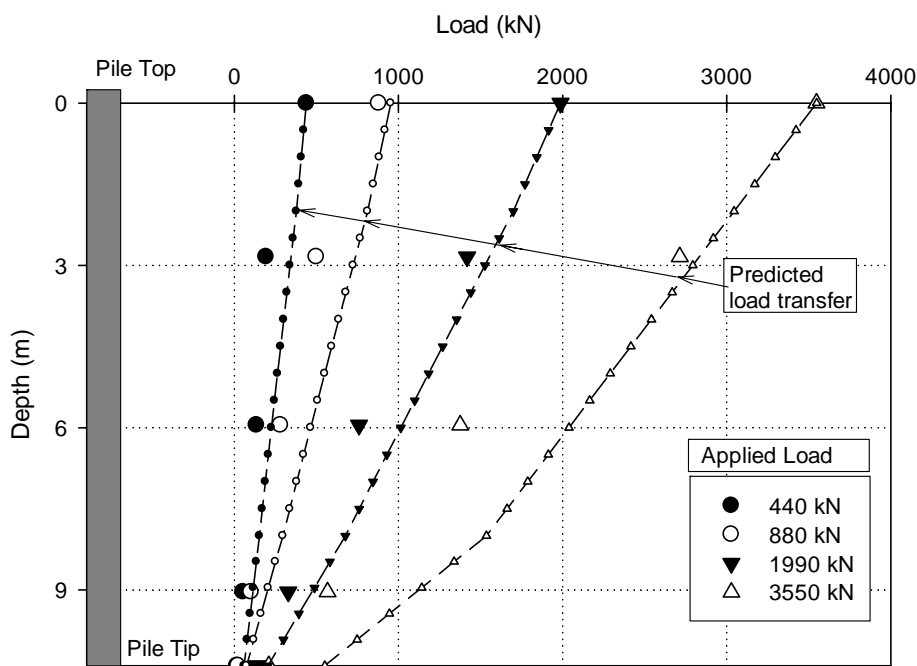


Figure 4-20 Predicted Vs. measured load transfer with depth for model 3

4.2.5 DRILLED SHAFT IN A PROJECT IN THE OLD SAN JUAN AREA, PUERTO RICO

The last case history treated in this chapter corresponds to a test pile for a project located in the Old San Juan area, in Puerto Rico. The project consisted of three high-rise apartment buildings founded on piles. An extensive pile testing program was developed at the site which allowed the designer/contractor to reduce the factor of safety for the piles.

The diameter of the pile being modeled was 0.41 and the tip depth was about 11.6 m. Results from two SCPT tests were used to determine the required asymptotic parameters for the load transfer curves. SCPT soundings and estimated shear wave velocity profile are shown in Figure 4-21.

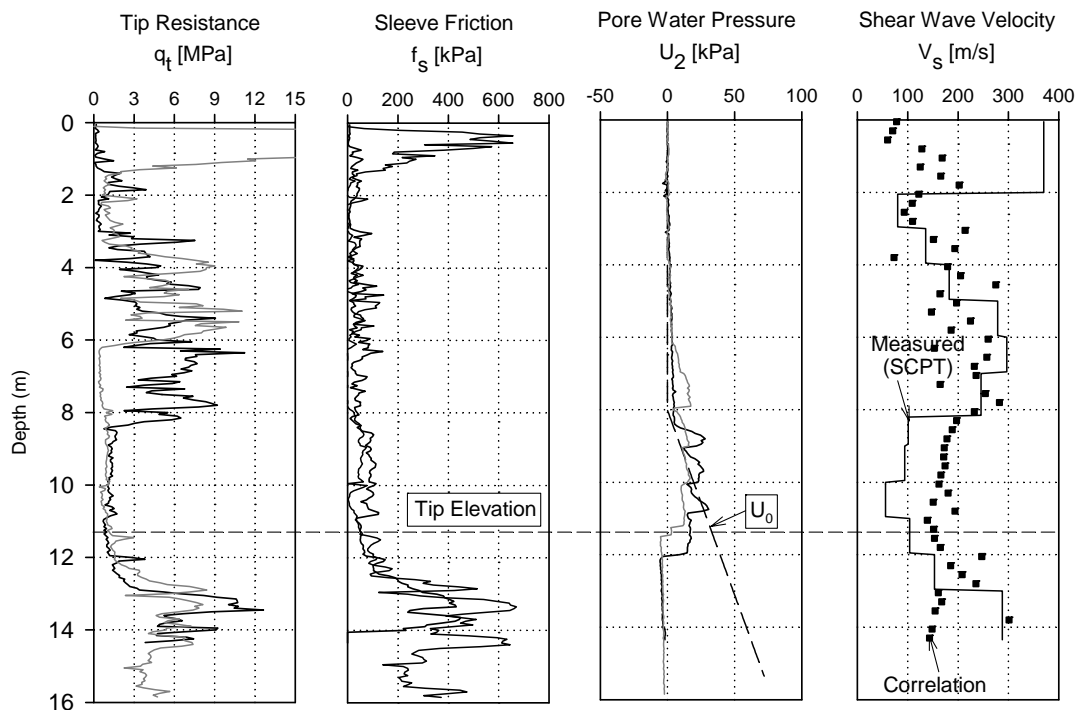


Figure 4-21 Shear wave velocity and CPT soundings advanced in the Old San Juan area, Puerto Rico

The results of the numerical model of the drilled shaft in Puerto Rico, obtained with the procedure outlined before are summarized in the following paragraphs.

Figure 4-22 shows the axial pile capacity for the drilled shaft in Puerto Rico estimated using each one of the three methods described in Chapter 3. Ultimate axial pile capacity is summarized in Table 4-6.

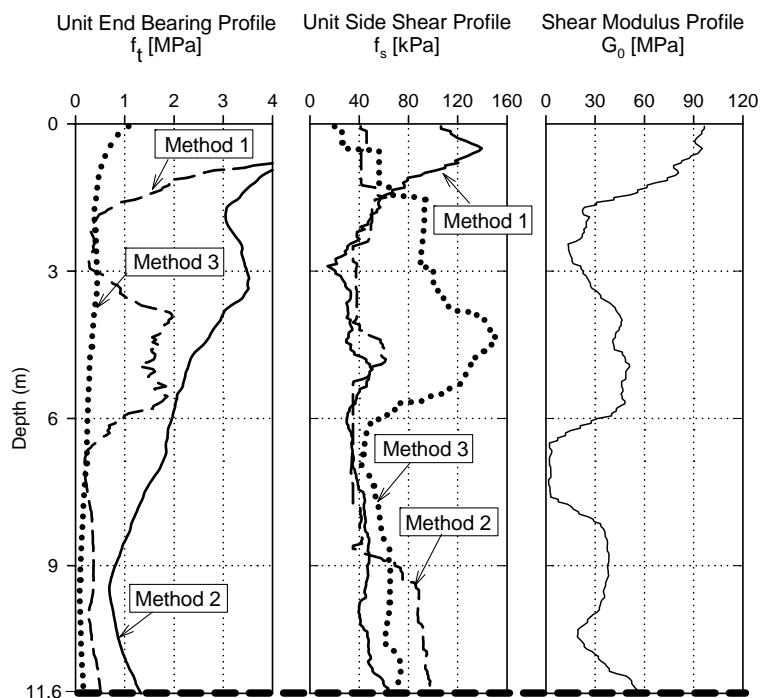


Figure 4-22 Static axial pile capacity and shear modulus profile for a 0.41 diameter drilled shaft in the Old San Juan area, Puerto Rico

Table 4-6 Predicted axial pile capacity for a drilled shaft in Puerto Rico

Method	Shaft Capacity [kN]	Tip Capacity [kN]	Total Capacity [kN]	Davisson Load [kN]
1	532	52	584	883
2	700	280	980	883
3	630	285	913	883
Load Test	-	-	1150	883

Results of class A predictions obtained with the numerical analyses are shown in Figure 4-23.

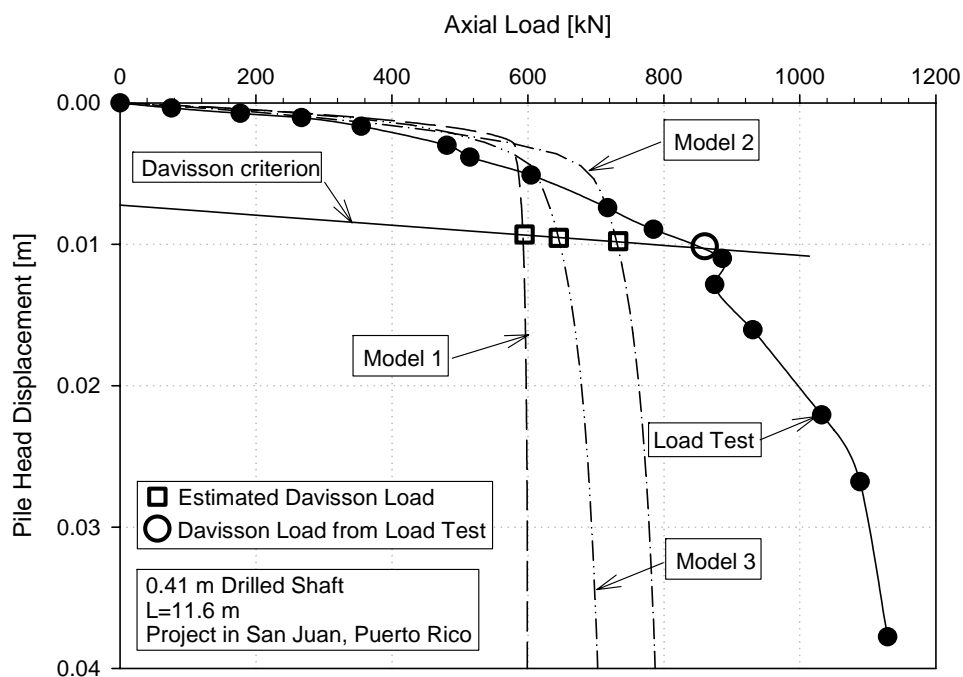


Figure 4-23 Type A predictions for axial pile tested at a project in the Old San Juan area, Puerto Rico

Class A predictions for the drilled shaft in Puerto Rico showed a highly underestimated pile capacity, for the three numerical models. As a consequence, predicted Davisson failure loads for models one through three were, respectively, 25%, 44%, and 30% smaller than that obtained from field measurements. No additional runs were performed in order to improve the type A predictions since the bad agreement was attributed to a very small pile tip capacity obtained with static methods 1, 2 and 3.

4.3 PILE CAPACITY PREDICTION USING THE PROPOSED METHODOLOGY

This sections presents comparisons of the ultimate axial capacity measured during the load test with the ultimate capacity predicted using the three CPT based static methods. It is known that the estimation of the ultimate pile capacity is a challenging task and

extremely erroneous results can be obtained (Eslami and Fellenius, 1997; O'Neill, 2001; and Olson, 2002). This is one of the reasons why safety factors in pile design are in the order of 3 or higher. Figure 4-24 shows predicted versus measured ultimate pile capacities, for the five cases studied in this chapter. As can be seen in that figure, ultimate pile capacity predictions using CPT based static methods did not give accurate results and only 50 % of the predictions are within a $\pm 20\%$ range with respect to the perfect match represented in the figure by the solid line.

From the approaches chosen to estimate pile axial capacity it was found that the method proposed by Eslami and Fellenius (1997) usually overpredicted the ultimate axial capacity of the pile. This was primarily related to an overestimated tip capacity. In this regard, the combination of side shear capacity estimated by Takesue et al. (1998) with end bearing capacity calculated using recommendations by Lee and Salgado (1999) gave the closest agreement to the pile ultimate load obtained from field data, as can be observed in Figure 4-24.

In order to assess the suitability of the proposed methodology to predict pile capacity, the Davisson failure loads of the numerical models were compared with those measured in the field. This is depicted in Figure 4-25.

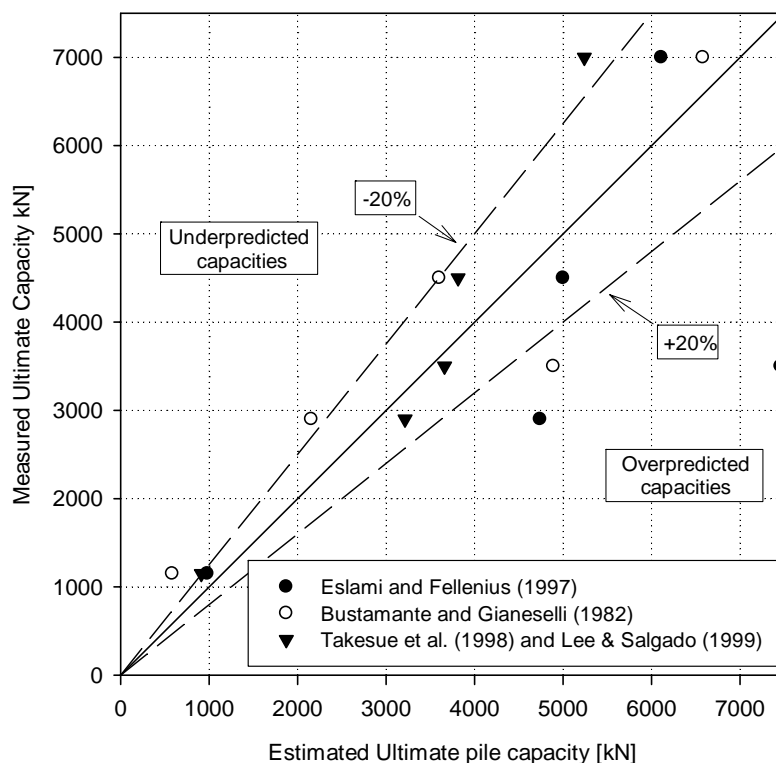


Figure 4-24 Ultimate pile capacity predicted vs Davisson failure load from load test for case studies one through five

Although the method by Eslami and Fellenius (1997) overpredicted ultimate pile capacity, load transfer models based on this method gave the best approximations to the measured Davisson failure load. In most cases, good agreement of the entire predicted and measured load settlement curve was observed for Model 3. In Figure 4-25 it can be seen that 30 % of the predictions lay outside the $\pm 20\%$ range. Furthermore, pile capacity obtained with Models 3 lay within a $\pm 10\%$ range for four out of the five cases. This may be attributed to a slightly underpredicted shaft capacity which seems to be counterbalanced with an overpredicted tip capacity when using the method by Eslami and Fellenius (1997) for estimating asymptotic values of the load transfer curves.

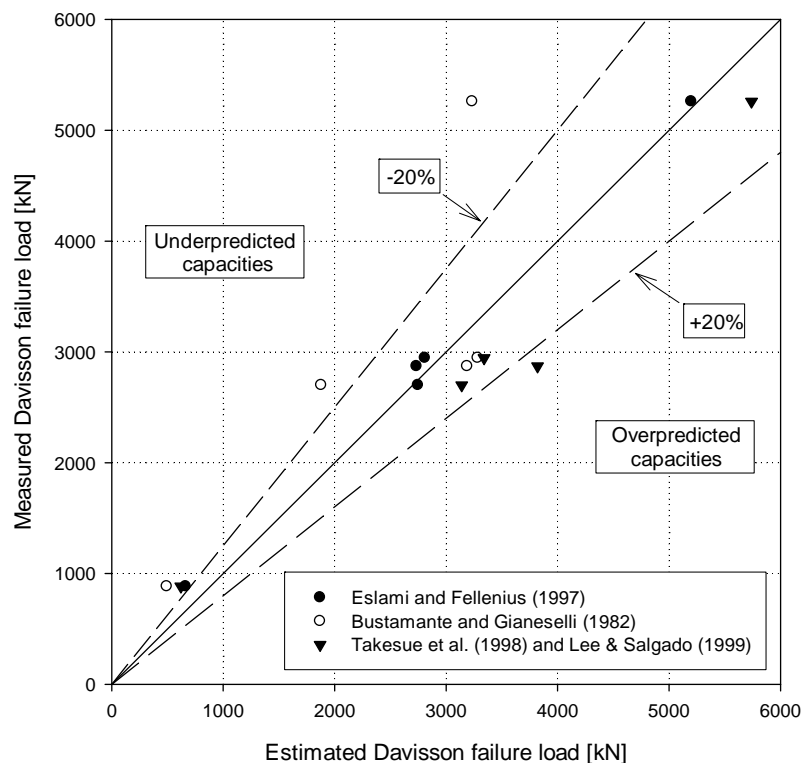


Figure 4-25 Davisson failure load estimated using the proposed CPT based load transfer approach methodology

4.4 SUMMARY AND CONCLUSIONS

The proposed methodology was applied to the study of five case histories for which the entire load settlement curve of the pile was available. For most of the cases reasonably good agreement was found between the predicted and measured load settlement curves for the type A predictions.

The theoretical load transfer curves chosen for this work include two fitting parameters: f and g . Values for these constants were unknown in advance, but they were found to have great influence on the load transfer curves. In this regard, Mayne and Schneider (2001) pointed out that parameter g ranges between 0.2 and 0.4 for most soils. These authors also stated that $g = 0.3$ and $f = 1$ were reasonable first-order estimates for

most cases. In all case studies presented in this chapter, initial values of $f = 0.98$ and $g = 0.3$ were used following the study by Mayne and Schneider (2001). These values were found to yield reasonably good results for all cases.

Of the five case histories presented, one showed improved agreement by slightly modifying the hyperbolic parameters f and g . However, for most cases, numerical results seemed to depend to a greater extent on the asymptotic values of the load transfer curves than on the fitting constants f and g . The fact that fitting constants f and g were kept constant for all case histories reduces the number of uncertainties involved in the proposed methodology improving the reliability of its application to other case studies.

Good agreement was found between predicted and measured Davisson failure loads, especially for models based on pile capacity estimated by Eslami and Fellnius (1997). It may be also noted that in all cases good agreement was found for the initial linear part of the load settlement curves recorded in the field. This may be useful in the designing stage of a project in order to obtain reliable estimates of pile settlements for working loads.

5 LOAD SETTLEMENT BEHAVIOR OF POST GROUTED PILES

5.1 INTRODUCTION

In the last 30 years, the trend in the design and construction of deep foundations has been seen to move towards the use of large diameter piles or piers to increase load bearing capacity (Stoker, 1983). However, for small to medium projects construction difficulties and higher associated costs usually continue to favor designs using conventional smaller pile diameters (Stocker, 1983). This is one of the reasons why continuous attempts are being made to improve deep foundation performance (i.e., increased load bearing capacity and lower settlements) without increasing pile diameter. In this regard, post grouted drilled shafts (PGDS) have shown good performance, especially in sandy soils (Bolognesi and Moretto, 1973; Stocker, 1983; Brusey, 2000; Mullins and Winters, 2004).

The main objective of this chapter is to present a description of the main factors that are believed to control the soil-foundation behavior of axially loaded post grouted piles. These factors are: (1) Compression of the soil under the pile tip due to tip grouting,

(2) Stress reversal along the shaft due to the upward movement of the shaft during tip grouting, and (3) increase of the effective pile tip area due to the formation of a grout bulb. Although the three mentioned factors may occur simultaneously, here are studied separately in order to: (a) examine the influence of each factor on the behavior of the post grouted pile, and (b) find an adequate representation of each factor within the proposed procedure for estimating pile settlements presented in Chapter 3.

In addition to describing the aforementioned factors, this chapter presents the proposed methodology to include these factors in the numerical modeling. The adequacy of the implementation of these factors in the numerical models will be assessed by comparisons with case histories in the next chapter. The manner in which each one of the aforementioned factors were included in the numerical models is also discussed in the following sections.

The following three subsections present a brief description of the effects that each of the factors mentioned above have on the behavior of the pile-soil system and how these factors can be incorporated in the load transfer model presented in Chapter 3. The last subsection presents a summary and conclusions of this chapter.

5.2 BEHAVIOR OF POST GROUTED DRILLED SHAFTS

As stated in Chapter 2, several researchers have reported important pile capacity improvements by pressure grouting of the pile tip. It was also discussed in that chapter, that up to date, the design of post grouted pile has been done using empirical approaches. Examples of the important benefits of pile tip grouting are shown in Figure 5-1-a and

Figure 5-1-b. In these figures it can be observed that the post grouted drilled (PGDS) is capable of carrying larger loads than a conventional pile installed in similar conditions, for a given pile head settlement.

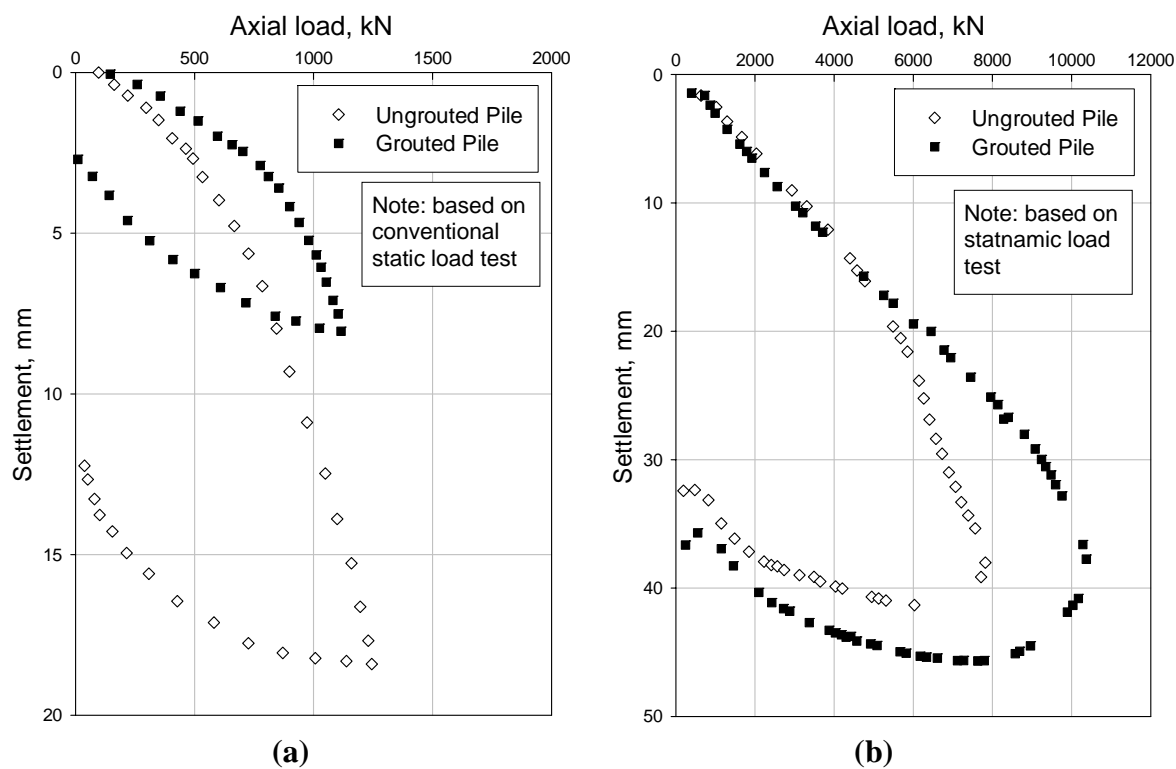


Figure 5-1 Pile capacity improvement for a drilled shaft in (a) Venezuela and (b) Florida

Despite that some researchers have attributed the pile capacity improvement to factors such as compression of the soil under the tip and the formation of a grout bulb under the shaft, to the best knowledge of the author, no attempts have been made to theoretically study or quantify these factors. Mullins and Winters (2004) reported that shear stress reversal occurs along the shaft of a pile during grouting, concluding that this effect may also contribute to the improved performance observed in PGDS. However, the research conducted by these investigators did not quantify the mentioned stress reversal and the

main focus of their work was aimed at pile end bearing improvement due to post grouting.

For the aforementioned reasons, the main motivation for this work was to study the behavior of post grouted drilled shafts within a theoretical framework. Factors believed to be the main contributors of the improved PGDS performance by previous researchers are discussed in this chapter and recommendation for their incorporation in load transfer models are given. It is believed that a theoretical framework for PGDS would improve the confidence in the use of this type of piles which, in turn, may increase the use of PGDS in the US mainstream engineering practice.

5.3 FACTOR 1: SOIL COMPRESSION UNDER THE PILE TIP

As explained earlier in Chapter 2, during the post grouting stage, cementitious slurry is injected at high pressure through pipes that exit at the pile tip. The grout is received by a flexible membrane that expands due to the incoming grout and hence is pushed against the soil. During this process the stress field in the nearby surrounding soil increases, resulting in a compression and densification of the soil under the pile tip. The magnitude of the densification and the extent of the zone of soil influenced by this grouting process are difficult to estimate. The improvement in the soil conditions under the pile tip would result in an increased cone tip resistance values which would not only correspond to an increased shear modulus but also to an increased ultimate unit end bearing. However, asymptotic values in Q_b - Z curves were not modified when modeling factor 1.

The compression effects due to tip post grouting can be included in the load transfer model by modifying the spring properties that represent the tip resistance (Q_b - Z load transfer curve). This is schematically shown in Figure 5-2. As shown in this figure, the resulting Q_b - Z curve represents a stiffer response of the pile tip and an increased ultimate resistance (asymptotic value of Q_b - Z curve). This is a reasonable assumption due to the post grouting process.

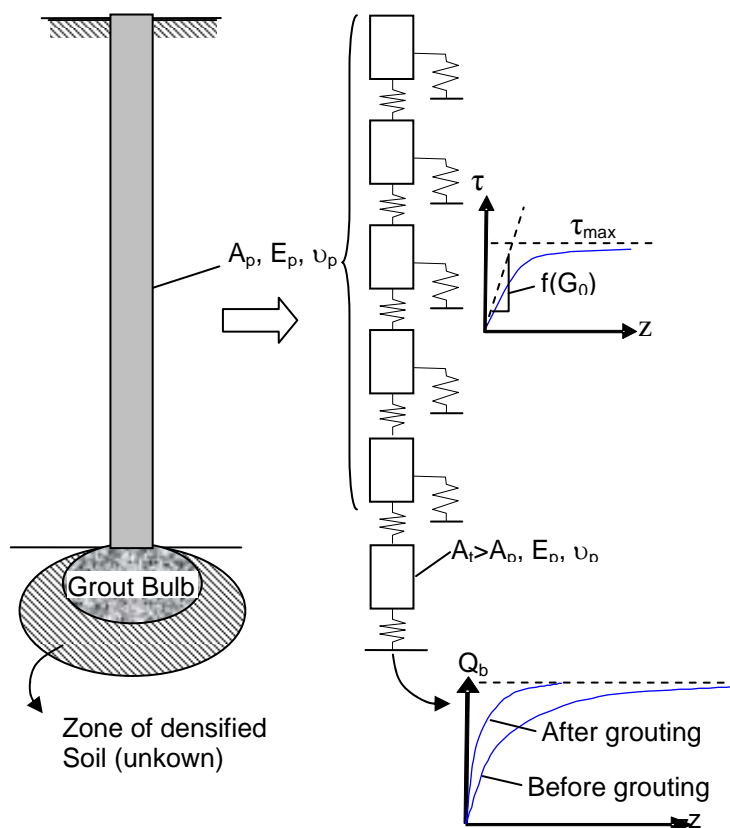


Figure 5-2 Effect of soil compression under the bottom of the pile on the load-transfer curve at the tip

However, normally, large deformations are required to mobilize the ultimate pile base resistance. Hence, for normal level of deformations measured in the case histories it was

considered adequate enough to only modify the initial stiffness of the load transfer curve. Therefore, to account for compression and densification effects in the soil under the pile tip due to tip post grouting the Q_b - Z curve was modified simply by assuming an increased shear modulus, G . The primary effect that an increased shear modulus has on the Q_b - Z curve is to provide a steeper initial slope. The influence of the shear modulus on the pile tip load transfer curve is illustrated in Figure 5-3.

As mentioned earlier, asymptotic values of the Q_b - Z curve were not modified due to the large deformations required to mobilize the ultimate tip resistance and also because the ultimate tip capacity, in CPT based static methods, is estimated using a weighted average cone tip resistance values averaged over a large depth range that will still include a large zone of unimproved ground (i.e., outside the zone of influence of the grout bulb).

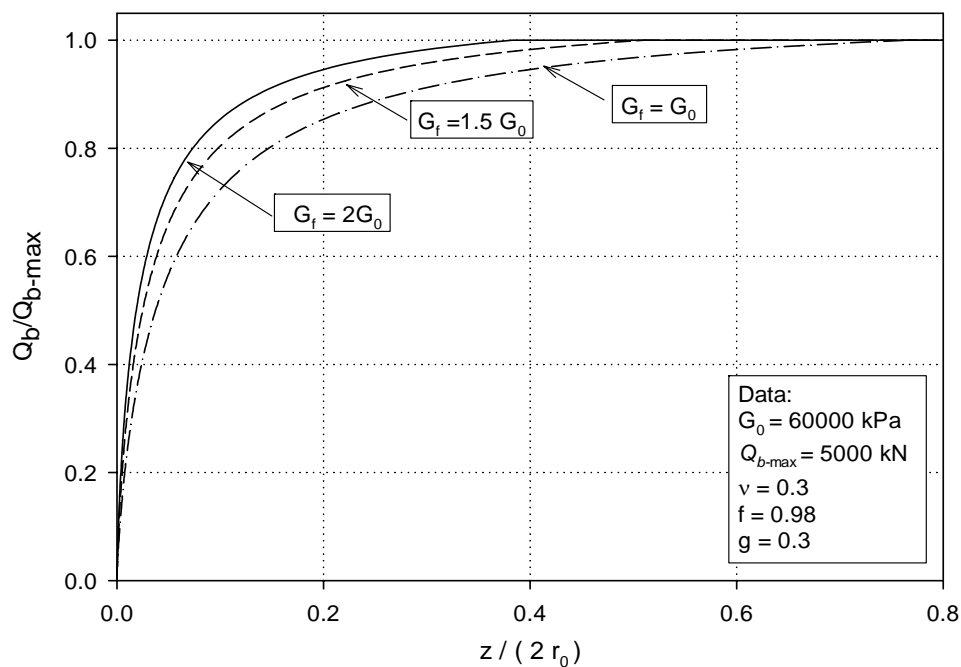


Figure 5-3 Effect of an increased soil shear modulus on the Q_b - Z curve

5.4 FACTOR 2: STRESS REVERSAL ALONG THE SHAFT

Another effect of the grouting of the pile tip is the upward movement of the drilled shaft. As the pile moves upward shaft resistance is mobilized in negative skin friction (i.e., the mobilized shear stresses point downwards reacting to the upward movement of the pile). This effect can be incorporated in the analysis if some rule of cyclic loading is used. A commonly used cyclic model for soils is the one proposed by Masing (1926), known as the Masing rule. This model assumes that the soil presents a symmetric backbone curve. Thus, if this soil behavior can be attributed to the soil along the pile shaft, the Masing rule can be applied to load transfer curves which represent the pile resistance in skin friction, as illustrated schematically in Figure 5-4.

The Masing rule states that a hysteresis loop can be described by two branches, one above the backbone curve of the soil (Figure 5-4, curve **acb**) and one below (Figure 5-4, curve **adb**). According to the Masing rule, the upper branch is equal to the backbone curve located in the first quadrant (curve **Ob**), but it has ordinates and abscissas doubled in value. In the same way, the lower branch is equal to the backbone curve branch located in the third quadrant (curve **aO**), also extended to the double in ordinates and abscissas.

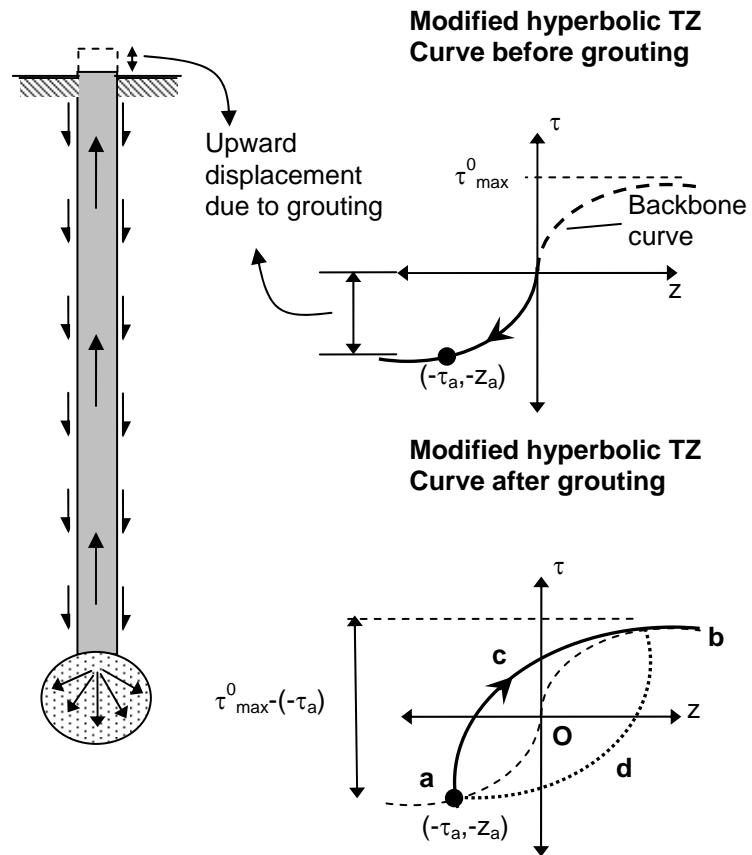


Figure 5-4 Effect of stress reversal on the load-transfer curve of soil along the shaft

Assuming that a constitutive law for the soil of the form $\tau = f(\gamma)$ is known, the Masing rule described before can be expressed as (Suárez, 2003):

$$\tau = \tau_a + n \cdot f\left(\frac{\gamma - \gamma_a}{n}\right) \quad (5.1)$$

Where: τ_a = shear stress resulting from the stress reversal due to grouting

γ = angular distortion of the soil

γ_a = angular distortion of the soil corresponding to τ_a

n = coefficient equal to 1 to recover the backbone curve and equal to 2 for subsequent loading and reloading cycles.

Equation (5.1) needs to be modified to include the constitutive law defined in Chapter 3 as $z = f(\tau_0/\tau_{\max})$. Incorporating this into equation (5.1) results in:

$$z = z_a + n \cdot f\left(\frac{\tau_0/\tau_{\max} - \tau_a/\tau_{\max}}{n}\right) \quad (5.2)$$

Applying the above general expression to the load transfer curve derived in Chapter 3 (Equation (3.26) and (3.27)), results in the following modified hyperbolic load transfer curve that accounts for shear stress reversal:

$$z = z_a + \frac{(\tau_0 - \tau_a)r_0}{G_0g} \ln \left(\frac{\left(\frac{r_m}{r_0}\right)^g - f\left(\frac{\tau_0 - \tau_a}{\tau_{\max} \cdot n}\right)^g}{1 - f\left(\frac{\tau_0 - \tau_a}{\tau_{\max} \cdot n}\right)^g} \right) \quad (5.3)$$

Where: τ_a = maximum negative shear stress resulting from the upward movement during grouting, at a given elevation

z_a = maximum upward movement due to grouting, measured at the same elevation of τ_a

Incorporating the Masing rule in the T-Z formulation is equivalent to shifting the origin of the T-Z curve to the point with coordinates $(-\tau_a, -Z_a)$ which is shown for a specific load transfer curve, obtained using equation (5.3), in Figure 5-5. In this figure,

only the upper branch of the hysteresis loop was plotted since it is assumed that the pile undergoes only one reloading cycle after grouting.

If the shaft uplift is measured during grouting, the amount of stress mobilized along the shaft can be estimated, once load transfer curves are available for the layers along the shaft. Negative stresses developed in the soil after grouting can be used to redefine the load transfer curve for each one of the soil layers along the shaft. The resulting TZ-curve will reflect the effect of upward loading in that the asymptotic value of the new curve will be increased by the amount of the mobilized negative stress due to grouting.

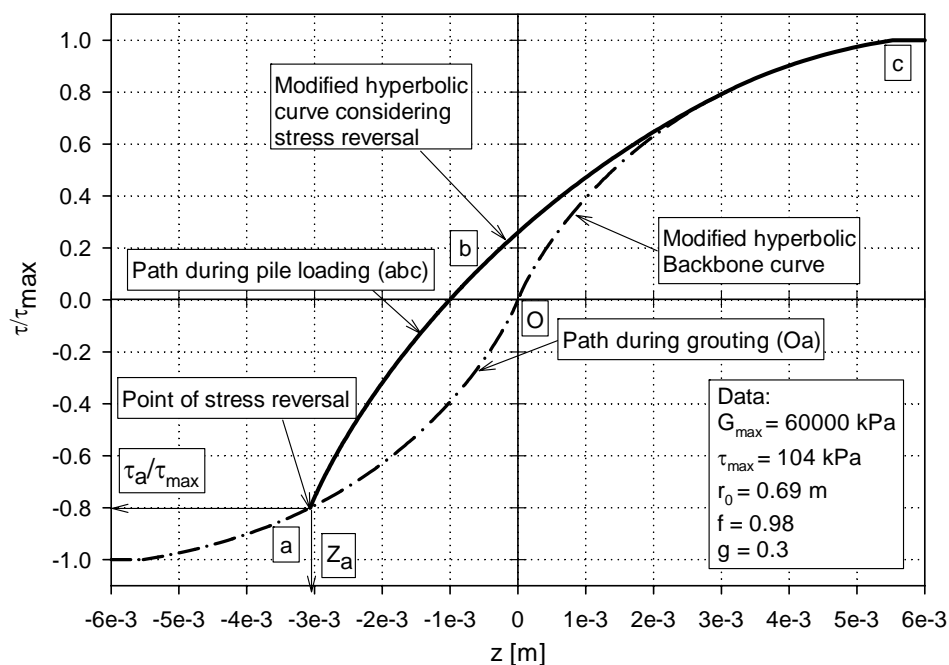


Figure 5-5 Masing rule applied to a TZ curve

For stiff or sensitive soils that show a marked post-peak strain softening, care must be taken during the grouting process. Excessive upward displacement of the shaft may result in a decreased shaft or skin friction resistance due to strain softening. For strain

softening soils the potential benefits of post grouting may not be as evident since at least the improvement due to shear stress reversal may be lost.

Since the soil under the pile tip does not experience a load-reversal after grouting, the Q_b -Z curve does not need to be modified by applying the Masing rule.

5.5 FACTOR 3: INCREASED TIP AREA DUE TO FORMATION OF A GROUT BULB UNDER THE PILE TIP

Laboratory tests on small scale piles have shown evidence that a grout bulb usually forms under the pile tip after pressure grouting (Mullins and Winters, 2004). Stress levels between laboratory and actual drilled shafts in the field are recognized as different in spite of the fact that laboratory testing techniques tend to reproduce stress gradients similar to those occurring in the field. Mullins and Winters (2004) reported the formation of grout bulbs under PGDS tested at a National Geotechnical Experimental Site at Auburn University based on the observation of four PGDS exhumed at the mentioned site. However, no detailed study was made to investigate the characteristics of grout bulb formation. The extent of the grout bulb including shape, dimension, etc. needs further study. Despite this absence of field verification studies, the formation of a grout bulb under the pile is generally believed to occur as a consequence of tip grouting.

As part of the first phase of the research conducted by Mullins and Winters (2004) several laboratory tests were carried out in order to assess the pile capacity improvement with post grouting. Laboratory tests were conducted aiming at reproducing actual pile construction and grouting procedures as well as stress gradients present in the field. Test

specimens were built in a frustum confining vessel, used to reproduce the stress field in the soil mass surrounding the pile. A total of eleven post grouted specimens were cast in the frustum vessels filled with saturated sand. The specimens were 0.11 m in diameter and 0.84 m in length. Important capacity improvement was observed with respect to ungrouted specimens constructed under similar laboratory conditions and using the same construction procedure as the grouted specimens.

One of the effects resulting from the formation of the grout bulb at the bottom of the shaft would be to provide an increased tip bearing area which results in an increased end bearing capacity of the pile (effects of densification were discussed in Factor 1). To model the augmented tip area due to the formation of a grout bulb under the tip of the shaft, the load transfer curve Q_b - Z is calculated (using Equation (3.29) presented in Chapter 3) assuming an increased radius for the shaft tip. The asymptotic value $Q_{b\text{-max}}$ changes according to the square of the ratio between the radius of the bulb and the radius of the shaft. The modified load transfer curve for the pile tip considering the increased radius due to the presence of the grout bulb is as follows:

$$z_b = \frac{Q_b(1-\nu)}{4r'_0 G_0 \left(1 - f \left(\frac{Q_b}{Q_{b\text{-max}} \cdot \left(\frac{r'_0}{r_0} \right)^2} \right)^g \right)} \quad (5.4)$$

Where: r'_0 = radius of the grout bulb under the pile tip

r_0 = radius of the shaft

The load transfer model used to represent the pile with an increased tip area is shown in Figure 5-6. It can be seen that only the area of the last segment is increased to match that of the grout bulb formed after grouting. It is worth to note that no side friction resistance is assigned to the grout bulb under the pile tip since it is considered to have a small height and its shape is not known.

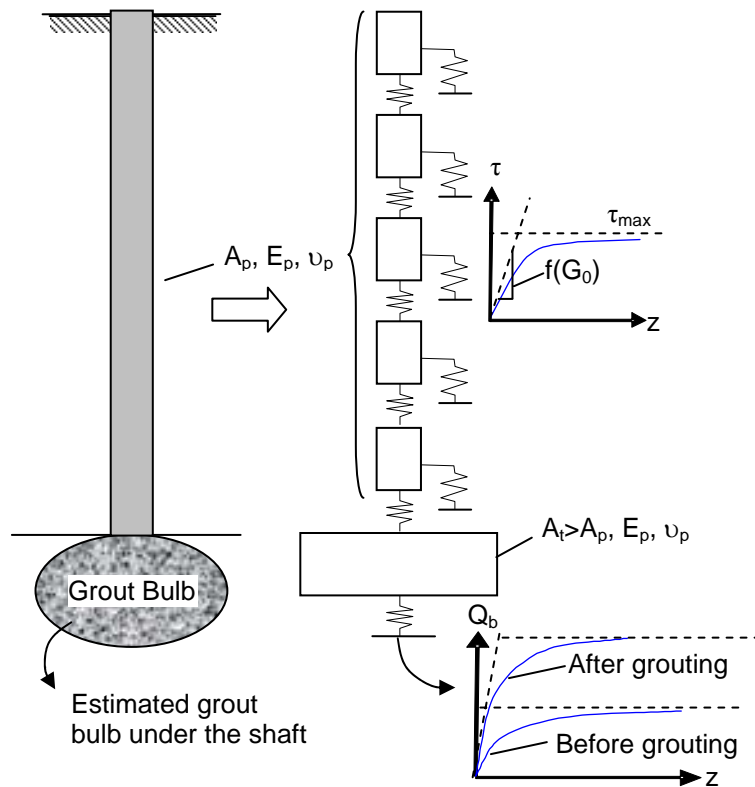


Figure 5-6 Effect of the augmented tip area on the load-transfer at the tip

The influence of the increased tip area in the Q_b - Z curve is shown in Figure 5-7. This figure shows Q_b - Z curves plotted for various ratios r'_0/r_0 using Equation (5.4). It can be seen that increasing the tip radius has a big influence in the resulting tip load transfer curve since it yields stiffer curves and increased asymptotic values.

The shape and size of the grout bulb that may result formed under the shaft after grouting is currently difficult to predict. However, as stated before, in the drilled shaft grouting the slurry is injected into a flexible membrane, which is deformed and pushed against the surrounding soil. Therefore the formation of the grout bulb can be thought as a process analogous to a cavity expansion process.

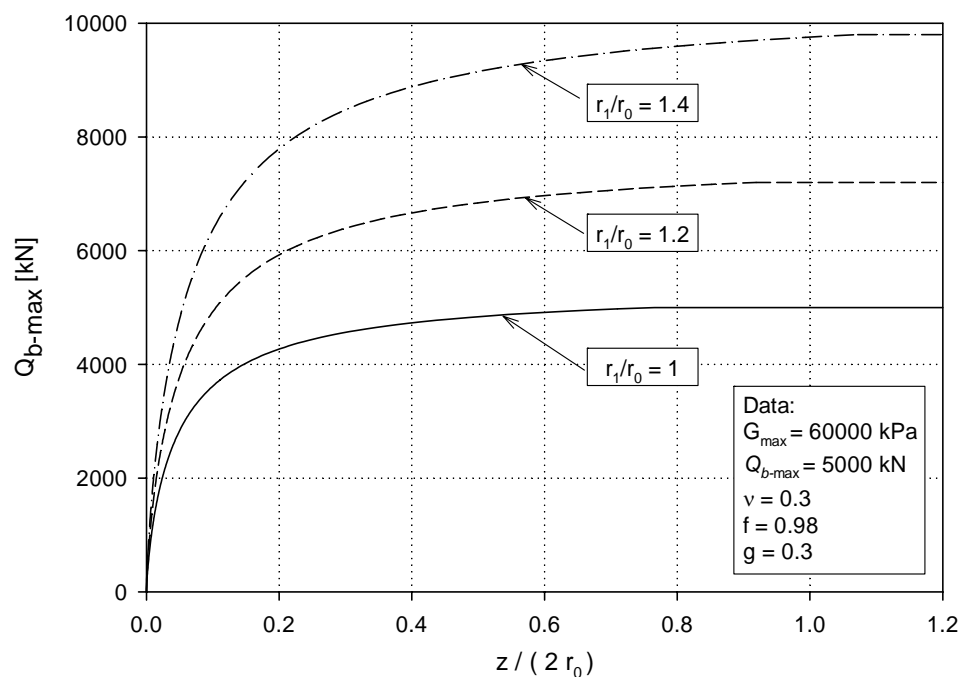


Figure 5-7 Effect of an increased pile tip area on the load transfer curve Q_b - Z

Cavity expansion theory can be used to calculate initial estimates of the radius of the grout bulb that may result for certain grout pressures. In this regard, the work by El-Kelesh et al. (2001) provides a good theoretical framework which allows the determination of the radius of a spherical cavity within a uniform elastic – perfectly plastic soil mass. The methodology proposed by El-Kelesh et al. (2001) can be used to

estimate approximate values for r'_0 of the grout bulb of a post grouted pile. The formulas proposed by the authors are:

$$r'_0 = \frac{R_i}{\left[a_1 \left(\frac{p + a_2}{a_3} \right)^{a_4} + \left(\frac{a_3}{p + a_2} \right)^{a_4} - a_5 \right]^{1/3}} \quad (5.5)$$

Where: r'_0 = Final radius of the cavity (i.e. radius of the grout bulb)

R_i = Initial radius of the cavity (i.e. radius of the shaft)

p = grout pressure

$$a_1 = \frac{1}{I_r} - 1 + \left(1 - \frac{4 \cdot (1 + \nu) \cdot \sin \phi}{2E \cdot (3 - \sin \phi)} (q + c \cdot \cot \phi) \right)^3$$

$$a_2 = c \cdot \cot \phi$$

$$a_3 = \frac{3 \cdot (1 + \sin \phi)}{3 - \sin \phi} (q + c \cdot \cot \phi)$$

$$a_4 = \frac{3 \cdot (1 + \sin \phi)}{4 \cdot \sin \phi}$$

I_r = rigidity index of the soil which is equal to the shear modulus divided by shear strength of the soil. Typical values for I_r for different soil types can be found in Vesic (1972).

ϕ = angle of internal friction of the soil

c = cohesion of the soil

Two disadvantages can be observed from the derivation of El-Kelesh et al. (2001): (1) only a uniform soil layer is considered, and (2) the derivation has not been validated with experimental results. Despite these disadvantages, numerical models using the initial radius obtained with the formulation proposed by El-Kelesh et al. (2001), gave reasonable good results when modeling PGDS behavior as presented later in this work. However, small adjustments had to be made in the bulb radiuses estimated with the above formulas to improve the agreement between measured and predicted PGDS load settlement curve for the full scale tests that will be presented in the next chapter.

Both size and shape of the grout bulb formed after grouting under the shaft are still under investigation. Another important consideration is that one should ensure that the grout bulb is strongly attached to the shaft to safely include the benefits of the augmented tip area. However, whether the bulb is well attached to the shaft or not is difficult to corroborate in the field and sometimes the grout bulb may separate from the shaft after loading the pile. In that case, the benefits of factors 1 and 2 only remain to increase pile capacity after grouting.

From the previous discussion it is observed that the formation of the grout bulb is subject to a number of uncertainties. Therefore, results from laboratory tests carried out by Mullins and Winters (2004) were used to approximately quantify the ratio of the bulb radius to the shaft radius for the post grouted specimens. Measurements of bulb and shaft radiuses were made on photographs of the extracted post grouted specimens included in the report by Mullins and Winters (2004). Some of the photographs used to estimate the

ratio between the bulb radius and the shaft radius are depicted in Figure 5-8 and 5-9. Some of the post grouted specimens presented fractured bulbs (Figure 5-8), while others presented a bulb firmly attached to the shaft (Figure 5-9 a, b and c).

It was found that the ratio between the bulb radius and the shaft radius (for those specimens which presented an unbroken bulb) ranged between 1.15 and 1.9. These values will be used as the upper and lower bulb radius limits for the case studies that will be presented in the next chapter.

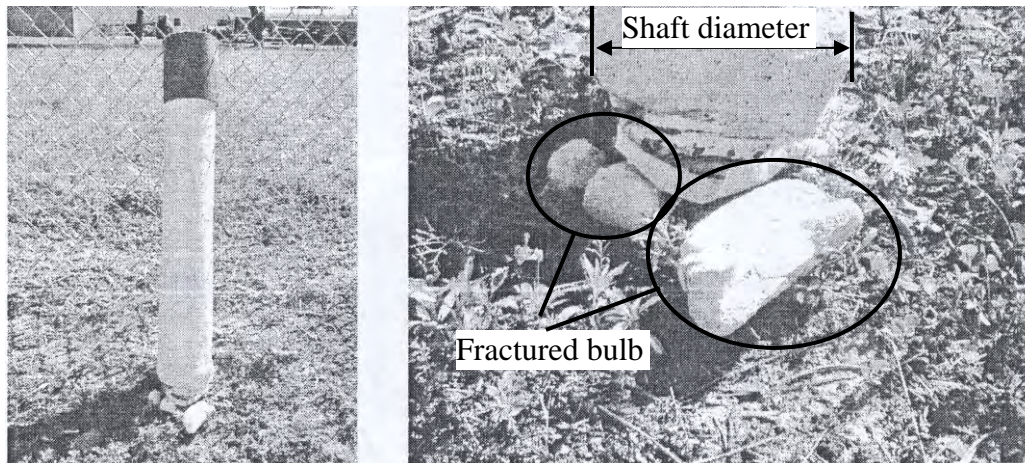
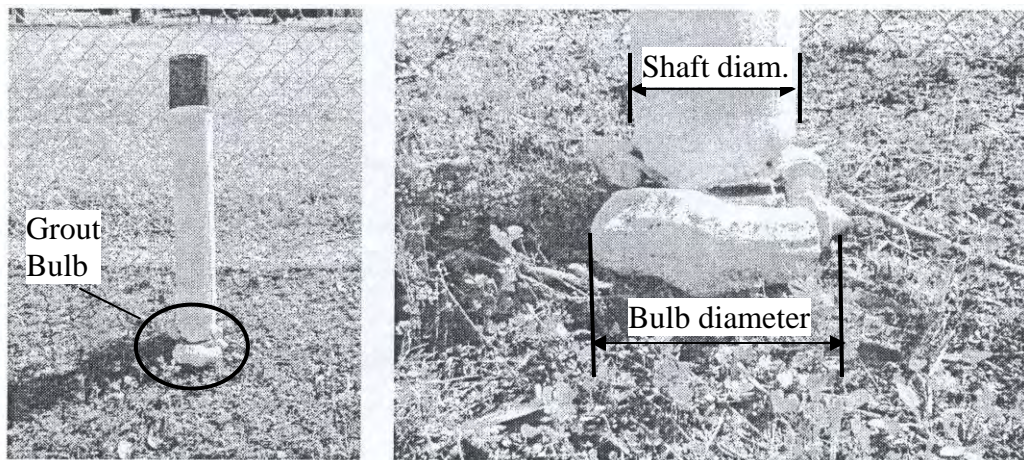


Figure 5-8 Post grouted laboratory specimen with fractured grout bulb (from Mullins and Winters, 2004)

Three examples of the test specimens used to quantify the extent of the grout bulb radiuses are shown in Figure 5-9. In this figure it can be seen that the grout bulbs do not have regular shapes, thus their volume is difficult to quantify and because of this, their size would be difficult to predict.

The grout volume injected to the pile tip is also difficult to quantify since the rubber membrane that holds the grout may result broken and migration of the grout may occur.

Thus, not the total grout volume injected through the pile tip would contribute to the formation of the bulb. For these reasons, the cavity expansion theory developed by El-Kelesh et al. (2004) may not strictly represent the grout bulb formation process due to grouting. However, as stated earlier, this formulation will be only used to perform initial estimates of the bulb size. This initial estimate will be adjusted in order to calibrate the predicted and measured load settlement curves of full scale PGDS.



(a)

Figure 5-9 Post grouted laboratory specimens with grout bulb (from Mullins and Winters, 2004)

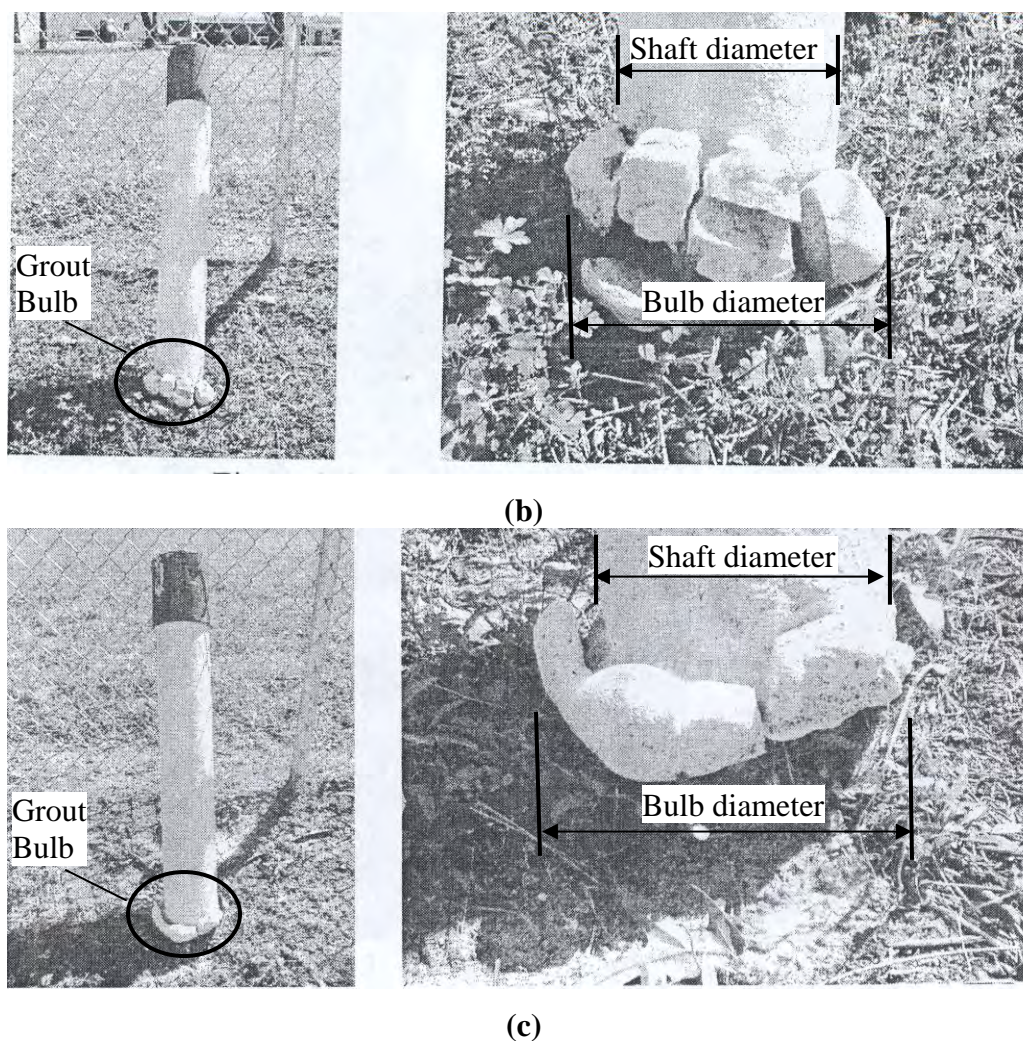


Figure 5-9 (Continued) Post grouted laboratory specimens with grout bulb (from Mullins and Winters, 2004)

5.6 SUMMARY AND CONCLUSIONS

In order to study the behavior of PGDS, three factors were assumed to control the increase in pile capacity achieved with tip grouting. These factors are: (1) Soil compression under the pile tip, (2) Shear stress reversal along the shaft due to grouting, and (3) Augmented tip area due to the formation of a grout bulb.

The manner in which the aforementioned factors can be included into the load transfer approach in order to model the PGDS behavior was discussed. The soil compression under the pile tip is incorporated in the model through an increased shear modulus of the Q_b -Z spring. Shear stress reversal along the shaft is accounted for by applying the Masing rule. The augmented pile tip area is considered assuming an increase pile shaft radius. Evidence of the formation of grout bulb was found from laboratory tests results on post grouted specimens.

The factors assumed to control the PGDS increased capacity will be used in the next chapter in order to systematically simulate available load tests performed on full scale PGDS.

6 POST GROUTED PILES: CASE STUDIES

6.1 INTRODUCTION

This chapter presents nine case histories where Post Grouted Drilled Shafts (PGDS) were tested at well characterized sites. The load test data for each PGDS case study is compared with predictions made with the load transfer analysis procedure described in Chapter 3. For each case history the predictions were made using a systematic procedure that involved varying independently each one of the influence factors discussed in Chapter 5 (i.e., compression of the soil under the pile tip, shear stress reversal along the shaft, and formation of a grout bulb under the pile tip). The final match was based on analysis that included a combination of two or more factors.

All case histories included load tests on ungrouted drilled shafts installed in the same site using the same general construction procedure. This pile is referred to as the control pile and its capacity will be used to assess the improvement in the overall pile performance due to grouting.

To study PGDS behavior in each case history the load transfer models were first carried out for the ungrouted piles (control piles). These analyses were performed following the step by step procedure presented in Chapter 3. Some small initial calibrations were made to obtain a good representation of the load settlement curve of the control pile. The parameters obtained from the control shaft were used as baselines for the additional runs performed to obtain the load-settlement curve of the PGDS. The contribution to the increased PGDS capacity from each of the factors considered in the previous chapter was investigated by performing several load transfer analyzes, modifying only one factor at a time, while keeping the other parameters constant. In order to account for each one of the three factors, modifications to the numerical model were made according to the methodology described in Chapter 5.

6.2 ORGANIZATION OF CASE STUDIES

In order to systematize the study the influence of each of the factors presented in Chapter 5, the following procedure will be followed for each case history presented in this chapter:

- (1) **Develop a load transfer model for an ungrouted (control) pile:** Obtain the pile – soil system characteristics before grouting, following the step by step procedure outlined in Chapter 3. Axial pile capacity will be estimated using the method by Eslami and Fellenius (1997) since it gave the closest representations of field measurements for all case studies presented in Chapter 4. If a load test for a control pile is available, calibrate model parameters until a good

representation of its load settlement curve is obtained with the numerical model.

- (2) **Load transfer model for PGDS including only Factor 1:** Increase shear modulus of the soil under the pile tip. Since soil compression under the pile tip does not seem to control the PGDS behavior, a 100% increment in shear modulus for the Q_b - Z curve was considered large enough to test factor 1.
- (3) **Load transfer model for PGDS including only Factor 2:** Consider stress reversal along the shaft by using the Masing approach. The magnitude of the stress reversal was estimated by means of the maximum upward movement of the shaft measured in the field, during grouting.
- (4) **Load transfer model for PGDS including only Factor 3:** Consider the formation of a grout bulb under the pile tip. Initial estimation for the bulb radius was made using the approach described in Chapter 5. The ratio of bulb to shaft radius is limited to the range obtained from laboratory tests mentioned in Chapter 5 (i.e. $1.1 \leq r_{bulb}/r_{shaft} \leq 2$).
- (5) **Load transfer model for PGDS including a combination of factors:** Calibration of the PGDS model will be performed by combining Factors 1 through 3, if necessary.

Ideally, a perfect procedure to compare post grouted and ungrouted pile behavior would involve a control shaft placed under the exact conditions that the PGDS. However, some soil variability between PGDS location and control pile location is expected and

this will have an incidence on the analysis results that study the influence of each factor on the PGDS behavior. The ungrouted or control pile for all case studies, was placed near the PGDS location and in some cases CPT data was available for each location.

In some of the case studies presented in the following subsections, differences were observed between CPT sounding performed at the control shaft location and those advanced at the PGDS locations. This suggested that new calculations should be carried out to estimate axial pile capacity for each one of the PGDS using CPT soundings at the exact PGDS locations (as if a control shaft were constructed at the exact location of each PGDS). Since reasonable good results were obtained with the methodology presented in Chapter 4, numerical models for control piles will be type A predictions assuming the ungrouted pile is located at the exact location of the PGDS. In other words, the benefit of PGDS was assessed based on comparisons with the load settlement curve from load transfer analyses that assumed an ungrouted pile condition and used the soil condition from CPT advanced at the location of the PGDS.

A total of nine case histories are presented in this chapter. The first eight are from the study by Mullins and Winters (2004) and the ninth case was provided by A. H. Beck Co Inc. and involves a PGDS constructed at Carolina Bays Parkway Project, in South Carolina State. The case histories studied in this chapter are listed in Table 6-1.

Table 6-1 PGDS Case histories

Case No	Location	Predominant Soil Type	Soil at the pile tip elevation	Embedded length [m]	Diameter [m]	Maximum sustained grout pressure [kPa]	Maximum measured uplift [mm]
1	Site I - Florida	Sand	Sand	4.6	0.61	587	3.78
2	Site I - Florida	Sand	Sand	4.6	0.61	462	4.83
3	Site I - Florida	Sand	Sand	4.6	0.61	1139	2.74
4	Site I - Florida	Sand	Sand	4.6	0.61	1221	1.42
5	Houston, TX	Sand	Sand	6.4	1.22	1517	12
6	NGES, Auburn University	Sandy silts to silty sands	Clay	7.3	1.06	565	2.7
7	NGES, Auburn University	Sandy silts to silty sands	Clay	7.3	1.06	602	1.9
8	NGES, Auburn University	Sandy silts to silty sands	Clay	7.3	1.06	689	3.3
9	South Carolina	Clayey sand	Sand	20.1	1.372	2130	10.5

Section 6.3 describes the results obtained with numerical models of PGDS corresponding to the Phase I of the research project conducted by Mullins and Winters (2004). Sections 6.4 and 6.5 describe the modeling of PGDS load tested during the second phase of the same research project. The last case history is studied in section 6.6. In the last section of this chapter conclusions extracted from the results obtained with the numerical models are presented.

CPT soundings, shear wave velocities, pile resistance profiles, and additional information regarding each case study are included in Appendix B.

6.3 SITE I, CLEARWATER, FLORIDA

A total of four PGDS were constructed and tested in Site I, located in the Coastal Caisson Corporation equipment yard in Clearwater, Florida. Each shaft had a diameter of 0.61 m and was approximately 4.6 m long. A control shaft was constructed in the same site in order to compare grouted capacities to ungrouted pile capacities. A total of seven CPT soundings were advanced at the site. Five of which were conducted at the exact drilled shaft locations. A schematic plan view showing the relative location of the five drilled shafts tested at this site is depicted in Figure 6-1. In the same figure, CPT soundings advanced at Site I are also shown.

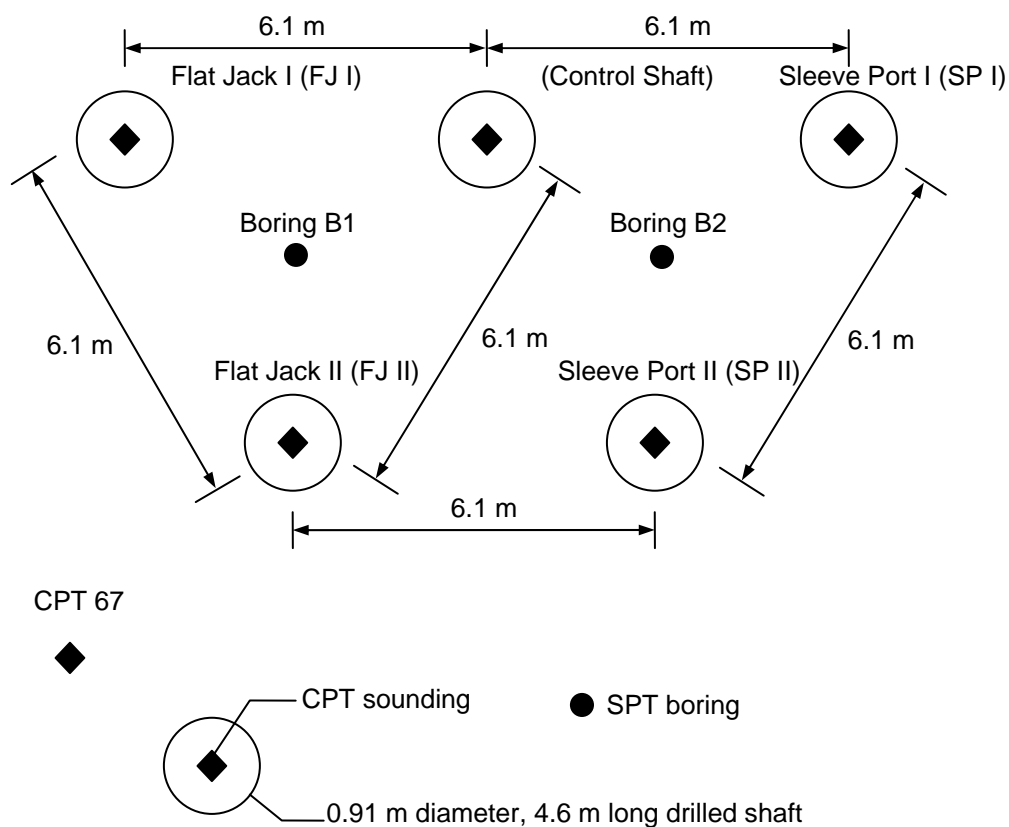


Figure 6-1 Site I layout

The general soil conditions at this site consisted of a medium dense sand fill about 1 m thick, with some silt and fine grained underlain by loose to very loose sand with shell fragments that extended in most cases to the final depth investigated of 8 m. For the control pile a medium dense sand layer was found from 4.8 to 5.2 m depth. In Figure 6-2 the most relevant geotechnical information gathered at this site is shown.

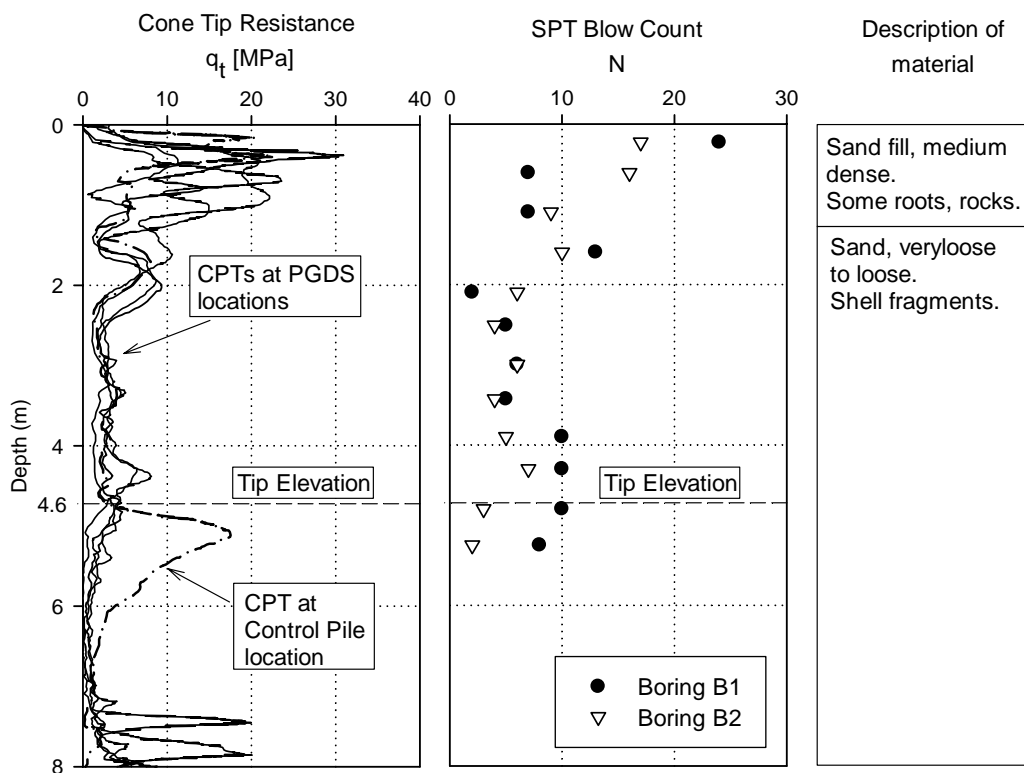


Figure 6-2 Geotechnical information gathered at testing Site I, Clearwater, Florida

It is important to point out that two of the PGDS were grouted using a flat jack apparatus. These two piles are referred to as FJ I and FJ II. The other two PGDS piles were grouted using a sleeve port device and are referred to as SP I and SP II. A detailed description of these two types of grouting apparatuses can be found in Mullins and Winters (2004).

All load testing was carried out using a 4.45 MN Statnamic device. The results presented herein are presented as equivalent static load tests were as reported by Mullins and Winters (2004). The load settlement curves for the control pile and for the four PGDS tested at this site are depicted in Figure 6-3.

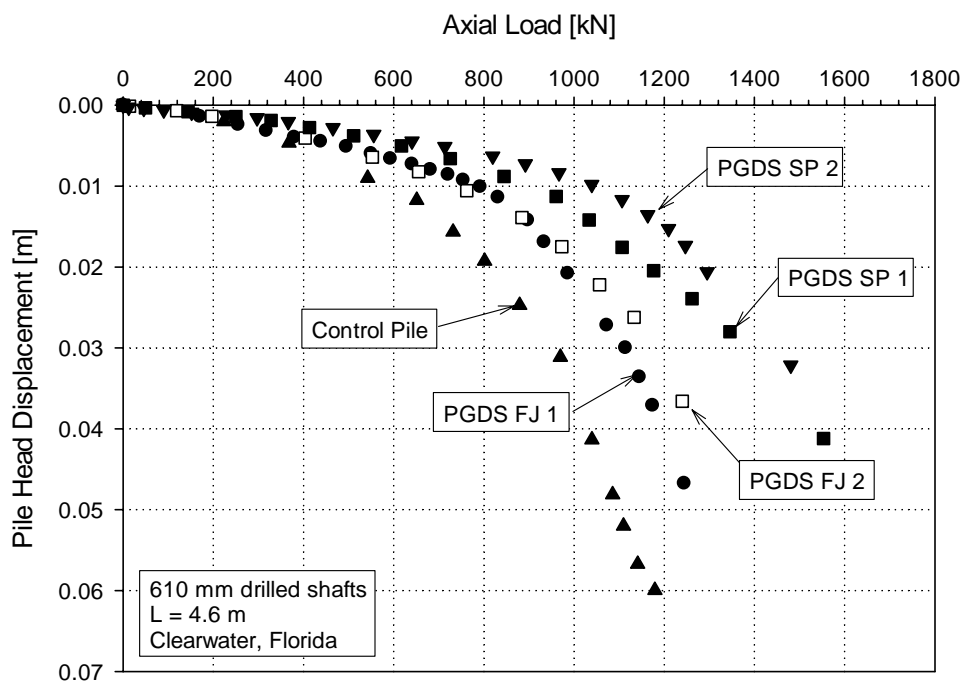


Figure 6-3 Equivalent static load test data for four PGDS and one control pile at Clearwater, Florida

In the following sections numerical models for the PGDS tested at the site in Clearwater, Florida are presented.

6.3.1 CONTROL PILE

As mentioned earlier, the control shaft was located at the center of the four PGDS tested in Site I as a means to ensure that results from the ungrouted pile could be extrapolated to the locations of the PGDS.

The CPT sounding and shear wave velocity estimations at the location of the control pile are shown in Figure A-1, in Appendix A. The control pile capacity derived from the CPT data depicted in Figure A-1 is shown in Figure A-2. The pile load test result as reported by Mullins and Winters (2004) is shown in Figure 6-4. A type A prediction obtained using the proposed load transfer methodology (presented in Chapter 6), for the

load settlement curve of the control shaft is also depicted in the same figure. The figure shows good agreement between measured and predicted load settlement curves for the entire curve.

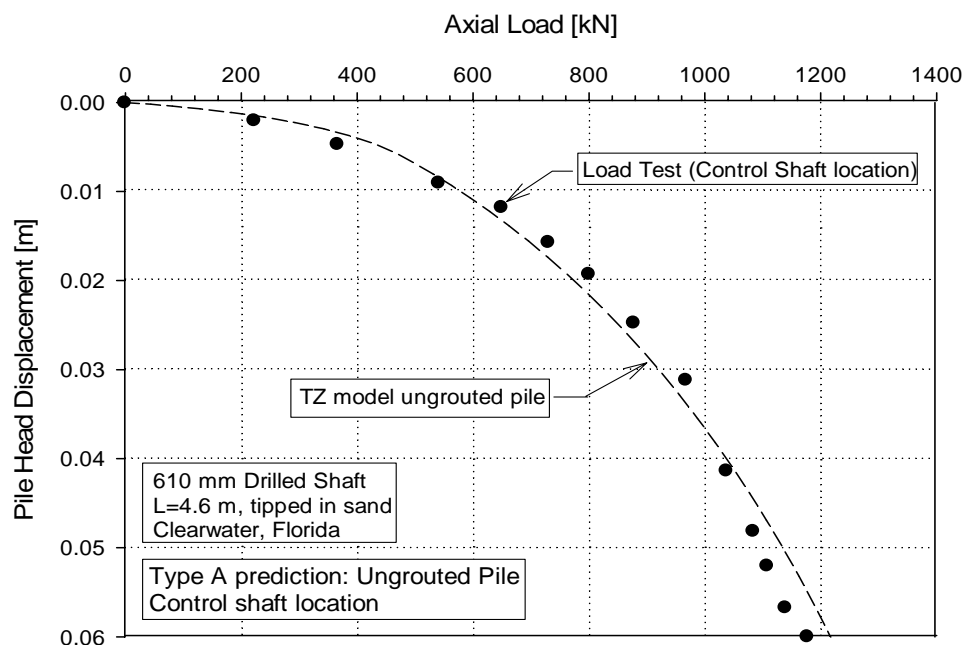


Figure 6-4 Type A prediction for control shaft in Site I

The CPT soundings presented in Appendix A, some differences of the soil conditions between the control pile and the PGDS locations. The main difference is the presence of a medium dense sand layer near the tip of the control pile. Hence, the benefits of pile tip post grouting will not be apparent from comparing PGDS load settlement curves with the control load test results. As shown later, to evaluate improvements in the load settlement behavior of PGDS it was necessary to compare the PGDS response with load settlement curves predicted using the proposed load transfer methodology applied to the actual CPT measurements at the PGDS.

6.3.2 PGDS INSTALLED USING THE FLAT JACK GROUTING APPARATUS

The following two subsections present numerical analyses for the PGDS using the flat jack grouting apparatus and are referred herein to as Flat Jack I (FJ I) and Flat Jack II (FJ II).

6.3.2.1 FLAT JACK I (FJ I)

Grout data recorded during the grouting process of FJ I showed a maximum sustained grout pressure of about 587 kPa and a maximum upward displacement of the shaft, measured with tension telltales of 3.78 mm (measured at the pile tip level). The total volume of grout injected was reported as being about 0.05 m³.

The CPT sounding and shear wave velocity estimations using correlations with CPT data at the location of FJ I are shown in Figure A-3, in Appendix A. Numerical results obtained for the PGDS are presented following the structure outlined in subsection 6.2.

(1) Load settlement curve for ungrouted pile at the FJ I location

The load settlement curve estimated using ungrouted conditions for an ungrouted drilled shaft at FJ I location is depicted in Figure 6-5. This was obtained using the CPT based pile capacity shown in Figure A-4. In Figure 6-5, the load test on the Control shaft is also shown. Good agreement between measured and predicted load settlement curve is restricted only to the initial portion of the curve, up to 400 kN. The differences can be attributed to the weaker soil at the tip elevation and to inherent soil variability between pile locations.

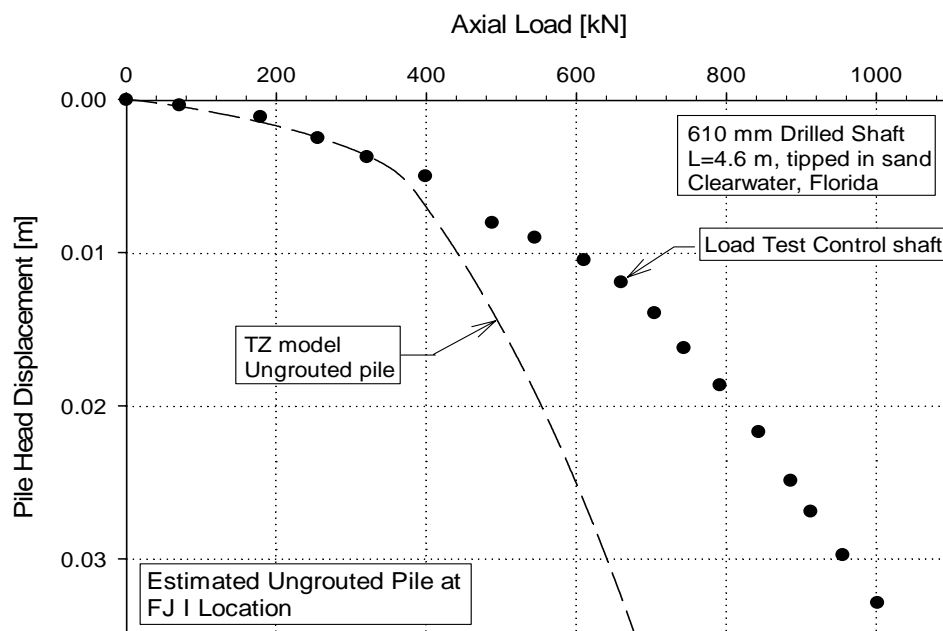


Figure 6-5 Predicted load settlement curve for an ungrouted drilled shaft at FJ I location

This numerical model was used as baselines to study the influence of post grouting on the measured PGDS behavior. This is presented in the following paragraphs.

(2) Factor 1: Increased shear modulus of the soil under the pile tip.

This run was carried out assuming that post grouting resulted only in an increased shear modulus of the soil under the pile tip. Results of the load transfer analyses using Factor 1 are shown in Figure 6-6.

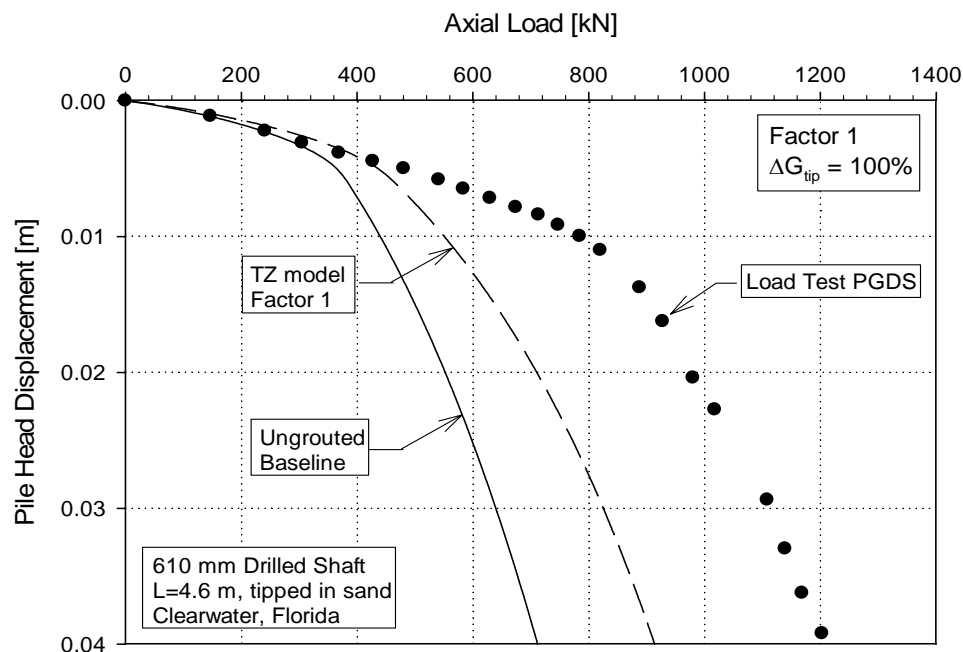


Figure 6-6 FJ I – Factor 1: Prediction of the load-settlement curve of PGDS with densified soil under the pile tip

As can be seen, good agreement with test data was only obtained for the initial part of the curve up to an axial load of 400 kN. This analysis was done with different levels of increased shear modulus of the soil near the pile tip. Figure 6-6 shows the results corresponding to a 100 % increase of the shear modulus. Even this relatively high degree of shear modulus improvement was insufficient to capture the measured load settlement response of the PGDS foundation.

(3) Factor 2: Consider stress reversal along the shaft

Load transfer analyses were carried out assuming that the only effect of post grouting on the pile was the development of residual stresses along the shaft due to shear stress reversal. Results of the numerical analyses that consider only Factor 2 are shown in Figure 6-7.

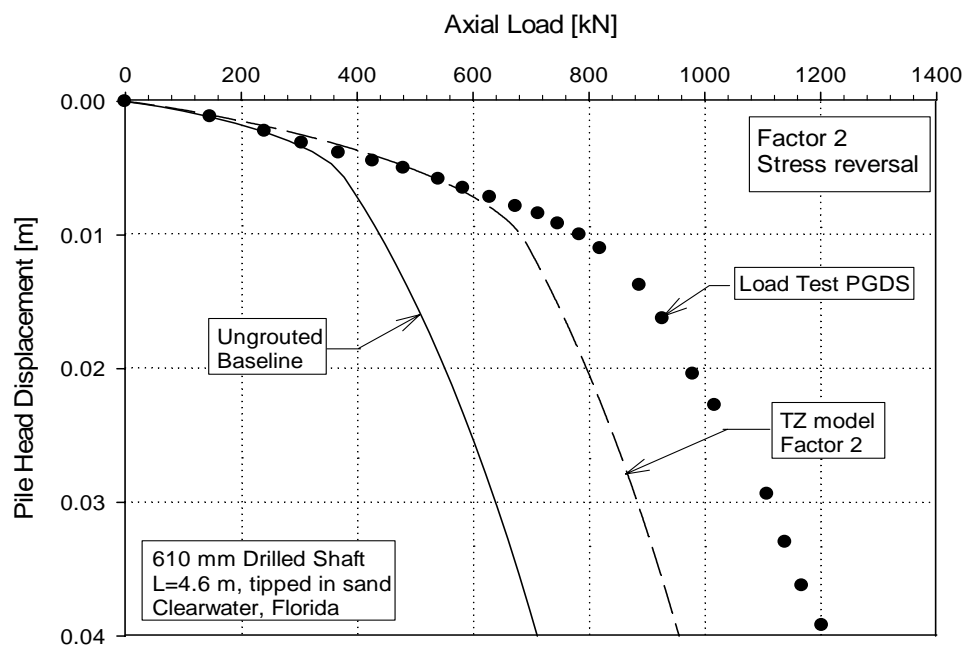


Figure 6-7 FJ I – Factor 2: Prediction of the load-settlement curve of PGDS considering stress reversal along the shaft

The analysis that considers only second factor shows a better agreement between the predicted and measured curves. However, the agreement is good only up to an axial load of about 600 kN and the ultimate axial capacity of the PGDS foundation is significantly under-predicted.

(4) Factor 3: Consider the formation of a grout bulb under the pile tip

Analyses for this factor assumed an increased pile tip area for the PGDS. This enlarged tip area simulates the formation of a grout bulb. Using the cavity expansion theory approach presented in Chapter 5 a bulb radius of 1.8 times that of the shaft was calculated. Load transfer analysis using this enlarged tip area (Factor 3) is presented in Figure 6-8.

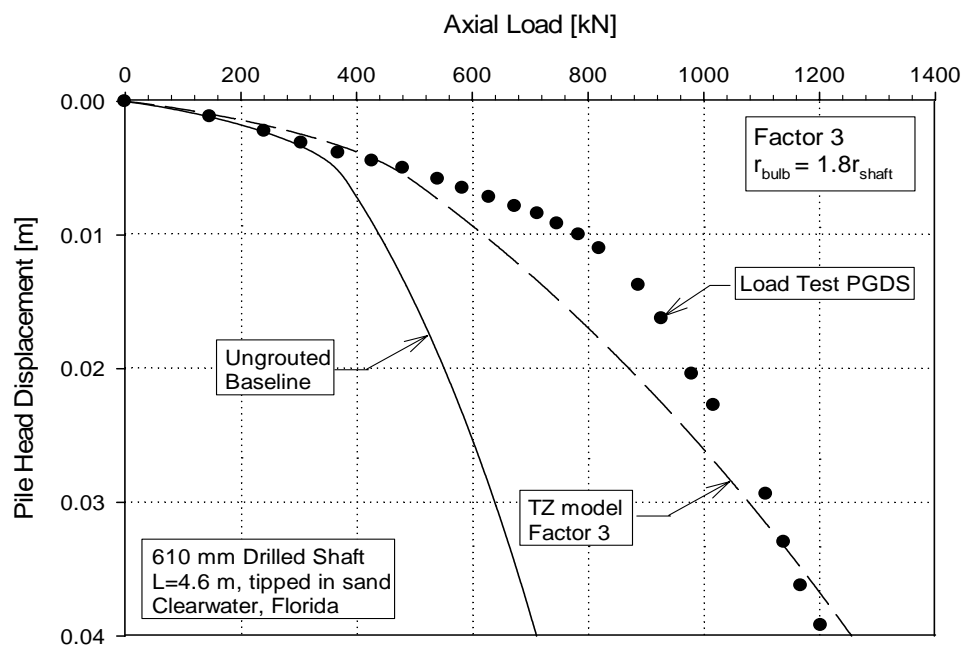


Figure 6-8 FJ I – Factor 3: Prediction of the load-settlement curve of PGDS considering augmented tip area

This figure shows that the assumption that post grouting only resulted in an enlarged tip area due to the grout bulb formation does not adequately capture the measured load settlement curve for the FJI PGDS. In addition, the the bulb radius estimated using the cavity expansion approach, seems to be too large and pile capacity results over-predicted. This can be seen in Figure 6-8 for loads larger than 1000 kN.

(5) Combination of factors

Since none of the three factors alone could adequately represent the measured response of the PGDS, additional analyses were performed combining these factors, in order to improve the prediction of the actual PGDS load-settlement curve.

The best representation of the measured load-settlement curve for the PGDS was obtained combining Factor 2 and Factor 3. This is shown in Figure 6-9.

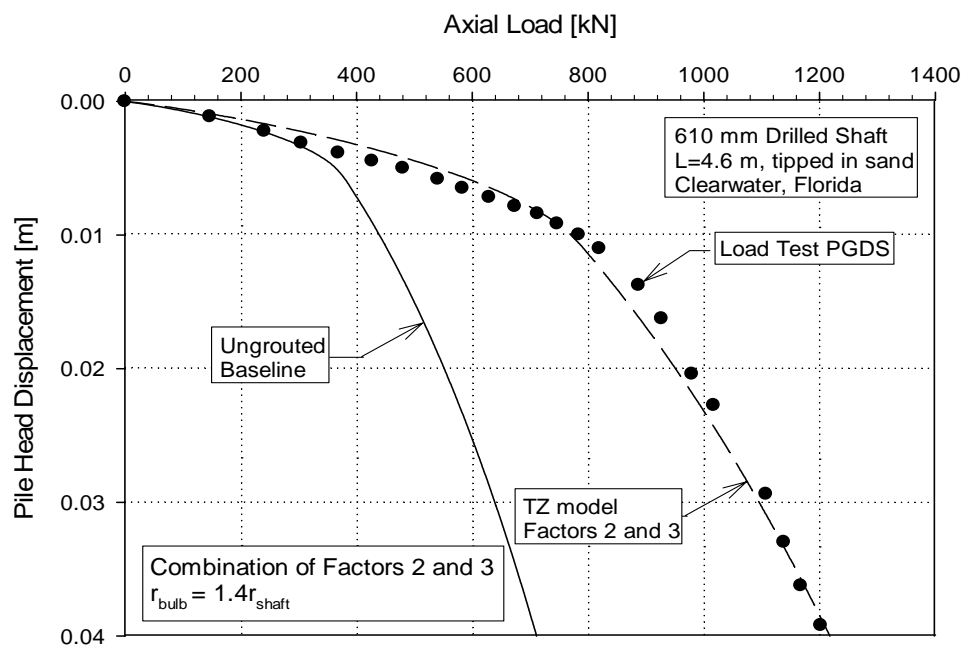


Figure 6-9 FJ I – Factors 2 and 3: Calibrated load-settlement curve

The enlarged tip area of the PGDS in this analysis was calibrated to match the load settlement curve recorded in the field. The adjusted bulb radius was 1.4 times that of the shaft, which represents a reduction of 29 % with respect to the first estimation of the bulb radius used in (4).

6.3.2.2 FLAT JACK II (FJ II)

Grout data recorded during grouting process of FJ II showed a maximum sustained pressure of about 462 kPa and a maximum uplift displacement of the shaft, measured with tension telltales of 4.83 mm. The volume of grout injected was about 0.107 m³.

The CPT sounding and shear wave velocity estimations using correlations with CPT data at the location of FJ II are shown in Figure A-5, in Appendix A. Numerical results obtained for the PGDS are presented following the structure outlined in subsection 6.2.

(1) Load settlement curve for ungrouted pile at FJ I location

The predicted load settlement curve for an equivalent ungrouted shaft carried out using the CPT data at FJ II location is depicted in Figure 6-10. In the same figure, the load test on the Control shaft is also shown. The pile capacity derived from CPT data at FJ II location is shown in Figure A-6. Very good agreement is observed between predicted and measured curves for the first portion of the curve. However, as expected, the ultimate pile capacity was extremely underpredicted with respect to that of the control shaft, similar to FJ I. The differences can be attributed to the weaker soil at the tip elevation and to inherent soil variability between pile locations.

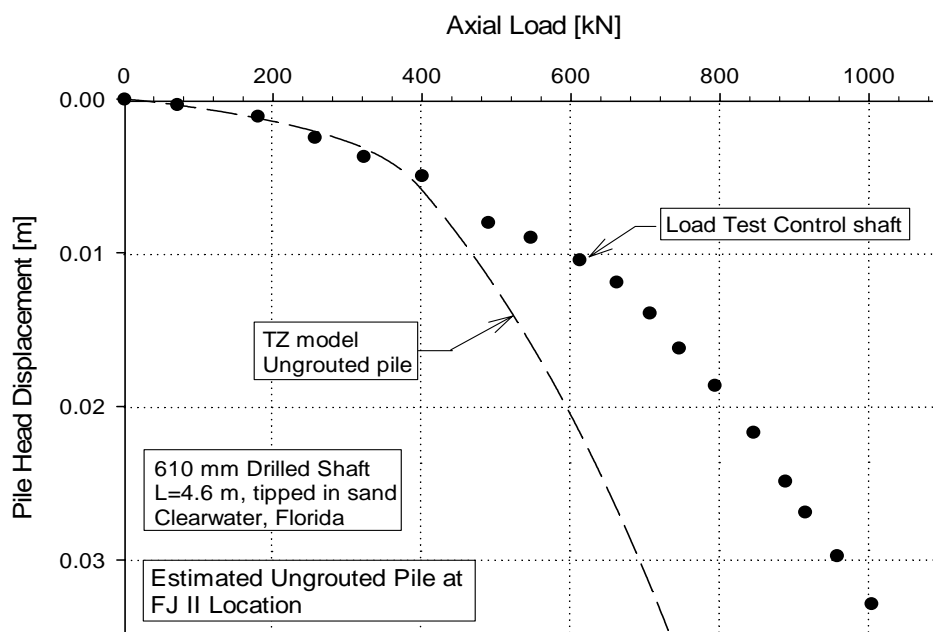


Figure 6-10 Predicted load settlement curve for an ungrouted drilled shaft at FJ II location

(2) Factor 1: Increased shear modulus of the soil under the pile tip.

As before, analyses for the Factor 1 assume that post grouting only resulted in an increased shear modulus for the soil under the pile tip. The results of this set of analyses are shown in Figure 6-11.

Similar to the case of FJ I, good agreement with test data was only obtained for the initial part of the curve, up to a load of about 500 kN. Analyses were done with different levels of shear modulus improvement of the soil near the pile tip. The analysis shown in Figure 6-11 corresponds to shear modulus improvement of a 100%. Even this level of shear modulus improvement was inadequate to capture the measured response FJ II PGDS foundation beyond 500 kN.

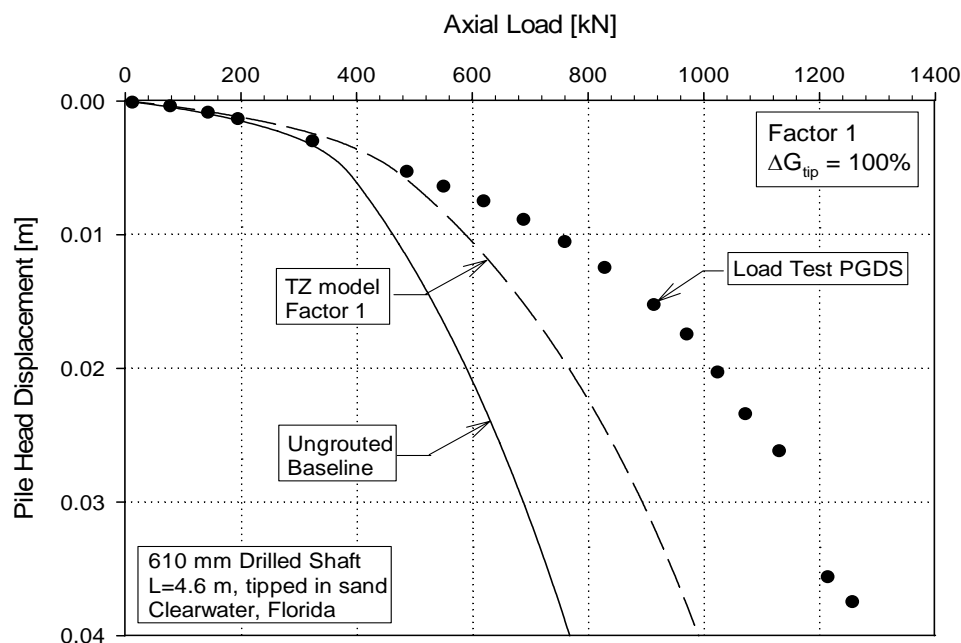


Figure 6-11 FJ II – Factor 1: Prediction of the load-settlement curve of PGDS with densified soil under the pile tip

(3) Factor 2: Consider stress reversal along the shaft

Results of the analyses considering Factor 2, i.e., only shear stress reversal along the shaft contributed to the PGDS performance improvement are shown in Figure 6-12.

The second factor shows a better agreement between predicted and measured curves. However, beyond 800 kN the agreement is poor and the ultimate axial capacity of the PGDS foundation is under-predicted.

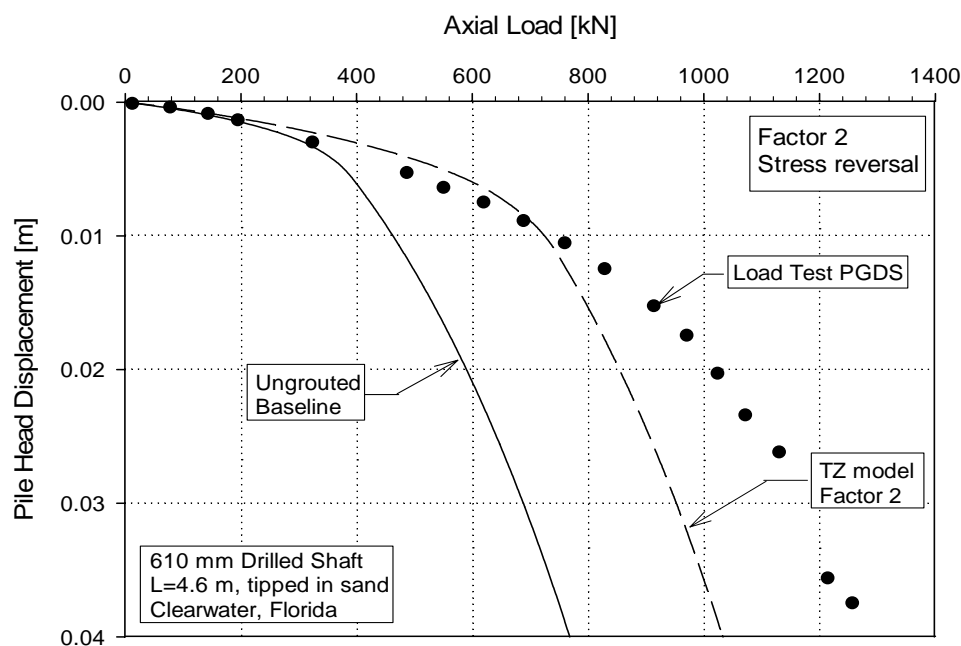


Figure 6-12 FJ II – Factor 2: Prediction of the load-settlement curve of PGDS considering stress reversal along the shaft

(4) Factor 3: Consider the formation of a grout bulb under the pile tip

A bulb radius of 1.5 times that of the shaft was estimated using the cavity expansion approach presented in Chapter 5. Results for the third factor using this new tip dimension are presented in Figure 6-13. The figure shows that the assumption of augmented tip area alone significantly underpredicts the capacity measured for the PGDS.

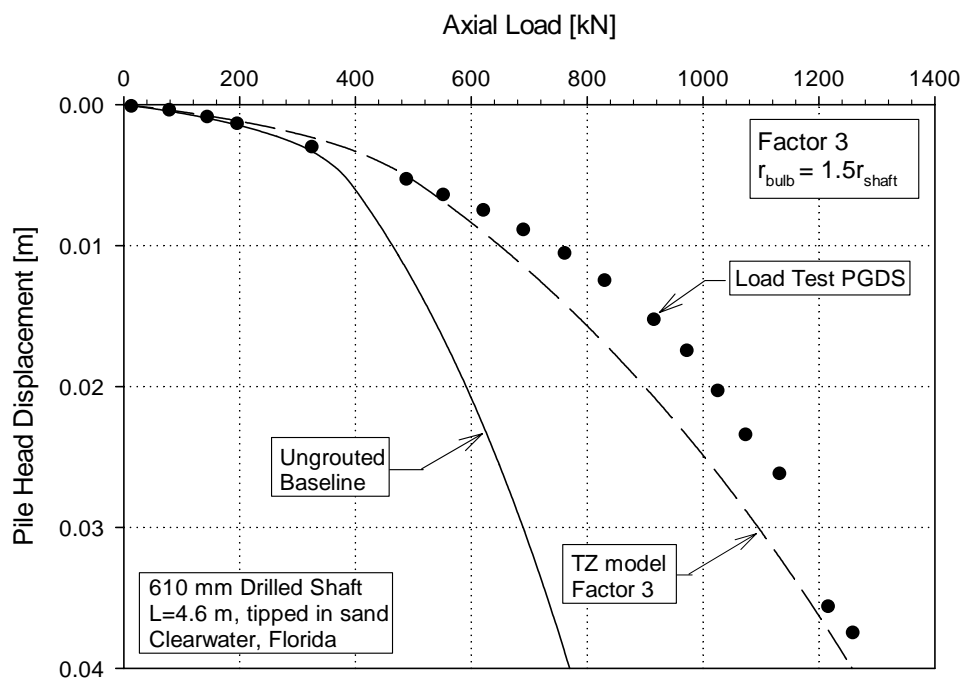


Figure 6-13 FJ II – Factor 3: Prediction of the load-settlement curve of PGDS considering augmented tip area

(5) Combination of factors

Since none of the three factors alone could adequately represent the measured response of the post grouted drilled shaft, additional analyses were performed combining these effects, in order to improve the prediction of the actual PGDS load-settlement curve.

The best representation of the measured load-settlement curve for the PGDS was obtained combining Factors 2 and 3. This is shown in Figure 6-14. The enlarged tip area of the PGDS in this analysis was calibrated to match the load settlement curve recorded in the field. The adjusted bulb radius was 1.35 times that of the shaft, which represents a reduction of 10 % with respect to the first estimation of the bulb radius used in Step 4.

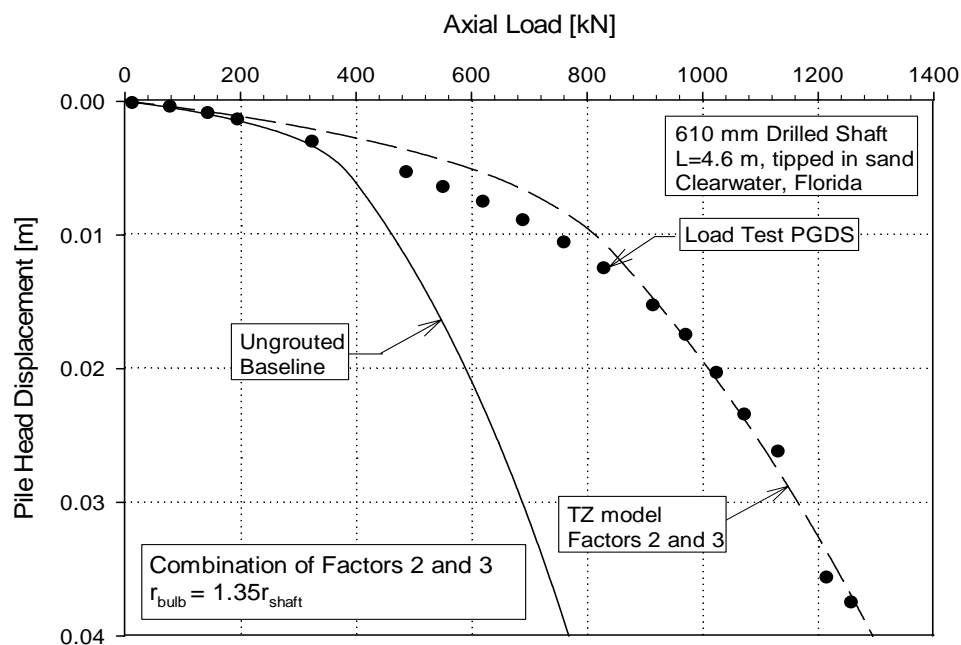


Figure 6-14 FJ II – Factors 2 and 3: Calibrated load-settlement curve

6.3.3 PGDS INSTALLED WITH SLEEVE PORT GROUTING APPARATUS

In the following two sections numerical analyses for two PGDS equipped with the sleeve port grouting apparatus located at Site I are presented. This piles are referred to as Sleeve port I (SP I) and Sleeve port II (SP II).

6.3.3.1 SLEEVE PORT I (SP I)

Grout data recorded during grouting process of SP I showed a maximum sustained pressure of about 1139 kPa and a maximum uplift displacement of the shaft, measured with tension telltales of 2.74 mm. The volume of grout injected was about 0.165 m³.

The CPT sounding and shear wave velocity estimations using correlations with CPT data at the location of SP I are shown in Figure A-7, in Appendix A. Numerical results obtained for the PGDS are presented following the structure outlined in subsection 6.2.

(1) Load settlement curve for ungrouted pile at SP I location

The estimated load settlement curve for a hypothetical ungrouted pile at the location of SP I is depicted in Figure 6-15. The pile capacity derived from CPT data at SP I location is shown in Figure A-8. Very good agreement is observed between the estimated curve and the measured curve for the control pile located at a different location.

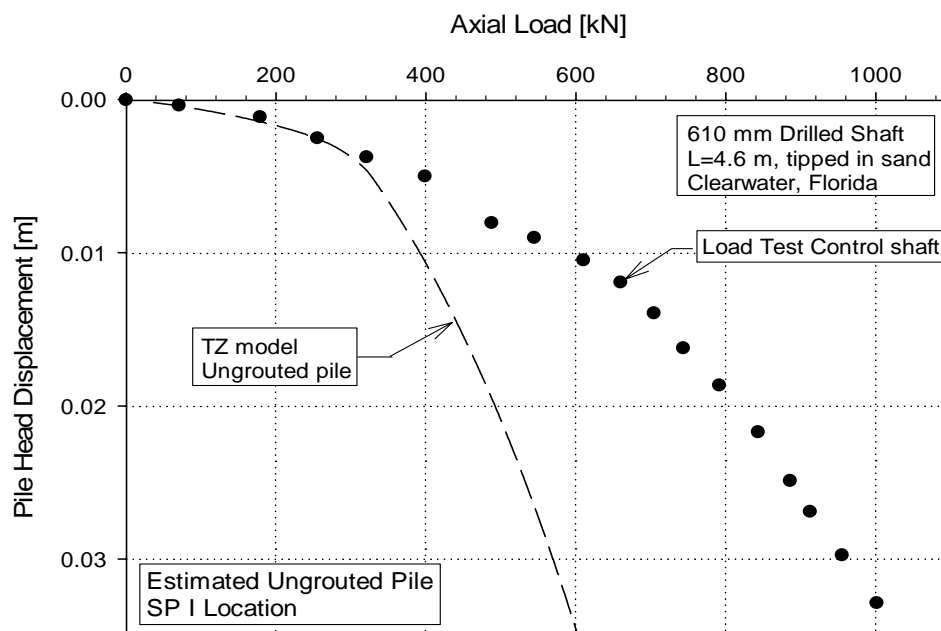


Figure 6-15 Predicted load settlement curve for an ungrouted drilled shaft at SP I location

The differences can be attributed to the weaker soil at the tip elevation and to inherent soil variability between pile locations. However, ultimate pile capacity was extremely underpredicted with respect to that of the control shaft, presumably due to reduced cone tip resistance recorded during CPT sounding over the pile tip influence zone (similar to FJ I and FJ II).

(2) Factor 1: Increased shear modulus of the soil under the pile tip.

Similar to previous PGDS located at this site, analyses considering Factor 1 only were carried out assuming that post grouting only resulted in an increased shear modulus for the soil under the pile tip. Results are shown in Figure 6-16.

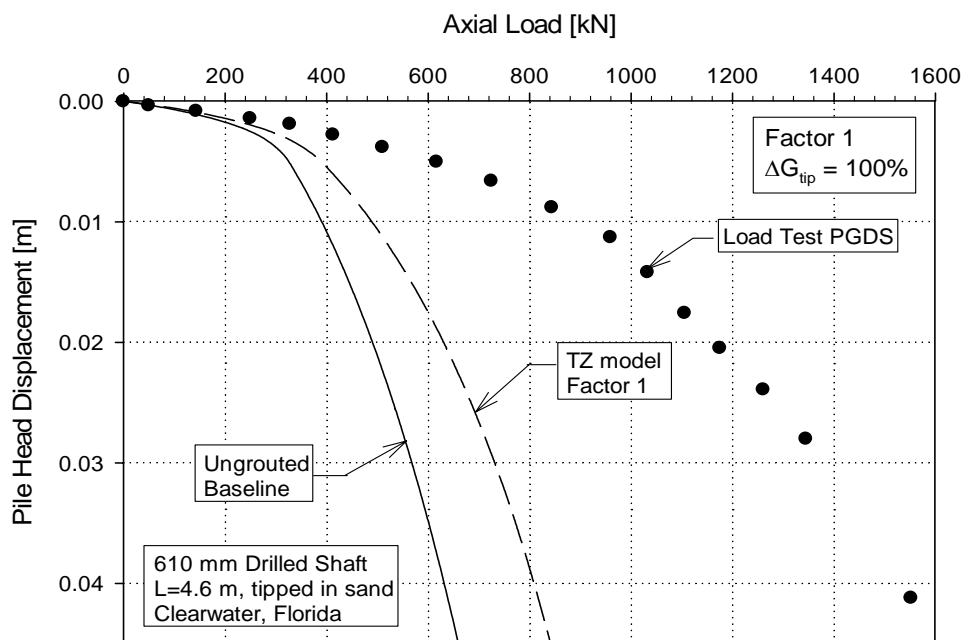


Figure 6-16 SP I – Factor 1: Prediction of the load-settlement curve of PGDS with densified soil under the pile tip

Good agreement with test data was only obtained for a small portion of the curve. Analyses were done with different levels of shear modulus improvement of the soil near the pile tip. The analysis shown in Figure 6-16 corresponds to shear modulus improvement of a 100%. Even this level of shear modulus improvement was inadequate to capture the measured response SP I PGDS.

(3) Factor 2: Consider stress reversal along the shaft

Results of the analyses considering Factor 2, i.e., only shear stress reversal along the shaft contributed to the PGDS performance improvement are shown in Figure 6-17.

The second factor shows a slight better agreement between predicted and measured curves. However, the agreement is poor and the ultimate axial capacity of the PGDS foundation is under-predicted, similar to analyses considering Factor 1.

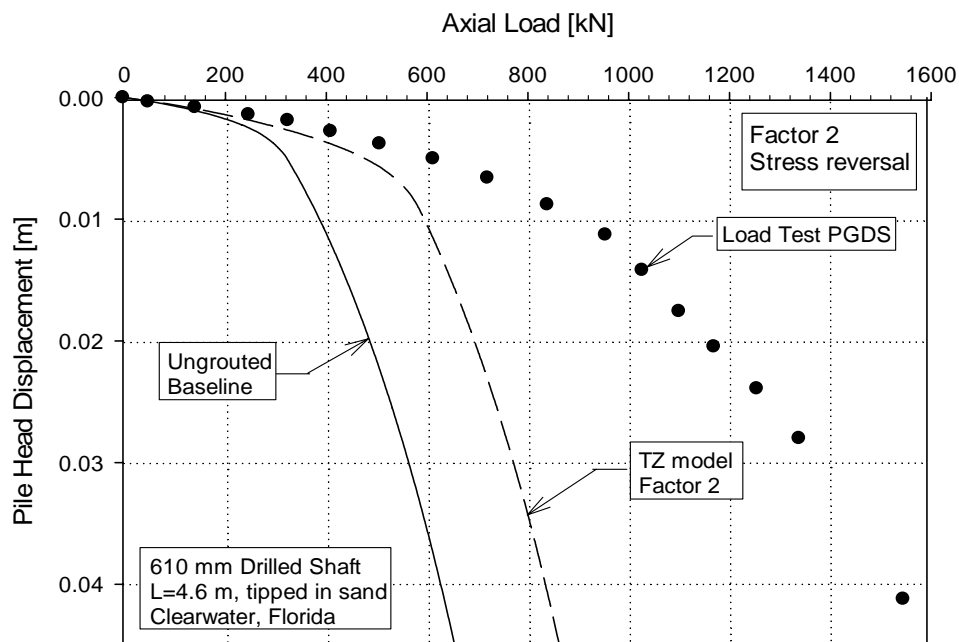


Figure 6-17 SP I – Factor 2: Prediction of the load-settlement curve of PGDS considering stress reversal along the shaft

(4) Factor 3: Consider the formation of a grout bulb under the pile tip

An increased pile tip area was assumed for the PGDS in order to simulate the formation of a grout bulb. A bulb radius of 1.7 times that of the shaft was obtained with the cavity expansion approach presented in Chapter 5. Results for this third factor are presented in Figure 6-18.

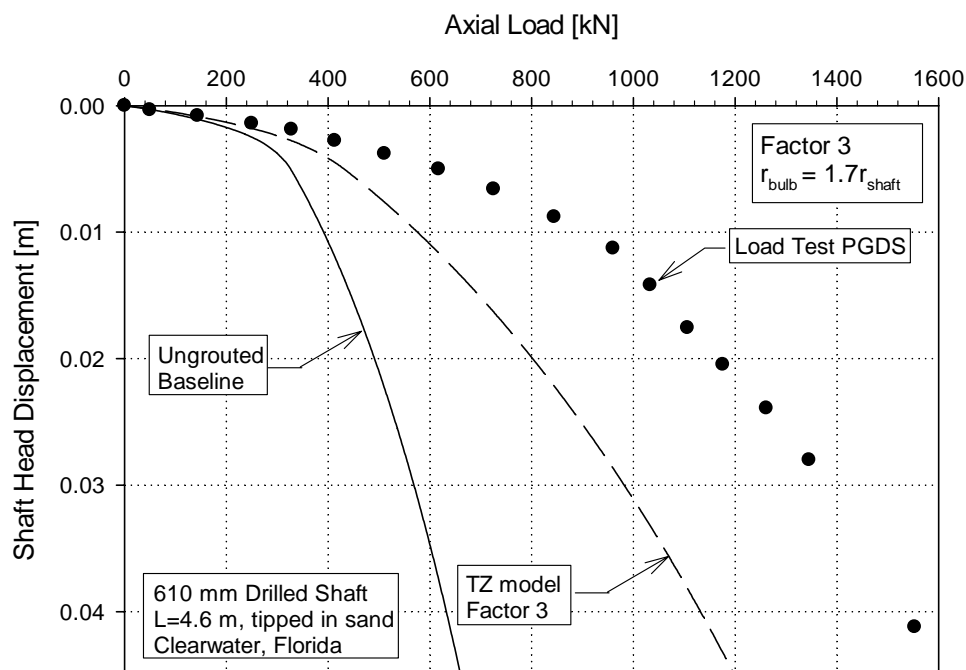


Figure 6-18 SP I – Factor 3: Prediction of the load-settlement curve of PGDS considering augmented tip area

This figure shows that the assumption that post grouting had only created a grout bulb under the tip area, significantly underpredicts the capacity measured for the PGDS, similar to the results obtained in the previous case studies.

(5) Combination of factors

Since none of the three aforementioned factors alone could adequately represent the measured response of the post grouted drilled shaft, additional analyses were performed combining these effects, in order to improve the prediction of the actual PGDS load-settlement curve.

For PGDS SP I, the best match between measured and predicted load-settlement curves was obtained combining all three factors. The best prediction is shown in Figure

6-19. The enlarged tip area of the PGDS in this analysis was calibrated to match the load settlement curve recorded in the field. The adjusted bulb radius is 1.3 times that of the shaft, which represents a reduction of 31 % with respect to the first estimation of the bulb radius.

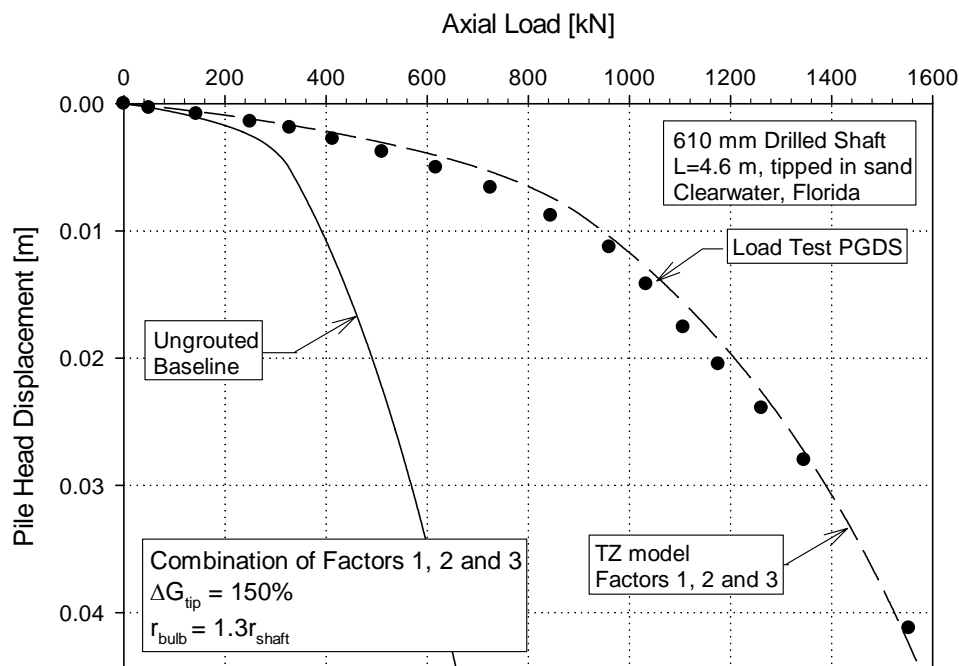


Figure 6-19 SP I – Factors 1, 2 and 3: Calibrated load-settlement curve

The calibrated PGDS model also assumed an increase in the shear modulus for the Q_b - Z curve of 150 % with respect to the original value used in the ungrouted model. This high level of shear modulus improvement may be indicative of a soil – grout mix that may had formed under the shaft rather than indicative of a compression of the lower soil layer (note that the Sleeve Port apparatus does not involves a membrane which separates the slurry from the soil).

6.3.3.2 SLEEVE PORT II (SP II)

Grout data recorded during grouting process of SP II showed a maximum sustained pressure of about 1221 kPa and a maximum uplift displacement of the shaft, measured with tension telltales of 1.42 mm. The volume of grout injected was about 0.086 m³.

The CPT sounding and shear wave velocity estimations using correlations with CPT data at the location of SP I are shown in Figure A-9, in Appendix A. Numerical results obtained for the PGDS are presented following the structure outlined in subsection 6.2

(1) Load settlement curve for ungrouted pile at SP II location

The load settlement curve of the type A prediction for an ungrouted shaft carried out using CPT data at FJ I location is depicted in Figure 6-20.

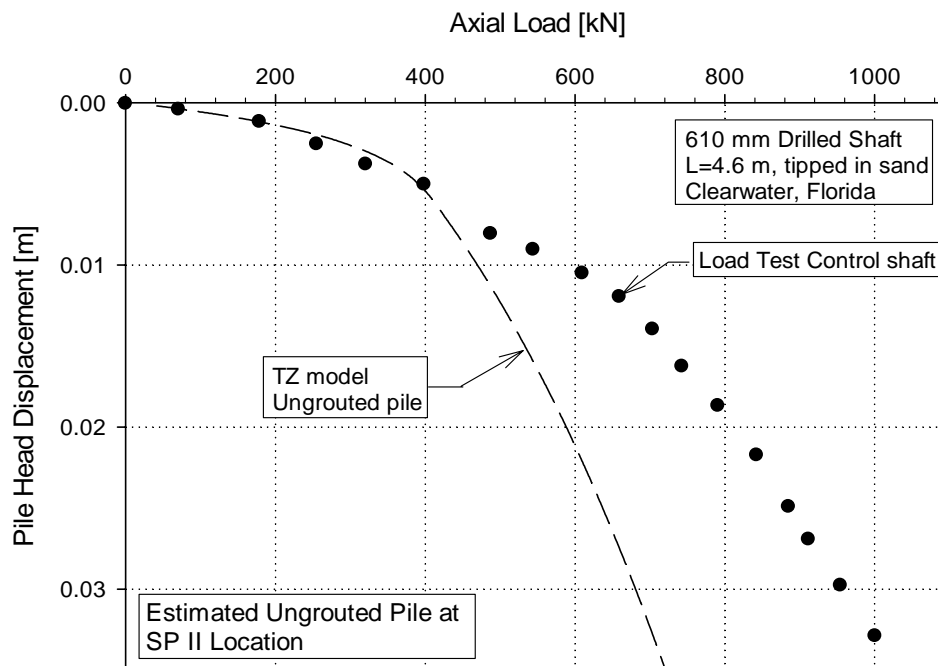


Figure 6-20 Predicted load settlement curve for an ungrouted drilled shaft at SP II location

Very good agreement is observed between predicted and measured curves for the first portion of the curve, up to a load of about 400 kN. However, ultimate pile capacity was extremely underpredicted with respect to that of the control shaft, similar to all three previous cases presented for this site.

(2) Factor 1: Increased shear modulus of the soil under the pile tip.

Similar to previous PGDS located at this site, analyses considering Factor 1 only were carried out assuming that post grouting only resulted in an increased shear modulus for the soil under the pile tip. Results are shown in Figure 6-21.

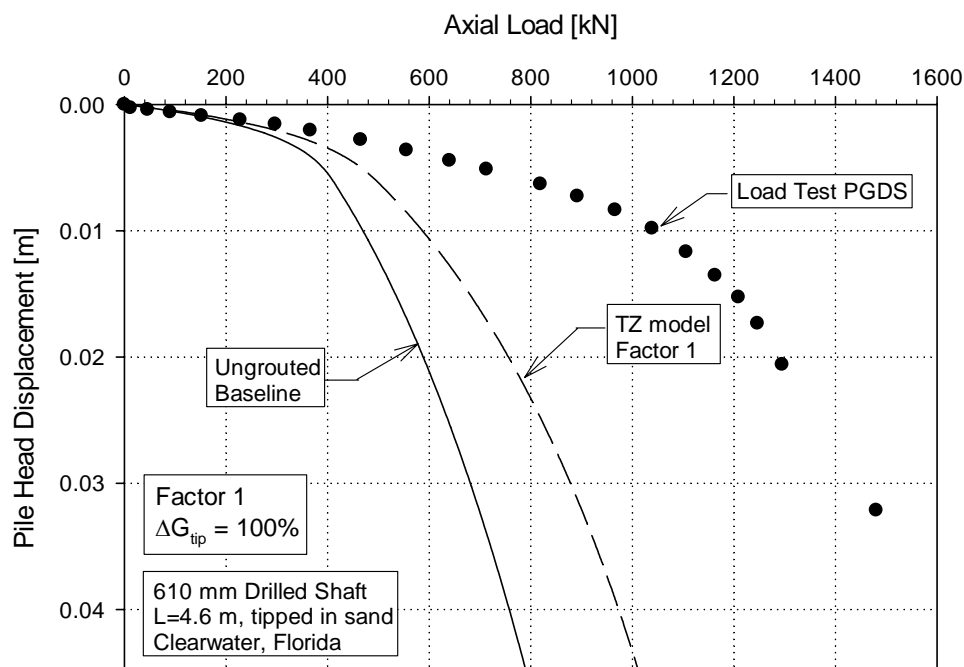


Figure 6-21 SP II – Factor 1: Prediction of the load-settlement curve of PGDS with densified soil under the pile tip

Good agreement with test data was only obtained for the initial part of the curve, up to 400 kN. This analysis was done with different levels of increased shear modulus of the

soil near the pile tip. Figure 6-21 corresponds to an increase level of 100%, and even this high level of shear modulus improvement was inadequate to capture the measured ultimate capacity of the PGDS foundation.

(3) Factor 2: Consider stress reversal along the shaft

Results of the analyses considering Factor 2, i.e., only shear stress reversal along the shaft contributed to the PGDS performance improvement are shown in Figure 6-22.

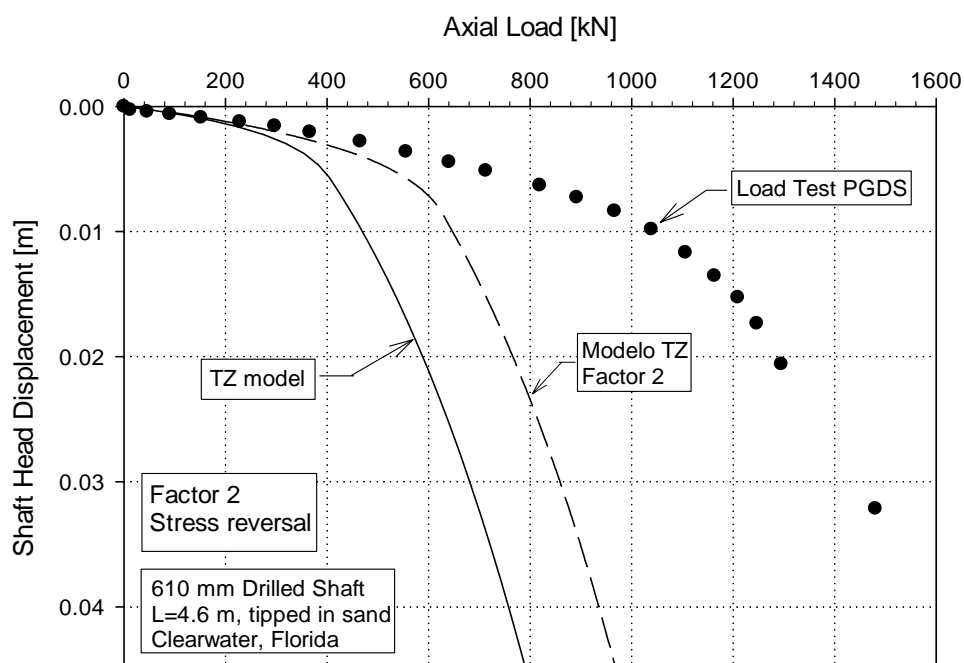


Figure 6-22 SP II – Factor 2: Prediction of the load-settlement curve of PGDS considering stress reversal along the shaft

Once more, good agreement between numerical and field results is restricted only to a small portion of the load settlement curve and the PGDS capacity is underpredicted.

(4) Factor 3: Consider the formation of a grout bulb under the pile tip

Results for the third factor are presented in Figure 6-23. A bulb radius of 1.8 times that of the shaft was obtained with the cavity expansion approach presented in Chapter 5. The figure shows that the assumption of augmented tip area alone significantly under-predicts the capacity measured for the PGDS.

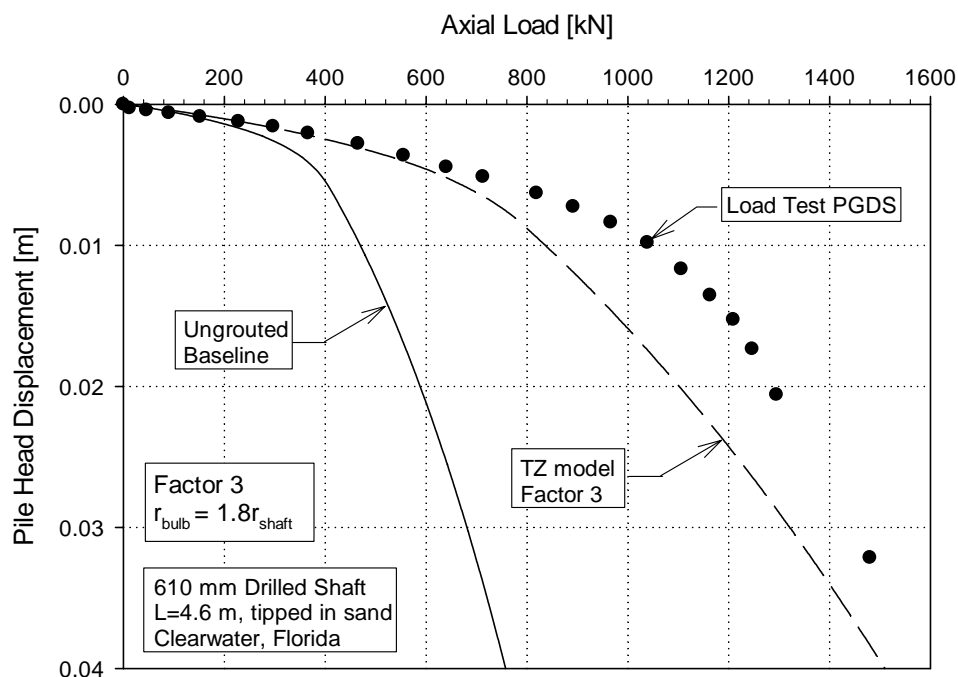


Figure 6-23 SP II – Factor 3: Prediction of the load-settlement curve of PGDS considering augmented tip area

(5) Combination of factors

Since none of the three factors alone could adequately represent the measured response of the post grouted drilled shaft, additional analyses were performed combining these effects, in order to improve the prediction of the actual PGDS load-settlement curve.

The best representation of the measured load-settlement curve for the PGDS was obtained combining all three factors. This is shown in Figure 6-24. The enlarged tip area of the PGDS in this analysis was calibrated to match the load settlement curve recorded in the field. The adjusted bulb radius was 1.3 times that of the shaft, which represents a reduction of 38 % with respect to the first estimation.

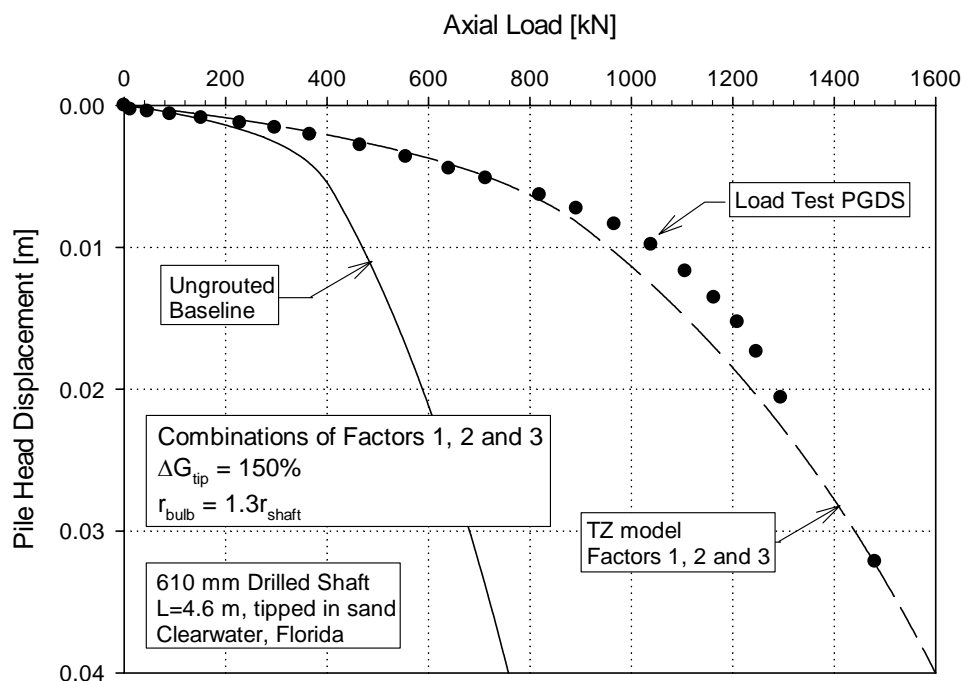


Figure 6-24 SP II – Factors 2 and 3: Calibrated load-settlement curve

The calibrated PGDS model also assumed an increase in the shear modulus for the Q_b - Z curve of 150 % with respect to the original curve in the ungrouted model. Similar to the previous case, this high shear modulus may be indicative of a soil – grout mix that may have formed under the shaft rather than indicative of a large compression of the lower soil layer (note that the Sleeve Port apparatus does not involve a membrane which separates the slurry from the soil).

As can be observed, results from cases SP I and SP II were reasonably similar as may be expected since both PGDS were equipped with the same grouting apparatus and installed one near the other in the same site. The same can be said regarding FJ I and FJ II.

6.4 LOAD TESTS AT THE UNIVERSITY OF HOUSTON

This section presents analyses for drilled shafts tested in a joint effort by the University of South Florida and the University of Houston to assess the effectiveness of PGDS. This effort involved testing four 1.22 m in diameter drilled shafts at a test site near the University of Houston. The test piles were instrumented with three levels of strain gages that were used to evaluate the load distribution along the shaft.

The site was characterized by means of (6) CPT soundings, (2) Standard Penetration Test borings, and (2) Texas Cone Penetrometer soundings. However, the site seemed to be fairly uniform throughout. Because of this, it was decided to develop a unique soil profile (and therefore a unique axial pile capacity profile) for the site by averaging the available CPT soundings. The soil conditions are shown in Appendix A, for four CPT soundings and for the average CPT profile developed for the site. The field exploration program revealed little soil variability (Mullins and Winters, 2004). In Figure 6-25 the most relevant geotechnical information gathered at this site is shown. The specific soil information for each test pile is provided in Appendix A. A schematic plan view showing the relative location of the five drilled shafts tested at this site is depicted in Figure 6-25.

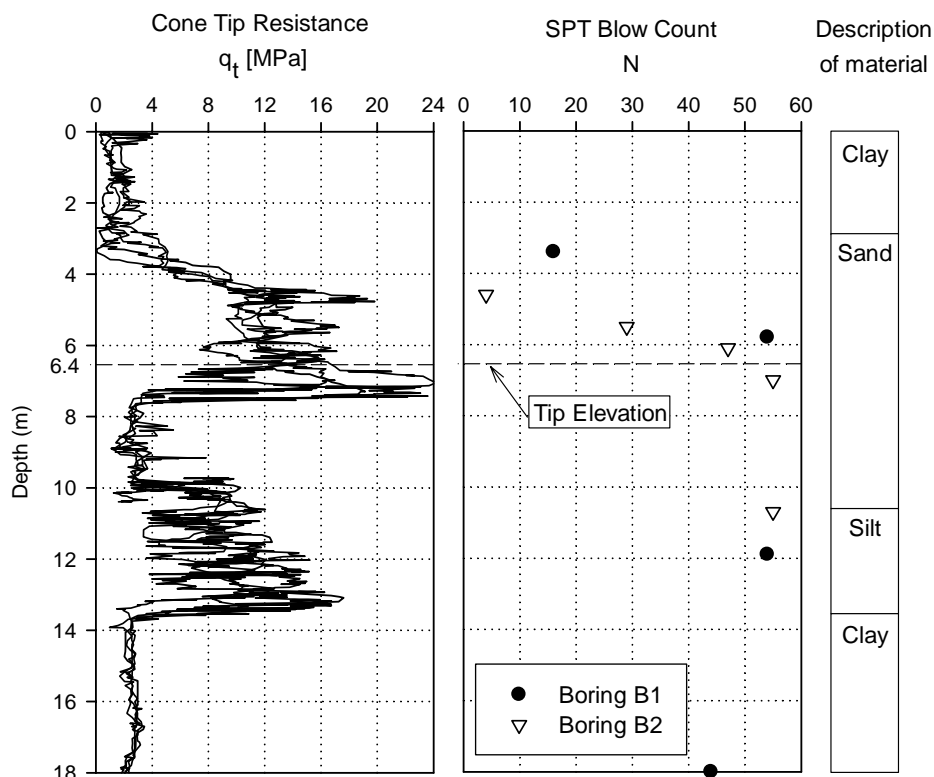


Figure 6-25 Geotechnical information gathered at testing site near University of Houston, Texas

The test program involved two sets of test piles. The first set of drilled shafts was excavated to a depth of 6.4 m such that the pile tips were embedded in sand. The test piles of this set were denoted as S1 and S2, where the 1 and 2 refer to ungrouted (control) and grouted piles, respectively. The second set of test piles was excavated to a depth of 15.2 m such that the pile tips were embedded in clay. The control pile and PGDS were denoted C1 and C2, respectively. The following section presents results of the load transfer analyses carried out for test piles S1 and S2. Test piles C1 and C2 were not analyzed due to insufficient information available for these piles.

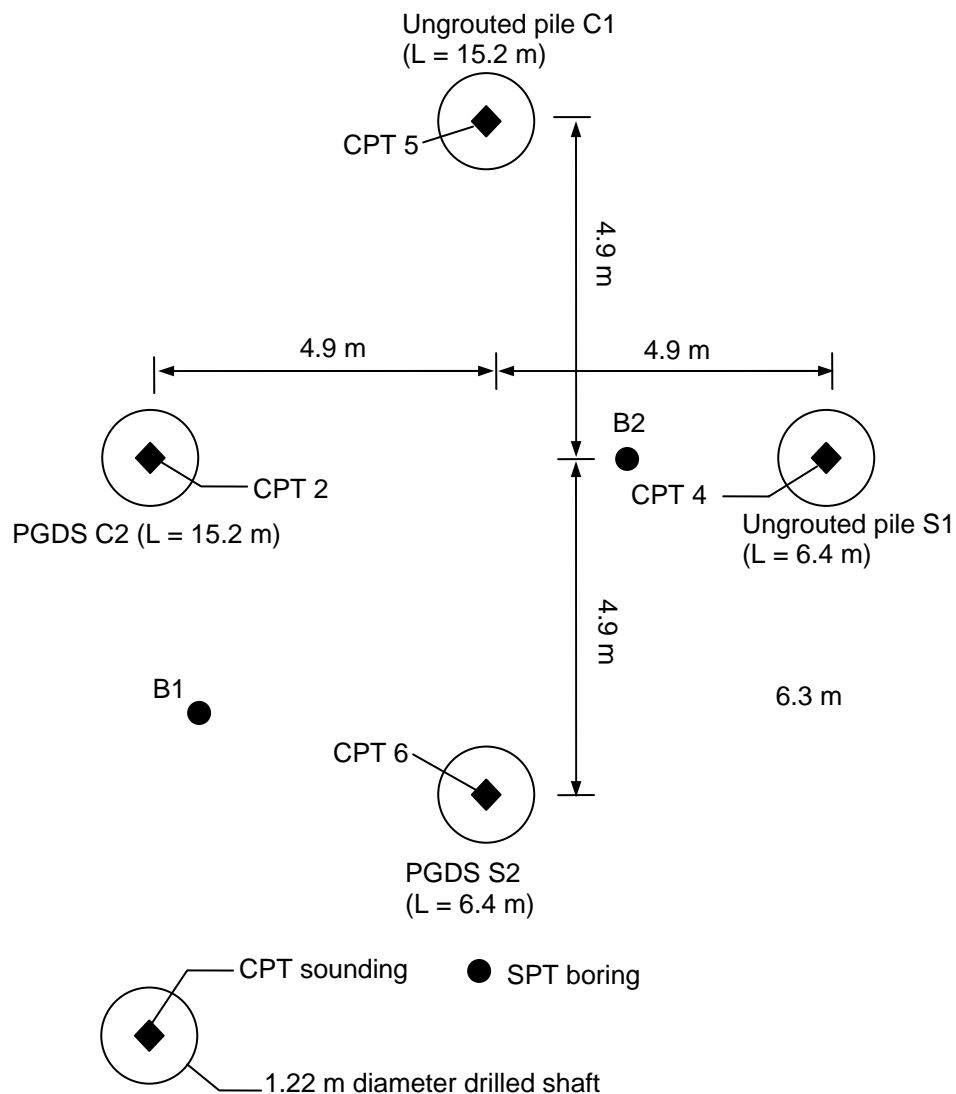


Figure 6-26 Layout of Site near the University of Houston

All load testing was carried out using a 16 MN Statnamic device. The results presented herein are presented as equivalent static load tests were as reported by Mullins and Winters (2004). The load settlement curves for the control pile S1 and for the PGDS S2 tested at this site are depicted in Figure 6-27.

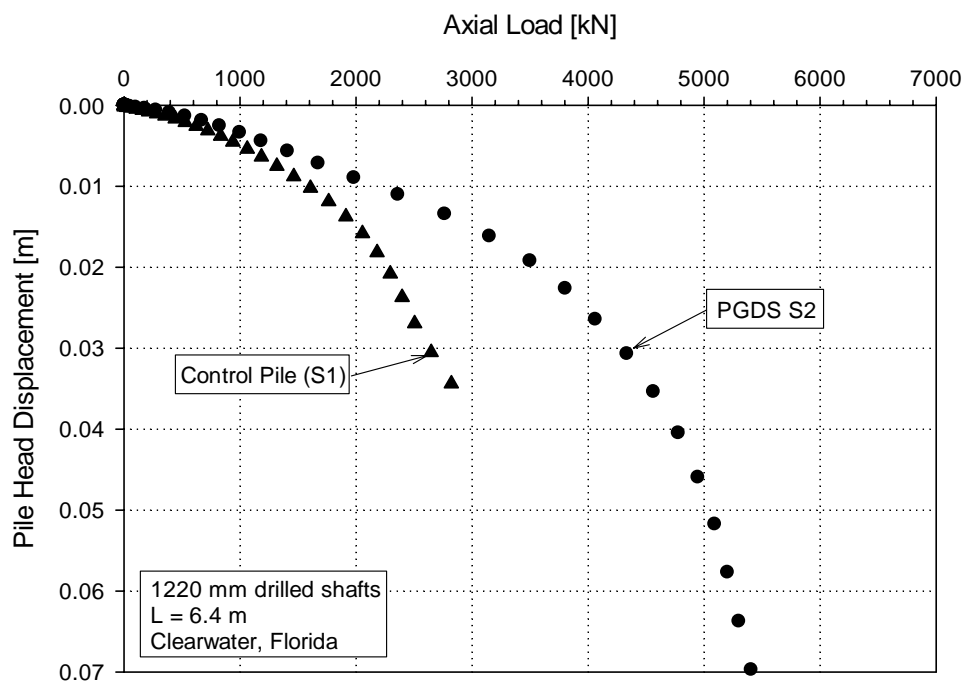


Figure 6-27 Equivalent static load test data for PGDS S2 and control pile S1 at the testing near University of Houston

In the following sections numerical models for the PGDS tested at the site near the University of Houston are presented.

6.4.1 CONTROL PILE

A Type A prediction for the load settlement curve of the ungrouted control drilled shaft near the University of Houston is depicted in Figure 6-28.

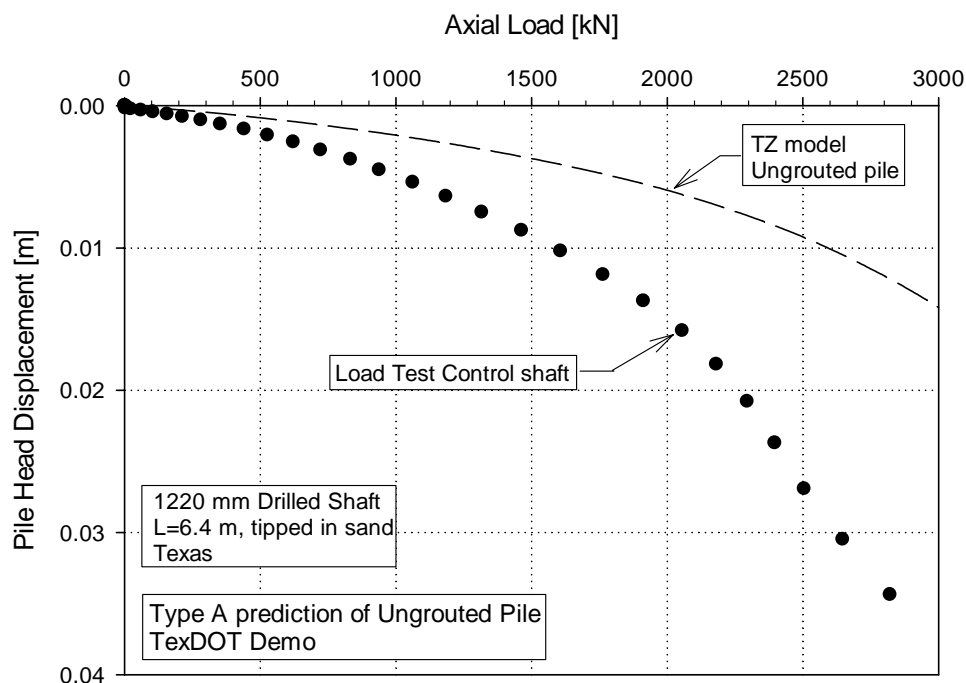


Figure 6-28 Predicted and measured control pile load settlement curves for the Texas DOT Demo (type A prediction)

Figure 6-28 shows that pile stiffness of the control pile was significantly overpredicted. Dissimilar from the previous case studies, in this site, soil characteristics for the control pile location are the same as those for the PGDS location because of the relatively uniform soil conditions at the site (see Appendix B). For this reason the numerical model for the ungrouted pile was calibrated to match the load settlement curve of the control pile measured in the field. Results of the calibrated model and the measured load settlement curve of the control pile are shown in Figure 6-29. In order to obtain a good representation of the load settlement curve for the control pile measured in the field, both asymptotic values of the T-Z curves and shear modulus of the soil along the shaft had to be modified. These values had to be reduced with respect to the original values

used in the type A prediction. The adjusted model was used as baseline to develop the load transfer model for the PGDS which is described in the following paragraphs.

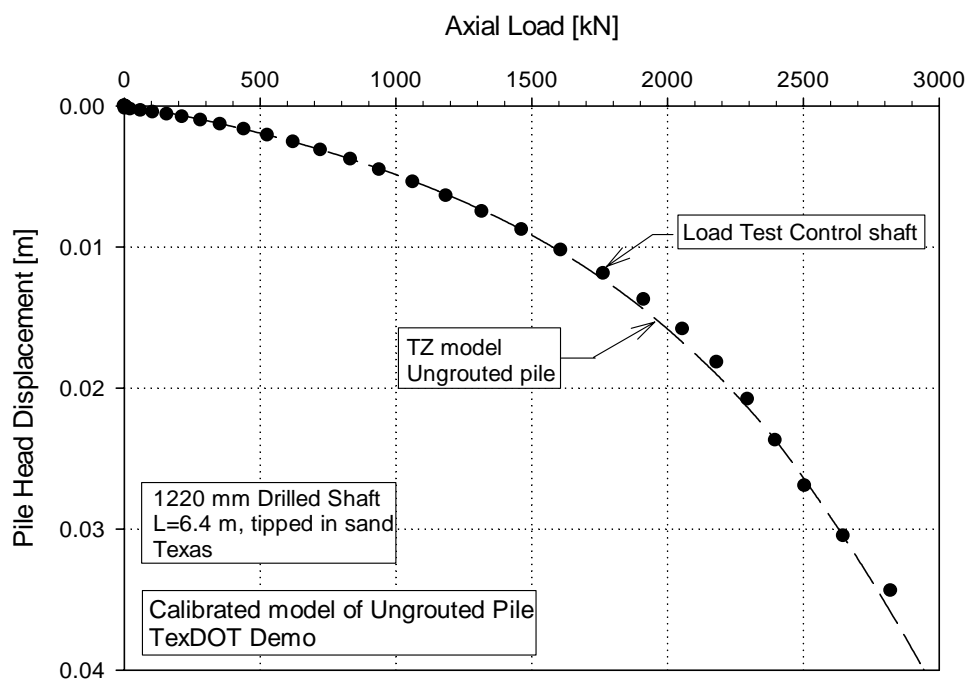


Figure 6-29 Calibrated control pile model for the Texas DOT Demo

6.4.2 PGDS: S2

The grouting process for this PGDS was reported as occurring in two stages since permeation of the grout was observed (Mullins and Winters, 2004). During the first grouting stage, a maximum sustained grout pressure of 7 kPa and a maximum uplift displacement of the shaft of 3.2 mm were recorded. The volume of grout injected in this first stage was about 0.2 m³. During the second grouting stage the maximum sustained grout pressure reached 1517 kPa and the maximum cumulative upward displacement was about 12 mm. The total grout volume injected was 0.25 m³. The CPT soundings and shear wave velocity estimations using correlations with CPT data at this testing site are

shown in Figures A-13 through A-18, in Appendix A. Numerical results obtained for the PGDS are presented following the structure outlined in subsection 6.2

(1) **Load settlement curve for ungrouted pile:** Due to the relative uniform soil conditions it was considered reasonable to use the calibrate model presented in subsection 6.4.1. The load settlement curve for this model was presented in Figure 6-28.

(2) **Factor 1: Increased shear modulus of the soil under the pile tip.**

This run was carried out assuming that post grouting resulted only in an increased shear modulus of the soil under the pile tip. Results of the load transfer analyses using Factor 1 are shown in Figure 6-30.

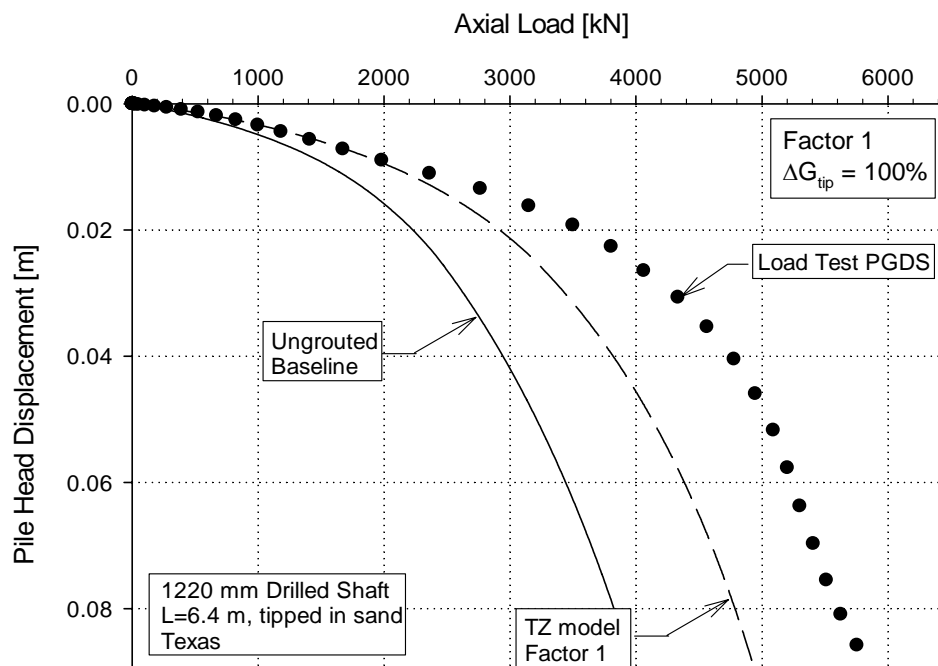


Figure 6-30 S2 – Factor 1: Prediction of the load-settlement curve of PGDS with densified soil under the pile tip

Good agreement with test data was only obtained for the initial part of the curve for axial loads up to 2000 kN. The curve shown in Figure 6-30 corresponds to a shear modulus increase of 100%. Even this relatively high level of shear modulus improvement was inadequate to capture the measured response of the PGDS.

(3) Factor 2: Consider stress reversal along the shaft

Load transfer analyses were carried out assuming that the only effect of post grouting on the pile was the development of residual stresses along the shaft due to shear stress reversal. Results of the numerical analyses that consider only Factor 2 are shown in Figure 6-31.

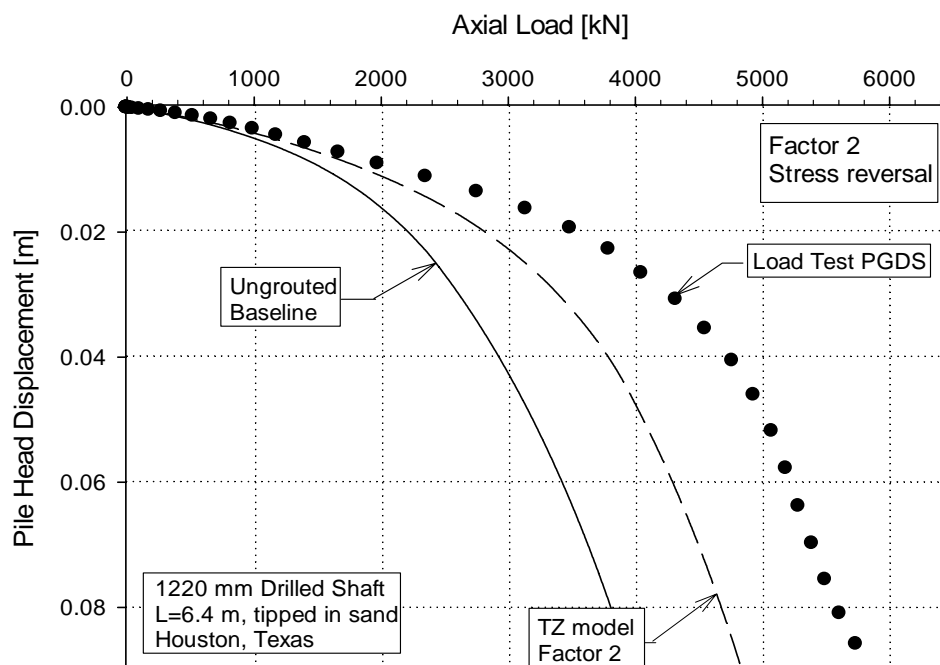


Figure 6-31 S2 – Factor 2: Prediction of the load-settlement curve of PGDS considering stress reversal along the shaft

Relatively good agreement between numerical and field results is observed only in a small portion of the load settlement curve (for axial loads below 2000 kN). The PGDS ultimate capacity is still underpredicted by about 20 %.

(4) Factor 3: Consider the formation of a grout bulb under the pile tip

Analyses for this factor assumed an increased pile tip area for the PGDS in order to simulate the formation of a grout bulb. Using the cavity expansion theory approach presented in Chapter 5 a bulb radius of 1.8 times that of the shaft was estimated. Load transfer analysis using this enlarged tip area (Factor 3) is presented in Figure 6-29.

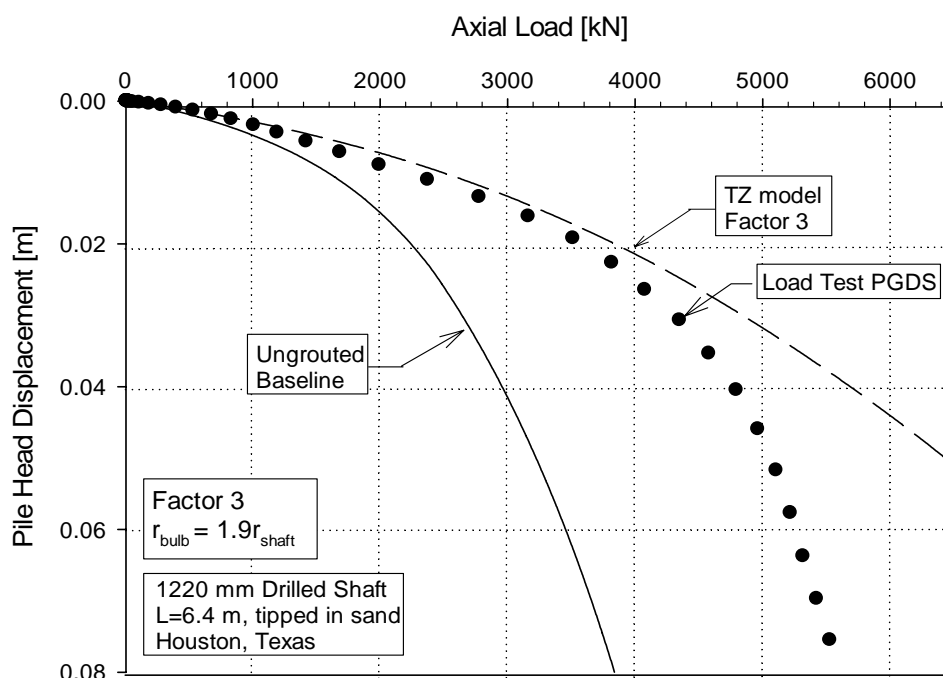


Figure 6-32 S2 – Factor 3: Prediction of the load-settlement curve of PGDS considering augmented tip area

Figure 6-19 shows a significantly overpredicted pile capacity with an estimated bulb radius 1.9 times bigger than that of the shaft. Although this bulb radius is relative large, for smaller radiuses PGDS capacity is still significantly overpredicted.

Post grouting of this drilled shaft was conducted in two stages. The first grouting stage was stopped as no sustained grout pressure could be maintained due to high grout volume losses. The second grouting stage was performed the day after (when the grout injected in the first staged had begun to set). A sustained pressure of 1516 kPa was reached at the end of the second stage. A total cumulative uplift of 12 mm was measured. This situation may be considered representative of stage grouting and not compaction grouting. For these reasons the formation of a grout bulb was considered unlikely.

(5) Combination of factors

The best representation of the measured load-settlement curve for the PGDS was obtained by combining Factors 1 and 2. This is shown in Figure 6-33. The calibrated model was obtained by increasing the shear modulus for the Q_b -Z curve a 100 % with respect to that of the control pile.

This 100 % increase may be representative of the shear modulus of a soil – grout mix produced by the staged - grouting process rather than representative of the modulus of a densified soil. The formation of a soil – grout mix may be attributed to a rupture of the membrane included in the flat jack apparatus soon after grouting started, since permeation of the grout was observed and grouting process had to be divided into two stages.

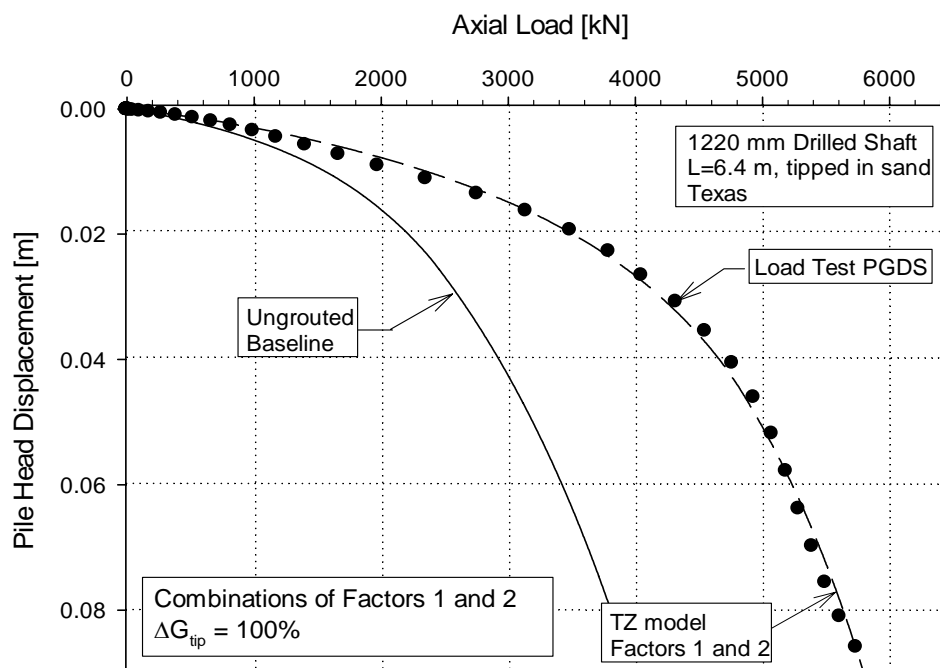


Figure 6-33 S 2 – Factors 1 and 2: Calibrated load-settlement curve

6.5 LOAD TESTS AT THE NGES AT AUBURN UNIVERSITY

This section presents analyses of three drilled shafts constructed and tested at the National Geotechnical Experimentation Site at Auburn University. A total of four PGDS were constructed and tested at the site. Each shaft had a diameter of 1.06 m and was approximately 7.3 m long. One additional pile was constructed and was taken as control pile. The four PGDS were equipped with a flat jack apparatus in order to carry out post grouting. All load testing was carried out using a 4 MN Statnamic device. The results presented herein are presented as equivalent static load tests were as reported by Mullins and Winters (2004).

The piles were embedded in a fairly uniform soil profile classified as ML – SM. Site characterization consisted in a series of five CPT soundings advanced at the centerline of

each test pile location. Little variability was observed from the site exploration results (Mullins and Winters, 2004). Results from the CPT soundings as well as pile capacity profiles are included in Appendix A for all soundings advanced at the site. In Figure 6-34 a summary of the most relevant geotechnical information gathered at this site is shown.

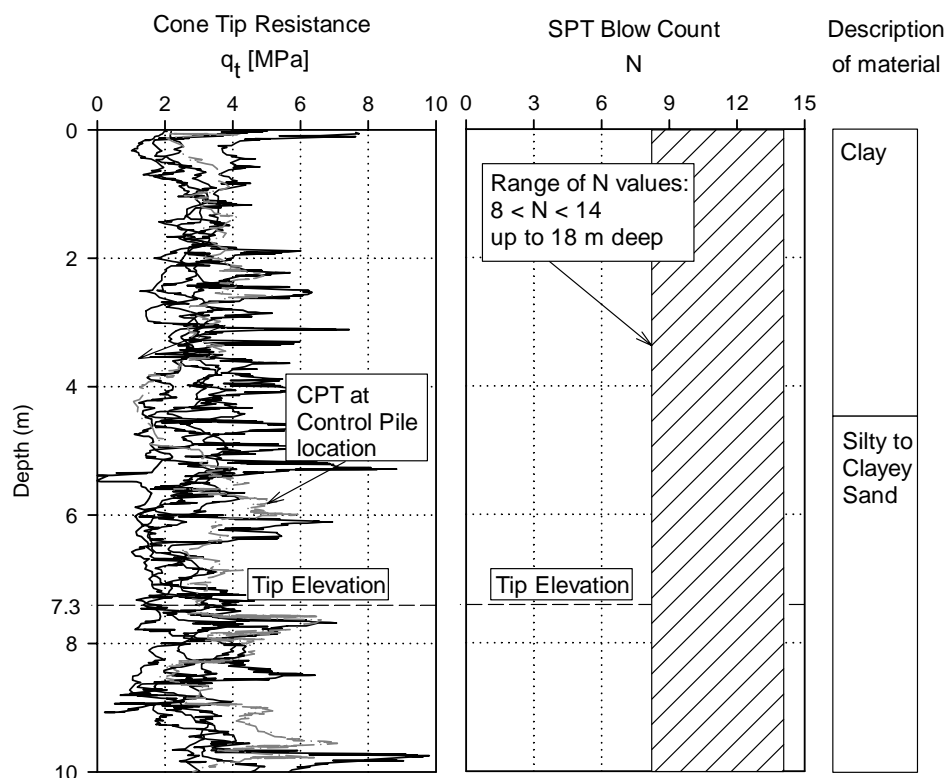


Figure 6-34 Geotechnical information gathered at NGES at Auburn University

The NGES at Auburn University is a well characterized geotechnical site and detailed information can be found elsewhere (Brown and Drew, 2000; Mayne et al., 2000; and Brown and Vinson, 1998). A schematic plan view showing the relative location of the five drilled shafts tested at this site is depicted in Figure 6-35. In the same figure, CPT soundings advanced at NGES at Auburn University are also shown.

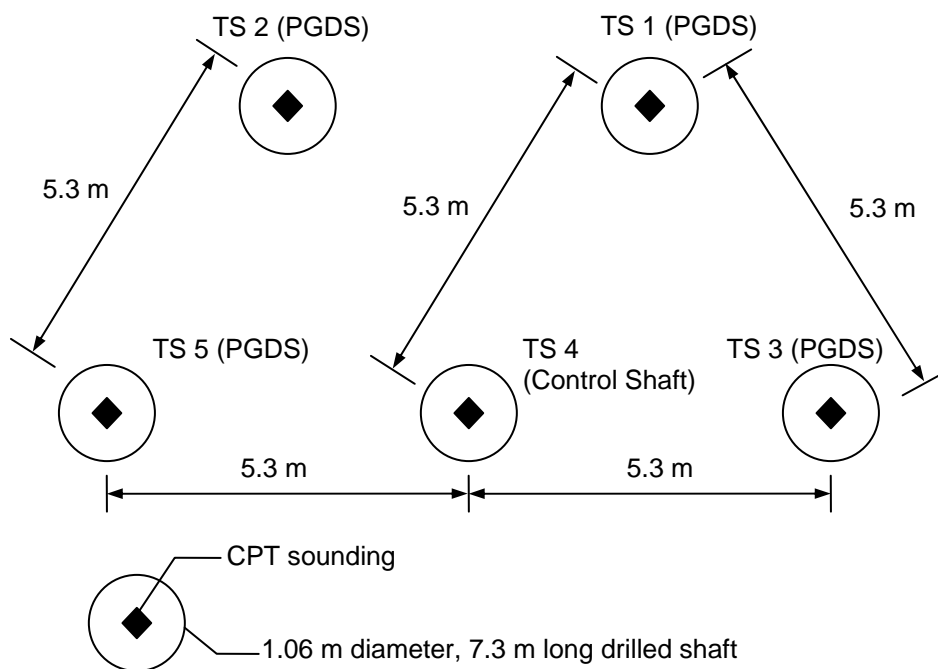


Figure 6-35 Layout of five drilled shafts tested at NGES Auburn University

All load testing was carried out using a 4 MN Statnamic device. The results presented herein are presented as equivalent static load tests were as reported by Mullins and Winters (2004). The load settlement curves for the control pile TS4 and for the three PGDS available tested at this site are depicted in Figure 6-36.

Figure 6-36 show that the control pile had a higher ultimate axial capacity. The exact reason for this is not known and was not explored in detail in this thesis. A possible reason could be differences in soil conditions between the locations of the control pile and the PGDS. This hypothesis is somehow reinforced later with the results of load transfer analyses performed using CPT data extracted from the locations of the PGDS. However, the CPT information depicted in Figure 6-34 does not show important differences between CPT soundings to fully support this hypothesis.

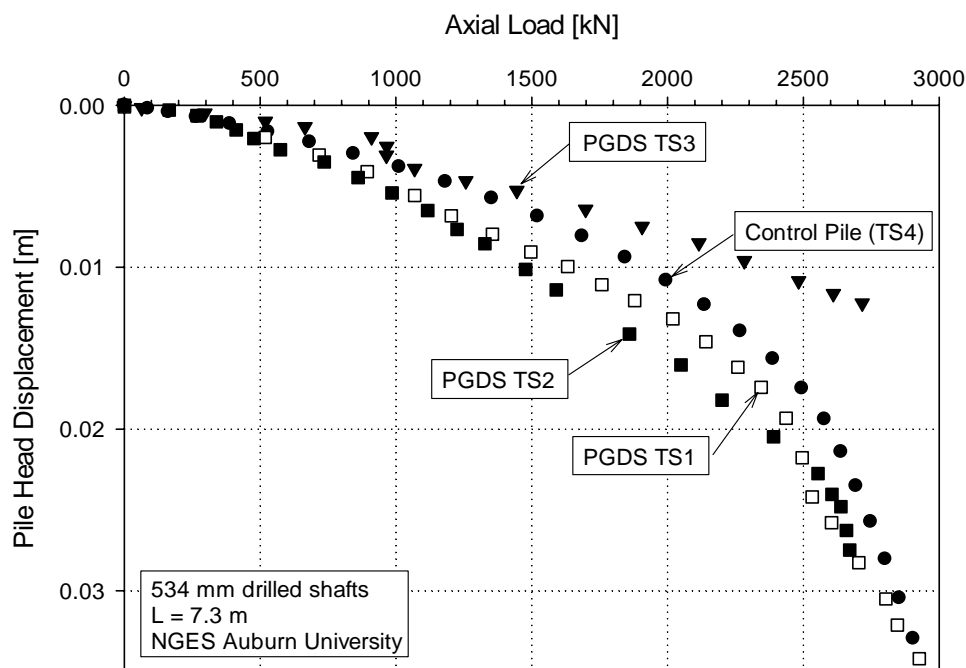


Figure 6-36 Equivalent static load test data for PGDS S2 and control pile S1 at the testing near University of Houston

The grouting process in clayey soil, such as the ones present at this site, may not result in a beneficial effect. This could be related to strain softening of the soil along the shaft and of the soil under the pile tip occurred during stress reversal. Another possible reason could be related to the interpreted equivalent static load derived from the Statnamic testing. It has been reported that high damping in clayey soils make this interpretation difficult. (Middendorp et al., 1992)

In the following sections numerical models for the PGDS tested at the University of Auburn are presented.

6.5.1 CONTROL PILE

The CPT sounding and shear wave velocity estimations at the location of the control pile are shown in Figure A-1, in Appendix A. The control pile capacity derived from the

CPT data depicted in Figure A-1 is shown in Figure A-2. The pile load test result as reported by Mullins and Winters (2004) is shown in. A type A prediction obtained using the proposed load transfer methodology (presented in Chapter 3), for the load settlement curve of the control shaft is also depicted in the same figure. The figure shows good agreement between measured and predicted load settlement curves for the entire curve, even though the ultimate pile capacity was slightly underpredicted by a 5 %.

Due to the fairly good agreement obtained with the type A prediction for the control pile, additional type A predictions were performed using CPT data obtained for each PGDS location using the methodology described in Chapter 3 in order to avoid the effects of soil variability on the results. Figure 6-38 shows these predictions for all CPT soundings available at the site.

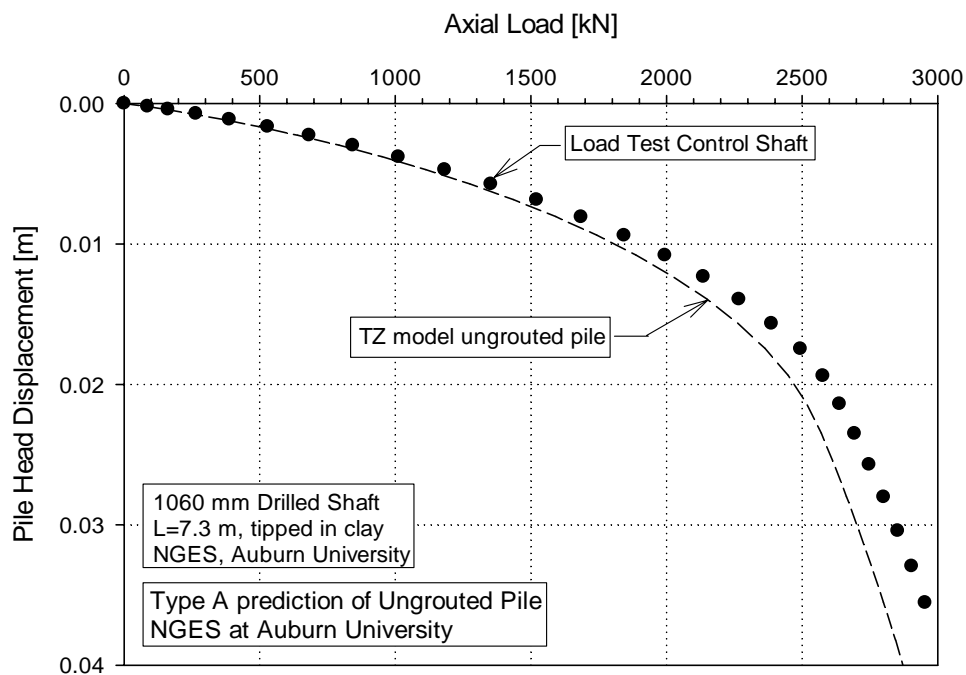


Figure 6-37 Type A prediction for control shaft at NGES at Auburn University

Although CPT readings show a fairly uniform soil profile throughout the site (see Appendix A), pile capacity seems to vary from one pile location to another. This variation is expected to impact the resulting PGDS behavior and the increase in pile capacity due to grouting. For this reason, Type A predictions depicted in Figure 6-38 will be used as baseline to develop load transfer models for the PGDS tested at the geotechnical site at Auburn University.

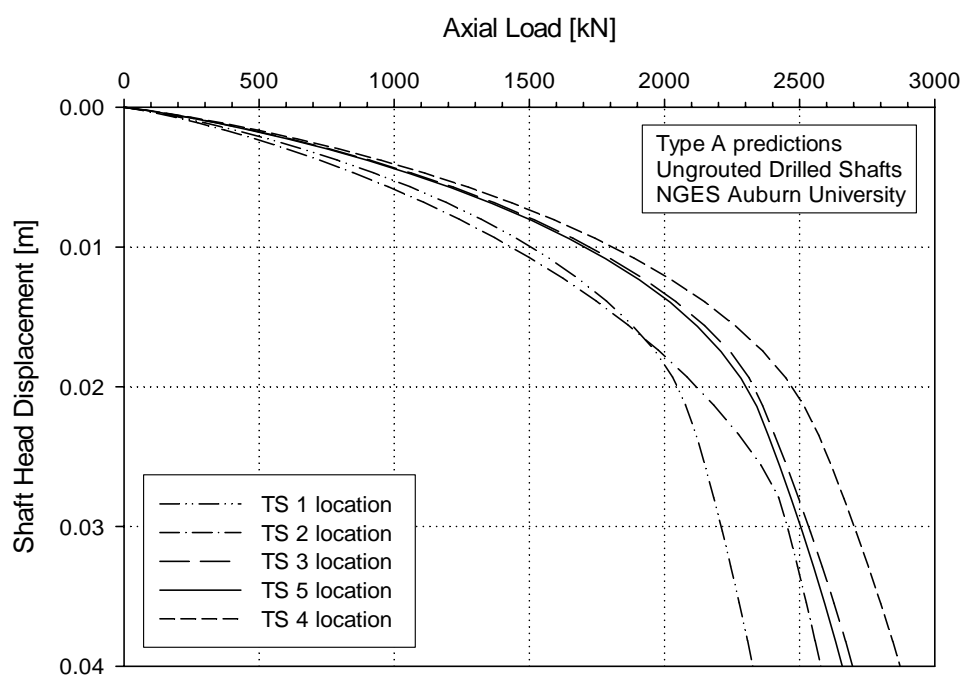


Figure 6-38 Type A prediction for ungrouted piles using data from 5 CPT soundings advanced at the site

6.5.2 PGDS: TS1

Grout data recorded during grouting process of TS 1 showed a maximum sustained pressure of about 565 kPa and a maximum uplift displacement of the shaft of 2.7 mm. The previous values of shaft uplift and grout pressure correspond to an injected grout volume of 0.28 m³.

The CPT sounding and shear wave velocity estimations using correlations with CPT data at the location of FJ I are shown in Figure A-19, in Appendix A. Numerical results obtained for the PGDS are presented following the structure outlined in subsection 6.2.

(1) Load settlement curve for ungrouted pile at TS 1 location

The load settlement curve estimated using ungrouted conditions for an ungrouted drilled shaft at FJ I location is depicted in Figure 6-38. This was obtained using the CPT based pile capacity shown in Figure A-20. This ungrouted pile model was used as baseline for the PGDS numerical models.

(2) Factor 1: Increased shear modulus of the soil under the pile tip.

This run was carried out assuming that post grouting resulted only in an increased shear modulus of the soil under the pile tip. Results of the load transfer analyses using Factor 1 are shown in Figure 6-39.

As can be seen, relatively good agreement with test data was obtained for the initial part of the curve. This analysis was done with different levels of increased shear modulus of the soil near the pile tip. Figure 6-39 corresponds to an increase level of 100%. This level of modulus improvement was seen to overpredict by itself the capacity of the PGDS. However, as said earlier, it is expected a much smaller compression of the soil under the pile tip than the one assumed for this model.

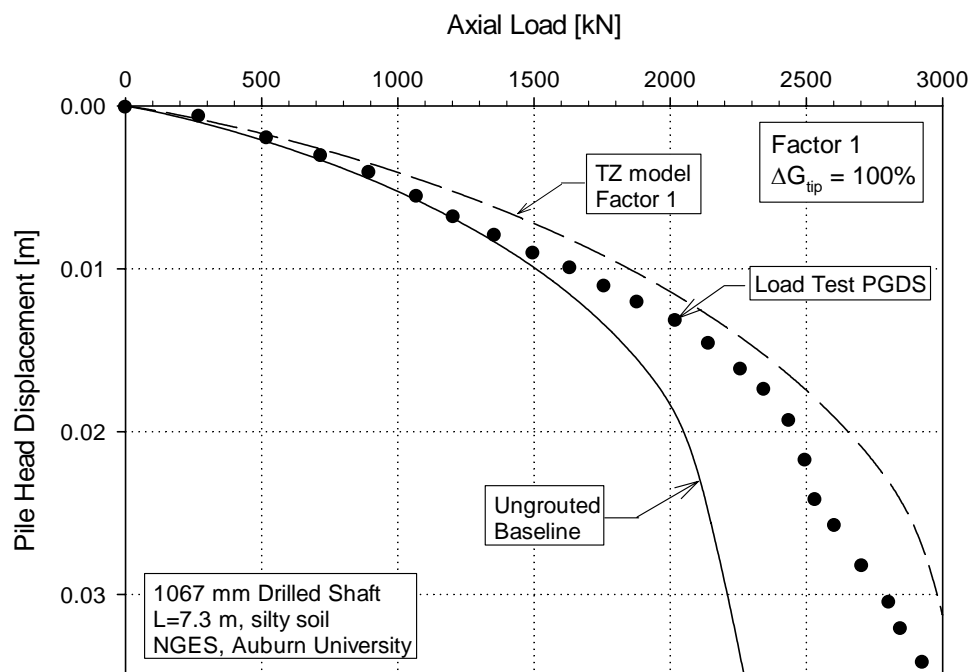


Figure 6-39 TS 1 – Factor 1: Prediction of the load-settlement curve of PGDS with densified soil under the pile tip

(3) Factor 2: Consider stress reversal along the shaft

Load transfer analyses were carried out assuming that the only effect of post grouting on the pile was the development of residual stresses along the shaft due to shear stress reversal. Results of the numerical analyses that consider only Factor 2 are shown in Figure 6-40.

Relatively good agreement is observed for almost the entire load settlement curve of the PGDS. However the PGDS ultimate capacity was slightly underpredicted.

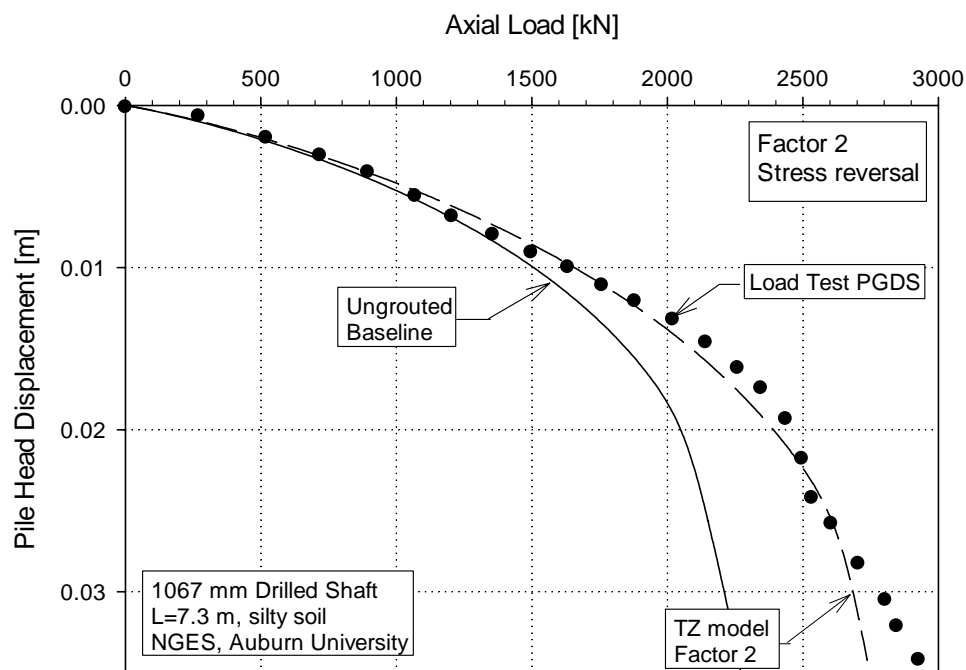


Figure 6-40 TS 1 – Factor 2: Prediction of the load-settlement curve of PGDS considering stress reversal along the shaft

(4) Factor 3: Consider the formation of a grout bulb under the pile tip

Analyses for this factor assumed an increased pile tip area for the PGDS. This enlarged tip area simulates the formation of a grout bulb. Using the cavity expansion theory approach presented in Chapter 5 a bulb radius of 1.4 times that of the shaft was calculated. Load transfer analysis using this enlarged tip area (Factor 3) is presented in Figure 6-41.

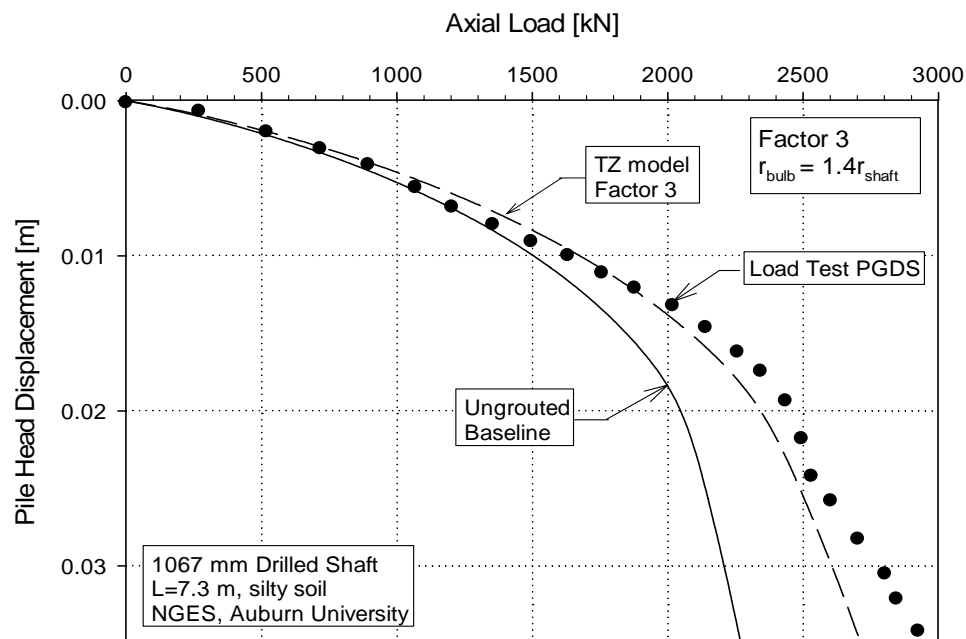


Figure 6-41 TS 1 – Factor 3: Prediction of the load-settlement curve of PGDS considering augmented tip area

This figure shows that, for this case, the assumption that post grouting had only created a grout bulb under the tip area, slightly underpredicts the capacity measured for the PGDS.

(5) Combination of factors

Dissimilar from the previous case studies, both factors 1 and 3 seem to adequately represent the PGDS behavior by themselves. However, factor 2 cannot be neglected since the upward pile head movement of 3 mm recorded during grouting implies a mobilization of about 50 % of the pile side resistance in negative skin friction. Besides, considering that a relatively small grouting pressure was attained in the field, the compression of the soil under the pile is considered unlikely. For these reasons, a numerical model combining factors 2 and 3 was run.

The estimated load-settlement curve for the PGDS obtained combining Factor 2 and Factor 3 is shown in Figure 6-42. The enlarged tip area of the PGDS in this analysis was calibrated to match the load settlement curve recorded in the field. The adjusted bulb radius was 1.1 times that of the shaft, which represents a reduction of about 27 % with respect to the first estimation of the bulb radius. This site had the advantage that the test piles were exhumed. Mullins and Winters (2004) reported that all piles presented a grout bulb attached to the shaft. The reduced bulb radius obtained for this case is consistent with photographs reported by Mullins and Winters (2004) taken to one of the exhumed piles at the site.

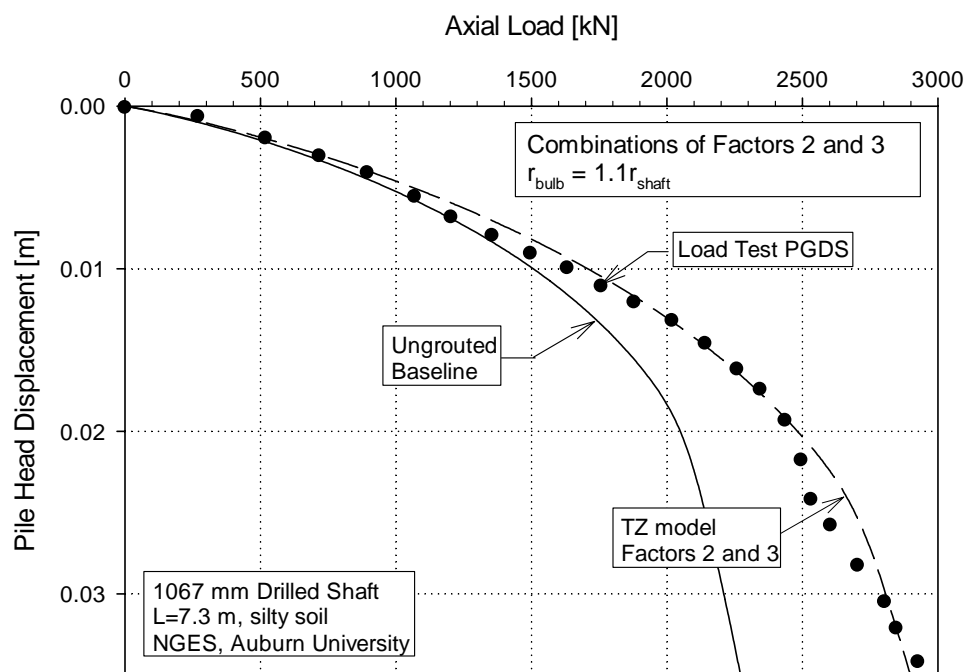


Figure 6-42 TS 1 – Factors 2 and 3: Calibrated load-settlement curve

6.5.3 PGDS: TS2

Grout data recorded during grouting process of TS 2 showed a maximum sustained pressure of about 607 kPa and a maximum uplift displacement of the shaft of 1.9 mm. The previous values of shaft uplift and grout pressure correspond to an injected grout volume of 0.28 m³.

The CPT sounding and shear wave velocity estimations using correlations with CPT data at the location of FJ I are shown in Figure A-21, in Appendix A. Numerical results obtained for the PGDS are presented following the structure outlined in subsection 6.2.

(1) Load settlement curve for ungrouted pile at TS 2 location

The load settlement curve estimated using ungrouted conditions for an ungrouted drilled shaft at FJ I location is depicted in Figure 6-38. This was obtained using the CPT based pile capacity shown in Figure A-22. This ungrouted pile model was used as baseline for the PGDS numerical models.

(2) Factor 1: Increased shear modulus of the soil under the pile tip.

This run was carried out assuming that post grouting resulted only in an increased shear modulus of the soil under the pile tip. Results of the load transfer analyses using Factor 1 are shown in Figure 6-43.

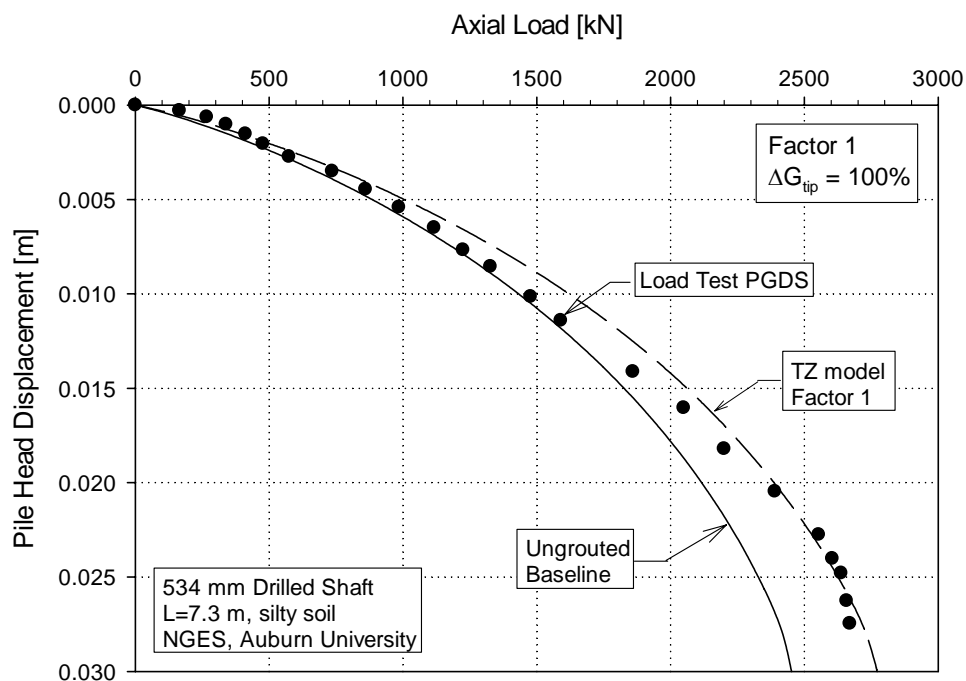


Figure 6-43 TS 2 – Factor 1: Prediction of the load-settlement curve of PGDS with densified soil under the pile tip

As can be seen, reasonably good agreement with test data was obtained incorporating only Factor 1. Figure 6-43 corresponds to a shear modulus increase level of 100%. Although this level of shear modulus improvement appears to adequately represent the PGDS behavior, it seems to be excessively high and this level of shear modulus improvement is considered unlikely to occur.

As seen in Figure 6-36, the post grouting of TS2 improved the pile capacity only by a small percentage. Thus, small modifications of each one of the factors may be enough to explain the PGDS improved capacity. Dissimilar to the previous cases, this site presented a clayey soil profile, which may explain the small improvement obtained with tip post grouting.

(3) Factor 2: Consider stress reversal along the shaft

Load transfer analyses were carried out assuming that the only effect of post grouting on the pile was the development of residual stresses along the shaft due to shear stress reversal. Results of the numerical analyses that consider only Factor 2 are shown in Figure 6-44.

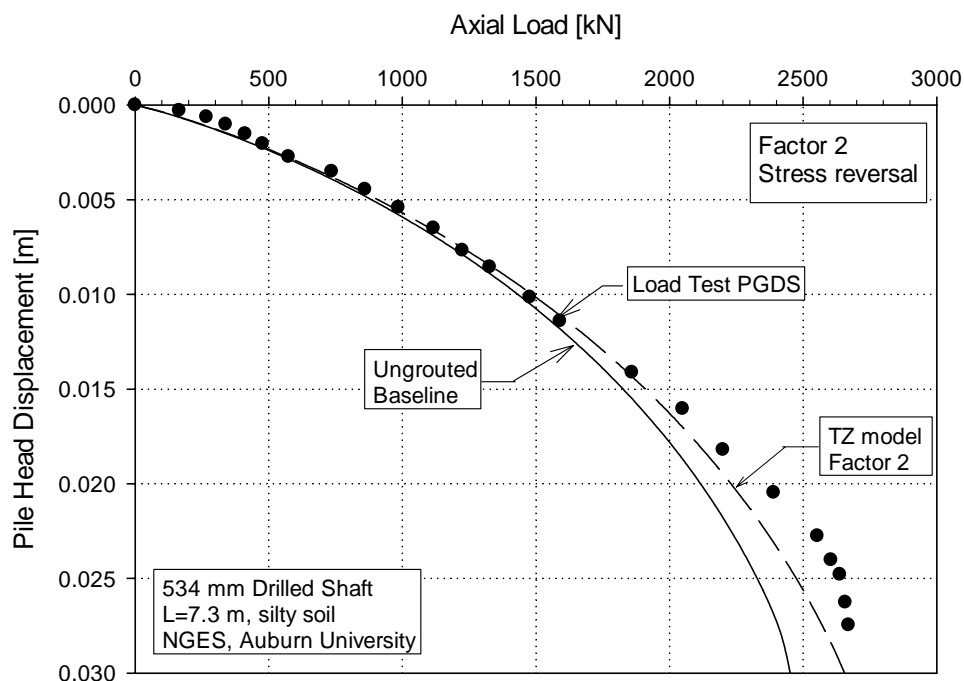


Figure 6-44 TS 2 – Factor 2: Prediction of the load-settlement curve of PGDS considering stress reversal along the shaft

The inclusion of factor 2 alone in the numerical model seems to underpredict the PGDS response including the ultimate capacity. In Figure 6-44 it can be seen that only a small improvement due to shear stress reversal was obtained in this case.

(4) Factor 3: Consider the formation of a grout bulb under the pile tip

Analyses for this factor assumed an increased pile tip area for the PGDS. This enlarged tip area simulates the formation of a grout bulb. Using the cavity expansion theory approach presented in Chapter 5 a bulb radius of 1.4 times that of the shaft was calculated. Load transfer analysis using this enlarged tip area (Factor 3) is presented in Figure 6-45.

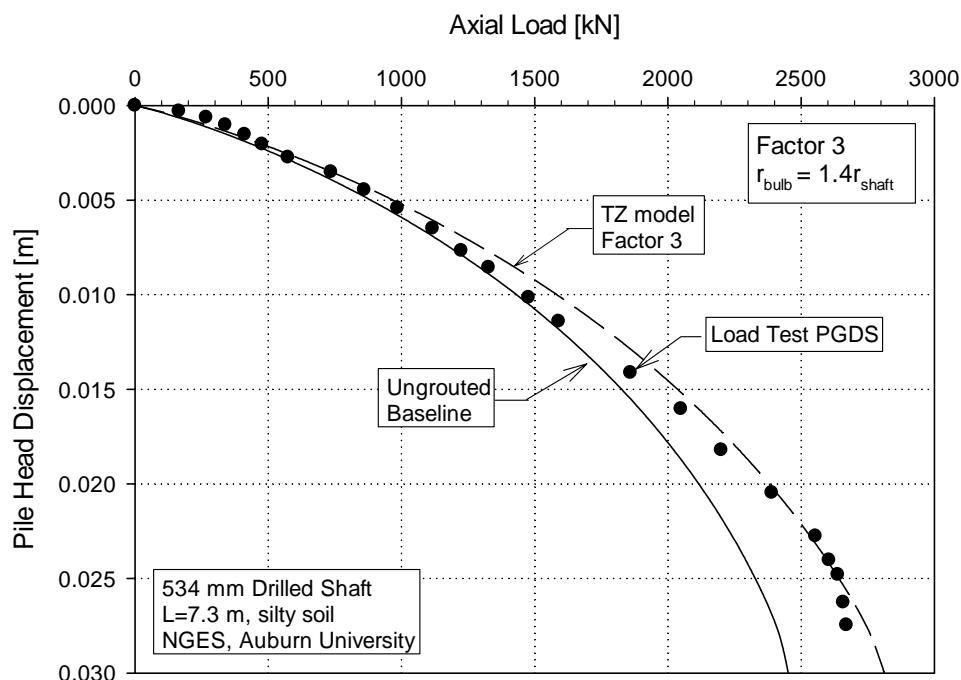


Figure 6-45 TS 2 – Factor 3: Prediction of the load-settlement curve of PGDS considering augmented tip area

This figure shows that the assumption that post grouting had only created a grout bulb under the tip area, for this case seems to adequately represent the capacity measured for the PGDS. The results obtained by incorporating Factor 3 in the load transfer model were similar to those obtained by incorporating Factors 1 and 2 in that, for this case, each one of the three factors appeared to be enough to represent the PGDS behavior. However, as

explained previously, a shear modulus increase of 100 % is believed to be excessively high. Moreover, Factor 3 may have been overpredicted since it was accounted for using the cavity the expansion approach presented in Chapter 5, which does not represent closely the pile post grouting process. For these reasons, a model combining factors 2 and 3 will be performed in order to adequately capture the PGDS behavior.

(5) Combination of factors

Although each one of the factors gave relative close estimates of the PGDS behavior, a combination of factors was found necessary in order to improve the agreement between measured and predicted curves.

The best representation of the measured load-settlement curve for the PGDS was obtained combining Factor 2 and Factor 3. This is shown in Figure 6-46. The enlarged tip area of the PGDS in this analysis was calibrated to match the load settlement curve recorded in the field. The adjusted bulb radius was 1.15 times that of the shaft, which represents a reduction of 20 % with respect to the first estimation of the bulb radius.

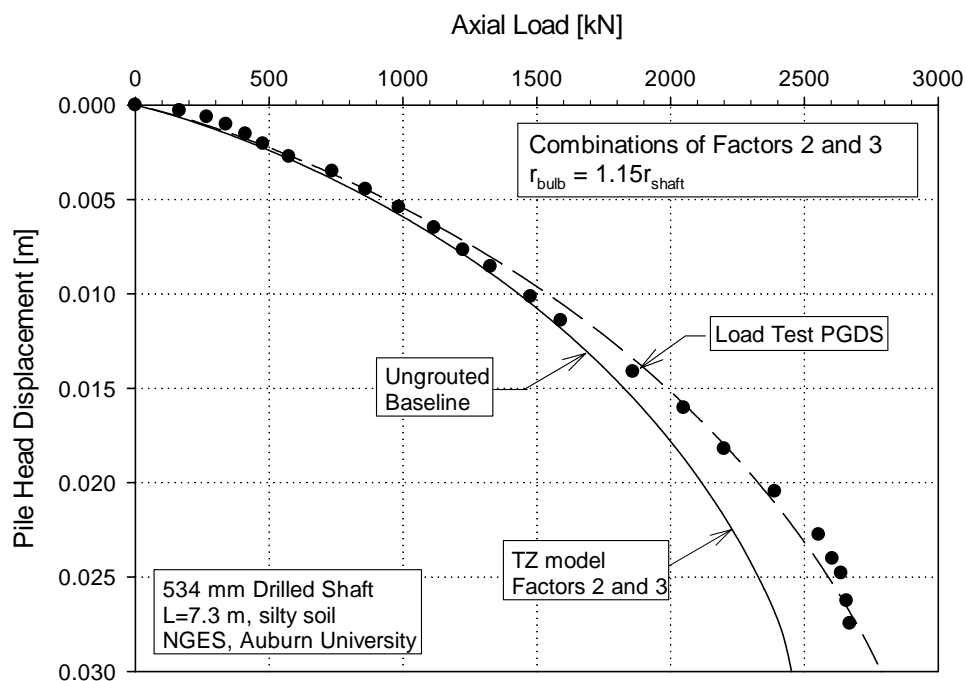


Figure 6-46 TS 2 – Factors 2 and 3: Calibrated load-settlement curve

Similar to case study TS 1, compression of the soil under the pile was considered unlikely because of the low grouting pressure attained in the field. For this PGDS in particular, the improvement of pile resistance obtained with post grouting seems to be extremely small. As stated earlier, this can be observed from results of the previous steps where each factor alone gave close estimates of the overall PGDS behavior even for relatively small variations of the parameters for each factor (i. e. bulb radius 1.4 times bigger than that of the shaft and a small pile upward movement of less than 2 mm which implies that only a 10 % of the available side shear was mobilized in negative skin friction).

6.5.4 PGDS: TS3

Grout data recorded during grouting process of TS 3 showed a maximum sustained pressure of about 689 kPa and a maximum uplift displacement of the shaft of 3.3 mm. The previous values of shaft uplift and grout pressure correspond to an injected grout volume of 0.28 m³.

The CPT sounding and shear wave velocity estimations using correlations with CPT data at the location of FJ I are shown in Figure A-23, in Appendix A. Numerical results obtained for the PGDS are presented following the structure outlined in subsection 6.2.

(1) Load settlement curve for ungrouted pile at TS 3 location

The load settlement curve estimated using ungrouted conditions for an ungrouted drilled shaft at FJ I location is depicted in Figure 6-38. This was obtained using the CPT based pile capacity shown in Figure A-24. This ungrouted pile model was used as baseline for the PGDS numerical models.

(2) Factor 1: Increased shear modulus of the soil under the pile tip.

This run was carried out assuming that post grouting resulted only in an increased shear modulus of the soil under the pile tip. Results of the load transfer analyses using Factor 1 are shown in Figure 6-47.

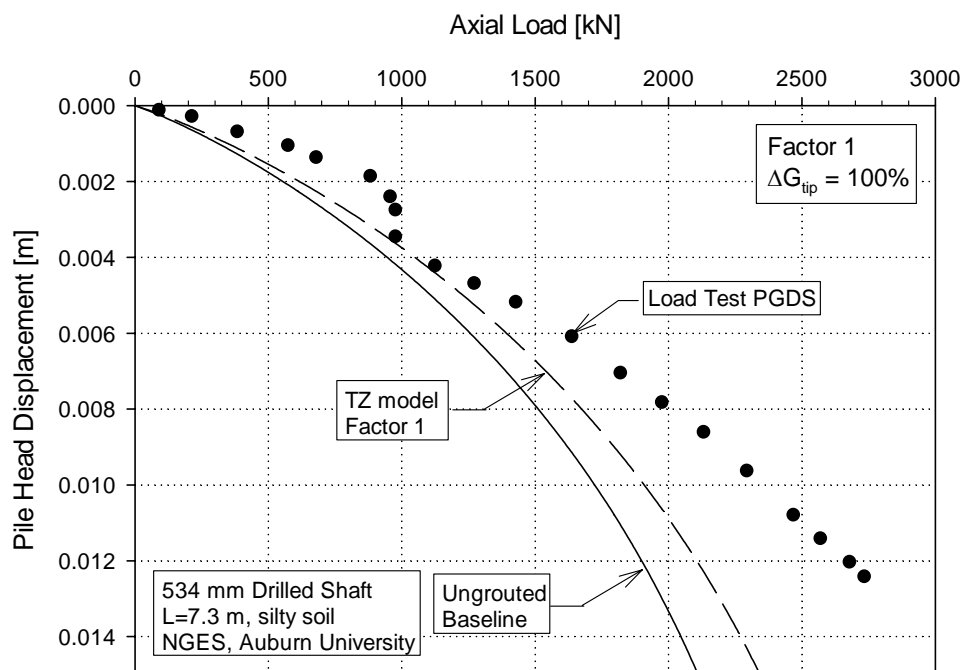


Figure 6-47 TS 3 – Factor 1: Prediction of the load-settlement curve of PGDS with densified soil under the pile tip

As can be seen, good agreement with test data was only obtained for the initial part of the curve. This analysis was done with different levels of increased shear modulus of the soil near the pile tip. Figure 6-47 corresponds to an increase level of 100%, and even this level of shear modulus improvement was inadequate to capture the measured ultimate capacity of the PGDS foundation.

(3) Factor 2: Consider stress reversal along the shaft

Load transfer analyses were carried out assuming that the only effect of post grouting on the pile was the development of residual stresses along the shaft due to shear stress reversal. Results of the numerical analyses that consider only Factor 2 are shown in Figure 6-48.

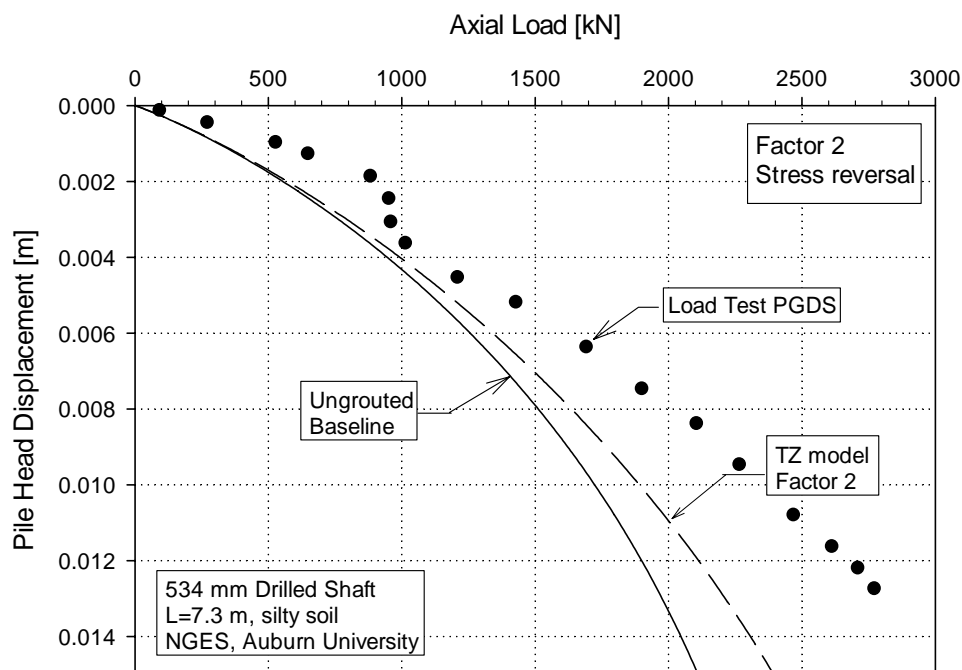


Figure 6-48 TS 3 – Factor 2: Prediction of the load-settlement curve of PGDS considering stress reversal along the shaft

Similar to results obtained with factor 1, the ultimate axial capacity of the PGDS foundation is still significantly underpredicted assuming that only factor 2 was mobilized by grouting.

(4) Factor 3: Consider the formation of a grout bulb under the pile tip

Analyses for this factor assumed an increased pile tip area for the PGDS. This enlarged tip area simulates the formation of a grout bulb. Using the cavity expansion theory approach presented in Chapter 5 resulted in a bulb radius of 1.5 times that of the shaft. Load transfer analysis using this enlarged tip area (Factor 3) is presented in Figure 6-49.

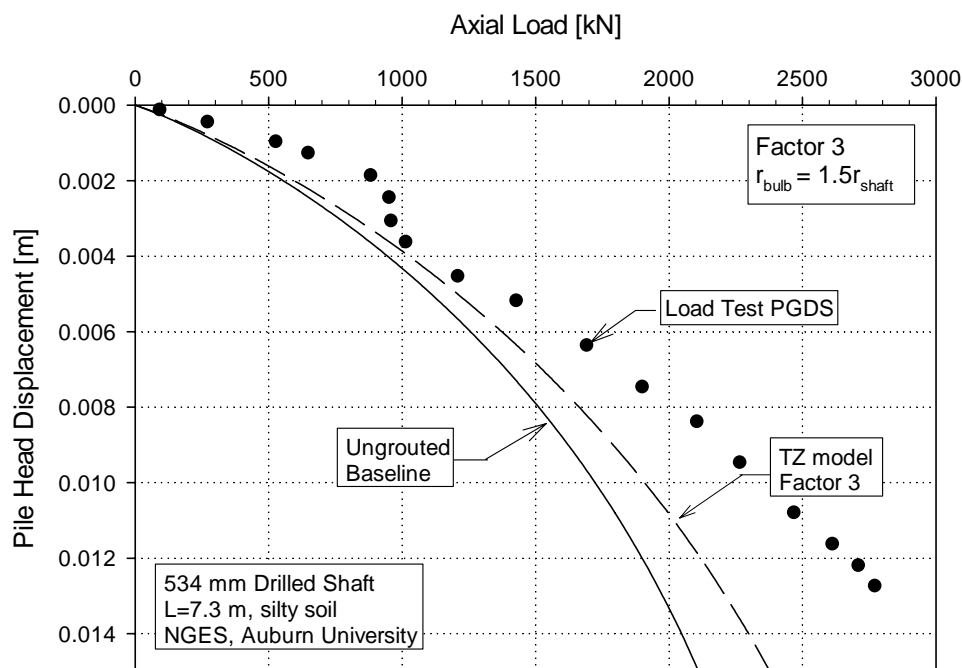


Figure 6-49 TS 3 – Factor 3: Prediction of the load-settlement curve of PGDS considering augmented tip area

This figure shows that the assumption that post grouting had only created a grout bulb under the tip area, significantly under-predicts the capacity measured for the PGDS.

(5) Combination of factors

Since none of the three aforementioned factors alone could adequately represent the measured response of the post grouted drilled shaft, additional analyses were performed combining these effects, in order to improve the prediction of the actual PGDS load-settlement curve. The best representation of the measured load-settlement curve for the PGDS was obtained combining factors 1, 2, and 3. This is shown in Figure 6-50.

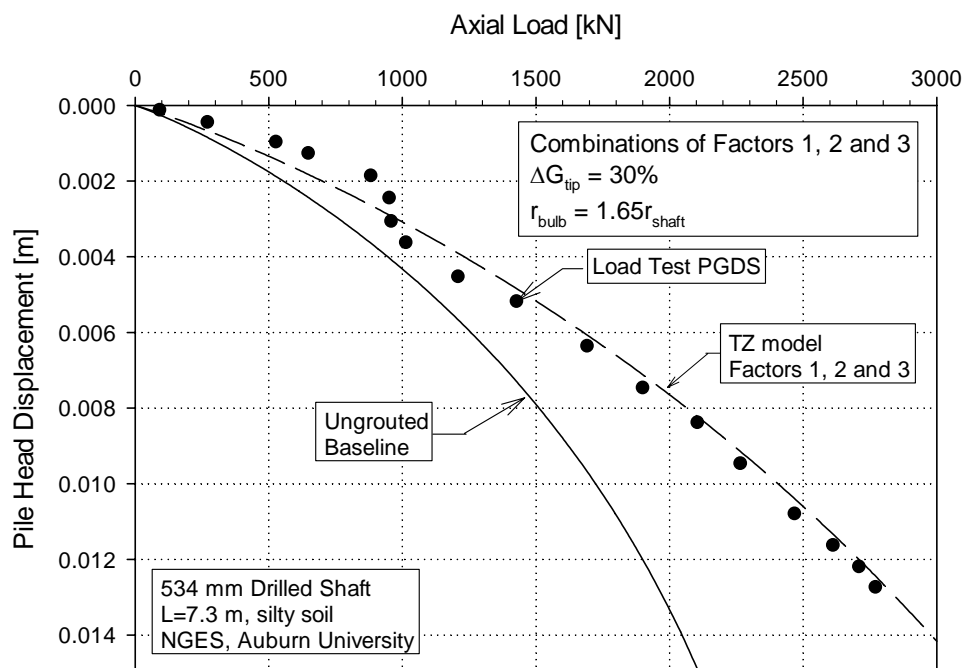


Figure 6-50 TS 3 – Factors 1, 2 and 3: Calibrated load-settlement curve

The enlarged tip area of the PGDS in this analysis was calibrated to match the load settlement curve recorded in the field. The adjusted bulb radius was 1.65 times that of the shaft, which represents an increase of 10 % with respect to the first estimation of the bulb radius. Since the increase in shear modulus of the Q_b -Z curve is relatively small, it may be attributed in this case, to a compression of the soil under the shaft.

Similar to case studies covered in subsection 6.3, results for the three PGDS tested at the NGES of Auburn University were reasonably similar. This was expected since all PGDS were equipped with the same grouting apparatus and installed in a fairly uniform geotechnical testing site.

6.6 DRILLED SHAFT IN A SOUTH CAROLINA STATE PROJECT

The final case history analyzed was a test pile provided by A. H. Beck Co. Inc. This load test was part of the Carolina Bays Parkway Project in Myrtle Beach, South Carolina. The pile was installed on February 6, 2004 and had a diameter of 1.372 m and a length of 20.1 m. The general soil conditions at this site consisted of layers of sand and clay of different thicknesses along the explored depth. The available geotechnical information included conventional SPT borings carried out for the Project. A CPT sounding near the test pile was available and is shown in Figure 6-51, together with the SPT boring advanced at the site.

The objective of the load test was to define a grouting criteria for the production drilled shafts of the project. Since this was not a research project no ungrouted control pile was available. Thus, the predicted load settlement curve of an ungrouted drilled shaft could not be evaluated against actual field data.

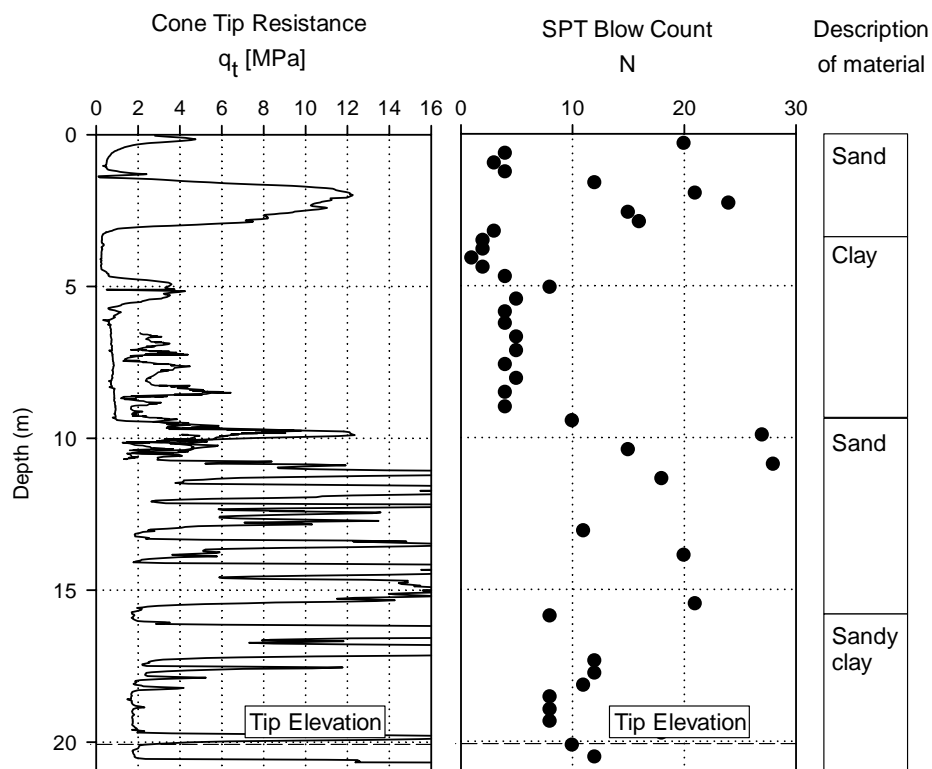


Figure 6-51 Geotechnical information gathered at Carolina Bays project

6.6.1 PGDS AT CAROLINA BAYS PROJECT

Grout data recorded during grouting process of this PGDS showed a maximum sustained pressure of about 2130 kPa and a maximum uplift displacement of the shaft of 10.5 mm (Muchard, 2004). The previous values of shaft uplift and grout pressure correspond to an injected grout volume of 0.55 m³.

The CPT sounding and shear wave velocity estimations using correlations with CPT data at the location of FJ I are shown in Figure A-30, in Appendix A. Numerical results obtained for the PGDS are presented following the structure outlined in subsection 6.2.

(1) Load settlement curve for ungrouted pile

The load settlement curve estimated using ungrouted conditions for an ungrouted drilled shaft at FJ I location is depicted in Figure 6-52. This was obtained using the CPT based pile capacity shown in Figure A-30.

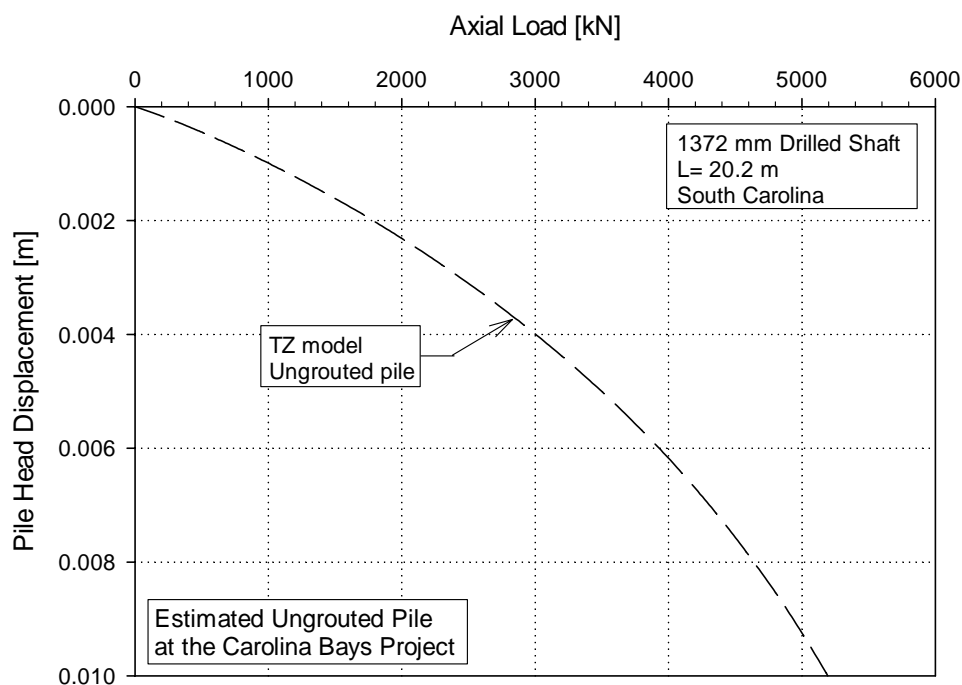


Figure 6-52 Predicted load settlement curve for an ungrouted drilled shaft at Carolina Bays project

This numerical model for the ungrouted drilled shaft was used as baseline for the models of the PGDS. The results of the load transfer analyses for the PGDS are presented in the followings paragraphs.

(2) Factor 1: Increased shear modulus of the soil under the pile tip.

This run was carried out assuming that post grouting resulted only in an increased shear modulus of the soil under the pile tip. Results of the load transfer analyses using Factor 1 are shown in Figure 6-53.

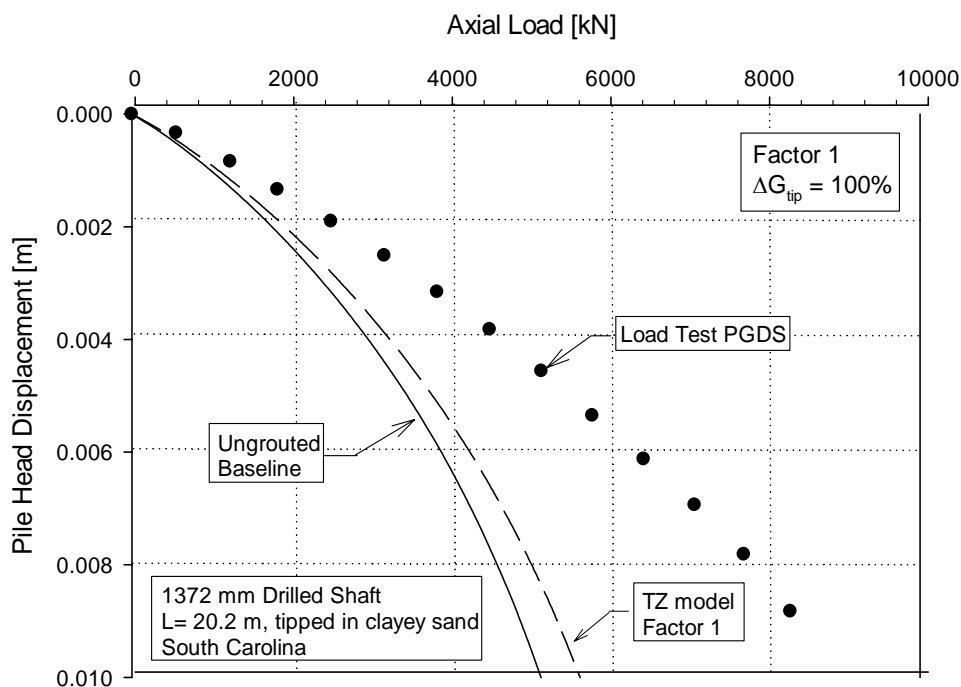


Figure 6-53 Carolina Bays – Factor 1: Prediction of the load-settlement curve of PGDS with densified soil under the pile tip

This figure shows poor agreement between measured and predicted load settlement curves. Analyses were done with different levels of increased shear modulus of the soil near the pile tip. The curve shown in Figure 6-53 corresponds to an increase level of 100%. Even this relatively high level of shear modulus improvement was inadequate to capture the measured ultimate capacity of the PGDS foundation.

(3) Factor 2: Consider stress reversal along the shaft

Load transfer analyses were carried out assuming that the only effect of post grouting on the pile was the development of residual stresses along the shaft due to shear stress reversal. Results of the numerical analyses that consider only Factor 2 are shown in Figure 6-54.

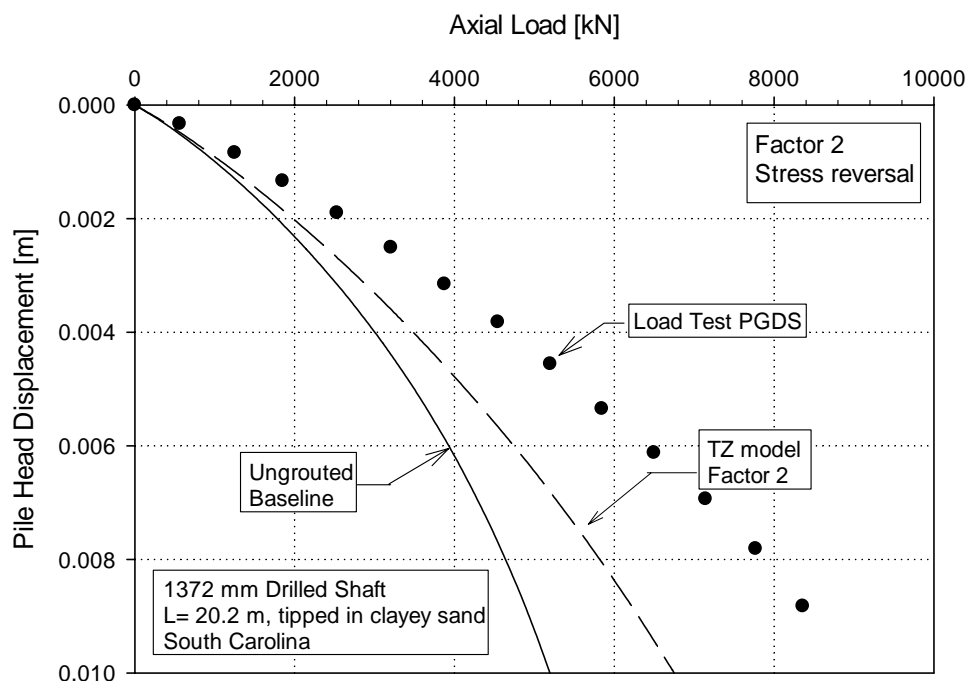


Figure 6-54 Carolina Bays – Factor 2: Prediction of the load-settlement curve of PGDS considering stress reversal along the shaft

Analysis incorporating the second factor shows an improvement in the estimated load settlement curve, but still showed poor match with the measured load settlement curve.

(4) Factor 3: Consider the formation of a grout bulb under the pile tip

Analyses for this factor assumed an increased pile tip area for the PGDS. This enlarged tip area simulates the formation of a grout bulb. Using the cavity expansion theory

approach presented in Chapter 5 a bulb radius of 1.6 times that of the shaft was calculated. Load transfer analysis using this enlarged tip area (Factor 3) is presented in Figure 6-55.

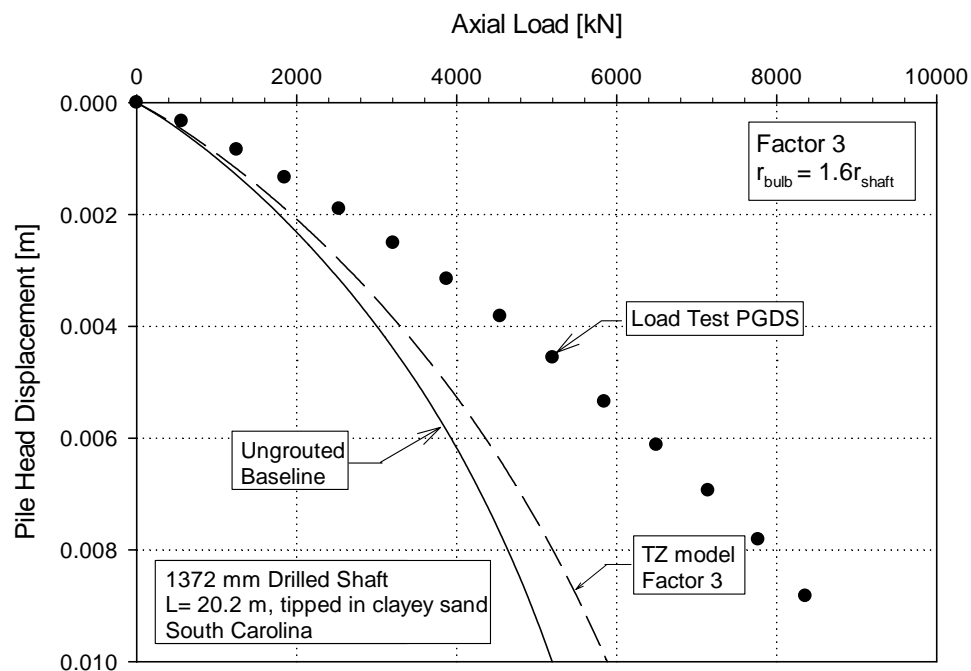


Figure 6-55 Carolina Bays – Factor 3: Prediction of the load-settlement curve of PGDS considering augmented tip area

This figure shows that the assumption that post grouting had only created a grout bulb under the tip area, significantly under-predicts the capacity measured for the PGDS.

(5) Combination of factors

Since none of the three aforementioned factors alone could adequately represent the measured response of the post grouted drilled shaft, additional analyses were performed combining these effects, in order to improve the prediction of the actual PGDS load-settlement curve.

The best representation of the measured load-settlement curve for the PGDS was obtained combining factors 1, 2, and 3. This is shown in Figure 6-56.

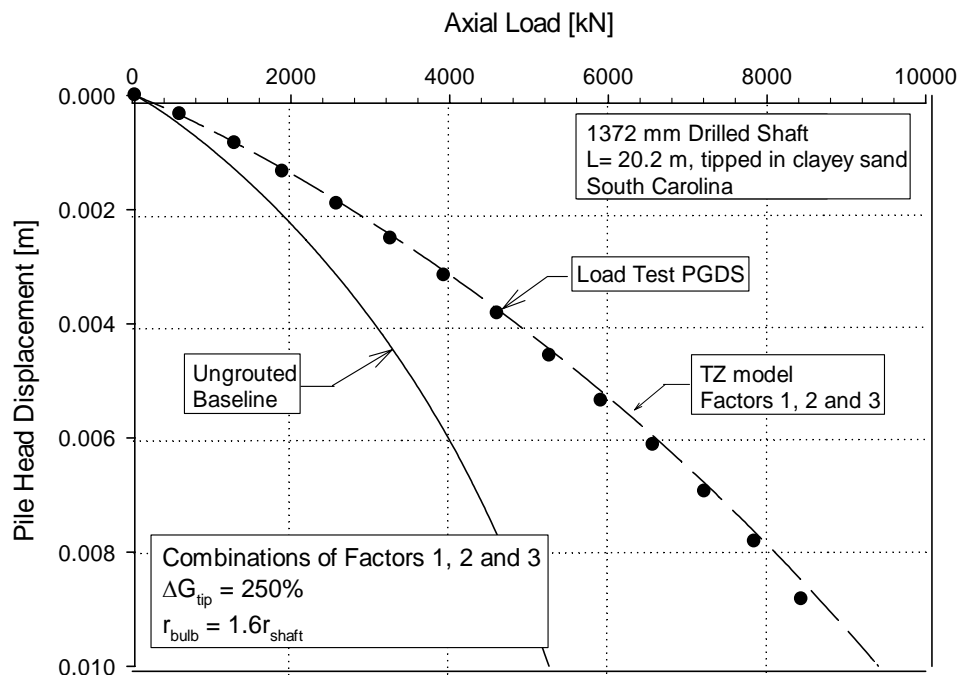


Figure 6-56 Carolina Bays – Factors 2 and 3: Calibrated load-settlement curve

For this case study, the calibration of the PGDS model was difficult to achieve. The best fit was achieved using an enlarged tip area with a bulb radius 1.6 times that of the shaft (Factor 3), consideration of fully developed stress reversal along the shaft (Factor 2), and an increment of the shear modulus for the Q_b -Z curve of 250 % (Factor 1).

The assumed size of the grout bulb seems to be reasonable when compared with the bulb radiuses obtained for the previous case studies. With regard to factor 2, an upward movement of 10.5 mm recorded during grouting seems to support the assumption of maximum side shear capacity in negative skin friction developed along the shaft. Finally, Factor 1 involved an extremely high increase in shear modulus when calculating the

improved Q_b - Z curve. This level of increase seems excessive but was necessary to achieve a good match. It could be justified somewhat if during grouting the soil and grout mixed rather than having compaction grouting. This is considered feasible because of the amount of grout injected (0.55 m^3) and the high sustained pressure reached during grouting.

6.7 SUMMARY AND CONCLUSIONS

A total of nine PGDS were studied in order to test the assumptions made in Chapter 5. Each PGDS was studied using the load transfer methodology which included a systematic study of the influence that three factors, which are believed to control PGDS behavior, had on the PGDS response. This systematic study of the three factors showed that for all case histories one factor alone could not adequately explain the overall pile capacity improvement observed due to post grouting of the pile tip.

For all nine PGDS studied, the consideration of the stress reversal along the shaft (Factor 2) was found to be a factor required in order to obtain an adequate representation of the measured load settlement curve of the PGDS. In addition, the use of the Masing rule seems to be a good methodology to account for the residual stresses that develop along the shaft due to grouting.

In those cases in which it was necessary to consider the formation of a grout bulb under the pile tip (Factor 3), the ratio of the calibrated bulb radius to the radius of the shaft agreed reasonably well with those ratios obtained from laboratory tests.

The consideration of the improvement of the shear modulus of the soil under the pile tip (Factor 1) was required for four of the nine PGDS modeled in this Chapter. However, it is believed that in some cases the high increase of shear modulus required to obtain a good match can only be attributed to the formation of a stiff soil – grout mix under the shaft. Large shear modulus increases are not expected to occur due to compaction grouting. The high increase in shear modulus for the soil under the shaft was required whether when the PGDS was equipped with a sleeve port grouting apparatus or when important migration of the grout was observed. For these cases it is considered feasible the formation of a soil – grout mix since the grout is injected directly into the soil.

Finally, similar soil conditions and grouting records yielded similar combination of factors in order to obtain a relatively good representation of the PGDS load settlement curve. This may be of significance when defining a grouting criteria for production of PGDS in the same site, provided the site is sufficiently uniform throughout. The methodology used for the analyses presented in this chapter provided reasonably good prediction of the measured load settlement curves of PGDS.

7 THEORETICALLY BASED DESIGN CHARTS FOR POST GROUTED DRILLED SHAFTS

7.1 INTRODUCTION

Mullins et al. (1991) and Mullins and Winters (2004) carried out an extensive two phase experimental program to study the axial behavior of PGDS. As a result of this comprehensive experimental study Mullins and Winters (2004) proposed an empirical design method for estimating the axial capacity of PGDS. Their proposed method is based on estimating an improved end bearing using design charts based on two proposed empirically derived parameters referred to as Tip Capacity Multiplier (TCM) and the Grout Pressure Index (GPI). This methodology assumes that the tip post grouting process results mainly in an increased tip end bearing. However the load transfer analyses presented earlier in this thesis seem to suggest that other factors are involved in the observed improved performance of PGDS. The methodology by Mullins and Winters (2004) also neglects any tip area increase due to tip grouting. This chapter is divided into five subsections. The first subsection compares TCM values derived using the theoretically based load transfer curves with the empirical charts by Mullins and Winters

(2004). The second subsection presents new design parameters that will be the basis of the proposed alternative design method discussed in Chapter 8. The third subsection of this chapter presents design charts based on these new design parameters. Conclusions extracted from this chapter are summarized in the last subsection.

7.2 THEORETICALLY DERIVED TIP CAPACITY MULTIPLIERS

As stated earlier in this work, the PGDS design method proposed by Mullins and Winters (2004) provides a set of three design charts based on experimental results. These charts relate the improved PGDS end bearing to the maximum sustained grout pressure achieved during the grouting process. Two parameters (discussed in Chapter 2) were defined by Mullins and Winters (2004) in order to develop the design charts. The expressions to calculate these parameters are:

$$TCM_{i,j} = \frac{(q_t^{grouted})_i}{(q_t^{ungrouded})_j} \quad (7.1)$$

$$GPI_j = \frac{G_p}{(q_t^{ungrouded})_j} \quad (7.2)$$

Where: $(q_t^{grouted})_i$ = Unit end bearing of grouted pile at tip displacement i

$(q_t^{ungrouded})_j$ = Unit end bearing of ungrouted pile at tip displacement j

i = Displacement of grouted tip, as a percentage of the pile diameter.

j = Displacement of ungrouted tip, as a percentage of the pile diameter.

$TCM_{i,j}$ = Tip Capacity Multiplier which relates PGDS unit end bearing at displacement i given an ungrouted tip capacity at displacement j .

GPI = Grout Pressure Index for an ungrouted tip displacement j

G_p = maximum sustained pressure obtained in the field during grouting

It can be seen from expressions (7.1) and (7.2) that the TCM and GPI parameters can be easily calculated for any tip displacement i and j , if the load settlement curves for the PGDS and its ungrouted control pile are available. Thus, the results obtained from load transfer models presented in the previous chapter one can calculate theoretical values of TCM and GPI.

Data points of TCM and GPI were calculated using the results for all the case histories presented in Chapter 6. These data points are presented in Figure 7-1, Figure 7-2, and Figure 7-3 for ungrouted tip displacements of 1 %, 2 %, and 5 % of the pile diameter, respectively. In each figure, the calculated data is represented with a solid inverted triangle, open circles, or solid circles depending if the grouted tip displacement is 1 %, 2 %, or 5 %, respectively.

Each of these figures show the design lines proposed by Mullins and Winters (2004) as well as the linear fits obtained for the load transfer based data points. The linear fits shown were obtained by forcing their intercepts to be the ratio of ungrouted tip capacities (i.e. $(q_t^{ungrouted})_i / (q_t^{ungrouted})_j$). In doing so, it is ensured that the design charts will reflect

the fact that if no grouting has taken place, no tip capacity improvement is obtained from the charts. Table 7-1 through Table 7-3 show the parameters which define the linear fits of these linear regressions for ungrouted tip displacements of 1 %, 2 %, and 5 % of the pile diameter.

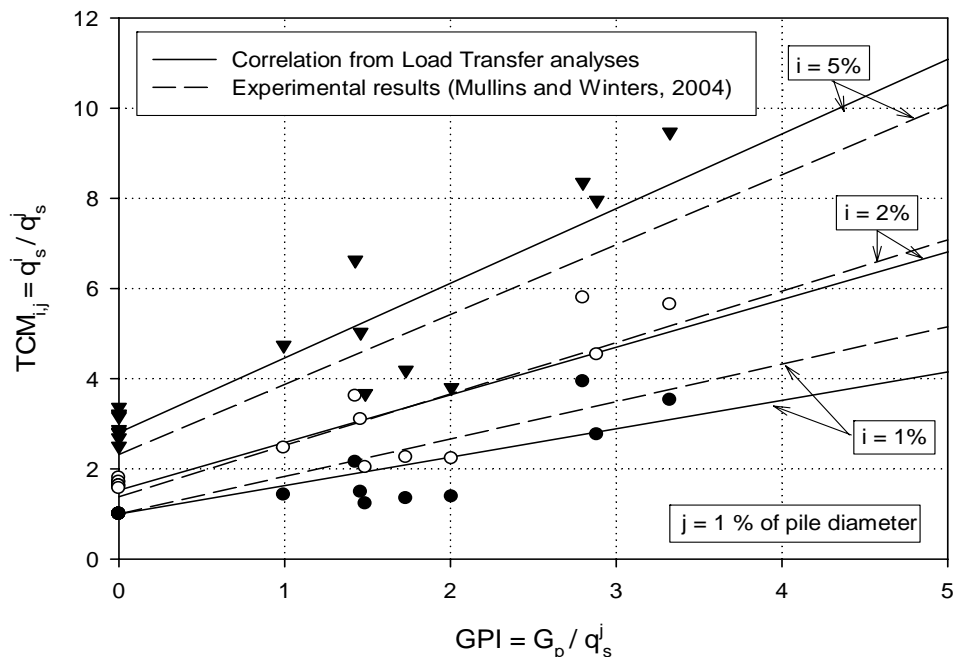


Figure 7-1 TCM vs. GPI applied to ungrouted tip capacities at 1% of diameter displacement

Table 7-1 Empirical and theoretical slopes and intercepts for the design charts proposed by Mullins and Winters (2004) for ungrouted tip displacement $j = 1\%$

Tip disp. j (as % of pile diameter)	This Work			Regressions by Mullins and Winters (2004)		
	Slope	Intercept	R^2	Slope	Intercept	R^2
1	0.63	1.00	0.62	0.82	1.00	0.85
2	1.06	1.53	0.65	1.14	1.38	0.86
5	1.66	2.80	0.67	1.55	2.32	0.88

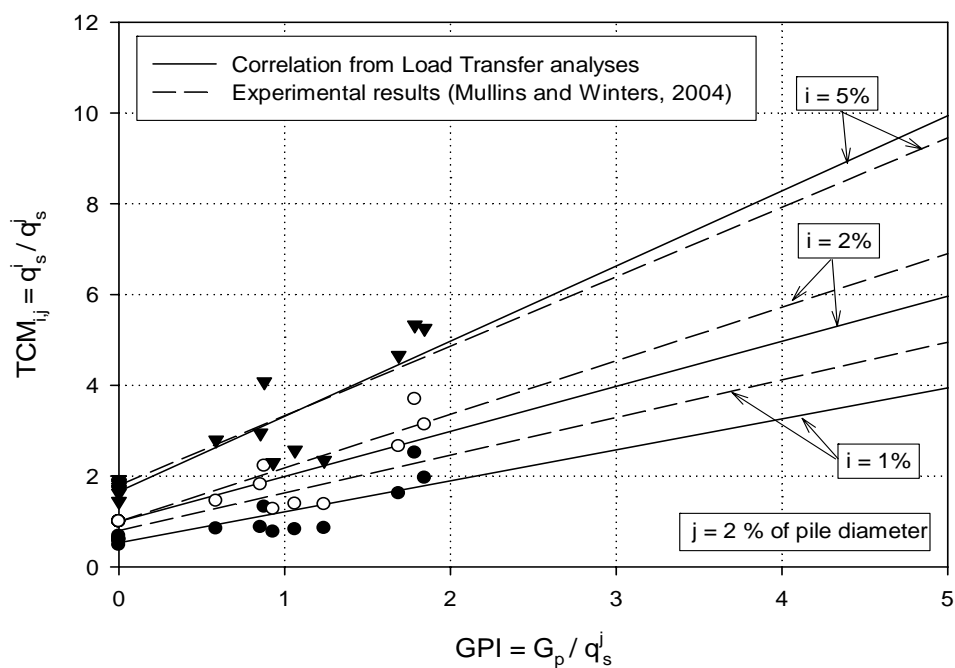


Figure 7-2 TCM vs. GPI applied to ungrouted tip capacities at 2% of diameter displacement

Table 7-2 Empirical and theoretical slopes and intercepts for the design charts proposed by Mullins and Winters (2004) for ungrouted tip displacement $j = 2\%$

Tip disp. j (as % of pile diameter)	This Work			Regressions by Mullins and Winters (2004)		
	Slope	Intercept	R^2	Slope	Intercept	R^2
1	0.68	0.53	0.60	0.83	0.80	0.85
2	0.99	1.00	0.63	1.18	1.00	0.81
5	1.66	1.65	0.66	1.53	1.80	0.89

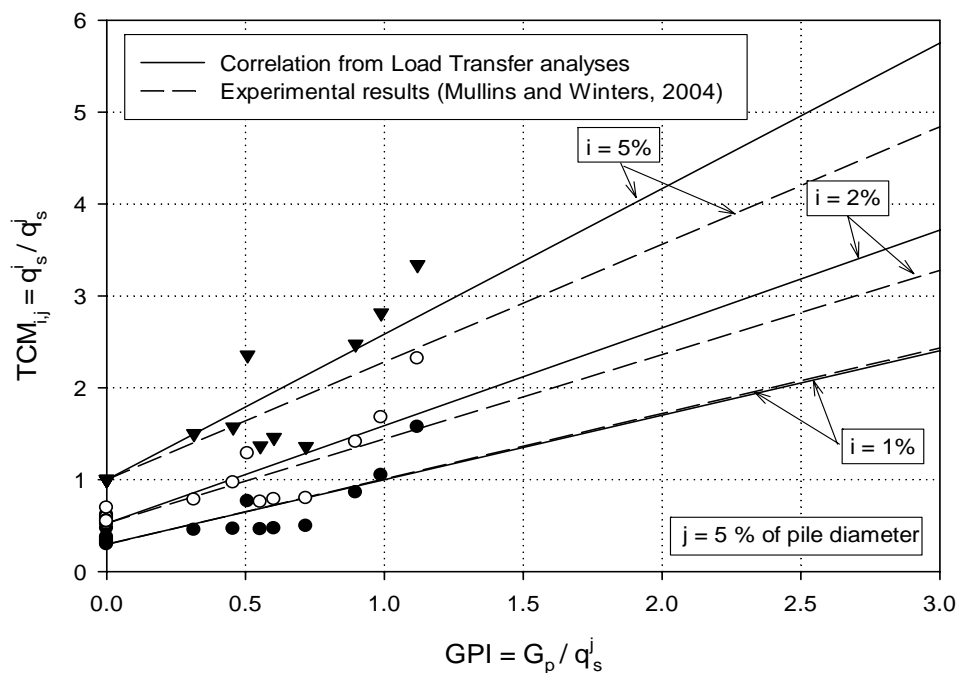


Figure 7-3 TCM vs. GPI applied to ungrouted tip capacities at 5% of diameter displacement

Table 7-3 Empirical and theoretical slopes and intercepts for the design charts proposed by Mullins and Winters (2004) for ungrouted tip displacement $j = 5\%$

Tip disp. j (as % of pile diameter)	This Work			Regressions by Mullins and Winters (2004)		
	Slope	Intercept	R^2	Slope	Intercept	R^2
1	0.70	0.30	0.58	0.71	0.30	-
2	1.06	0.53	0.62	0.92	0.53	-
5	1.58	1.00	0.66	1.28	1.00	-

Figure 7-1 through Figure 7-3 show a reasonably good approximation between theoretical and empirical design charts. However, for large values of GPI, theoretically derived charts seem to predict larger post grouted tip capacities than those that would be obtained from the empirical charts. It can be seen from Table 7-1 through Table 7-3 that correlation coefficients for the linear regressions of the load transfer data have a smaller value than those estimated by Mullins and Winters (2004) for data points obtained from

field tests. However, the number of data points used by these researchers is less than the number of the case studies included in this work.

The design charts proposed by Mullins and Winters (2004), are easy to use and provide a direct approach to estimate the improved end bearing due to grouting. However, they are only based on observed end bearing improvements. Analyses presented in Chapter 6 indicated that improvements in performance of PGDS piles can depend on several factors. Because of that, end bearing based design charts may not be appropriate for estimating the PGDS capacity.

The currently available design charts by Mullins and Winters (2004) are solely based on end bearing capacity, and hence may entail some limitations regarding their applicability:

- Shear reversal along the shaft is not considered in the end bearing based design charts.
- PGDS tip capacity obtained from the previous design charts will depend to a great extent on the ungrouted end bearing used to calculate the TCM and GPI parameters. End bearing values predicted using standard static methods usually show great scatter. This was confirmed in Chapter 4 where ungrouted end bearing values were found to have great variability among the three CPT based static methods used. This uncertainty will be transferred to the PGDS capacity predictions.

- PGDS end bearing is not univocally defined by design charts proposed by Mullins and Winters (2004). In effect, if the ungrouted end bearing $(q_t^{ungrouted})_j$ can be calculated for $j = 1\%$, 2% , and 5% of the pile diameter, three values for $(q_t^{grouted})_i$ can be obtained, for the same PGDS tip displacement i .
- The increased pile tip capacity according to Mullins and Winters (2004) is given as:

$$(Q_t^i)_{grouted} = [TCM_{i,j} \cdot (q_t^{ungrouted})_j] \cdot A_t \quad (7.3)$$

Where: $(Q_t^i)_{grouted}$ = PGDS tip capacity

A_t = PGDS tip area

It seems that the authors assume that the tip area of the PGDS is equal to that of the ungrouted pile. This assumption ignores the potential benefits of the formation of a grout bulb under the pile. This assumption is on the safe side for design purposes, but as shown in Chapter 6, in some cases ignoring enlarged tip area can result in PGDS capacity estimates considerably lower than observed in the field.

Due to the aforementioned reasons the following subsection explores the possibility of using new parameters to estimate PGDS capacity. The proposed new parameters were defined in terms of total pile capacity as opposed to tip capacity. The motivation for developing these new parameters is to try to overcome the uncertainties associated with

the estimation of unit end bearings and to include in the formulation the benefits that shear stress reversal has on the improved PGDS capacity.

7.3 MODIFIED DESIGN PARAMETERS

As stated in the previous subsection, PGDS capacity may not be appropriately estimated solely on the basis of an improved pile tip capacity. Consequently, design charts may be more conveniently defined by means of total pile capacities instead of tip end bearings only. This can be accomplished through an appropriate redefinition of factors TCM and GPI, as described in the followings subsections.

7.3.1 SHAFT GROUT PRESSURE INDEX (SGPI)

Mullins and Winters (2004) reported that the pile capacity improvement due to tip post grouting is proportional to the volume of grout injected and the maximum sustained pressure attained during grouting. The greater the grout pressure and the larger the grout volume injected, the greater benefits of post grouting. However, these parameters have practical limits, hence grouting is usually stopped if one of the two following limiting states is reached: (a) the maximum pressure of the pump is reached which impedes further increase of the grout pressure, or (b) upward displacement of the pile is observed for constant grout pressure (meaning that shaft resistance has been fully mobilized in negative skin friction). The latter limiting state is reached when the force exerted by the grout pressure on the pile base equals the pile shaft resistance. Thus, a modified parameter, called the Shaft Grout Pressure Index (SGPI) is proposed to relate the available side shear to the grout pressure applied at the pile base.

This parameter is defined as follows:

$$SGPI = \frac{G_p}{q_f^{AVE}} \quad (7.4)$$

Where: G_p = maximum sustained grout pressure

q_f^{AVE} = average available side shear before grouting, with same units as G_p

(i.e. pile shaft resistance divided by the shaft area)

The above equation assumes that the average shaft friction, q_f^{AVE} , is mobilized when the maximum grout pressure G_p is applied. This assumption is considered reasonable since shaft capacity is usually mobilized at small pile displacements. Only one value of SGPI is calculated for a given set of PGDS grouting conditions.

The grout pressure required to develop all the shaft resistance can be estimated by equating the total force exerted by the grout pressure acting upon the pile tip to the shaft capacity of the ungrouted pile, i.e.:

$$G_p A_t = Q_{fu} \quad (7.5)$$

Where Q_{fu} is the ultimate pile shaft capacity, then:

$$G_p = \frac{Q_{fu}}{A_t} \quad (7.6)$$

In some geomaterials, the side resistance of drilled shafts may develop fully at small displacements and then tend to decrease with further displacement while the base

resistance may still be showing a tendency to increase (O'Neill and Reese, 1999). Such geomaterials are termed displacement softening materials, and for these materials the shaft capacity has to be calculated based on the average shaft friction mobilized for the level of deformations induced in the PGDS during grouting. If the average unit shaft friction is used to estimate Q_{fu} , Equation (7.6) becomes:

$$G_p = \frac{4 \cdot q_f^{AVE} \cdot (\pi DL)}{\pi D^2} \quad (7.7)$$

$$G_p = 4 \cdot q_f^{AVE} \cdot \frac{L}{D} \quad (7.8)$$

Where L is the pile length and D is the pile diameter, before grouting. As mentioned before, Equation (7.8) can be used to estimate the maximum grout pressure that must be applied at the pile tip to mobilize the ultimate or limiting average side shear resistance along the pile shaft. This value should consider the level of deformations expected in the field and also the nature of the geomaterials (i.e., displacement softening or not) present along the shaft of the PGDS foundation.

In other words, q_f^{AVE} in expression (7.8) represents the average mobilized side shear resistance along the shaft. The calculated value of G_p can be based on a limiting value of q_f^{AVE} selected by the designer if evidence is found that a layer within the soil profile presents a strain softening behavior.

7.3.2 AXIAL CAPACITY MULTIPLIER (ACM)

As stated in Chapter 2, PGDS have been reported in the literature as presenting higher axial capacity than conventional drilled shafts installed in similar conditions. The main reasons that may be responsible for this increased capacity were found to be (Chapter 5) the compression of the soil under the pile tip, shear stress reversal along the shaft, and the increased pile tip area due to the formation of a grout bulb. Considering these three factors, the overall capacity improvement can be attributed to two effects: (1) increased pile tip capacity, and (2) increased shaft stiffness. The increased pile tip capacity is obtained through increased tip area and increased unit end bearing. The increased unit end bearing is obtained primarily through compression or densification of the soil under the pile tip and, in some instances, through soil stiffening due to soil-cement mixing that may occur during grouting under certain conditions. The increased pile tip capacity may be the main factor responsible for the observed increased ultimate axial capacity in PGDS foundations. The second effect, i.e., increased the stiffness of the system, is believed to be mainly due to the “pre-stressing effect” from the shear stress reversal that occurs along the shaft after tip post grouting. The shear stress reversal has a pre-stressing effect on the soil along the shaft, thus, the post grouting does not necessarily increase the pile shaft capacity but rather increases the available shaft capacity for a certain pile settlement level. In other words, the second effect of increased stiffness of the foundation system permits the PGDS support larger loads than conventional drilled shafts for a given pile settlement level. The observed improved stiffness of the PGDS foundation system is believed to also be due to stiffening of the soil under the pile tip after tip post-grouting.

In summary, the combination of an increased pile end bearing and increased foundation stiffness are the main reasons for the observed improved performance and increased capacity of PGDS foundations.

Ideally the improved performance of the PGDS should be evaluated with respect to a conventional drilled shaft by comparing axial capacities for a given level of displacement. In practice, it is common to specify axial capacities as loads at the head of the pile for a given pile head displacement. Hence, the second proposed parameter is defined to represent the PGDS axial capacity improvement obtained due to pile tip post grouting process. The proposed parameter is defined similarly as the Tip Capacity Multiplier proposed by Mullins and Winters (2004). However, it is calculated using a ratio of total pile capacities (at the pile head) instead of using unit end bearings, and the displacement levels refer to pile head displacements and not toe displacements as proposed by Mullins and Winters (2004). The new proposed parameter is termed axial capacity multiplier or ACM, and it is defined as:

$$ACM = \frac{Q_{grouted}^i}{Q_{ungrounded}^j} \quad (7.9)$$

Where: $Q_{grouted}^i$ = total PGDS capacity after grouting at pile head displacement i

$Q_{ungrounded}^j$ = total ungrouted pile capacity at pile head displacement j

$ACM_{i,j}$ = Axial Capacity Multiplier relating ungrouted pile head displacement j to grouted pile head displacement i .

It is worth to note that the convenience of defining a capacity multiplier in terms of total capacities relies upon the fact that it implicitly involves the three factors that are believed to control the increased PGDS capacity as discussed in Chapter 5. Another convenience of expressing the multiplier in terms of total capacities is that in practice pile capacities are usually measured at the head level. Even during conventional load tests it is common to measure the applied load at the head and not at the pile tip.

Note that since the new definition of ACM involves total pile capacities, i and j correspond to displacements of the pile head and do not correspond to tip displacements, as it was the case of the Tip Capacity Multiplier proposed by Mullins and Winters (2004).

7.3.3 ULTIMATE CAPACITY MULTIPLIER (UCM)

An additional parameter was defined similar to the ACM parameter, but in terms of ultimate axial load capacities. The ultimate capacity multiplier parameter, or UCM, is in a similar way as the ACM but the numerator and denominator in Equation (7.9) correspond to the ultimate or failure loads for the PGDS and conventional drilled shaft, respectively. The values of the ultimate axial loads for both the grouted and ungrouted piles can be calculated using any failure criterion. For example, if the Davisson failure criterion (Davisson, 1972), is chosen, which is the commonly used in the US, the UCM results as follows:

$$UCM = \frac{Q_{grouted}^{Davisson}}{Q_{ungrouted}^{Davisson}} \quad (7.10)$$

Where: $Q_{grouted}^{Davisson}$ = Davisson failure load for the PGDS

$Q_{ungROUTED}^{Davisson}$ = Davisson failure load for the ungrouted pile (i.e. control pile)

UCM = Ultimate Capacity Multiplier

A reasonably good linear correlation was found between the UCM parameter and the Shaft Grout Pressure Index defined earlier. This will be presented and discussed in the next subsection.

7.4 TOTAL CAPACITY DESIGN CHARTS

A PGDS design chart was developed by relating the axial capacity multiplier (ACM), the shaft grout pressure index (SGPI), and the PGDS head displacement. This design chart is depicted in Figure 7-4. The ACM values plotted in this chart were calculated for eight of the nine case histories included in Chapter 6 by setting in Equation 7.9 the numerator as the axial load in the PGDS corresponding to a certain head displacement (i), and the denominator as the Davisson failure load for the ungrouted pile. In other words, the head displacement of the ungrouted pile (j) corresponds to the pile head displacements at the ultimate pile load calculated using the Davisson failure criterion. Case history involving PGDS TS3 (subsection 6.5.4) was not included in Figure 7-4 because this pile presented an unexpected high improved performance when compared with similar PGDS (TS1 and TS2) installed under similar conditions at the same site. Thus, it is believed that PGDS TS3 is not representative of the improved performance that can be obtained by post grouting at that site.

Figure 7-4 can be used to estimate the PGDS capacity for pile head displacements up to 5 % of the pile diameter. The chart was not extended for larger displacements since it

is believed that pile head settlements beyond 5% of the pile diameter may be excessive for most foundation systems supporting conventional civil structures.

The design chart shown in Figure 7-4 allows the determination of PGDS capacities for a given pile head displacement and a certain SGPI, once the Davisson failure load has been estimated for an ungrouted pile installed under similar conditions as the PGDS. In Figure 7-4 best fits for each value of PGDS head displacement are also depicted.

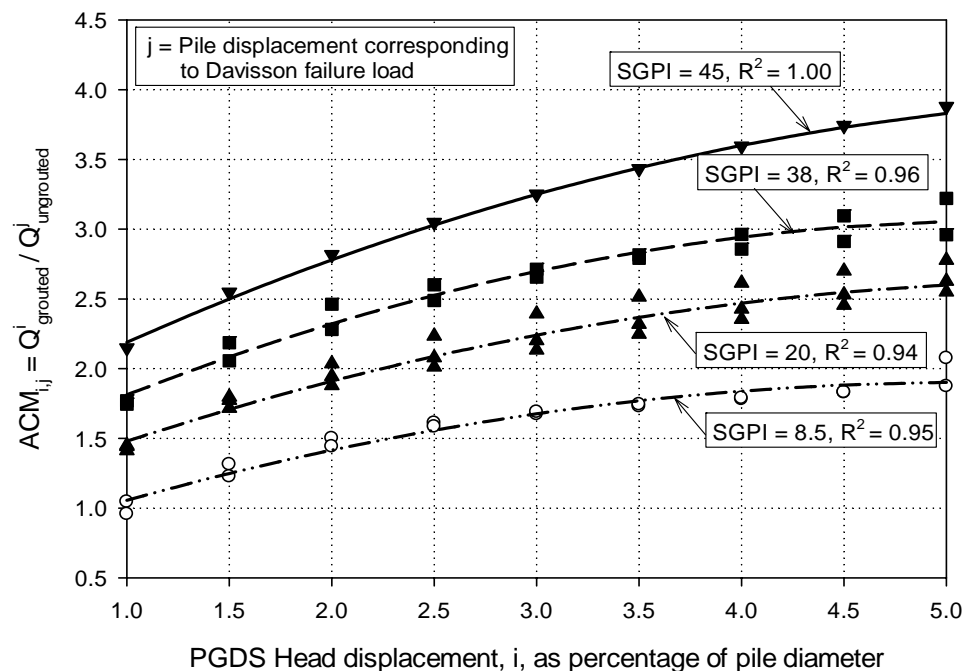


Figure 7-4 Total Capacity design chart applied to grouted total capacities for different levels of SGPI

It is important to point out that the ACM values are not expected to increase indefinitely as suggested by the correlations shown in Figure 7-4. The correlations were used to fit the available data; however SGPI values are not expected to increase indefinitely as discussed later in this chapter. Use of these correlations outside the range

of SGPI values presented in this chart is not recommended without field validation or additional case histories.

Another important consideration regarding the design chart depicted in Figure 7-4 is that, as stated before, ACM values relate the PGDS capacity for a certain pile head displacement to the Davisson capacity of the ungrouted pile. This definition of the ACM yields a relation between pile capacities developed at different pile head displacements. Since the improved performance observed in PGDS relies upon the fact that a PGDS can support larger loads than conventional drilled shafts for a certain displacement, a more appropriate definition of the parameter ACM would entail the ratio of grouted and ungrouted capacities measured at the same pile head settlement. If the ACM is defined in this way, it would result in larger capacity multipliers than the ones calculated by means of Equation (7.9). However, the design chart shown in Figure 7-4 can be used as a reasonable initial approximation to conservatively estimate the PGDS capacity.

Additional to the design chart in Figure 7-4, two more design charts are proposed. The first of them relates SGPI with UCM (Figure 7-5), while the second one relates SGPI to the size of the grout bulb that may be formed under the pile after grouting (Figure 7-6).

In Figure 7-5 the values of UCM were obtained from expression (7.10) for all case studies included in Chapter 6. Similarly, the corresponding SGPI values were calculated from Equation (7.4). Figure 7-6 also shows the best fit of the data.

In Figure 7-6 values of the adimensional number $(r_1/r_0)(\sigma_v^{\text{tip elev}}/G_p)^2$ calculated for all cases studied in Chapter 6 were plotted in ordinates against their corresponding SGPI

values. In the adimensional factor, r_l corresponds to the grout bulb radius, r_0 is the shaft radius, G_p is the maximum grout pressure, and $\sigma_v^{\text{tip elev}}$ is the effective overburden pressure at the pile tip elevation. The adimensional factor plotted in ordinates represents, somehow, the influence that both grout pressure and effective overburden pressure have on the formation of a grout bulb under the pile.

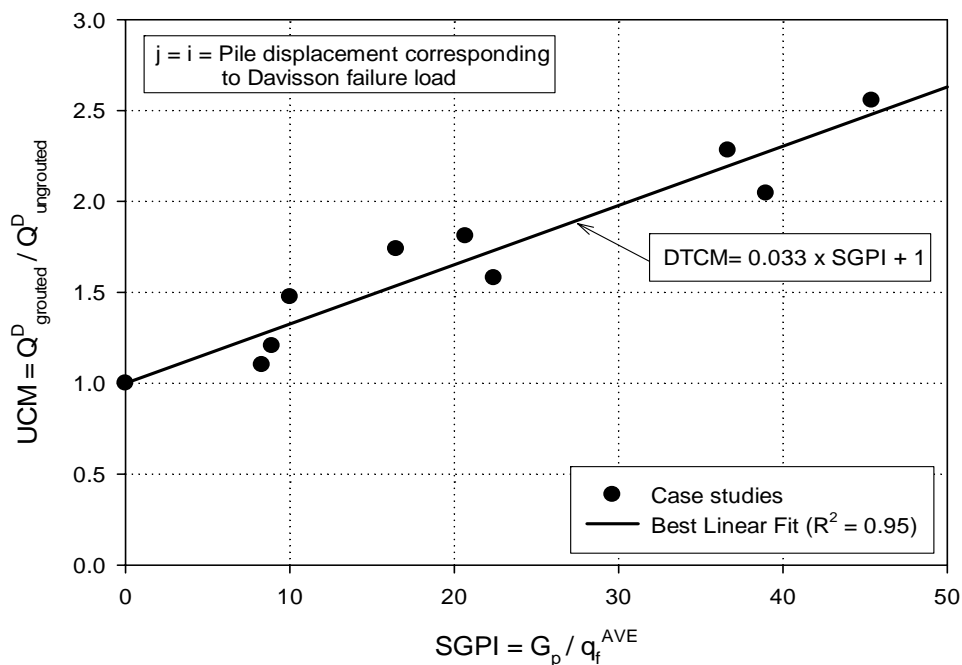


Figure 7-5 UCM vs. SGPI design chart

The design charts depicted in Figure 7-4 and Figure 7-5 will be used in the following chapter as part of a proposed design procedure for PGDS using a load transfer approach.

Figure 7-6 seems to give a good correlation for estimating the radius of the grout bulb that may formed due to grouting. However, it is recommended that this figure only be used for preliminary estimates since the correlation is based on limited data and there are several factors that influence the grout bulb formation that are not included in the

proposed design chart. Some of the important factors not included in this correlation are: shear resistance of the soil being grouted, viscosity of the grout, local soil conditions at the tip elevation, and permeation of the grout, etc.

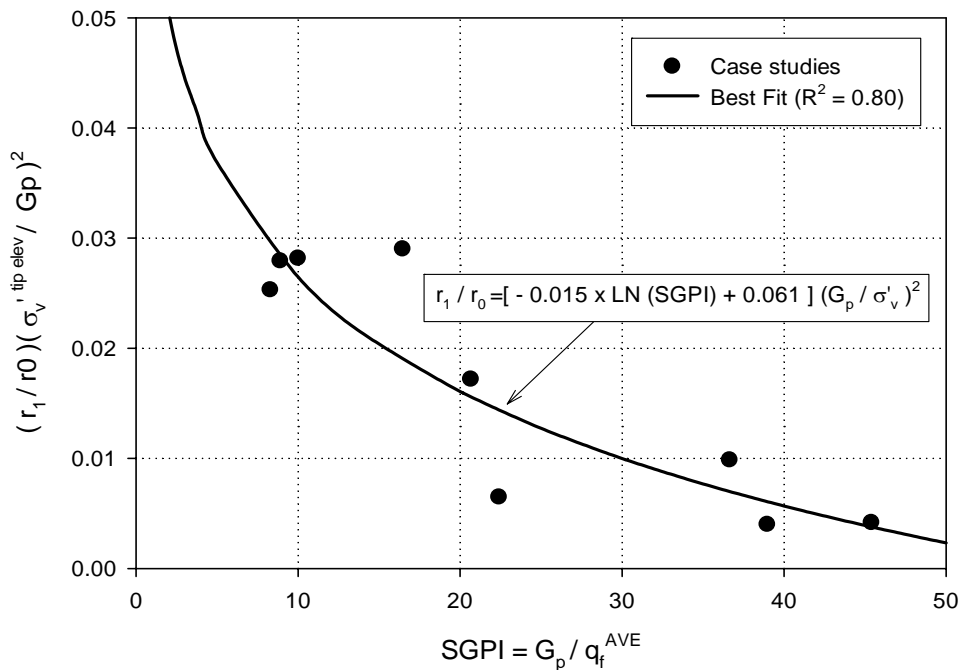


Figure 7-6 Design chart to approximately estimate the grout bulb radius of a PGDS in terms of the SGPI

Another important consideration to keep in mind, regarding the proposed design charts, involves the SGPI defined in section 7.3.1. Equation (7.4) seems to suggest that SGPI can increase indefinitely. However, if the expression for the grout pressure from Equation (7.8) is replaced into Equation (7.4), the SGPI becomes:

$$SGPI = 4 \frac{L}{D} \quad (7.11)$$

Equation (7.11) indicates that the SGPI is directly proportional to the pile slenderness ratio. However, the SGPI has practical limits based on typical pile slenderness ratios used

in conventional drilled shaft construction practice. Pile dimensions are typically selected based on constructability considerations and loading considerations that not only include axial load requirements but also lateral load demands. In North America, drilled shafts lengths typically range between 6 m and 40 m, and their diameters are selected based on availability of the auger diameters. For short drilled shafts diameters range between is between 0.91 m and 2.44 m, while for long drilled shafts pile diameters usually range between 1.5 m and 3 m. Thus, slenderness ratios typically range between 2.5 and 25. This range of slenderness ratios with Equation (7.11) results in a practical range of SGPI between 10 and 100. However, the derivation of the design charts were based on field data that included piles with a maximum SGPI of about 50 (which corresponds to a maximum slenderness ratio of about 13). The proposed design charts are not recommended for piles with slenderness ratios above 15 unless the database is extended to include field data from piles with slenderness ratios higher than 15. Slender piles where $L/D > 15$ should be treated as special cases and thorough analyses should be carried out in order to assess the pile capacity that may be gained with post grouting in these piles.

The maximum SGPI value is not only related to slenderness ratio, but also to limitations in the grouting pressure that can be applied in the field and its relationship with the specific average mobilized side shear resistance along the shaft. For example, if a typical grout pump has a maximum achievable grout pressure of about 6900 kPa and an average shaft side resistance of about 50 kPa is assumed, the maximum SGPI would be about 140. Lower SGPI values are expected for pumps with lower grout pumping

pressures, or for higher mobilized average shaft resistances. Therefore the recommended practical SGPI range is between 10 and 100.

These maximum and minimum SGPI values may be useful when designing PGDS since they would help limiting the pile capacity improvement obtained with post grouting the pile tip. Limiting SGPI to about 60, would limit the maximum level of improvement of PGD axial capacity to about 3 times the capacity of the ungrouted pile.

7.5 SUMMARY AND CONCLUSIONS

Theoretical values for the Tip Capacity Multiplier and Grout Pressure Index parameters proposed by Mullins and Winters (2004) were calculated using the load settlement curves obtained in Chapter 6 using the load transfer analyses. These theoretical values for these parameters were plotted in the design charts proposed by Mullins and Winters (2004) and showed reasonably good agreement with design lines proposed by these authors. Linear regressions were calculated for the theoretical values calculated, and the intercepts were defined to values that reflected no capacity improvement for the case of no grouting. However, theoretical tip capacity multipliers obtained from the linear regression were found to be slightly larger than their corresponding design lines of Mullins and Winters (2004). This was particularly evident for large grout pressure indexes and for PGDS tip displacements of 5 % of the pile diameter.

New parameters and design charts were developed in order to overcome some uncertainties associated with the original methodology proposed by Mullins and Winters (2004). The new methodology is based on total pile capacity as opposed to tip capacity.

This approach implicitly considers all factors discussed in Chapter 5. The new charts consider the increased pile tip capacity due to compression of the soil under the pile and the formation of a grout bulb at the pile tip, and the increased shaft stiffness due to shear stress reversal. Design charts were developed to estimate the increased total capacity of PGDS piles using the new parameters UCM and SGPI parameters.

Practical limiting values for the SGPI were established based on commonly used drilled shafts dimensions. The expected SGPI values limit the increased capacity that can be obtained for PGDS foundations to a maximum of about 3 times the capacity of the ungrouted pile.

8 DESIGN METHODOLOGY FOR POST GROUTED DRILLED SHAFTS

8.1 INTRODUCTION

This chapter presents a proposed methodology for estimating the PGDS total capacity and settlements developed using a load transfer approach. The methodology makes use of the design charts presented in Chapter 7 and aims at providing a rational approach for the PGDS design. This method is an alternative to the method by Mullins et al. (2001) which considers tip end bearing improvement only.

The proposed methodology for PGDS design is discussed in the following subsection and the recommended procedure is presented as a series of steps required.

8.2 PROPOSED METHODOLOGY

The proposed methodology consists of two main parts: (1) the estimation of the PGDS capacity (for a certain pile head displacement), and (2) the estimation of the load settlement curve for the PGDS.

The PGDS capacity is calculated taking into consideration factors identified in Chapter 5. Three factors were identified in Chapter 5 as possible contributors to the PGDS increased capacity. Moreover, the design methodology proposed herein includes only the following: (a) the increased pile shaft capacity due to stress reversal (factor 2, as referred to in Chapter 5) and (b) the increased pile tip capacity due to the formation of a grout bulb under the pile (factor 3, as referred to in Chapter 5). Factor 1 (i.e. compression of the soil under the pile tip) was found to be difficult to incorporate. The extent of the increased of shear modulus (or initial stiffness of the Q_b -Z curve) could not be easily quantified to be incorporated into the numerical models. Since its influence was not as higher as the two other factors and since neglecting its contribution is conservative it was not included in the design methodology proposed herein.

As shown in Chapter 6, incorporating Factor 3 (enlarged tip area) was found to be necessary in order to adequately capture the observed PGDS behavior in almost all case studies discussed. This was confirmed through laboratory tests by Mullins and Winters (2004) which indicated bulb radiuses of up to two times that of the ungrouted pile tip. A design chart was developed in order to approximately estimate the bulb radius with a reasonably good correlation factor. Factor 2 (shear stress reversal) was also systematically considered in all PGDS load transfer analyses presented in Chapter 6.

As mentioned before, the proposed methodology has two main parts. Part I can be used to estimate the PGDS pile axial capacity given certain diameter and grouting conditions, or for estimating the pile dimensions and grouting pressure required to

support a certain design load. Part 2 can be used to estimate PGDS settlements for service loads.

The second part of the methodology is based on using a PGDS load transfer model obtained by modifying the ungrouted pile load transfer model by including shear stress reversal (Factor 2) and the formation of a grout bulb under the pile tip (Factor 3). This PGDS load transfer model is used to estimate the load settlement curve of the PGDS which can be used for estimating PGDS settlements under service loads. Since Part I involved the estimation of the PGDS capacity for a certain design pile head displacement, Part II is not strictly required, thus, it may be skipped. However, Part II of the proposed design procedure can be used to check if the PGDS capacity obtained in Part I is within reasonable limits and to obtain the full load settlement curve which can be useful if pile capacities for pile head displacements different from that specified in Part I are required.

PART I: Estimate PGDS capacity for a given pile settlement

The first part of the proposed methodology is similar to that proposed by Mullins and Winters (2004). However, here the design charts are used to estimate the total PGDS capacity for a given PGDS head settlement. The methodology presented in Chapter 3 is used in order to estimate the ungrouted pile load settlement curve which will provide the basis to estimate the PGDS response for Part II. Part I aims at providing a simple procedure for estimating the pile length and the grouting pressure required to support a certain design load using a PGDS. This part entails the following main steps:

- (1) Estimate the pile resistance profile based on the available CPT data and select the appropriate length. Assume an ungrouted pile condition. Note that if CPT data is not available the procedure can be modified for other in-situ testing.
- (2) Develop a load transfer model based on the axial pile capacity estimated in step (1). Use procedure described in Chapter 3. Obtain the ungrouted load settlement curve and estimate the Davisson failure load. This value is referred to as $Q_{ungrouted}^{Davisson}$.
- (3) Estimate the design grout pressure and the SGPI, as follows:

$$G_p = 4 \cdot q_f^{\text{lim}} \cdot \frac{L}{D} \quad (8.1)$$

$$SGPI = \frac{G_p}{q_f^{AVE}} \quad (8.2)$$

Where: G_p = Design grout pressure

q_f^{lim} = Limiting value of side friction along the pile shaft. Suggest using q_f^{min} which would be the minimum allowable side shear resistance along the shaft

L = pile length from step (1)

D = pile diameter

q_f^{AVE} = average side shear resistance (i.e. maximum shaft resistance divided by the shaft area)

Note that this step suggests calculating the design grout pressure using the minimum allowable unit side shear along the shaft. (i.e. using the value from the layer with the lowest unit side shear). Equation (8.1) with q_f^{\min} ensures that during grouting no peak shaft resistance will be exceeded. This may be important for situations where strain softening soils with a post-peak lower residual value. If the soil profile does not show any layer with strain softening behavior, the design grouting pressure can also be increased through increasing the limiting value of side friction in (8.1).

- (4) Estimate the axial capacity of the PGDS. This is done using the design chart that relates ACM to SGPI (presented in Chapter 7). The estimate is made for a certain design settlement of the PGDS head (i) and the SGPI calculated in step 3. The procedure is shown schematically in Figure 8-1.

Having ACM from the design chart (Figure 8-1) the PGDS capacity for the given pile displacement is calculated as follows:

$$Q_{grouted}^i = ACM_{i,Davison} \cdot Q_{ungouted}^{Davison} \quad (8.3)$$

- (5) Check if the estimated post grouted capacity meets the required design load specified for the pile. If not, increase either the pile length in step (1) and

repeat steps (2) through (5), or increase the pile diameter, or choose a bigger pile head displacement in step (4).

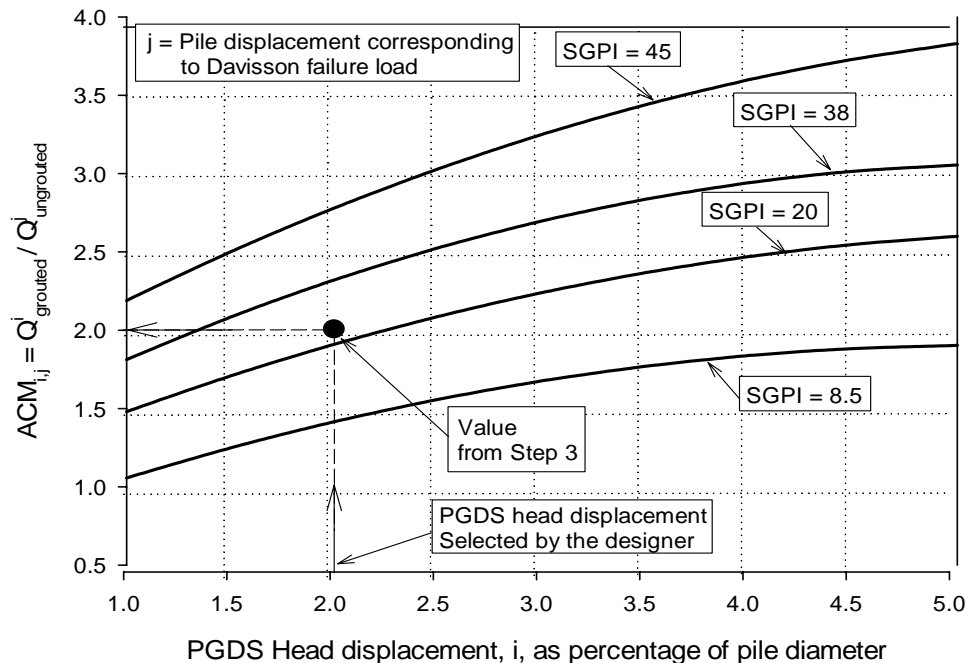


Figure 8-1 Example of calculation of the PGDS total capacity at pile head displacement for a given SGPI

PART II: Estimate the load-settlement curve for PGDS and design check

This part entails estimating the full load settlement curve for the PGDS using the load transfer methodology. Since this is not normally needed for design, this step is not strictly necessary, therefore is optional.

The methodology that will be presented in the following paragraphs is based on the load transfer methodology proposed earlier in this work (Chapter 3). Therefore, the methodology involves the use of methods based on CPT data in order to estimate the static axial capacity of a pile. However, other methods to estimate pile capacity may be used as well, even though load transfer models based on data from other types of in-situ

tests (such as SPT borings) have not been evaluated in this work. Part II of the proposed methodology, entails modifying the load transfer model used in Part I using the following steps:

- (1) Incorporate the stress reversal factor in the load transfer model. This can be done using the Masing rule discussed in Chapter 5. The resulting T-Z curve is obtained by modifying the load transfer model developed in step (2) of Part I. The amount of side friction increase will be controlled by q_f^{lim} used in Equation (8.1). The influence of shear stress reversal on the T-Z load transfer curve is illustrated in Figure 8-2.

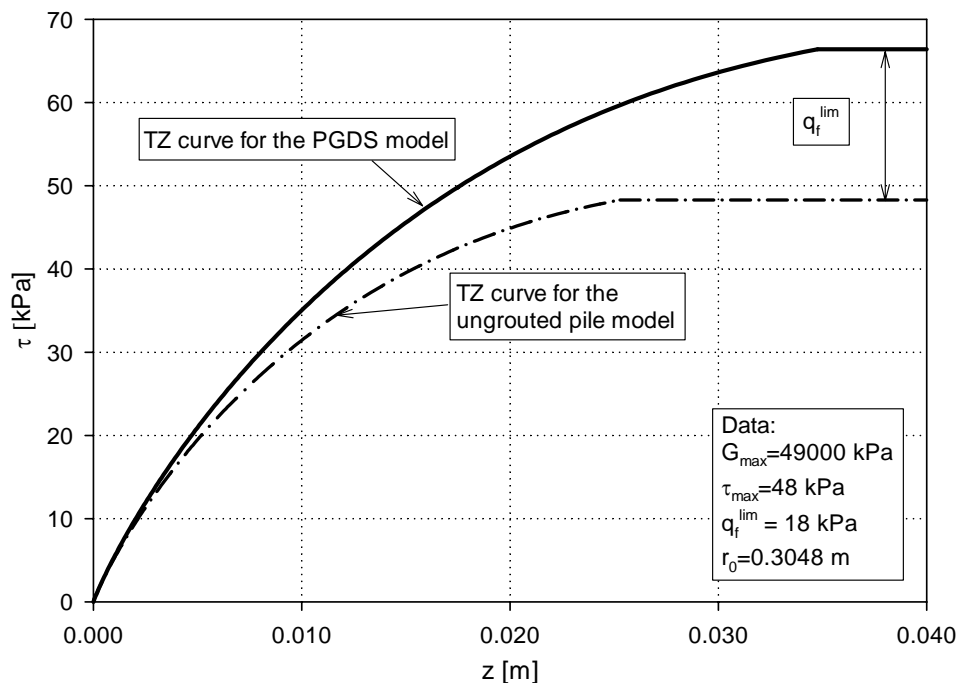


Figure 8-2 Example of the application of the resulting Modified Hyperbolic T-Z curve after applying the masing rule to consider stress reversal

- (2) Calculate the modified Q_b - Z load transfer curve considering the formation of a grout bulb under the pile. The grout bulb radius (r_1) can be estimated using the SGPI calculated in step (2) and the design chart in Figure 8-3. The suggested procedure to estimate the grout bulb radius is shown schematically in Figure 8-3. A limiting value of 2 for the ratio between grout bulb radius (r_1) and shaft radius (r_0) is recommended based on laboratory observations from Mullins and Winters (2004). Alternatively, one can use cavity expansion theory, such as the one presented in Chapter 5 and used in Chapter 6, to estimate the size of the grout bulb. With the new tip area recalculate the load transfer curve for the pile tip using the modified expression presented in Chapter 5 (Equation (5.4)).

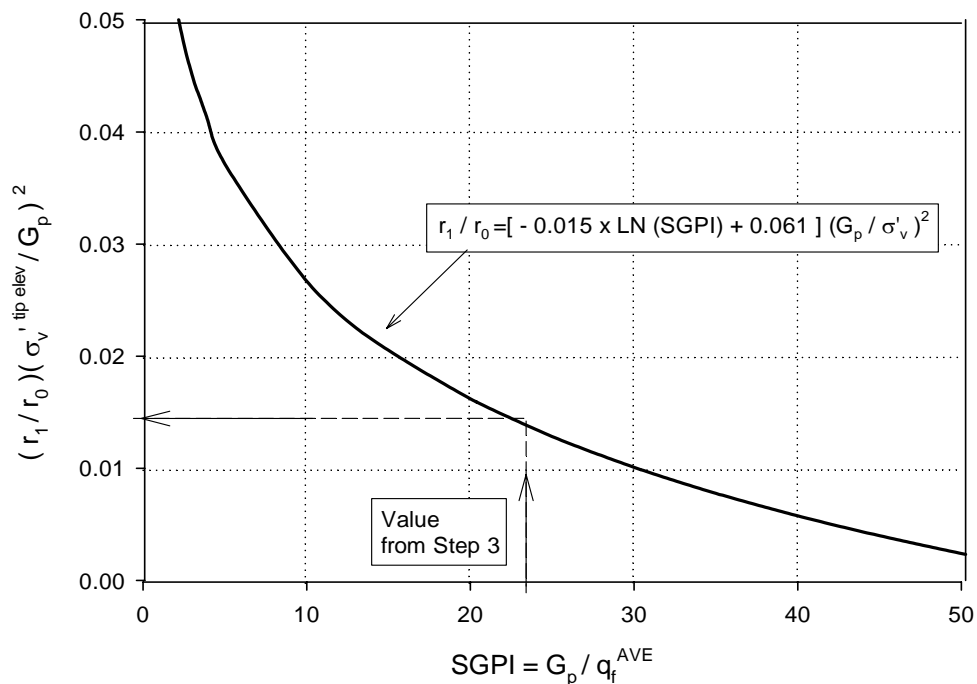


Figure 8-3 Example for the estimation of the bulb radius using the SGPI parameter

- (3) Estimate the load settlement curve of the PGDS. This is done using numerical analyses similar to the ones presented in Chapter 6 with the updated load transfer

curves. The load settlement curve obtained from these numerical analyses can be used as estimated settlements that the PGDS may undergo for service loads. The numerical analyses can be done with the aid of any load transfer analysis computer program. As mentioned earlier, a load transfer analysis computer program was developed to perform the analyses carried out for this research project. Details of this program are described in Appendix B.

- (4) Calculate the Davisson failure load using the predicted load settlement curve for the PGDS obtained in step (3) and estimate its corresponding DCM.
- (5) Enter the design chart with the DCM calculated step 4 and the SGPI calculated in step (3) and check that this point is below the lower limit depicted in the design chart (Figure 8-4).

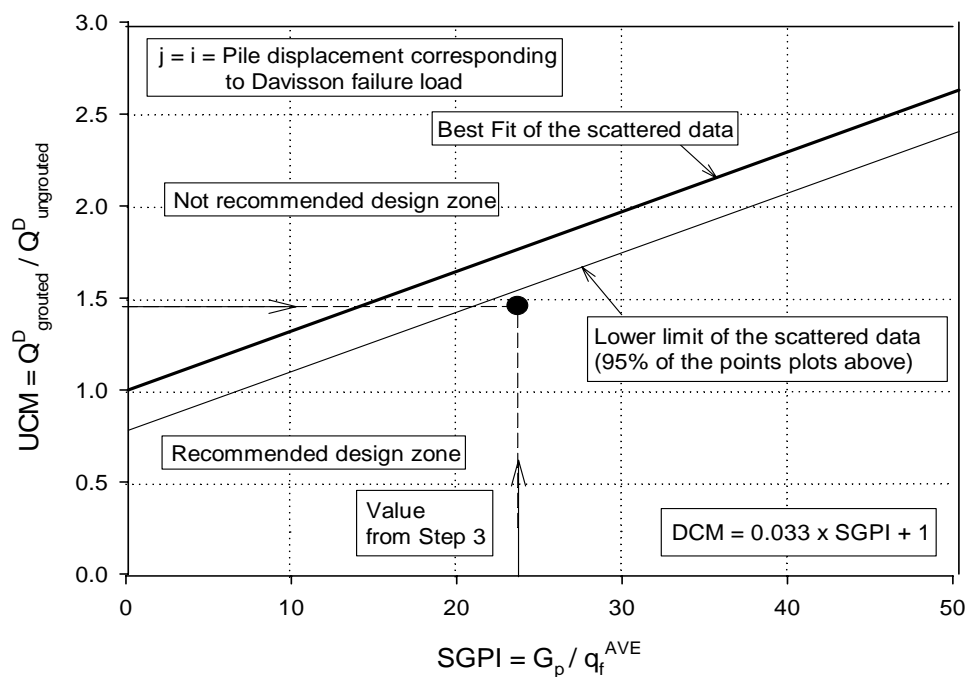


Figure 8-4 Example for checking the PGDS Davisson failure load

If the point falls above the solid line, the bulb radius may have been overestimated and should be reduced. Calibrate the model repeating steps (7) through (10) until the values of SGPI and DCM for the model plot below the design line. These limits are based on available case histories. As more cases become available this limit should be updated.

8.3 DESIGN EXAMPLE

A design example of a 0.61 m diameter drilled shaft is provided in this section in order to illustrate the application of the proposed PGDS design procedure. In order to simplify the example, a pile length of 4.6 m is used so the first part of the methodology can be skipped. It was assumed that the PGDS to be designed was located at Site I, presented in Chapter 6. The soil conditions assume to be those of CPT 67. Cone tip resistance and sleeve friction for this CPT sounding are shown in Figure 8-5.

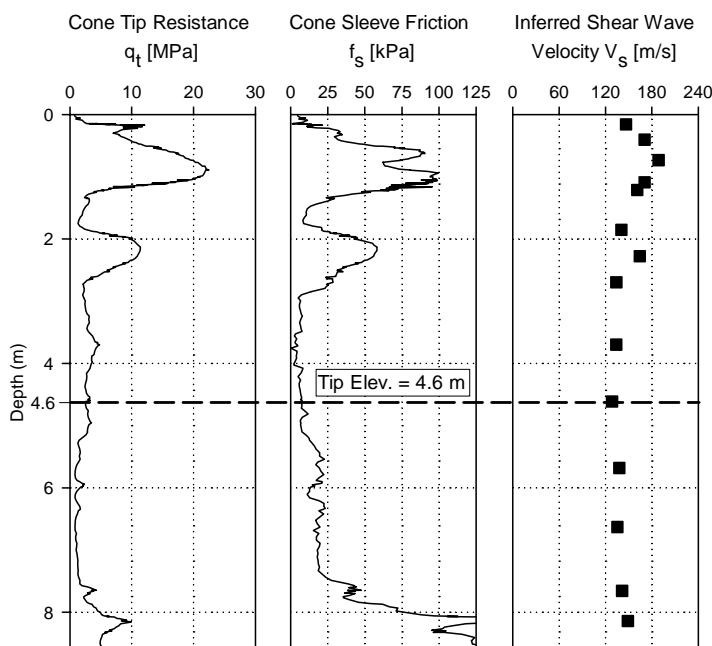


Figure 8-5 Shear wave velocity and CPT soundings advanced at the location of an additional CPT sounding (CPT 67) advanced at Site I, Clearwater, Florida

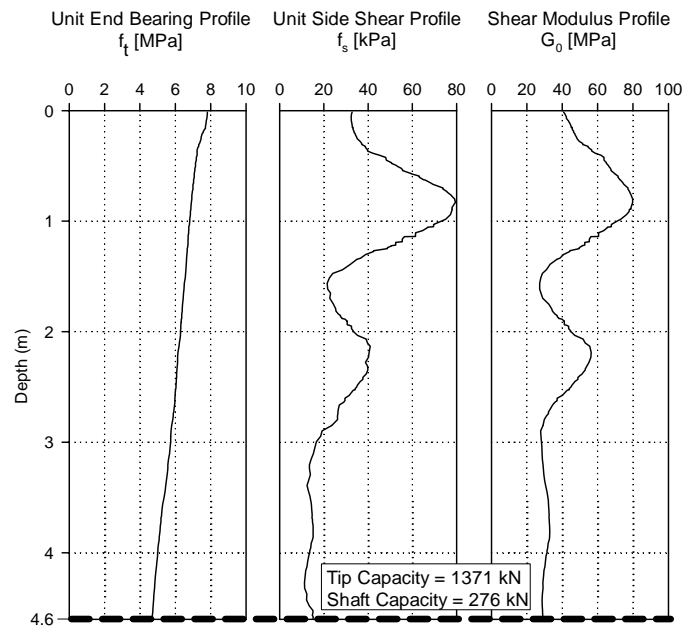


Figure 8-6 Static axial pile capacity and shear modulus profile for a 0.61 m diameter drilled shaft at the location of CPT 67 at Site I, Clearwater, Florida

PART I: Estimate PGDS total capacity for a given grout pressure

STEP 1: A pile length of 4.6 m was assumed in order to simplify the example.

STEP 2: Type A prediction for an ungrouted pile was made using axial a pile tip capacity of 1371 kN and a pile shaft capacity of 276 kN obtained with the static CPT based method by Eslami and Fellenius (1997). This type A prediction was carried out following the procedure outlined in Chapter 3. The load settlement curve for the ungrouted pile is shown in Figure 8-7. The ungrouted Davisson capacity was about 512 kN.

The shear wave profile shown in Figure 8-5 was inferred using the correlations proposed by Andrus et al. (2004). Ultimate axial pile capacity used to estimate asymptotic values for the numerical model is depicted in Figure 8-5.

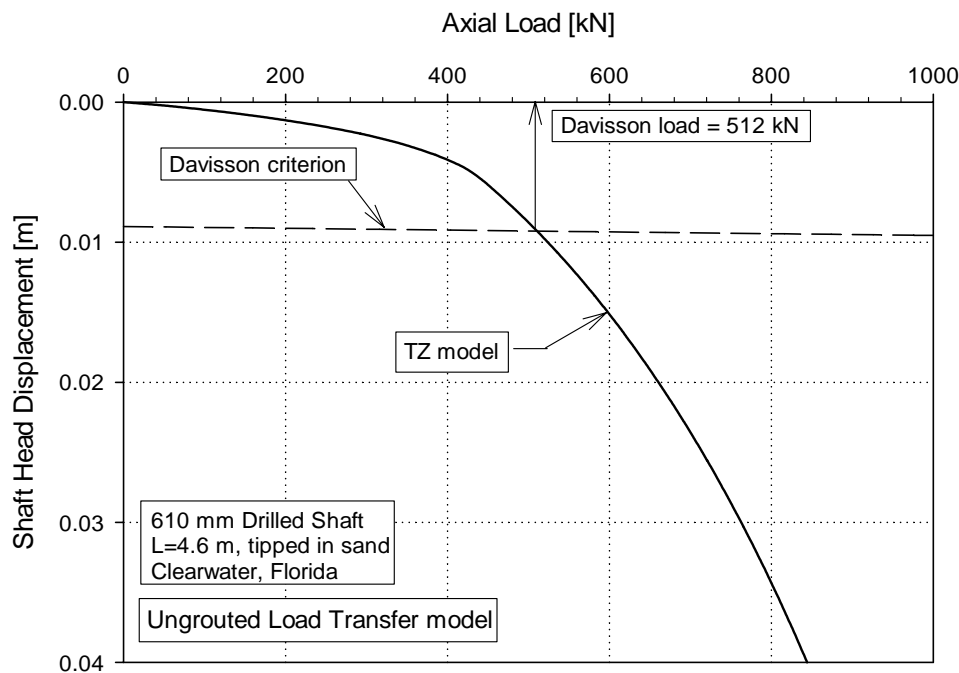


Figure 8-7 Load settlement curve for the ungrouted pile

STEP 3: From Figure 8-6, an average side shear resistance of 30 kPa can be estimated. This value is used to estimate the SGPI to enter the design charts. Note that this same value can be used as limiting side shear friction. However, for this case no evidence of soils with strain softening behavior, thus, a larger grout pressure may have been used during grouting. The maximum allowable grout pressure obtained using Equation (8.1) is:

$$G_p = 4 \times 30 \times \frac{4.6}{0.61} = 896 \text{ kPa} \quad (8.4)$$

And the SGPI, required to enter the design charts from Equation (8.2) is:

$$SGPI = \frac{896 \text{ kPa}}{30 \text{ kPa}} = 30.2 \quad (8.5)$$

STEP 4: Using the SGPI value and the design chart depicted in Figure 8-8, total capacity multipliers can be obtained for different pile head displacements. For example, head displacements equal to 1 %, 2 %, and 3 % of the pile diameter can be taken to estimate the PGDS capacity:

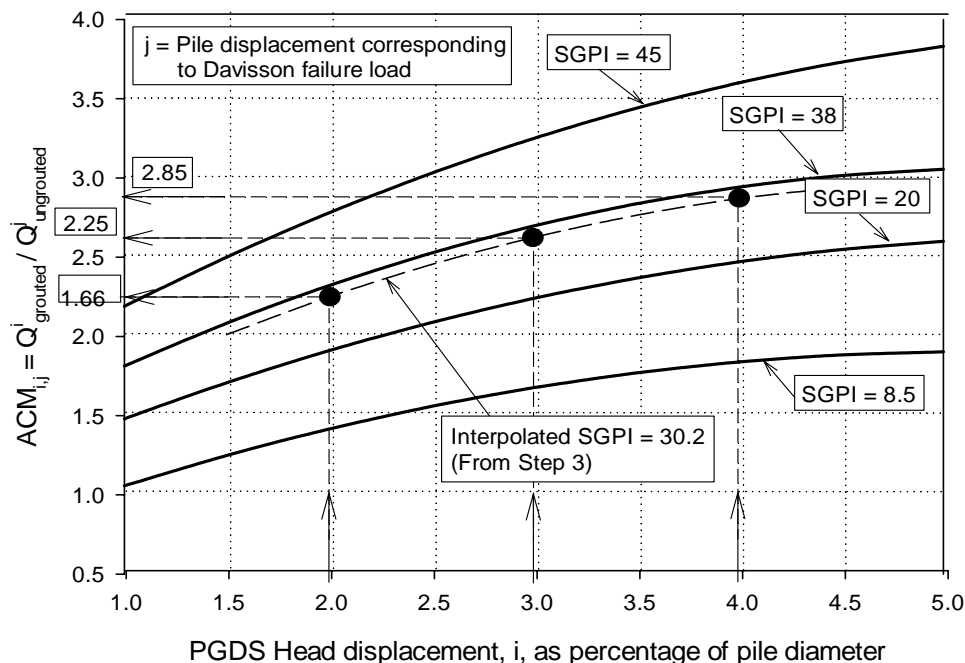


Figure 8-8 Total capacity multipliers for pile selected PGDS head displacements of 2 %, 3 %, and 4 % of the pile diameter

The estimated total axial capacities for the PGDS can be easily calculated for each PGDS pile head displacement, by means of expression (8.3):

$$Q_{grouned}^{2\%} = 2.25 \times 512 \text{ kN} = 1152 \text{ kN} \quad (8.6)$$

$$Q_{grouned}^{3\%} = 2.65 \times 512 \text{ kN} = 1357 \text{ kN} \quad (8.7)$$

$$Q_{grouned}^{4\%} = 2.85 \times 512 \text{ kN} = 1460 \text{ kN} \quad (8.8)$$

PART II: Estimate PGDS settlements

STEP 1: Apply the Masing rule for soil layer along the pile shaft. The asymptotic value should be increased by the amount used to estimate SGPI, which is 30 kPa in this case.

STEP 2: Estimate the radius of the grout bulb that will be developed below the pile shaft using the chart depicted in Figure 8-9:

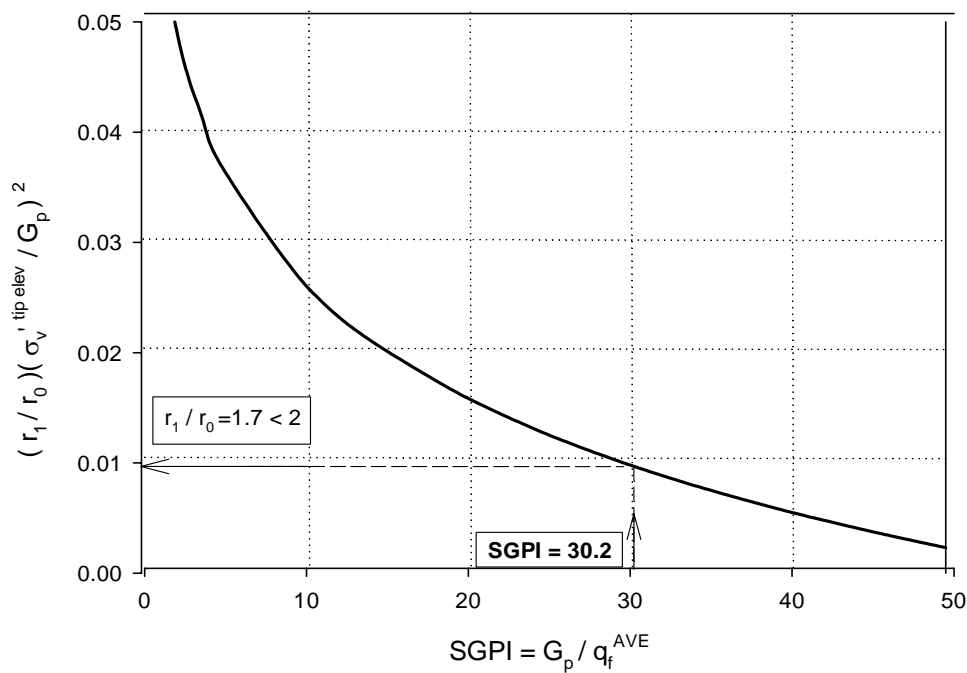


Figure 8-9 Estimated grout bulb radius from design chart

An increased pile tip area due to the presence of a grout bulb under the pile tip will be considered to estimate the PGDS settlements. The bulb radius was estimated using Figure 8-9 and a $G_p = 896$ kPa (From STEP 2, Part I) and an effective overburden pressure of about 85.5 kPa. The resulting bulb radius was 1.7 times that of the pile shaft.

STEP 3: The result from the numerical model of the PGDS is depicted in Figure 8-10. In the same figure the line that corresponds to the Davisson failure criterion is also shown. The Davisson failure load was found to be 925 kN for the PGDS.

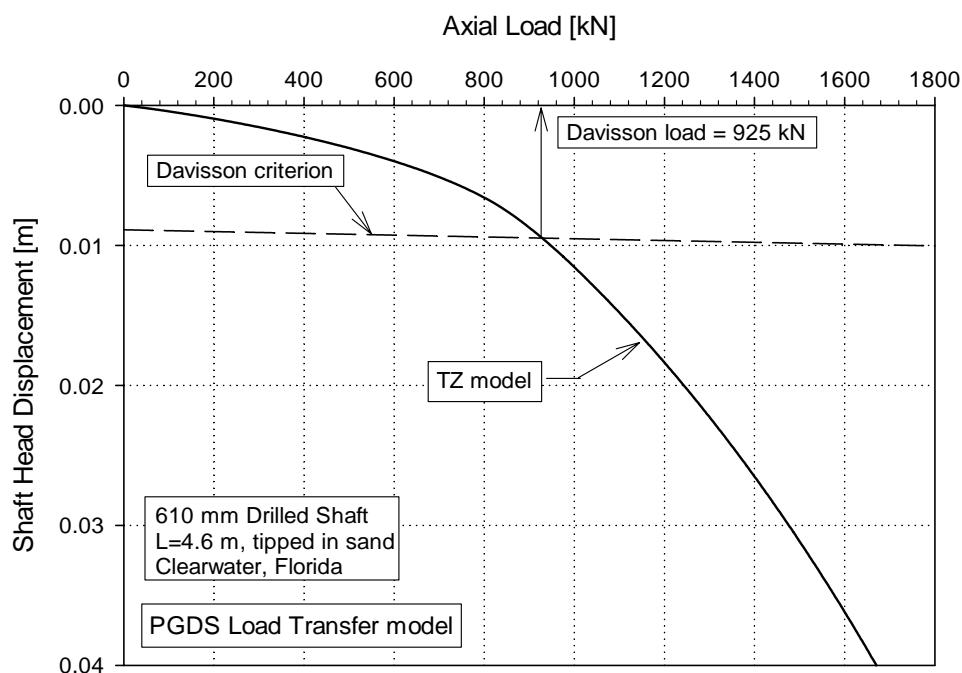


Figure 8-10 Load settlement curve for the PGDS assuming a grout bulb radius 1.7 times the shaft radius and stress reversal of 30 kPa along the shaft

STEP 4: The Davisson failure load obtained in the previous step is checked with the design chart depicted in Figure 8-4. This is shown in Figure 8-11 for $SGPI = 30.2$ and $DCM = 925/512 = 1.8$.

STEP 5: Check the capacity of the design PGDS, as shown in Figure 8-11.

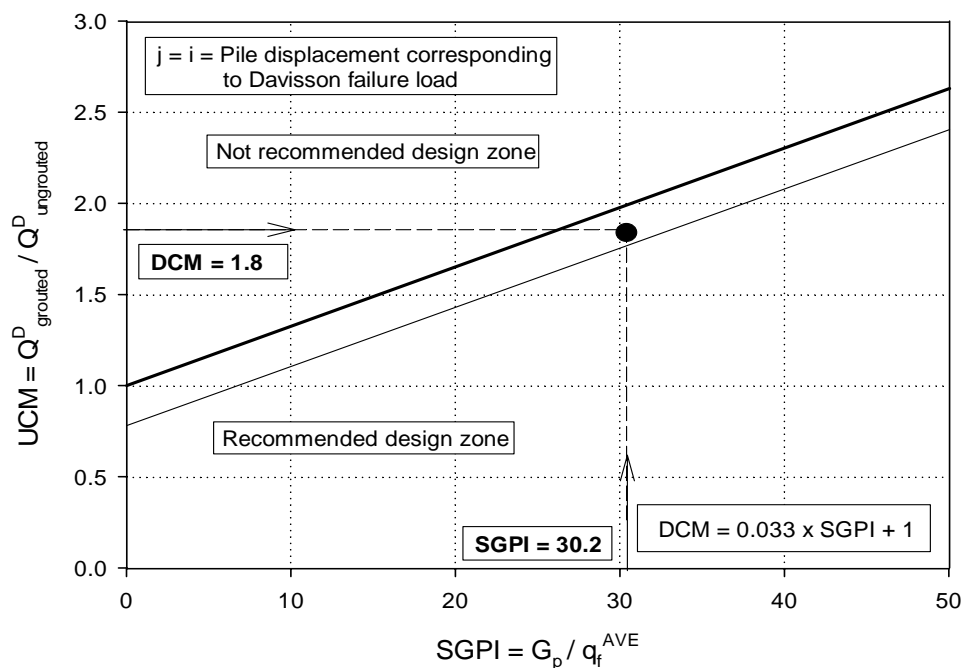


Figure 8-11 Davisson failure load for the designed PGDS

From the above figure it can be seen that the Davisson failure load for the design PGDS lays within reasonable limits. However, if a safer design is desired the grout pressure can be reduced in order to decrease the grout bulb radius and the amount of stress reversal along the shaft. This would require to recalculate SGPI with the selected grout pressure and to repeat steps 3 through 9.

The load settlement curve, depicted in Figure 8-10 can be used to approximately estimate pile settlements. With regard to this, pile settlements beyond the linear portion of the curve should not be trusted since it is controlled by the PGDS tip resistance, which is subject to a number of uncertainties, as stated earlier in this work. However, once a safety factor has been chosen a rough estimate of pile settlements for working loads may be estimated from Figure 8-10.

The final result of the design procedure are the grout pressure required to improve the ungrouted drilled shaft capacity to one of the capacities obtained in STEP 4 (pile length and diameter would also be part of the final result, however for this example these parameters were assumed in advance). Note that if a grout pressure of 896 kPa cannot be reached in the field, new calculations should be made in order to estimate the pile capacity improvement obtained with the actual grout pressure achieved in the field. For this reason it is recommended the construction and test of a PGDS, previously to pile production. This would allow to define a grouting criteria and to check if the design assumptions can be met in the field (i.e. the grout pressure used in the design).

8.4 SUMMARY AND CONCLUSIONS

A methodology composed of two parts was proposed to approximately estimate the total PGDS capacity and its settlements for working loads. The proposed procedure is based on both the results from the load transfer models presented in Chapter 6 and the methodology for estimating single pile settlements presented in Chapter 3. The procedure is based in using three design charts in order to: (a) determine PGDS total capacity for a given pile head displacement, (b) approximately estimate the grout bulb radius that may be formed under the pile tip, and (c) check if the Davisson failure load of the designed PGDS is within reasonable limits.

The proposed methodology represents a rational approach for the design of the PGDS. The procedure incorporates two of the three factors that are believed to control the PGDS capacity and load settlement behavior. The factor representing stiffness increase due to

compression of the soil under the pile tip was neglected in this methodology and can be thought to represent an additional safety factor in the design of PGDS.

9 SUMMARY AND CONCLUSIONS

9.1 INTRODUCTION

This study investigated the load settlement behavior of post grouted drilled shaft foundations (PGDS). PGDS foundations refer to drilled shafts in which cementitious slurry is injected through the pile tip after pile installation in order to improve pile capacity and stiffness. These piles have been found to have improved performance compared to conventional drilled shafts installed in similar soil conditions and with same dimensions. The improved performance is observed through a higher axial capacity and reduced settlements under the same level of service loads. This study investigated the reasons for this improved performance by means of theoretical load transfer analyses of both PGDS and conventional drilled shafts. This study involved developing a new theoretical load transfer analysis technique which was validated using five case studies that were well documented with full scale field load test data. The new technique was programmed into a pile load settlement program called TZASP. This program was used to study load settlement behavior of PGDS foundations. Load transfer analyses were carried out on nine case histories that included PGDS and conventional drilled shafts tested under similar geotechnical conditions.

This study revealed three possible factors that contribute to the observed improved performance of PGDS with respect to conventional drilled shafts. The results of this study were used as a basis to develop a design procedure of PGDS foundations.

The overall objective of this research project was to establish the mechanisms responsible for the improved axial load settlement behavior of PGDS foundations compared to conventional drilled shafts. Table 9-1 outlines the two main objectives of this project and indicates how each objective was met.

Table 9-1 Detailed project objectives

Objective	Evidence of objective completion
1. Develop a methodology to estimate the load settlement curve for single axially loaded piles using the load transfer method.	An analytical technique was formulated and programmed (Chapter 3). The technique was validated with five documented case histories (Chapter 4).
2. Assess the total pile capacity improvement gained by post grouting the pile tip of drilled shafts using the load transfer method.	Load transfer analyses indicated that compression of the soil under the pile, stress reversal along the shaft and the formation of a grout bulb at the pile tip elevation are the factors which contribute to the observed improved performance of PGDS. A design procedure for PGDS was developed based on the load transfer results (Chapters 5 through 8 are related to this objective).

9.2 SUMMARY AND CONCLUSIONS

This section summarizes the activities and conclusions for the following: Literature review, load settlement technique, analytical study of PGDS axial behavior, and the proposed procedure for PGDS design.

9.2.1 LITERATURE REVIEW

A literature review was performed to identify the research needs and to help design the work plan for this research project. The literature review covered the two areas that constitute the central topic of this work: (1) pile settlement estimation using the load transfer method and (2) study the post grouting technique to improve pile performance.

9.2.2 LOAD SETTLEMENT TECHNIQUE

A methodology was proposed for estimating settlements of single axially loaded piles. The methodology is based on the load transfer method and includes theoretically derived load transfer curves. These curves are capable of modeling the degradation of the maximum soil shear modulus through the use of a modified hyperbolic model. Asymptotic values for the load transfer curves were calculated using CPT based static methods for predicting axial pile capacity and the initial shear modulus for small strains was estimated using shear wave velocities from correlations with CPT.

A series of five case studies were analyzed by means of the proposed load transfer methodology in order to test and validate the procedure. Results obtained with the numerical analyses were found to be in good agreement with measured data. Furthermore, the Davisson failure loads for all five cases studies was reasonably close to

the values measured in the field. Of the three static methods tested to estimate the asymptotic values of the load transfer curves; the method by Eslami and Fellenius (1997) was found to give better results than the other two methods tested (namely those by Bustamante and Gianceselli, 1982 and Takesue et al., 1999).

9.2.3 ANALYTICAL STUDY OF PGDS AXIAL BEHAVIOR

The tested methodology for estimating conventional pile settlements was used as the starting point to study the behavior of PGDS. The load transfer methodology was applied systematically to nine PGDS case studies to recognize the influence of different factors to the observed improved axial capacity and stiffness of PGDS compared to control conventional drilled shafts installed under similar soil conditions and same dimensions.

The load transfer analyses were used to assess the effects of three of the main factors that were assumed in this work to contribute to the observed improved performance. These factors are: (1) Soil compression under the pile tip, (2) Shear stress reversal along the shaft due to grouting, and (3) Augmented tip area due to the formation of a grout bulb. Incorporating these factors into the analyses resulted in very good agreement with the observed field measurements. However, no single factor alone could explain the improved PGDS capacity. In all cases it was necessary to include a combination of factors.

Factor 2 (shear stress reversal) was incorporated in the load transfer models using the Masing rule and factor 3 (augmented tip area) was incorporated by enlarging the tip with initial estimates made with the aid of the cavity expansion theory. The initial estimate of the grout bulb radius was adjusted to match field data. Limiting values of the grout bulb

radiuses were established according to results from laboratory test on post grouted specimens. Factors 2 and 3 were systematically incorporated in the load transfer methodology in order to calibrate the numerical model with results from load tests on PGDS. Conversely, factor 1 (the compression of the soil under the pile tip) was not as influential and its incorporation was only required in few case studies. In these cases, it was found that a large increase of the shear modulus of the soil under the tip was required in order to obtain a good calibration of the model. This large shear modulus increase of the load transfer curve at the pile tip may be attributed to the formation of a soil cement mix under the pile and not to large densification of the soil under the pile tip.

9.2.4 PROPOSED PROCEDURE FOR PGDS DESIGN

Results from the nine PGDS case studies discussed in Chapter 6 were used to theoretically assess the currently available empirically derived design charts for PGDS. Results showed a fairly good agreement between theoretically based (derived from the load transfer results obtained in this work) and empirically based (derived by Mullins et al., 2001) design charts. However, these design charts were found to significantly depend on both grouted and ungrouted piles end bearings, which in turn, are subject to important uncertainties. For PGDS, these uncertainties are associated with the aforementioned factors (1) and (2). For conventional drilled shafts, the uncertainties involve the accuracy of the method used to estimate the end bearing capacity of the pile. Therefore, and since good agreement was found between predicted and measured load settlement curves for all nine PGDS case studies, new design charts were developed in terms of total pile capacity. These new design charts required the definition of three factors: Axial Capacity

Multiplier (ACM), Davisson Capacity Multiplier (DCM), and Shaft Grout Pressure Index (SGPI). The ACM relates the Davisson failure load of the PGDS to the axial capacity of the ungrouted pile for a certain pile head displacement. The DCM relates the Davisson failure load of the PGDS to the Davisson failure load of the ungrouted pile. The last factor, the SGPI, relates the grout pressure to the average side shear resistance of the pile. Reasonably good linear fits were found between the ACM and SGPI and between DCM and SGPI. These linear fits were used to develop design charts that allow estimating the PGDS capacity for a certain grout pressure and side shear resistance of an ungrouted pile of similar dimensions installed in similar geotechnical conditions as the PGDS. A third chart was developed to approximately estimate the grout bulb radius that may result under the pile due to grouting. This third chart relates SGPI and an dimensionless number that involves the grout pressure, effective overburden pressure at the tip elevation, the shaft radius, and the grout bulb radius.

The new design charts were incorporated into a procedure proposed for designing PGDS. The proposed methodology is based on the load transfer approach and is composed of two parts: Part I aims at determining the total PGDS capacity for a given grouting pressure, and Part II aims at estimating the load settlement curve for a PGDS through the inclusion of factors 2 and 3.

9.3 RECOMMENDATIONS FOR FUTURE RESEARCH

This research focused primarily on two objectives: development of a methodology for estimating pile settlements and development of a design method for PGDS foundations using a theoretical framework. This work is believed to have met these two objectives.

However, based on the findings from this investigation, the following recommendations are made for future work:

- **METHODOLOGY FOR ESTIMATING PILE SETTLEMENTS**

- More case studies are needed in order to extend the conclusions and recommendations of this study to other soil types. For example, layered soils and strain weakening soils. An extended database will strengthen the proposed methodology allowing a reduction of safety factors in design process of single piles. Well documented field loading tests of drilled shafts with adequate instrumentation (e.g., CPTU, measurement of shear wave velocities, etc.) are scarce.
- Extend the proposed methodology to other in-situ tests (e.g., Standard Penetration Test, DMT, pressuremeter, etc.). Comparison of the different methodologies would be useful for countries where CPT is not common.
- Determine the variability of hyperbolic parameter f and g . A table with recommended values of these parameters for different soil types is recommended.

- **DESIGN METHODOLOGY FOR PGDS**

- Processes that develop at the pile tip during grout injection are not completely understood. In this regard, more rigorous numerical models should be performed in order to simulate the post grouting process and determine the extent at which factors 1, 2 and 3 can be developed.

Moreover, a rigorous numerical model (i.e. finite element or finite differences models) might lead to additional factors that are probably involved in the PGDS improved capacity.

- Finite element analyses are recommended to model field tests on test piles. This type of analysis would take into account the continuous nature of soil deposits, as opposed to the T-Z approach used in this study. Comparison of the results of the two approaches would be useful and new conclusions may be drawn from these analyses.
- More case studies of instrumented PGDS foundations are needed in order to strengthen the database used to develop the proposed design charts. This will result in more reliable correlations which, in turn, would lead to safer designs.
- The design procedure has not been fully tested. Additional load tests performed on PGDS are required to test the accuracy of the methodology and calibrate the design procedure.
- The proposed design procedure is probably too conservative since the effects of soil compression under the pile tip were neglected and the Davisson failure load for the PGDS was limited. Further research on PGDS behavior would help to incorporate factor 3 into the design procedure and improve its accuracy and reliability.

- Additional research is required in order to more clearly understand the bulb formation process for different type of soils. In this regard, exhumation of PGDS would help to assess the formation of the grout bulb due to tip grouting.

REFERENCES

- Abendroth, R. E., and Greimann, L. F. (1988). "Pile Behaviour Established from Model Tests." *Journal of Geotechnical Engineering, ASCE*, 116(4), 571-588.
- Andrus, R. D., Piratheepan, P., and Juang, H., (2004). "Shear Wave Velocity – Penetration Resistance Correlations for Ground Shaking and Liquefaction Hazards Assessment" Report to the US Geological Survey, Department of Civil Engineering, Clemson University.
- API (1993). "Recommended Practice for Planning, Designing and Constructing Fixed Offshore Platforms - Working Stress Design." Washington, DC, 20th Edition, American Petroleum Institute.
- Armaleh, S., and Desai, C. S. (1987). "Load-Deformation Response of Axially Loaded Piles." *Journal of Geotechnical Engineering, ASCE*, 113(12), 1483-1500.
- Atkinson, J. H. (2000). "Non-linear soil stiffness in routine design." *Geotechnique*, 50(5), 487-508.
- Baguelin, F., and Frank, R. (1979). "Theoretical Studies of Piles Using the Finite Element Method." *Proceedings of the conference on Numerical Methods in Offshore Piling*, Ed. Institution of Civil Engineers, London, UK, 83-91.
- Baker, W. H., and Broadrick, R. L. (1997). *Ground Improvement, Reinforcement, and Treatment: A Twenty Year Update and a Vision for the 21st Century*, Earth Tech, Clearwater, Florida.
- Baldi, G., Bellotti, R., Ghionna, V. N., Jamiolkowski, M. and Lo Presti, D. F. C. (1989). "Modulus of Sands From CPTs and DMTs." *Proceedings of the 12th International Conference on soil Mechanics and Foundation Engineering*, Rio de Janeiro, 1, 165-170, Balkema Pub., Rotterdam.

- Bolognesi, A. J. L. and Moretto, O. (1973). "Stage Grouting Preloading of Large Piles on Sand." *Proceedings of the 8th ICSMFE*, Moscow.
- Boussinesq, J. (1885) "Application des potential a l'etude de l'equilibre et du mouvement des solides elastiques. " Lille, Paris, 57-75.
- Briaud, J-L. and Gibbens, R.M., editors (1994). "Predicted and Measured Behavior of Five Spread Footings on Sand." GSP 41, ASCE, Reston, Virginia, 255 pages.
- Brown, D.A. (2002). "Effect of construction on axial capacity of drilled foundations in Piedmont soils." *Journal of Geotechnical and Geoenvironmental Engineering, ASCE*, 128 (12), 967-973.
- Brown, D. A. and Vinson, J. (1998). "Comparison of Strength and Stiffness Parameters for a Piedmont Residual Soil". *Proceedings of the Geotechnical Site Characterization Conference*, Vol. 2, Balkema, Rotterdam, 1229-1234.
- Bruce, D. A. (1986). "Enhancing the Performance of Large Diameter Piles by Grouting." *Ground Engineering*(Parts 1 and 2, May and July respectively).
- Brusey, W. G. (2000). "Post-Grouted Test Shafts at JFK International Airport." *Proceedings of the New Technological and Design Developments in Deep Foundations*, Denver, Colorado, 18-32.
- Bustamante, M. and Gianceselli, L. (1982). "Pile bearing capacity prediction by means of static penetrometer CPT". *Proceedings of the 2nd European Symposium on Penetration Testing Amsterdam*, The Netherlands.
- Butterfield, R., and Banerjee, P. K. (1971). "The Elastic Analysis of Compressible Piles and Pile Groups." *Geotechnique*, 20(1), 43-60.
- Chow, F. C. (1996). "Investigations into the behaviour of displacement piles for offshore foundations." PhD thesis, Imperial College of Science, Technology, and Medicine, University of London, London, UK.
- Chow, Y. K. (1986). "Analysis of vertically loaded pile groups." *International Journal for Numerical and Analytical Methods in Geomechanics*, 10, 59-72.
- Coyle, H. M., and Reese, L. C. (1966). "Load Transfer for Axially Loaded Piles in Clay." *Journal of Soil Mechanics and Foundation Division, ASCE*, 92(2), 1-26.
- Coyle, H. M., and Sulaiman, I. H. (1967). "Load Transfer for Axially Loaded Piles in Clay." *Journal of Soil Mechanics and Foundation Division, ASCE*, 93(6), 261-278.
- Dawkins, W. P. (1982). "User's Guide: Computer Program for Soil-Structure Interaction Analysis of Axially Loaded Pile (CAXPILE)." *U.S Army Coprs of Engineers, Waterways Experiment Station, Vicksburg, MS*.

- Desai, C. S., and Christian, J. T. (1977). *Numerical Methods in Geotechnical Engineering*, New York: McGraw-Hill.
- Duncan, J. M., and Chang, C. (1970). "Nonlinear Analysis of Stress and Strain in Soils." *Journal of Soil Mechanics and Foundation Division, ASCE*, 96(SM5), 1629-1651.
- El-Kelesh, A. M., Mossaad, M. E., and Basha, I. M. (2001). "Model of Compaction Grouting." *Journal of Geotechnical and Geoenvironmental Engineering, ASCE*, 127(11), 955-964.
- Ensoft Inc. (1998) "Shaft, A program for the study of Drilled Shafts under axial loading", User's Manual.
- Eslami, A. and B. H. Fellenius (1997). "Pile capacity by direct CPT and CPTu methods applied to 102 case histories." *Canadian Geotechnical Journal*, 34, 886-904.
- Everett, J. P. (1991). "Load Transfer Functions and Pile Performance Modelling." *Proceedings of the Tenth Regional Conference for Africa on Soil Mechanics and Foundation Engineering and The Third International Conference on Tropical and Residual Soils*, Maseru, 23-27 September, 229-234.
- Fahey, M., and Carter, J. P. (1993). "A finite Element Study of the Pressuremeter test in Sand Using a Non-linear Elastic-Plastic model." *Canadian Geotechnical Journal*, 30(2), 348-362.
- Frank, R. (1974). "Etude théorique du comportement des pieux sous charge verticales: Introduction de la dilatance." Dr-Ing thesis, Université Pierre et Marie Curie, France.
- Frank, R., and Zhao, S. R. (1982). "Estimation par les Parametres pressiometriques de L'enfoncementt Soud Charge Axiale de Pieux Fores dans des Sols Fins." *Bull. Liaison Labo. P. et Ch.*, 119, 17-24. (in French).
- Frank, R., Kalteziotis, N., Bustamante, M., Christoulas, S., and Zervogiannis, H. (1991). "Evaluation of Performance of Two Piles Using Pressuremeter Method." *Journal of Geotechnical Engineering, ASCE*, 117(5), 695-713.
- Georgiadis, M., and Saflekou, S. (1990). "Piles Under Axial and Torsional Loads." *Computers and Geotechnics*, 9, 291-305.
- Gouvenot, D. and Gabiax, F. D. (1975). "A New Foundation Technique Using Piles Sealed by Concrete Under High Pressure." *Proceedings of the Seventh Annual Offshore Technical Conference*.
- Guo, W. D. (1996). "Analytical and Numerical Solutions for Pile Foundations," PhD. Thesis, Department of Civil Engineering, The University of Western Australia.

- Guo, W. D., and Randolph M. F. (1997). "Vertically Loaded Piles in Non-Homogeneous Media." *International Journal of Numerical and Analytical Methods in Geomechanics*, 21, 507-532.
- Guo, W. D. (2000). "Vertically Loaded Single Piles in Gibson Soil." *Journal of Geotechnical and Geoenvironmental Engineering, ASCE*, 126(2), 189-193.
- Guo, W. D., and Randolph M. F. (1997). "Vertically Loaded Piles in Non-Homogeneous Media." *International Journal of Numerical and Analytical Methods in Geomechanics*, 21, 507-532.
- Hirayama, H. (1990). "Load-Settlement Analysis for Bored Piles Using Hyperbolic Transfer Functions." *Soils and Foundations*, 30(1), 55-64.
- Hoit, M., Hays, C., McVay, M., and William, M. (2000). "FB-Pier v. 2.0." *Florida Bridge Software Institute*. <http://bsi-web.ce.ufl.edu>.
- Houdin, H., et al. (1968). "Le deuxieme pont d'Abidyan." *Annales de l'Institut Technique du Batiment et des Travaux Publics*, 1187-1193.
- Kezdi, A. (1975). "Chapter 19. Pile Foundations." *Foundation Engineering Handbook*, Ed. by Winterkorn, H. F. and Fang, H. Y., Van Nostrand Reinhold Company, New York, N. Y., 567.
- Kodikara, J. K., and Johnston, I. W. (1994). "Analysis of Compressible Axially Loaded Piles in Rock." *International Journal of Numerical and Analytical Methods in Geomechanics*, 12, 427-437.
- Kondner, R. L. (1963). "Hyperbolic stress-strain response: Cohesive soils." *Journal of Soil Mechanics and Foundation Division, ASCE*, 89(SM1), 115-143.
- Kondner, R. L., and Zelasko, J. S. (1963). "A hyperbolic stress-strain formulation for sands." *Proceedings, 2nd Pan-American Conference on Soil Mechanics and Foundations Engineering*, Sao Paulo, Brazil, 1, 289-324.
- Kraft, L. M. J., Ray, R. P., and Kagawa T. (1981). "Theoretical T-Z Curves." *Journal of Geotechnical Engineering Division, ASCE*, 107(GT11), 1543-1561.
- Lee, J. H., and Salgado, R (1999). "Determination of Pile Base Resistance in Sands." *Journal of Geotechnical and Geoenvironmental Engineering, ASCE*, 125(8), 673-683.
- Liu, J., and Zhang, K. (2003). "Analysis of Pile Load-Transfer Under Pile-Side softening." *J. of Cent. South Univ. of Technol.*, 10(3), 231-236.
- Liu, J., Xiao, H. B., Tang, J., Li, Q. S. (2004). "Analysis of Load-Transfer of Single Pile in Layered Soil." *Computers and Geotechnics*, 31, 127-135.

- Liu, Q. F., and Meyerhof, G. G. (1987). "New Method for Nonlinear Analysis of Rigid Piles in Clay." *Computers and Geotechnics*, 3, 185-212.
- Lizzi, F., Viggiani, C., and Vinale, F. (1983). "Some Experience with Pre-Loading Cells at the Base of Large Diameter Bored Piles." *Proceedings of the 7th Asian Regional Conference on Soil Mechanics and Foundation Engineering*, Haifa, Israel.
- Logie, C. V. (1984). "Drilled Pier Foundation Rehabilitation Using Cement Grouting." *Innovative Cement Grouting, SP-83*, American Concret Institute, Detroit, Michigan.
- Lunne, T., Robertson, P. K., and Powell, J. J. M. (1997). "Cone Penetration Testing in Geotechnical Practice." Blackie Academic and Professional, New York, 312p.
- McVay, M. C., Townsend, F. C., Bloomquist, D. G., O'Brien, M. O., Caliendo, J. A. (1989). "Numerical Analysis of Vertically Loaded Pile Groups." *Proceedings of the Foundation Engineering Congress*, North Western University, Illinois.
- Masing, G. (1926). "Eigenspannungen und Verfurigung beim Messing." *Proceedings of the 2nd International Congress on Applied Mechanics*, Zurich.
- Mayne, P. W., and Dumas, C. (1997). "Enhanced in-situ geotechnical testing for bridge foundation analyses." *Transportation Research Record 1569*, National Academy Press, Washington, D.C., 26-35.
- Mayne, P. W., Schneider, J.A., and Martin, G.K. (1999). "Small- and large-strain soil properties from seismic flat plate dilatometer tests." *Pre-Failure Deformation Characteristics of Geomaterials*, Vol. 1, (Torino), Balkema, Rotterdam, 419-426.
- Mayne, P. W., Brown, D., Vinson, J., Schneider, J. A. and Finke, K. (2000). "Site Characterization of Piedmont Residual Soils at the NGES, Opelika, Alabama." *ASCE Geotechnical Special Publication No. 93*, Ed. By Jean Benoit and Alan Lutenegeger, Reston, Virginia, April 2000, 160-185.
- Mayne, P. W. and Schneider, J. A. (2001). "Evaluating Axial Drilled Shaft Response by Seismic Cone" *Proceedings of Conference Foundations and Ground Improvement, GSP No 113*, Reston, Virginia, 655-669.
- Mayne, P. W. and Brown, D. A. (2003). "Site characterization of Piedmont residuum of North America". *Proceedings of Characterization and Engineering Properties of Natural Soils*, Vol. 2, Ed. Swets & Zeitlinger, Lisse, Netherlands, 1323-1339.
- Mayne, P. W. and Zavala, G. (2004). "Axial Shaft Response From Seismic Piezocone Tests." *Proceedings of Conference Geosupport 2004, GSP No. 124*, Ed. John P. Turner and P. W. Mayne.

- Midendorp, P., Bermingham, P., and Kuiper, B. (1992). "Statnamic Load Testing of Foundation Piles." *Proceedings of the 4th International Conference on the Application of Stress-Wave Theory to Piles*, A. A. Balkema, Rotterdam, 581-588.
- Mindlin, R. D. (1936). "Force at a Point in the Interior of a Semi-Infinite Solid." *Physics*, 7, 197-202.
- Mitchell, J. K. (1988). "New Developments in Penetration Tests and Equipment." *Penetration Testing 1988, ISOPT-1*, J. De Ruiter Ed. Vol. 1, A. A. Balkema, Rotterdam, The Netherlands, 245-261.
- Mullins, G. (1999). "Interviews with Engineers During Load Testing on the Taipei Financial Center," Taipei, Taiwan.
- Mullins, G., Dapp, S., Frederick, E., and Wagner, R. (2001). "Post grouting Drilled Shafts Tips – Phase I." Final Report to the Florida Department of Transportation, December, 2001.
- Mullins, G., and Winters, D. (2004). "Post grouting Drilled Shafts Tips – Phase II", Final Report to the Florida Department of Transportation, June, 2004.
- Murff, J. D. (1975). "Response of Axially Loaded Piles." *Journal of Geotechnical Engineering Division, ASCE*, 101(3), 357-360.
- Olson, R. E. (2002). "Axial Load Capacity of Driven Piles." *Proceedings of the 50th Annual Geotechnical Engineering Conference*. Ed. J. F. Labuz and J. G. Bentler. University of Minnesota, February 2002.
- O'Neill, M. W., and Raines, R. D. (1991). "Load Transfer for Pipe Piles in Highly Pressured Dense Sand." *Journal of Geotechnical Engineering, ASCE*, 117(8), 1208-1226.
- O'Neill, M. W. (2001). "Side resistance in Piles and Drilled Shafts" (The Thirty Fourth Terzaghi Lecture). *Journal of Geotechnical and Geoenvironmental Engineering, ASCE*, Vol. 127(1), 1-16.
- Pando, M. A., (2003). "A Laboratory and Field Study of Composite Piles for Bridge Substructures." PhD Thesis. Civil Engineering Department. Virginia Polytechnic Institute and State University, 412p.
- Piccione, M., Carletti, G., and Diamanti, L. (1984). "The Piled Foundations of the Al Gazira Hotel in Cairo." *Proceedings of the International Conference on Advances in Piling and Ground Treatment for Foundations*, London, UK.
- Poulos, H. G., and Davis, E. H. (1980). "Pile Foundation Analysis and Design", John Wiley and Sons, New York.

- Poulos, H. G. (1989). "Pile Behaviour-Theory and Application." *Rankin Lecture. Geotechnique*, 39(3), 365-415.
- Poulos, H. G. (2001). "Pile foundations." In *Geotechnical and Geoenvironmental engineering handbook*, Edited R. K. Rowe, Kluwer Academic Press.
- Rajapakse, R. K., N. D. (1990). "Response of Axially Loaded Elastic Piles in a Gibson Soil." *Geotechnique*, 40(2), 237-249.
- Randolph, M. F. (1994). "Design methods for pile groups and pile drafts." *Proceedings, XIII ICSMFE*, New Delhi, India, 61-82.
- Randolph, M. F., and Wroth, C. P. (1978). "Analysis of Deformation of Vertically Loaded Piles." *Journal of Geotechnical Engineering Division, ASCE*, 104(GT12), 1465-1488.
- Reese, L., C., Hudson, W. R., and Vijayvergiya, V. N. (1969). "An Investigation of the Interaction Between Bored Piles and Soil." *Proceedings of the 7th ICSMFE*, Mexico, 211-215.
- Rix, G. J., and Stokoe, K. H. (1991). "Correlation of initial tangent modulus and cone resistance." *Proceedings of the International Symposium on Calibration Chamber Testing*, Potsdam, NY, 351-362.
- Satou, S. (1965). "Bearing Mechanism of Pile (I), (II), (III), (IV), (V)." *Civil Engineering Technology*, 1-5 (in Japanese).
- Schmitt, K. (1971). "Spitzen-Verpressung von GROSSOHRPHÄLEN." *Die Bautechnik*, 44-71.
- Seed, H. B., and Reese, L. C. (1957). "The Action of Soft Clay Along Friction Piles." *Transactions, ASCE*, 122(731-754).
- Silwinski, Z. J., and Flemming, W. G. K. (1984). "The Integrity and Performance of Bored Piles." *Proceedings of the International Conference on Advances in Piling and Ground Treatment for Foundations*, London, UK.
- Simons, H., Wind, H., Bucksch, H., and Brückner, H. (1963). *The Bridge Spanning Lake Maracaibo in Venezuela*, Bauverlag GmbH, Wiesbaden, Berlin.
- Solera, S. A. and Mitchell, J. M. (1991). "Predicted and Observed Settlement of a Building Founded on Base Grouted Piles in the Thanet Sands, London." *Proceedings of the X ECSMFE*, Florence, Italy, 571-576.
- Stocker, M. F. (1983). "The Influence of Post Grouting on the Load Bearing Capacity of Bored Piles." *Proceedings of the 8th European Conference on Soil Mechanics and Foundations Engineering*, Helsinki, 167-170.

- Suárez, L. E. (2003). "Soil Dynamics" Graduate Course notes. University of Puerto Rico, Civil Engineering Department. (In Spanish).
- Takesue, K., Sasao, H., and Matsumoto, T. (1998). "Correlation Between Ultimate Pile Skin Friction and CPT Data." *Proceedings of the conference Geotechnical Site Characterization*, Balkema, Rotterdam, (2) 1177-1182.
- Tan, M. J. C., and Johnston, I. W. (1991). "Estimation of Side Resistance of Compressible Piles in a Softening Medium." *Australian Geomechanics*, 20, 24-39.
- Tumay, M.T. and Bynoe, Y. (1998). "In-situ testing at the national geotechnical experimentation sites (Phase 2)". Contract Report DTFH61-97-00161 to Federal Highway Administration, Louisiana Transportation Research Center, Baton Rouge.
- Vaziri, H. H., and Xie, J. (1990). "A Method for Analysis of Axially Loaded Piles in Nonlinear Soils." *Computers and Geotechnics*, 10(2), 149-159.
- Vesic, A. S. (1972). "Expansion of Cavities in Infinite Soil Mass." *Journal of Soil Mechanics and Foundation Division, ASCE*, 98(SM3), 265-290.
- Vijayvergiya, V. N. (1977). "Load-Movement Characteristics of Piles." *Proceedings of the 4th Symposium of Waterway*, Long Beach, California, 269-284.
- Xiao, H. (2003). "Analysis of Pile's Load Transfer in Layered Soils." *J. of Cent. South Univ. of Technol.*, 34(6), 687-690 (in chinese).
- Zhao, S. R. (1991). "Vertical Stiffness of Single Pile." *Proceedings of the 6th National Conf. on Soil Mech. and Found. Engrg.*, Shanghai, China.
- Zhu, H., and Chang, M. (2002). "Load Transfer Curves Along Bored Piles Considering Modulus Degradation." *Journal of Geotechnical and Geoenvironmental Engineering, ASCE*, 128(9), 764-774.
- Zienkiewicz, O. C. (1971). "The Finite Element Method in Engineering Science." *McGraw-Hill, London*.

APPENDIX

A

A.1 PHASE I – SITE I, CLEARWATER, FLORIDA

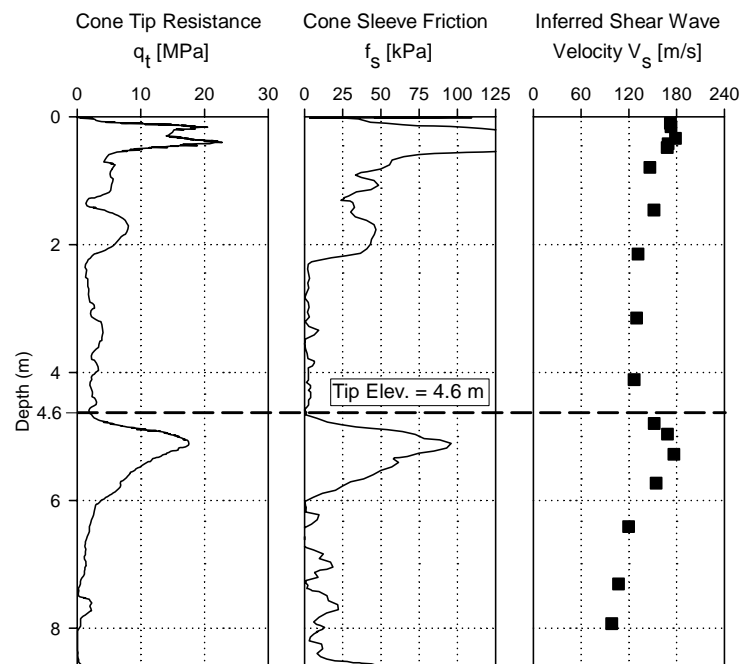


Figure A - 1 Shear wave velocity and CPT soundings advanced at the location of Control pile at Site I, Clearwater, Florida

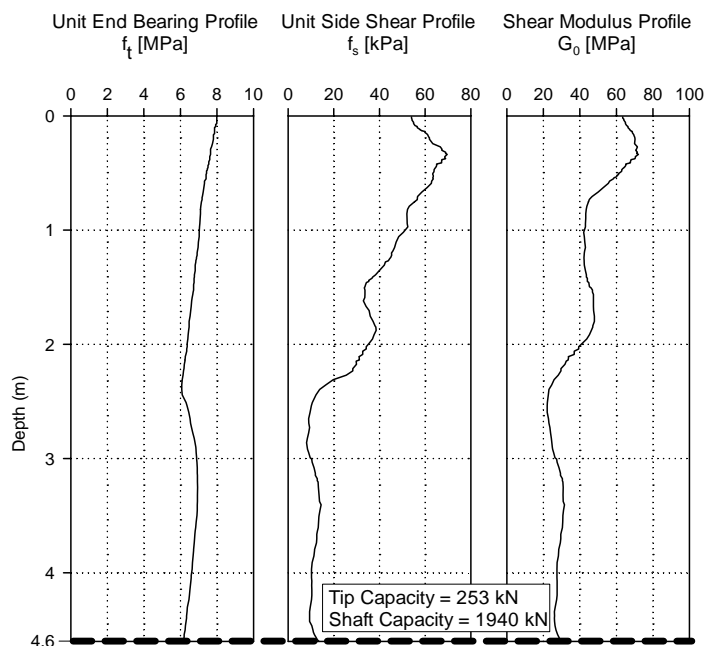


Figure A - 2 Static axial pile capacity and shear modulus profile for a 0.61 m diameter Control pile at Site I, Clearwater, Florida

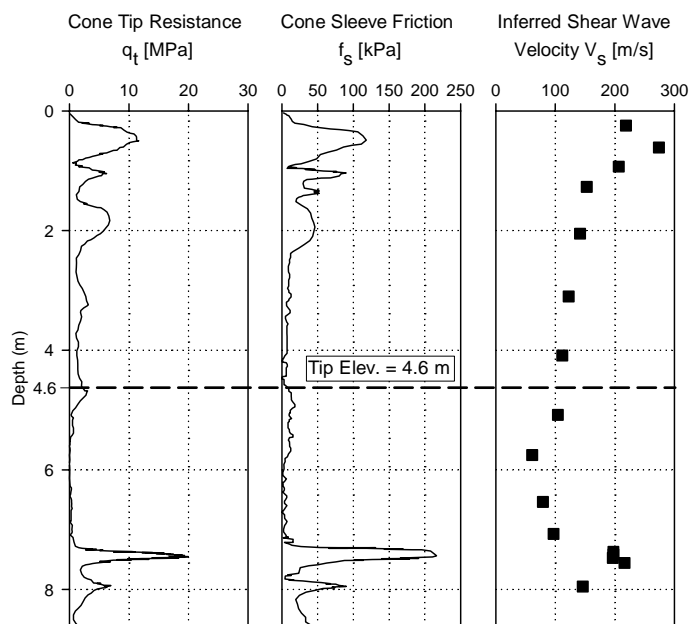


Figure A - 3 Shear wave velocity and CPT soundings advanced at the location of drilled shaft FJ 1 at Site I, Clearwater, Florida

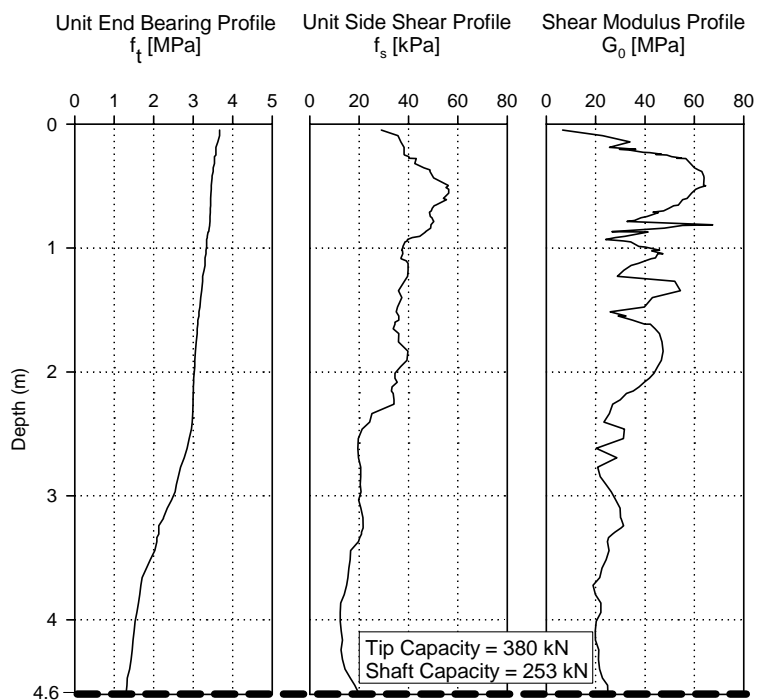


Figure A - 4 Static axial pile capacity and shear modulus profile for a 0.61 m diameter drilled shaft FJ 1 location at Site I, Clearwater, Florida

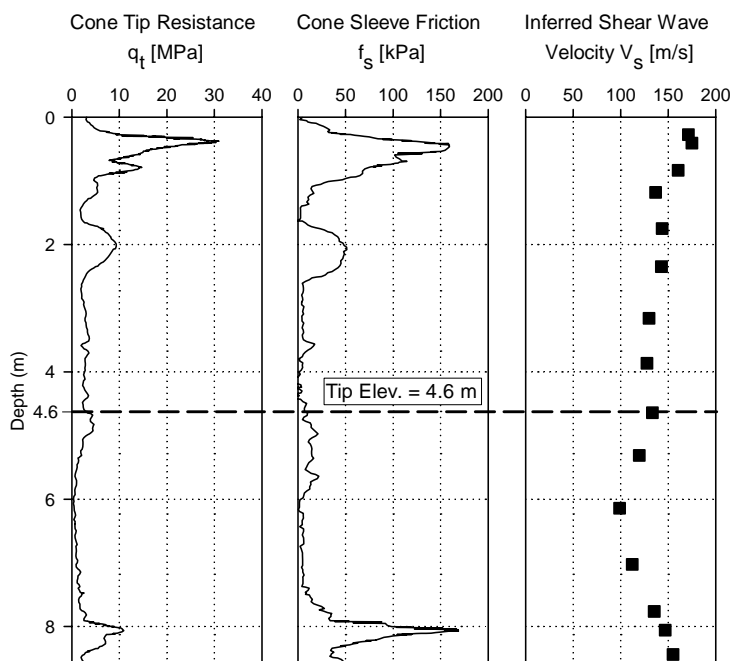


Figure A - 5 Shear wave velocity and CPT soundings advanced at the location of drilled shaft FJ 2 at Site I, Clearwater, Florida

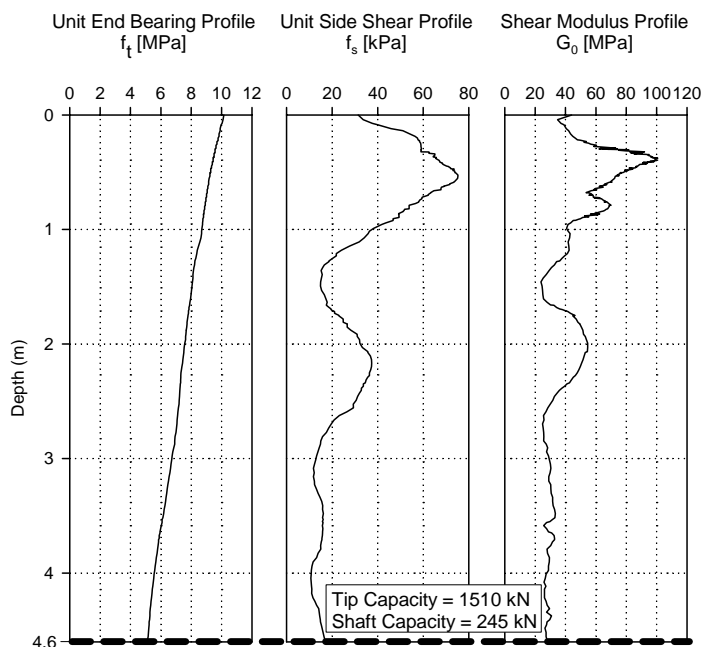


Figure A - 6 Static axial pile capacity and shear modulus profile for a 0.61 m diameter drilled shaft FJ 2 location at Site I, Clearwater, Florida

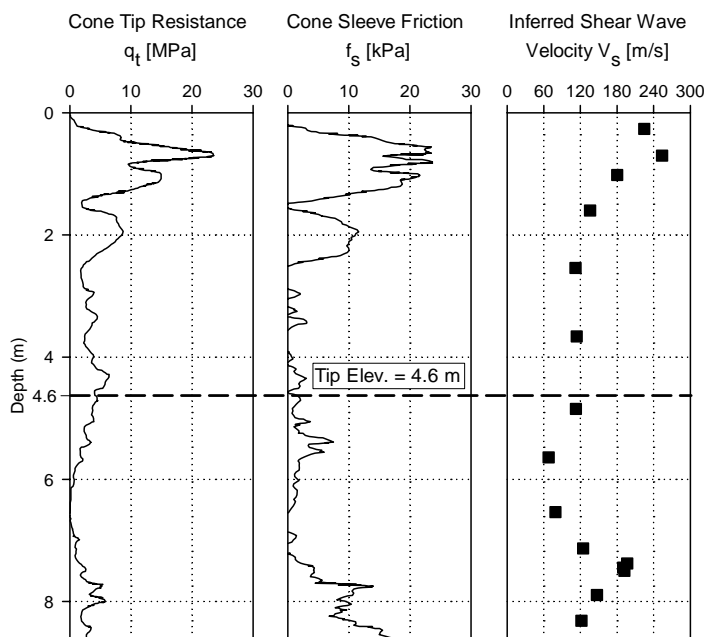


Figure A - 7 Shear wave velocity and CPT soundings advanced at the location of drilled shaft SP 1 at Site I, Clearwater, Florida

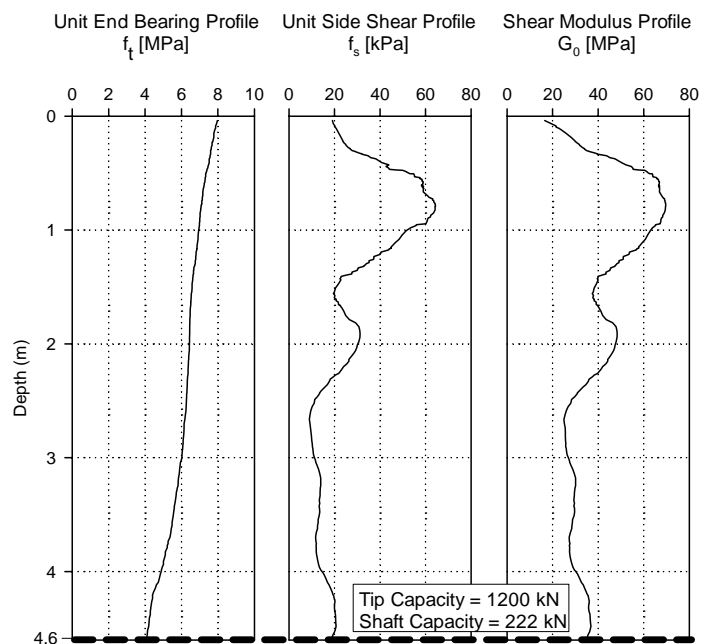


Figure A - 8 Static axial pile capacity and shear modulus profile for a 0.61 m diameter drilled shaft SP 1 location at Site I, Clearwater, Florida

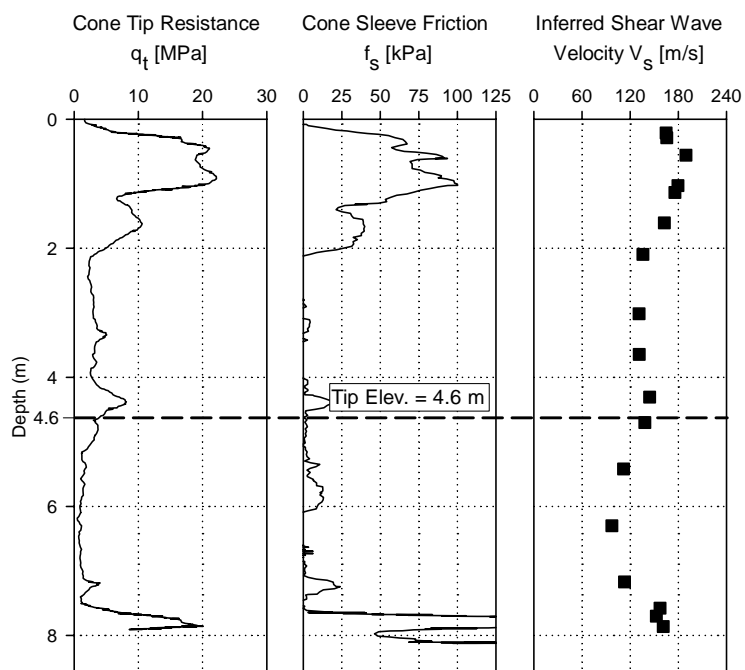


Figure A - 9 Shear wave velocity and CPT soundings advanced at the location of drilled shaft SP 2 at Site I, Clearwater, Florida

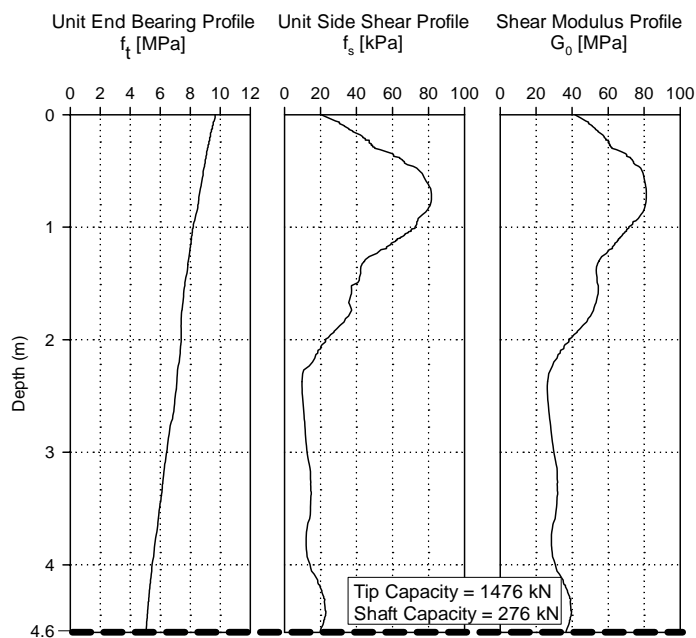


Figure A - 10 Static axial pile capacity and shear modulus profile for a 0.61 m diameter drilled shaft SP 2 location at Site I, Clearwater, Florida

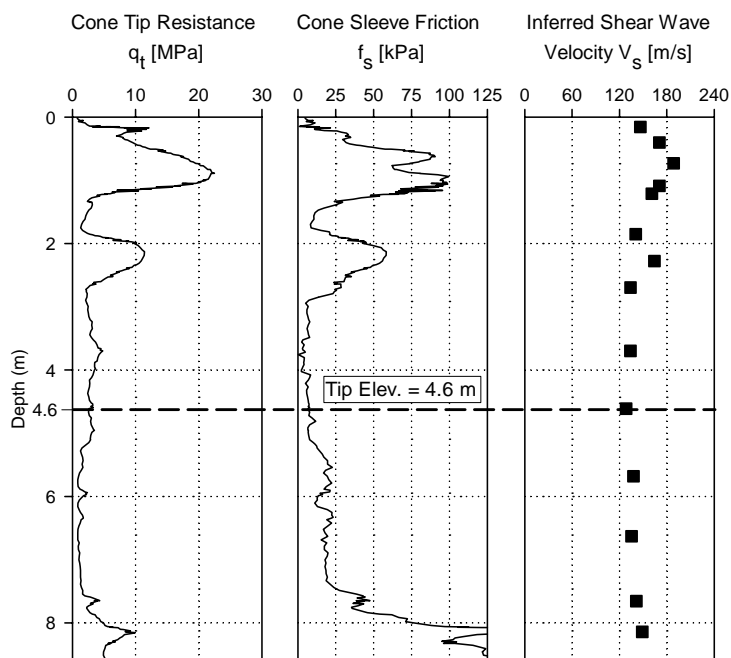


Figure A - 11 Shear wave velocity and CPT soundings advanced at the location of an additional CPT sounding (CPT 67) advanced at Site I, Clearwater, Florida

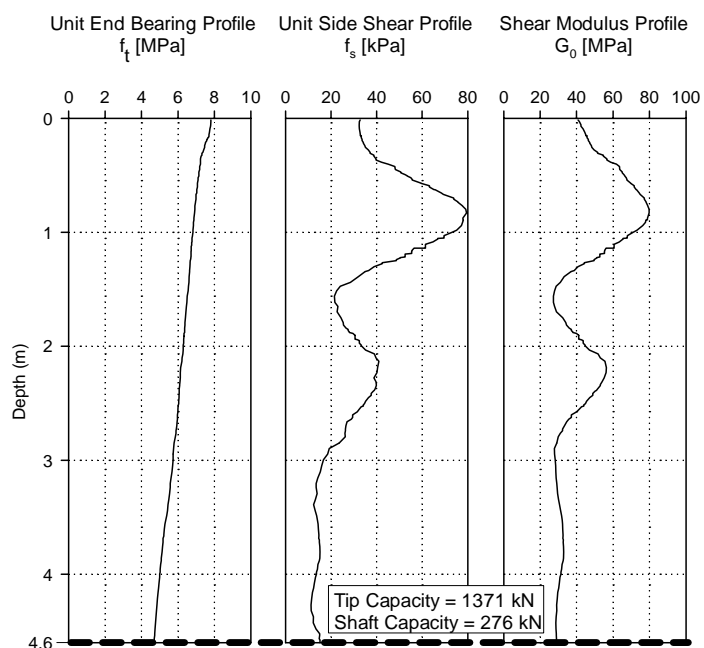


Figure A - 12 Static axial pile capacity and shear modulus profile for a 0.61 m diameter drilled shaft at the location of CPT 67 at Site I, Clearwater, Florida

A.2 TESTING SITE NEAR UNIVERSITY OF HOUSTON

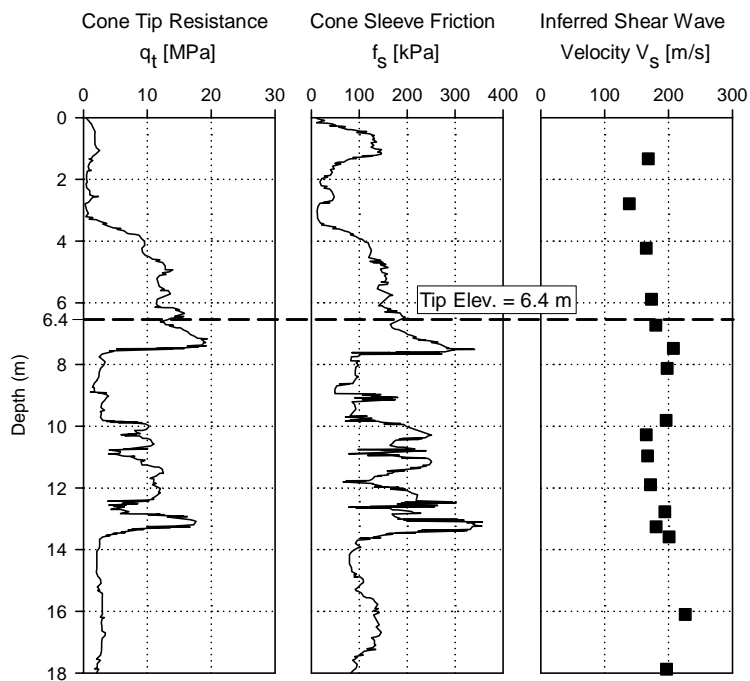


Figure A - 13 Shear wave velocity and sounding CPT 2 advanced at University of Houston, Texas

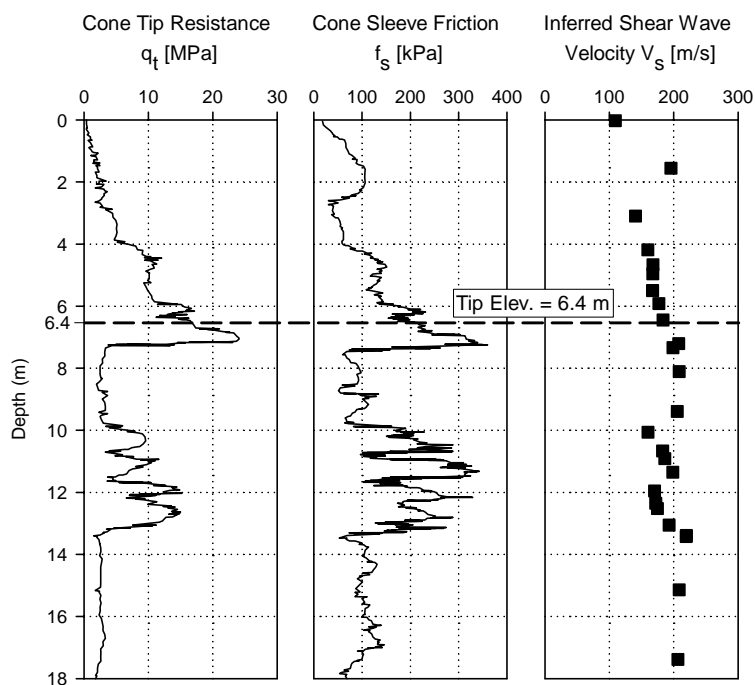


Figure A - 14 Shear wave velocity and sounding CPT 4 advanced at University of Houston, Texas

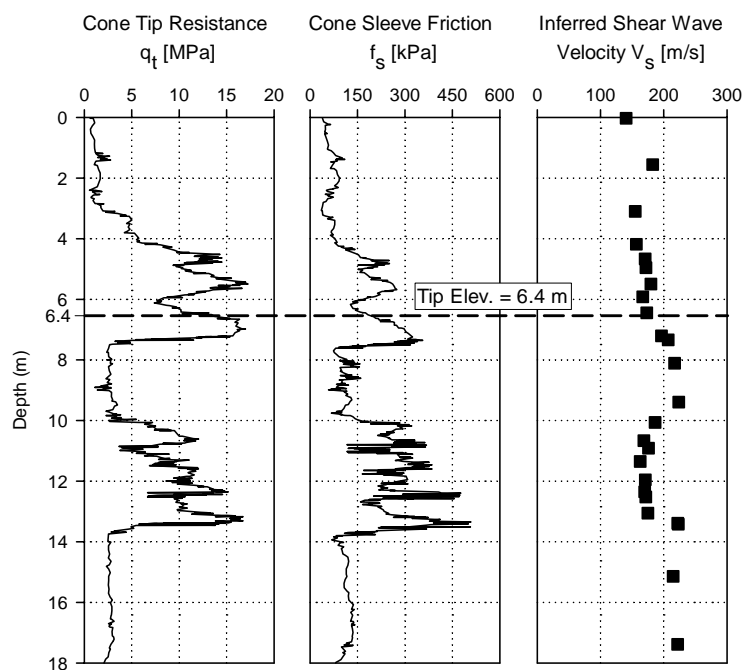


Figure A - 15 Shear wave velocity and sounding CPT 5 advanced at University of Houston, Texas

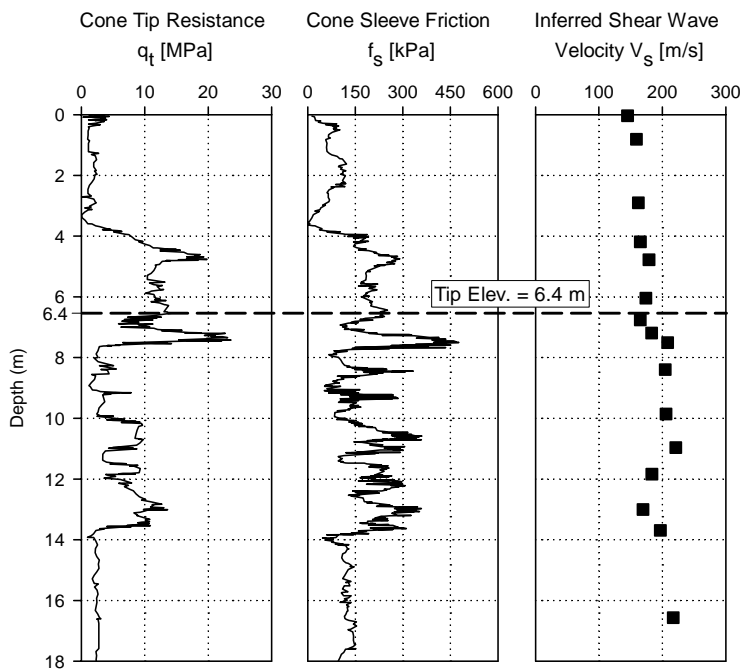


Figure A - 16 Shear wave velocity and sounding CPT 6 advanced at the location of drilled shaft S2 at University of Houston, Texas

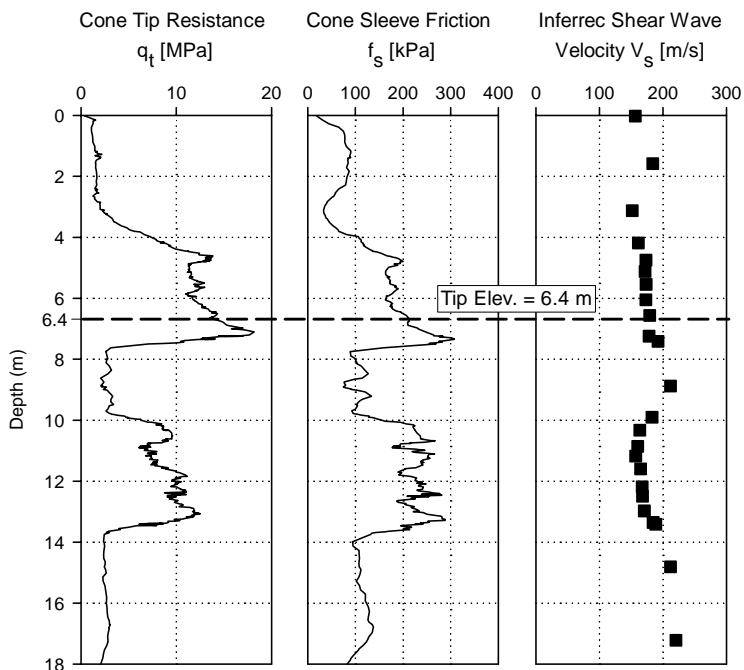


Figure A - 17 Shear wave velocity and average CPT sounding obtained from soundings depicted in Figure A - 13 through Figure A - 16

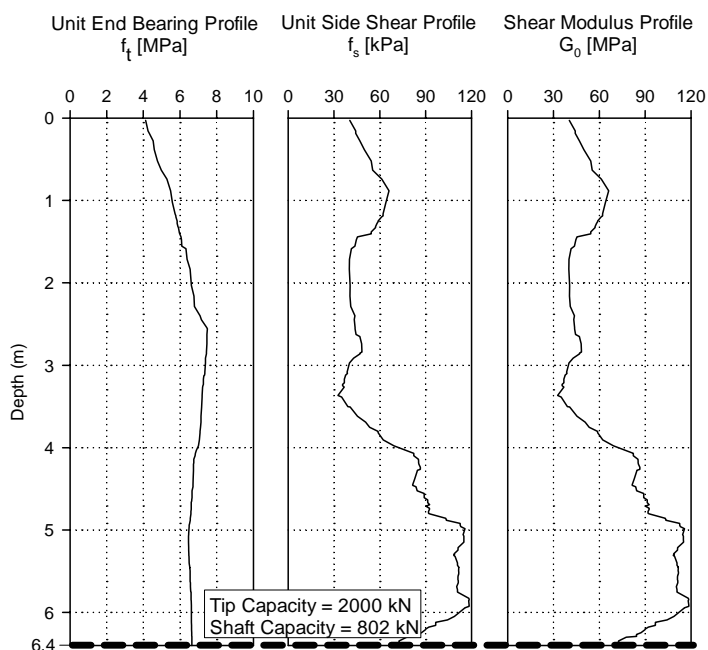


Figure A - 18 Static axial pile capacity and shear modulus profile for a 1.22 m diameter drilled shaft using the average soil profile depicted in Figure A - 17

A.3 NGES AUBURN UNIVERSITY

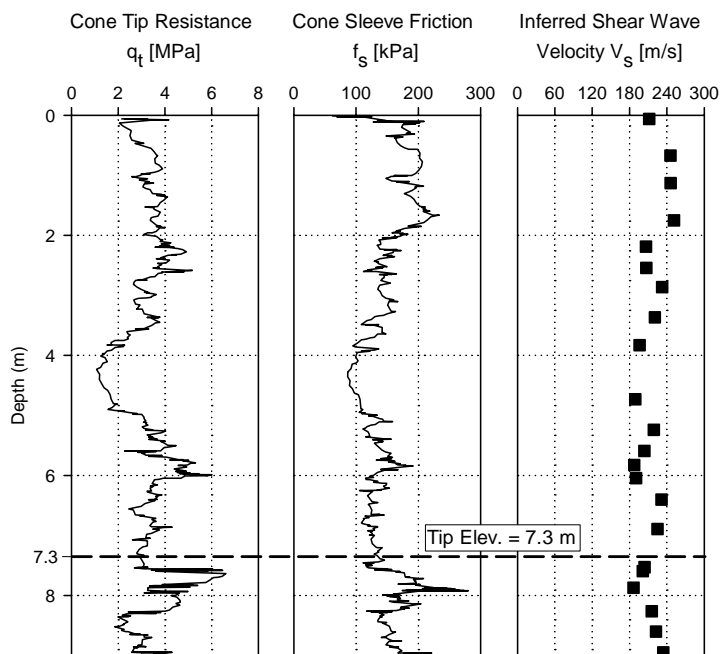


Figure A - 19 Shear wave velocity and CPT soundings advanced at the location of control pile TS-4 at NGES at Auburn University, Alabama

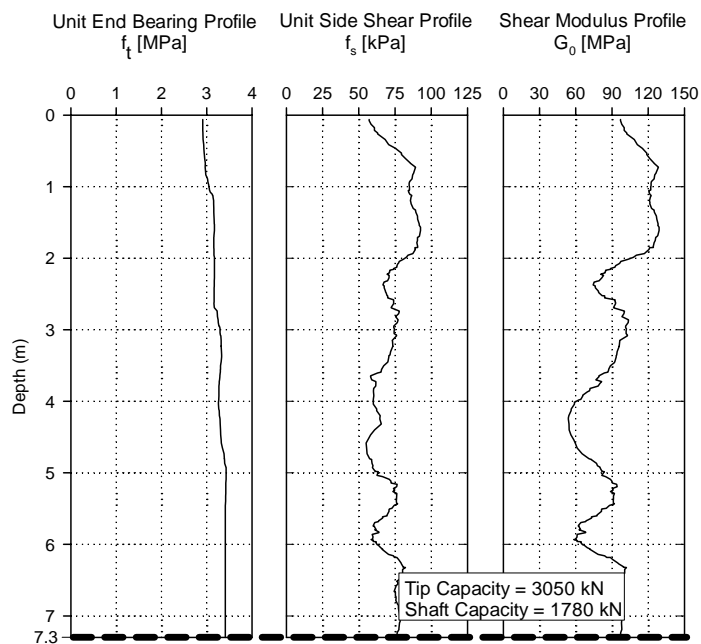


Figure A - 20 Static axial pile capacity and shear modulus profile for a 1.06 m diameter control pile TS-4 at Auburn University, Alabama

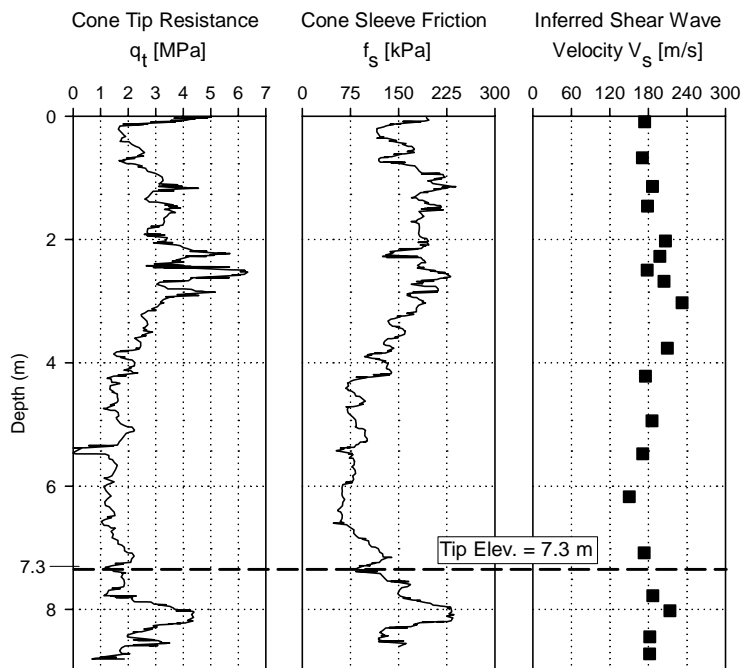


Figure A - 21 Shear wave velocity and CPT soundings advanced at the location of drilled shaft TS-1 at NGES at Auburn University, Alabama

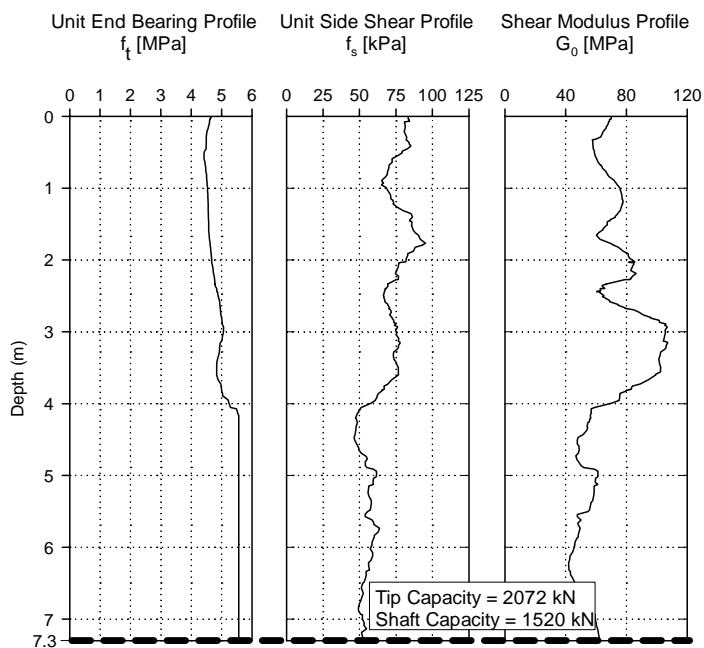


Figure A - 22 Static axial pile capacity and shear modulus profile for a 1.06 m diameter drilled shaft TS-1 at Auburn University, Alabama

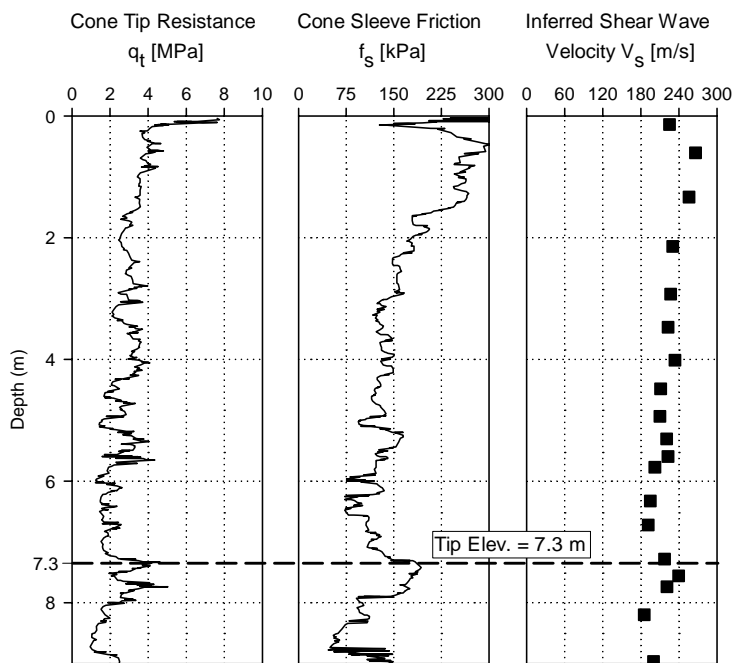


Figure A - 23 Shear wave velocity and CPT soundings advanced at the location of drilled shaft TS-2 at NGES at Auburn University, Alabama

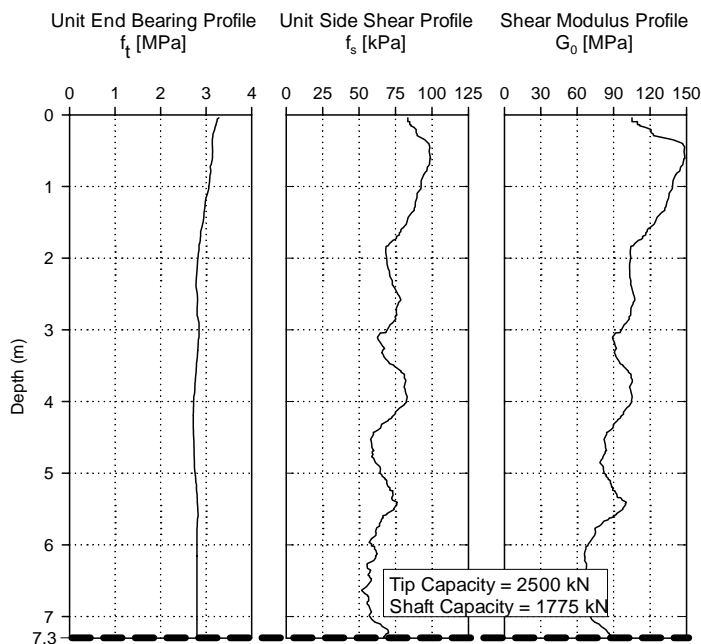


Figure A - 24 Static axial pile capacity and shear modulus profile for a 1.06 m diameter drilled shaft TS-2 at Auburn University, Alabama

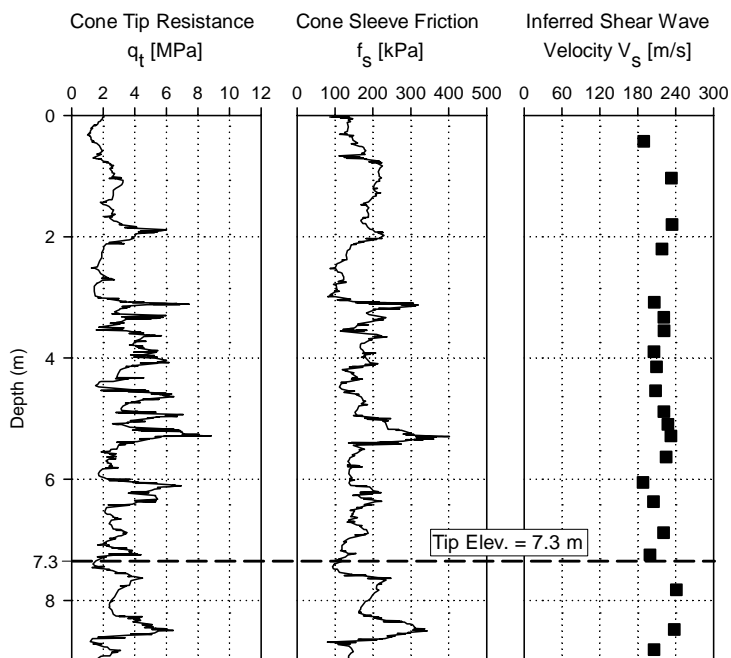


Figure A - 25 Shear wave velocity and CPT soundings advanced at the location of drilled shaft TS-3 at NGES at Auburn University, Alabama

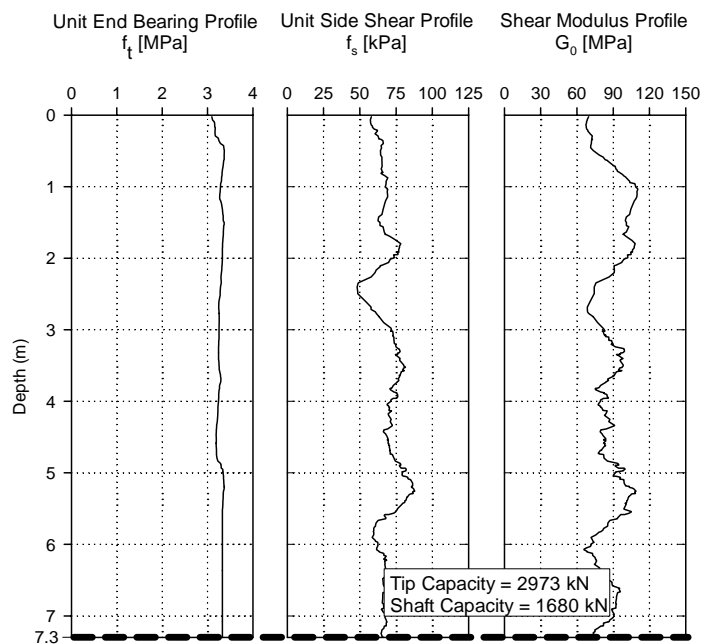


Figure A - 26 Static axial pile capacity and shear modulus profile for a 1.06 m diameter drilled shaft TS-3 at Auburn University, Alabama

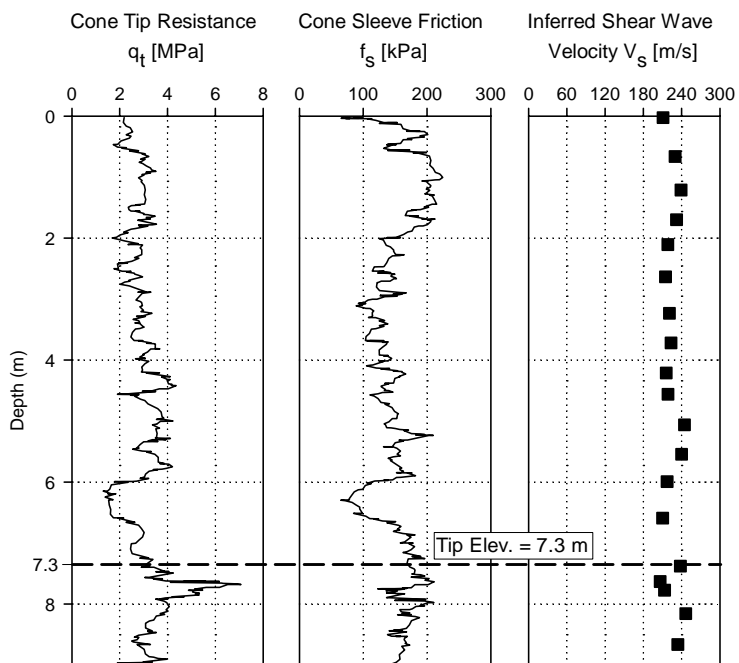


Figure A - 27 Shear wave velocity and CPT soundings advanced at the location of drilled shaft TS-5 at NGES at Auburn University, Alabama

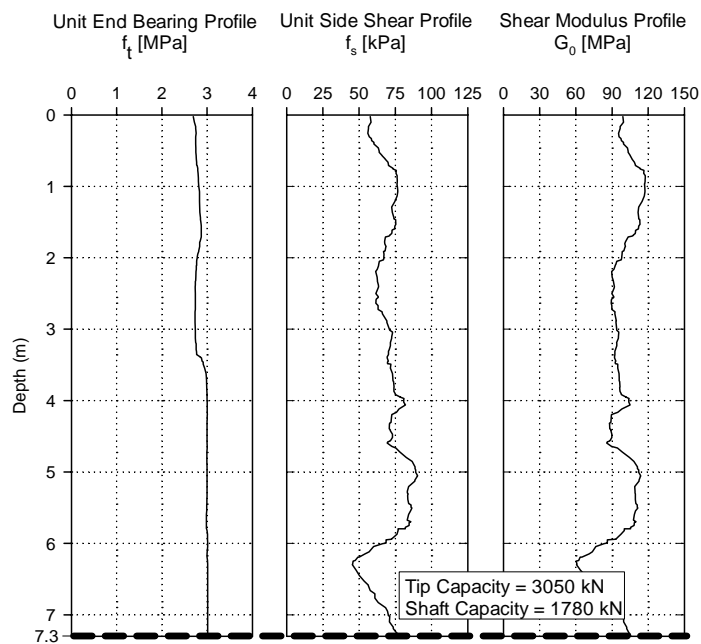


Figure A - 28 Static axial pile capacity and shear modulus profile for a 1.06 m diameter drilled shaft TS-5 at Auburn University, Alabama

A.4 CAROLINA BAYS PROJECT

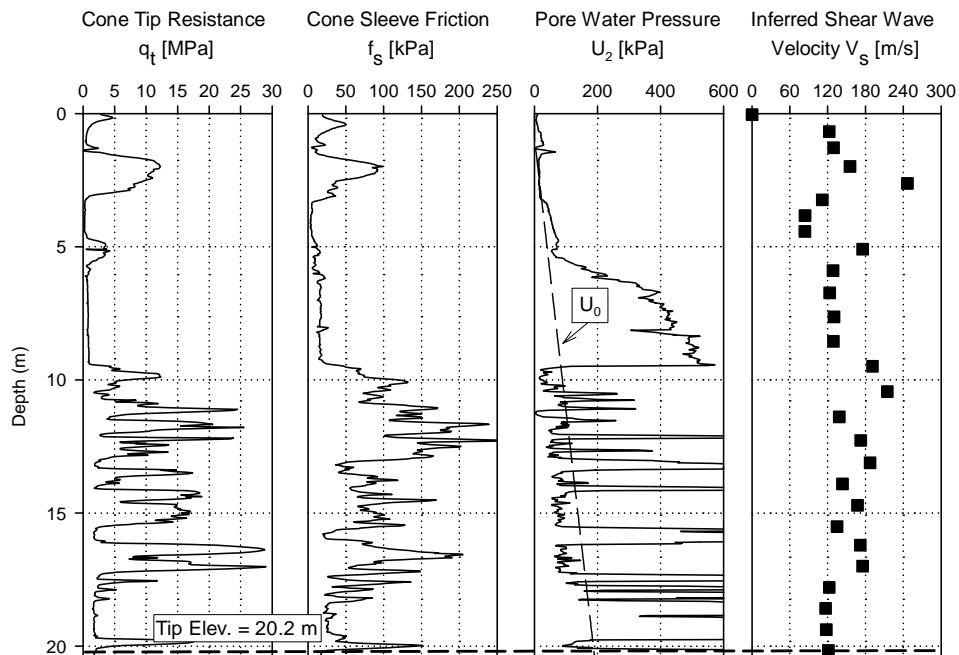


Figure A - 29 Shear wave velocity and CPT soundings advanced at the location of the PGDS at the Carolina Bays project, South Carolina

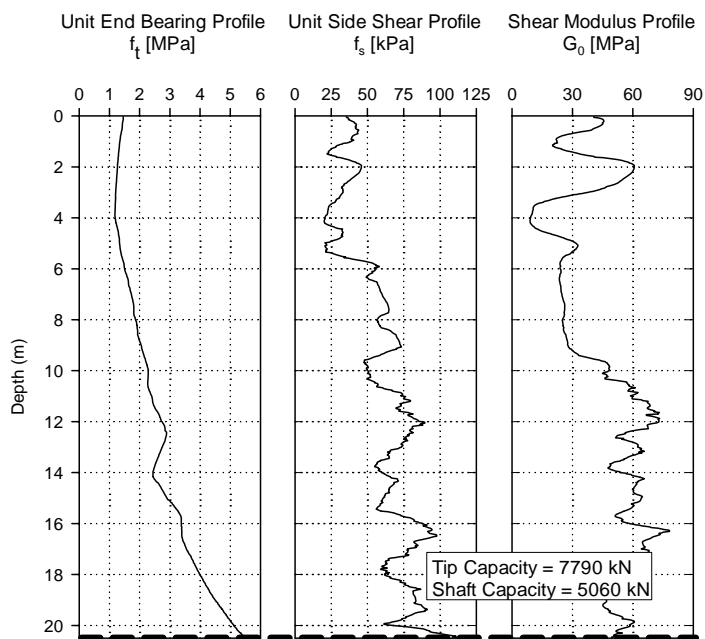


Figure A - 30 Static axial pile capacity and shear modulus profile for a 1.372 m diameter drilled shaft at the Carolina Bays project, South Carolina

APPENDIX

B

B.1 LOAD TRANSFER ANALYSIS OF SINGLE PILES

A program for estimating single pile settlements by means of the load transfer method was developed for this work. The program runs in macro driven worksheets within the Microsoft Excel environment.

The program has two worksheets named “Instructions” and “General Data”. In the “Instructions” worksheet the pile discretization assumed by the load transfer method is presented and a brief guide of the required steps to use the program is provided. In the same sheet the variables required by the program are defined and some typical values for these variables are suggested. The “Instructions” worksheet is depicted in Figure B-1 and Figure B-2.

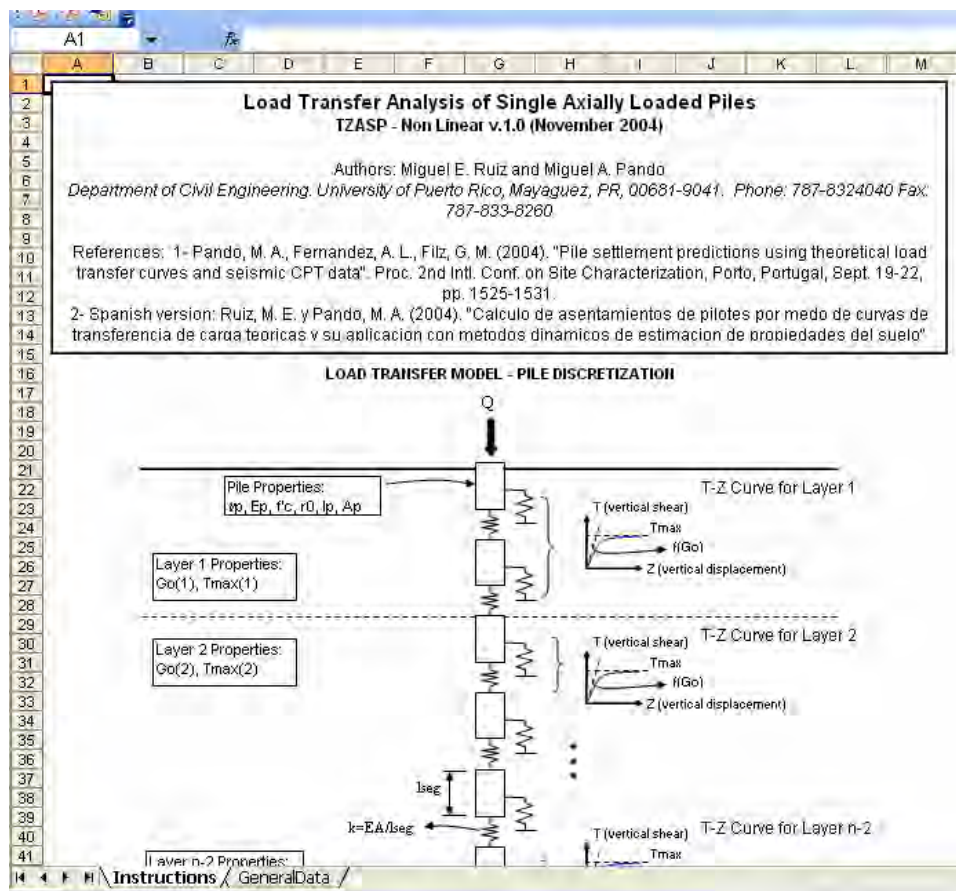


Figure B-1 "Instructions" Worksheet of the load transfer program: Pile discretization

M105		fx																	
	A	B	C	D	E	F	G	H	I	J	K	L	M	N	O	P	Q	R	S
58																			
59		GENERAL INSTRUCTIONS																	
60																			
61		A)	Steps to create new project																
62			1)	Select "General Data" worksheet.															
63			2)	Select the units system that you will use. Make sure to keep units consistent when entering all parameters															
64			3)	Input data in red cells only. Fill in the cells corresponding to the following fields:															
65				f _c , n _p , r ₀ , l _p , A _p , N _{layers} y Conv. Tolerance. (The elastic modulus of the pile is calculated automatically from f _c)															
66			4)	After entering basic input data press the "Step 1" Button. A dialog box will open. You can enter the properties of the soil layers in this dialog box.															
67			5)	Select from the drop down menu the type of Tz or G&Z curve you want to use															
68			6)	The "File segments" button allows you to discretize the pile into segments. You will be requested to enter the number of segments in which you want to divide the pile for each layer of soil.															
69			7)	Press the "Tip Displacements" button to generate a number of prescribed tip displacement that will be used to calculate the P-U curve of the pile.															
70			8)	Press the "Save New Project" button to save data to a file															
71			9)	Press "Run" button to perform Analysis															
72			10)	Press "View Results" button to save and open the results file.															
73																			
74																			
75		B)	Steps to open an existing project																
76			1)	Press the "Open existing project" button. A dialog box will appear, in which you can select your saved file.															
77			2)	After the file is open you can either view old results (pressing the "View Results" button or perform new analysis															
78			3)	To save changes, press the "Save Data" button. Changes will be saved in the existing file.															
79			4)	To save data in a new file, press the "Save New Project" button															
80																			
81																			
82																			
83																			
84																			
85																			
86																			
87			f_c=	Compressive strength of concrete. This value is used to calculate modulus of elasticity of concrete following ACI 318															
88			ν_p=	Poisson modulus of the pile															
89			r₀=	Radius of pile															
90			l_p=	Length of pile															
91			A_p=	Cross section of pile															
92			N_{layers}=	Number of layers in soil profile. The last layer is the layer under the pile tip.															
93			Conv. Tolerance=	Tolerance for convergence. It has units of Length. The default tolerance is 0.0001 m															
94																			
95																			
96																			
97			G0(j)=	Shear modulus of soil layer "j". Units [F]/[L ²]															
98			f=	Fitting parameter. Dimensional. This value is useful only if the "Modified Hyperbolic" curve type is selected															
99			g=	Fitting parameter. Dimensional. This value is useful only if the "Modified Hyperbolic" curve type is selected															
100			q_{max}=	Ultimate Shaft resistance for the layer. Units [F]/[L ²]															
101			q_{bmax}=	Ultimate Tip resistance. Units [F]															
102			ν_s=	Poisson modulus of the soil layer under the pile tip.															
103			r_m=	Radius of influence of pile [L]. Flandolph and Wroth proposed the following expression to calculate r _m =2.5r _p (1-ν _s), where r is the ratio of the shear modulus of the layer at the middle of the pile and the shear modulus of the soil under the pile tip, and l _p is the length of the pile															
104																			
105																			
106																			

Figure B-2 “Instructions” Worksheet of the load transfer program: General Instructions to run analysis and variable definition

In the second worksheet, named “General Data”, a series of buttons are provided in order to develop the numerical model. In this sheet, all pile and soil data required for the model should be entered by the user. In Figure B-3 fields for entering general model data and pile properties are shown.

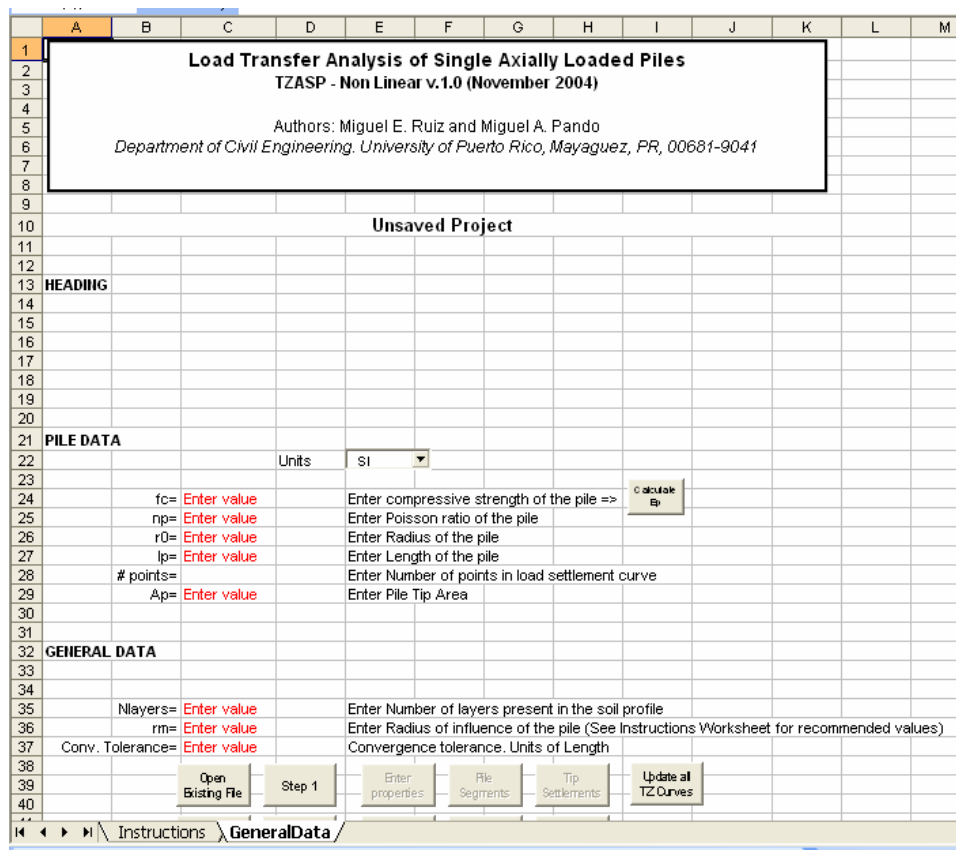


Figure B-3 “General Data” Worksheet of the load transfer program: General model data and pile properties

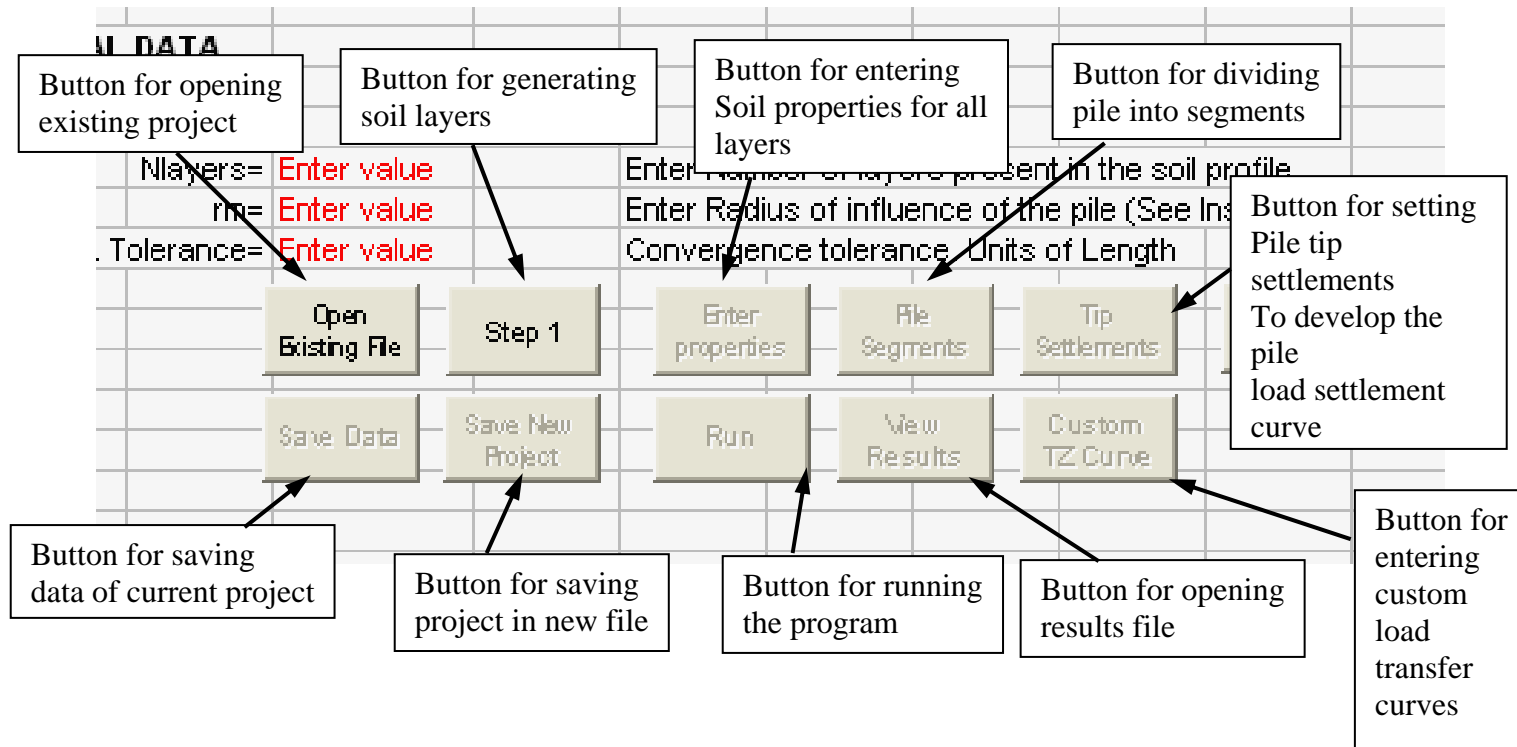


Figure B-4 “General Data” Worksheet of the load transfer program: Panel of Command Buttons

Results of the load transfer analyses are shown in a separate file which can be open pressing the “View Results” button. The results file shows an echo of the input data and the load settlement curve of the pile that is being analyzed. If several runs are made for the same model, data for each run is stored in separate worksheets in the results file. The program generates the pile load settlement curve for each run. A screenshot of the results file showing the echo of input data is shown Figure B-5.

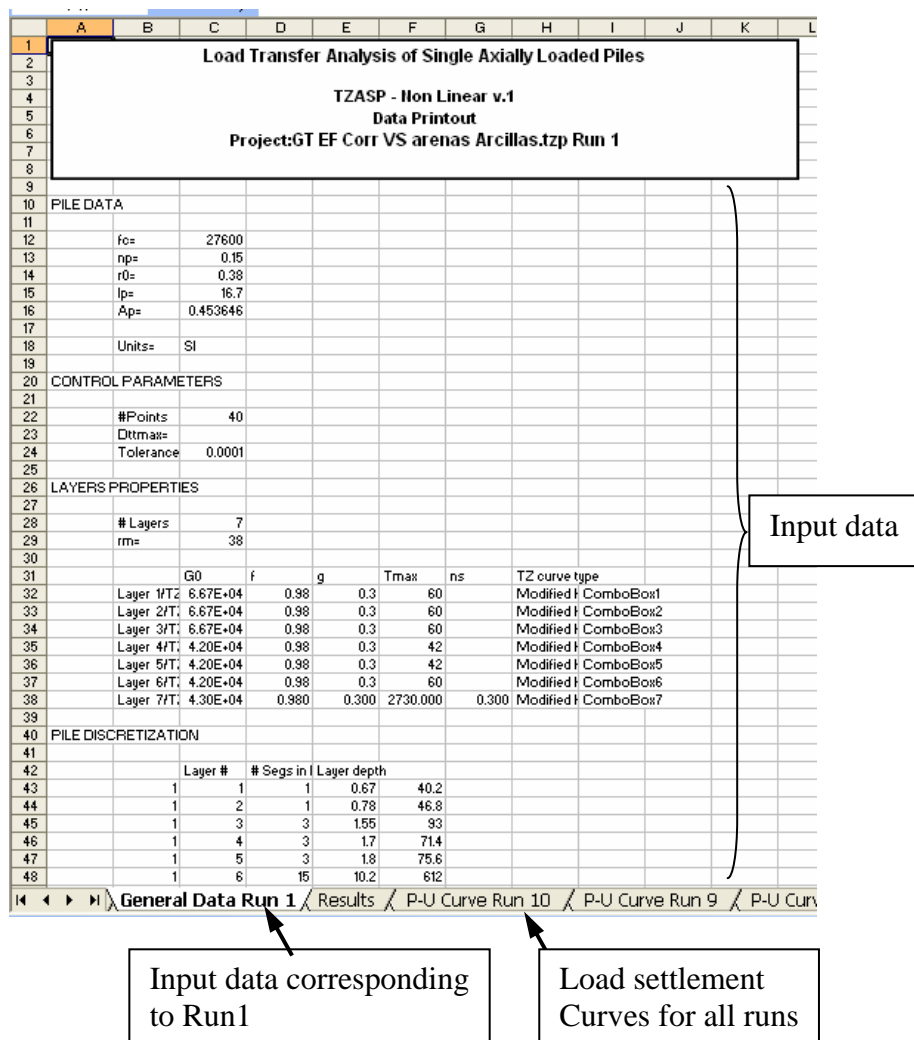


Figure B-5 Results file: Echo of input data